INFORMATION TO USERS

This manuscript has been reproduced from the microfilm master. UMI films the text directly from the original or copy submitted. Thus, some thesis and dissertation copies are in typewriter face, while others may be from any type of computer printer.

The quality of this reproduction is dependent upon the quality of the copy submitted. Broken or indistinct print, colored or poor quality illustrations and photographs, print bleedthrough, substandard margins, and improper alignment can adversely affect reproduction.

In the unlikely event that the author did not send UMI a complete manuscript and there are missing pages, these will be noted. Also, if unauthorized copyright material had to be removed, a note will indicate the deletion.

Oversize materials (e.g., maps, drawings, charts) are reproduced by sectioning the original, beginning at the upper left-hand corner and continuing from left to right in equal sections with small overlaps.

Photographs included in the original manuscript have been reproduced xerographically in this copy. Higher quality 6" x 9" black and white photographic prints are available for any photographs or illustrations appearing in this copy for an additional charge. Contact UMI directly to order.

Bell & Howell Information and Learning
300 North Zeeb Road, Ann Arbor, MI 48106-1346 USA

UMI®
800-521-0600

Behavior of FRP Reinforced and Partially Prestressed Concrete Members under the Effects of Temperature Gradients

Omer Ramadan El-Zaroug

A Thesis

in

The Department

of

Building, Civil, and Environmental Engineering

Presented in Partial Fulfillment of the Requirements

for the Degree of Master of Applied Science at

Concordia University

Montreal, Quebec, Canada

November 1999

0-612-47819-X

Abstract

Behavior of FRP Reinforced and Partially Prestressed Concrete Members under the Effects of Temperature Gradients

Omer Ramadan El-Zaroug

The use of fiber reinforced polymer (FRP) reinforcements in concrete structures has increased rapidly in recent years. FRP rods are made of high strength continuous carbon, aramid or glass fibers impregnated with resin and have some excellent properties such as high strength-to-weight ratio, high resistance to corrosion and good fatigue properties. However, the thermal characteristics of FRP rods can be substantially different from those of concrete and conventional steel bars. Such difference can have a significant influence on the behavior of FRP concrete members when subjected to temperature variations.

This research involves an experimental investigation into the effects of thermal characteristics of different types of FRP on the development of thermal stresses and on the control of thermal cracking in reinforced concrete (RC) and partially prestressed concrete (PPC) beams. A total of eleven RC and PPC beams using FRP rebars were tested. The test program consisted of two series; RC series and PPC series. The eleven beams had the same concrete cross-section dimensions. The RC series consisted of six beams. Three of the beams were reinforced with carbon fiber reinforced polymer (CFRP) rods of different amounts. The CFRP reinforcement is known as Leadline, manufactured and supplied by Mitsubishi Chemical Corporation. The other three beams were reinforced with glass fiber reinforced polymer (GFRP) grids known as NEFMAC, manufactured by

NEFCOM Corporation, Japan. Different locations of the grid were used in the three beams.

The PPC series consisted of two pretensioned beams and two post-tensioned beams using Leadline rods, in addition to one beam post-tensioned with prestressing steel strand. The Leadline rods and the steel strand were prestressed with the same force but were located at different eccentricities from the cross-section centroid.

The concrete specimens were tested under the effects of temperature gradients while the rotations at the two beam ends were prevented. The bending moment and cracking resulted from the temperature variations were monitored. The behavior of the thermally cracked concrete beams was also investigated under mechanically applied moments. Finally, in order to study the mode of failure and deflection after cracking, the concrete beams were loaded statically as simply supported beams subjected to two concentrated loads, each applied at one third of the span length. The results of RC beams were compared to those obtained from tests on beams of the same dimensions but reinforced with steel bars (Ariyawardena, Ghali and El-Badry, 1997), and to those obtained from analytical model developed by El-Badry and Ghali, (1995).

ACKNOWLEDGMENTS

I would like to express my sincere thanks to my supervisor Dr. Mamdouh M. El-Badry for his critical review of my research work. His assistance and valuable guidance are highly appreciated.

Special acknowledgement is due to my dear friend Ibrahim Balkir for his valuable help and encouragements throughout the work.

Thanks are due to Mr. Andrew Chociwski and Mr. Daniel Roy for their help during the experimental work conducted in the Structures Laboratory of Concordia University. I also extend my thanks to my friend Richard Tse for his appreciated help.

The financial support from the Secretariat of Education of Libya is highly appreciated. The financial assistance provided by ISIS Canada Network of Centers of Excellence and by the Department of Building, Civil and Environmental Engineering are also gratefully acknowledged.

The CFRP Leadline reinforcements were supplied by Mitsubishi Chemical Corporation, Japan. The donation of the GFRP NEFMAC reinforcement by the city of Calgary is greatly appreciated. Thanks are also extended to the University of Calgary for donating the testing frame and for providing the anchorage system developed by Dr. N. G. Shrive for prestressed Leadline rods.

I wish also to thank my family, my parents and my wife for their support and encouragement during the preparation of this work.

Table of Contents

List of Figures

List of Tables

List of Symbols

A = area of concrete section

A_f = area of CFRP reinforcement

A_g = gross area of concrete section

A_m = cross sectional area of masonry wall

A_P = area of prestressing FRP tendon

A_s = area of nonprestressed tension reinforcement

A_s' = area of nonprestressed compression reinforcement

b = width of section

d = depth from the concrete extreme compression fiber to the centroid of nonprestressed tension reinforcement

d_c = thickness of concrete cover measured from centroid of the bottom layer of tension reinforcement

d_f = depth from the concrete extreme compression fiber to the centroid of Leadline reinforcement

d_p = depth from the concrete extreme compression fiber to the centroid of prestressing tendon

d_s = thickness of concrete cover measured from centroid of tension reinforcement

d_s' = thickness of concrete cover measured from centroid of compression reinforcement

E_c = modulus of elasticity of concrete

E_f = modulus of elasticity of CFRP reinforcement

E_m = modulus of elasticity of masonry wall

E_p = modulus of elasticity of tendon materials

e = eccentricity

f_{all} = allowable prestressing

f_c' = concrete compressive strength

f_{ct} = concrete tensile strength

f_g = guaranteed tensile strength of Leadline

f_s' = splitting strength of concrete

h = total height of section

I = moment of inertia about the centroidal axis

I_1 = moment of inertia of transformed uncracked section

I_2 = moment of inertia of fully cracked section

I_e = effective moment of inertia

I_m = second moment of area of wall cross section

L = length of member

l = tested length

M = bending moment

M_{cr} = cracking moment

$M_{cr,m}$ = cracking moment at which the *m*th crack develops

M_i = initial applied moment before introducing the thermal moment

M_r = restraining moment

m = crack number

N_r = restraining force

n_f = E_f / E_c = modular ratio of CFRP

P = applied load

P_f = force in prestressing tendon

s = crack spacing

S_{avg} = average crack spacing

S_{max} = maximum crack spacing

S_{min} = minimum crack spacing

T = temperature

T_f = temperature at level of CFRP layer

T_O = temperature at the centroid of cross section

t = asphalt thickness

t_w = wall thickness

y_f = distance from the centroid of the cross section to centroid of CFRP reinforcement

y_m = distance measured upward from a point 1200 mm below the top of the concrete deck

Z_t = section modulus of a transformed noncracked section

α_c = coefficient of thermal expansion of concrete

α_f = coefficient of thermal expansion of CFRP

α_{Invar} = coefficient of thermal expansion of Invar bar

α_m = coefficient of thermal expansion of masonry wall

α_p = coefficient of thermal expansion of prestressing tendon

β = coefficient of reinforcement shape

Δ = mid-span deflection

ΔP = change in prestressing force

ΔT = temperature difference between the top and bottom fibers of the cross section

$\Delta T_{cr,1}$ = temperature difference at which first crack occurs

$\Delta T_{cr,m}$ = temperature difference at which the *m*th crack occurs

$\Delta \varepsilon_m$ = change in strain in masonry wall

$\Delta \varepsilon_p$ = change in strain in prestressing tendon

ε = normal strain

ε_O = normal strain at the centroid

λ = factor accounting for concrete density

ψ = curvature

ρ = reinforcement ratio

σ_c = concrete stress

σ_{ci} = stress at the extreme tension fiber before application of any thermal loading

σ_{cmax} = maximum stress at extreme tension fiber ignoring cracking

σ_f = stress in CFRP reinforcement

σ_r = restraining stress

σ_s = steel stress

ζ = interpolation coefficient

Chapter 1

Introduction

1.1 General

Increased cracking in newly constructed concrete bridge decks has been reported in recent years. There has been a growing awareness that an important aspect that should considered in the design, particularly of continuous concrete bridges, is the induction of thermal stresses by nonuniform temperature distributed through the depth of bridge decks. Comprehensive studies and successful tests have been carried out to fully understand the magnitude and significance of thermal stresses induced by ambient conditions in addition to the stresses due to dead and live loads in concrete bridges.

Daily changes in solar radiation and other weather conditions result in nonlinear distribution of temperature through the depth of a concrete bridge deck. Nuclear structures, thick concrete sections and floor slabs under boilers are also subjected to temperature gradients. In general, thermal loadings are caused by daily fluctuations in temperature. These gradients can, in some instances, represent the most critical loading condition, and can produce relatively high tensile stresses enough to produce cracking. This can adversely affect the serviceability and durability of concrete structures.

A reinforced concrete structure subjected to thermal loads will develop stresses when free thermal expansion, contraction or rotation is restrained. The restraints to thermal deformations can be external such as those provided by the supports in continuous structures or internal when the distribution of temperature across the section is nonlinear. Internal restraints occur also when the reinforcement has coefficient of thermal expansion different from that of concrete as in the case of Fiber Reinforced Polymer (FRP) reinforcement.

Although the technology of replacing steel with FRP reinforcement is gaining acceptance due to its higher strength and durability, corrosion resistance and light weight, the thermal behavior of FRP reinforced structures when subjected to large temperature variations (-40°C to 38°C), such as those found in North America remains an unresolved issue. Thermal characteristics of FRP rebars vary from one product to another and depend on the type of fiber and resin matrix used, the fiber volume ratio and the modulus of elasticity. Carbon fiber reinforced polymers (CFRP), for example, have a coefficient of thermal expansion in the longitudinal direction, α_L, close to zero (Erki and Rizkalla, 1993), while aramid fiber reinforced polymers (AFRP) have a negative coefficient varying from -2×10^{-6} /°C for Arapree to -15×10^{-6} /°C for Technora (Daniel and Ishai, 1994).

The effects of temperature on FRP rods in terms of prestressing applications and loss of strength at elevated temperature are an important aspect. Under increase of temperature, the difference in the coefficient of thermal expansion of CFRP from that of concrete may lead to compressive stresses in the concrete and tensile stresses in the CFRP rod. This can be beneficial in concrete members prestressed by CFRP. On the other hand, under temperature decrease. this may cause tensile stresses in the concrete and compressive stresses on the reinforcement, and hence increase in the prestress losses in prestressed members (El-Badry and Abdalla. 1998).

Experiments on FRP reinforcements have shown that the transverse coefficient of thermal expansion of FRP rebars is typically much higher than its longitudinal coefficient of thermal expansion and can be 5 to 8 times higher than the corresponding value of concrete. Thermal incompatibility in the transverse direction my create significant bursting stresses within the concrete members around the FRP reinforcement under temperature increase (Gentry and Hudak, 1996) or separation of the bars from the concrete under temperature decrease. This may adversely affect the bond between the reinforcement and the concrete and the minimum cover to the reinforcement (El-Badry and Abdalla, 1998).

1.2 Objectives and Scope

The main objective of the present research is to investigate experimentally the behavior of FRP reinforced and partially prestressed concrete members under the effects of thermal gradients while the end rotations are restrained.

The specific objectives of the research are:

1. To examine the effects of thermal characteristics of different types of FRP reinforcement on the development of thermal stresses and on the control of thermal cracking in concrete members.

2. To investigate the flexural behavior of concrete members, in terms of crack distribution, spacing and width and deflection after cracking under thermal loading and mechanical moments.
3. To study the behavior up to ultimate of thermally cracked concrete members under mechanical load.
4. To study the effects of the reinforcement ratio (ρ) and the level of partial prestressing with either concentric or eccentric tendons on the thermal behavior of concrete members.
5. To compare the experimental results with those available from tests carried out on beams reinforced or prestressed with conventional steel (Ariyawardena, 1993) and with the results obtained from analytical equations proposed by El-Badry and Ghali (1995).

The experimental program consists of testing a total of eleven reinforced and partially prestressed concrete beams, all having a 250 x 500mm rectangular cross-section. Each of the concrete beams was tested under three different conditions: first, under thermal loading, then under mechanically applied moment and, finally, under two symmetrical concentrated loads each applied at one third of the span length in small increments up to failure. The test specimens included two series, A and B. Series A consisted of six reinforced concrete beams, 250 x 500 x 3500 mm each, which were divided into two groups, A1 and A2. Group A1 consisted of three beams reinforced with CFRP Leadline bars with reinforcement area equal to 0.6%, 0.8% and 1.0% of the concrete section, respectively. Group A2 consisted of the remaining three beams which were reinforced with glass fiber reinforced (GFRP) grids, known as NEFMAC. The cross sectional area of each grid represents 0.5% of the cross sectional area of the concrete beam. The beams were reinforced with the grid placed at different location within the cross section of each beam.

Series B consisted of five beams, each of length 4500 mm, which were divided into two groups, B1 and B2. Group B1 consisted of two beams pretensioned with one Leadline tendon, placed at the centroid of the concrete section in one beam and at an eccentricity of 50 mm from the centroid in the second beam. Group B2 included three beams, two were post-tensioned with unbonded concentric and eccentric Leadline tendon. The third beam in Group B2 was post-tensioned with a concentric unbonded steel strand. This beam was used as control specimen.

1.3 Outline of Thesis

In the following chapter, the heat transfer processes that affect the development of temperature variations within a bridge cross-section, typical distributions of temperature that are considered in the design by different codes, and the analysis of stresses induced by temperature variations in concrete bridge are discussed. Temperature effects on material characteristics and mechanical properties of different types of fiber reinforced plastic are presented. Previous research work carried out on concrete member reinforced with FRP reinforcement under temperature gradients is also reviewed.

A detailed description of the experimental program is given in Chapter 3. The procedures for preparation, fabrication, and the instrumentation of the test specimens are explained in detail. The material properties of the concrete and steel and the characteristics of CFRP and NEFMAC reinforcements used in the test specimens are given. The test set-up and testing procedure are described in details.

The results of this experimental program are presented and discussed in Chapter 4. Graphs of temperature profile, variation of bending moment with temperature difference, crack pattern, and the change in the prestressing force in the tendons are presented. The ultimate strength of thermally cracked beams and the modes of failure are also discussed. Photographs of the failure modes of each test specimen are presented in Appendix A. Also, a comparison is made between the behavior of beams of Series A to the behavior of similar beams but reinforced with steel rebars and tested by Ariyawardena (1993).

In chapter 5, the analytical equations proposed by El-Badry and Ghali (1995) for prediction of the thermal moment-curvature relationships for concrete members are reviewed and modified to account for the effects of the difference between the coefficients of thermal expansion of CFRP and concrete. A comparison is made between the analytical M-ΔT diagrams and the experimental results.

Finally, a summary and conclusions are given in Chapter 6. Recommendations are also given for further research in the area of thermal behavior of concrete structure.

Chapter 2

Literature Review

2.1 General

Temperature variations can produce relatively high thermal stresses enough to cause cracking in a concrete structure. Such cracking can seriously affect the serviceability and durability of the structure. Several investigations have shown that many problems can arise if the effects of temperature gradients over the cross section depth of concrete members are ignored in the design calculations.

In this chapter, the heat transfer processes that take place between the atmosphere and concrete structures are briefly reviewed. The form of temperature distributions and the magnitude of thermal gradients and the corresponding stresses that develop in concrete bridges are discussed. The effects of thermal characteristics of different types of FRP reinforcement on their mechanical properties and on the behavior of concrete structures reinforced with FRP are also discussed. Very few investigations on the behavior of FRP reinforced concrete structures under temperature effects have been found in the literature. A brief review of the previous experimental studies on the thermal behavior of concrete members reinforced with FRP is presented.

2.2 Heat Transfer Processes and Bridge Temperature

2.2.1 Sources of Temperature Variations

The main sources of temperature variations that take place in concrete structures may be divided into two types:

- Insolation and ambient heating and cooling: Concrete structures thermally respond to solar radiation, wind exposure, and ambient temperature changes (both diurnal and seasonal cycles). An exposed bridge deck continuously gains and loses heat from solar radiation, radiation to the sky or surrounding objects, and convection to or from the surrounding atmosphere. In the daytime and especially during summer, the heat gain is greater than the heat loss, resulting in a temperature increase throughout the cross-section. During a typical winter night, the converse is true, and the temperature in the superstructure decreases. The heat flow processes for typical summer and winter conditions are shown in Figure 2.1. The amount of radiation absorbed by a bridge deck is a function of the nature and color of the surface. Convective heat transfer from atmosphere to bridge deck is a function of wind velocity, ambient air temperature, and deck surface temperature.
- The heat released during hydration of cement: This is only important in relatively thick sections, such as in concrete dams, retaining walls and foundation pads.

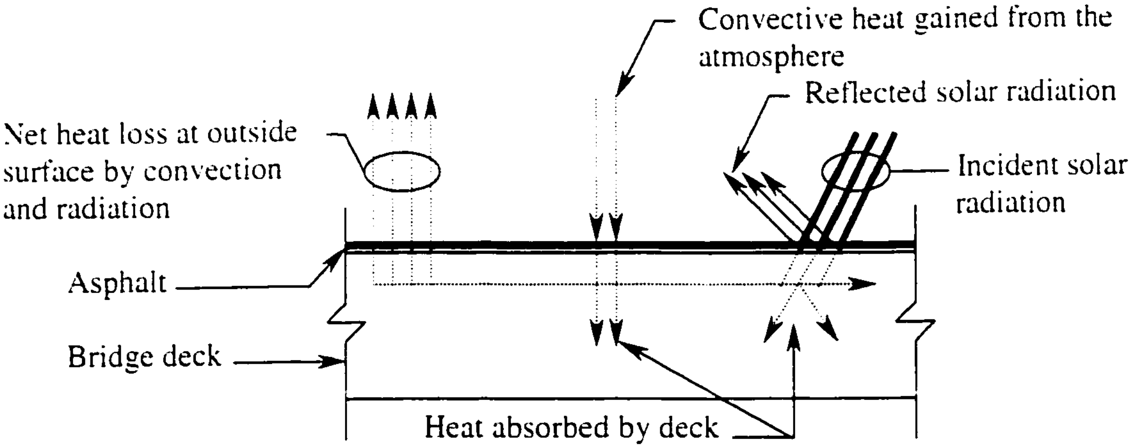

(a) Summer Daytime Conditions

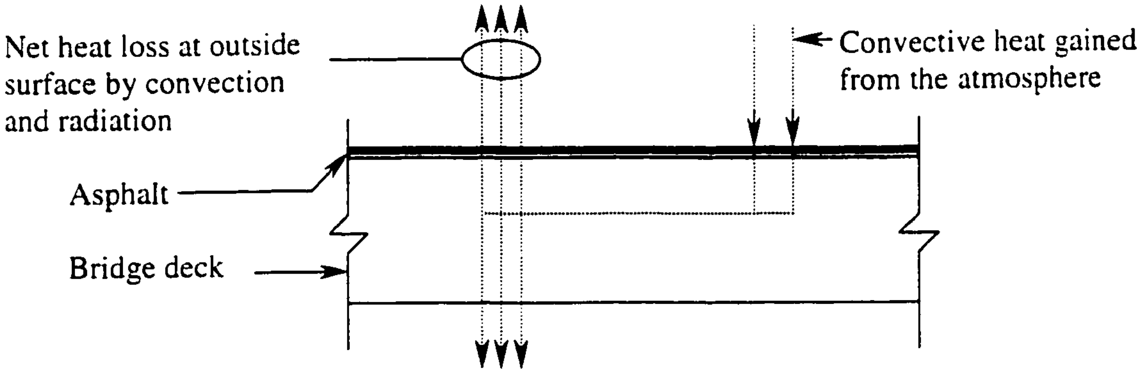

(b) Winter Night Conditions

Figure 2.1 Heat Gain and Loss Processes

2.2.2 Bridge Temperature

There are two types of temperature gradients: namely, positive and negative. A positive gradient is defined when the top surface of the structure is warmer than the bottom surface. As a result of the poor thermal conductivity of concrete, a temperature gradient will occur through the depth of a concrete member. In shallow sections (i.e. less than 0.3 m), temperature gradients are generally linear while in deeper sections gradients are nonlinear (El-Badry and Ghali, 1983). In order to determine the vertical temperature distribution, several codes have proposed different design temperature and thermal gradients to be used in the analysis methods. Suggestions for selecting of temperature gradients are briefly discussed and illustrated below.

The New Zealand Code adopted the temperature distribution shown in Figure 2.2 proposed by Priestley (1978) for box-girder bridges. The temperature distribution consists of a fifth power parabola for the cantilever parts and for the top 1200mm depth of the webs of box girders. This parabolic profile can be determined by:

$$T = (32 - 0.2t)\left(\frac{y_m}{1200}\right)^5 \tag{2.1}$$

Where:

t = asphalt thickness, mm

T = temperature, °C

y_m = distance measured up from a point 1200 mm below the top of the concrete deck.

For deck slabs above enclosed air-cells between the two webs, a linear gradient is used. A linear distribution increasing from 0°C to 1.5°C is also used over the bottom 200 mm of a section. For superstructures less than 1400 mm in depth, the top and bottom curves are to be superimposed.

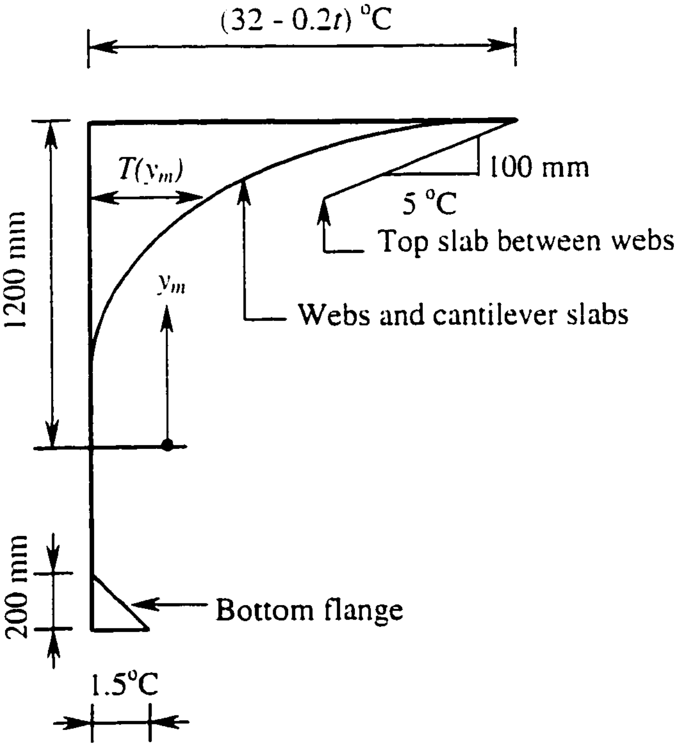

Figure 2.2 Suggested Temperature Distribution for Bridge Box Section (Priestley, 1978)

Podolny (1985) summarized briefly some design temperatures collected from different codes. He reported that most of these recommendations require different shaped gradients. He also noted that the design gradients are influenced by local meteorology and construction practices. In Australia, the design thermal gradients take the shape shown in Figure 2.3a. In France, a linear variation indicated in Figure 2.3b is used with a 10°C gradient used in combination with dead load, shrinkage, and creep. A 5°C gradient is used with all loads including live load and impact. Thermal gradients adopted in England are shown in Figure 2.3c for deck warming and deck cooling. A thickness of surfacing is assumed a 40mm for groups 1 and 2 loading and 100 mm for groups 3 and 4. For other thicknesses of surfacing, the values of T are adjusted according to the British Code of Practice.

2.3 Stresses due to Temperature

Two types of thermal stresses can be induced in the longitudinal direction of statically indeterminate concrete structures: 1) self-equilibrating stresses which develop when the temperature distribution of the cross-section is nonlinear, and 2) continuity stresses which develop because of the restraint provided by the supports to thermal deformations. In statically determinate structures, however, only self-equilibrating stresses develop due to nonlinear temperature distributions.

2.3.1 Self-Equilibrating Stresses

These stresses develop in a reinforced concrete member in two cases:

- when the reinforcement has a coefficient of thermal expansion different from that of concrete, as in the case of concrete members reinforced with FRP reinforcements.

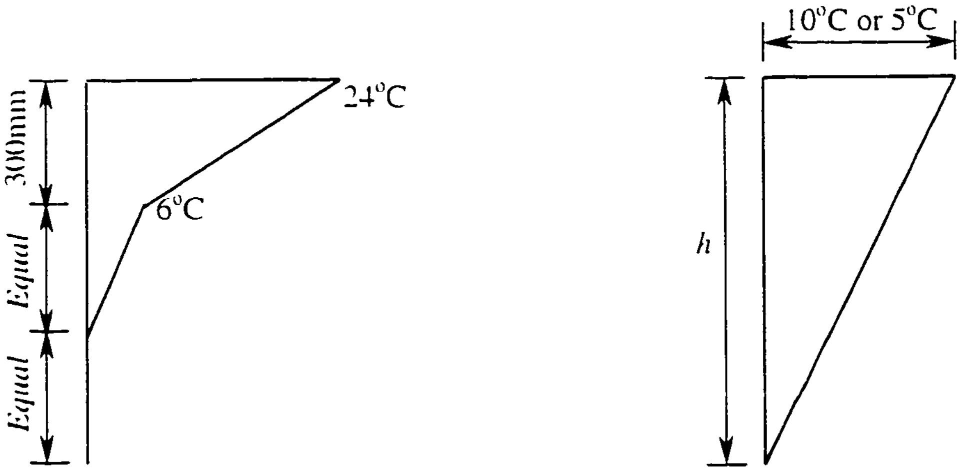

(a) Australia

(b) France

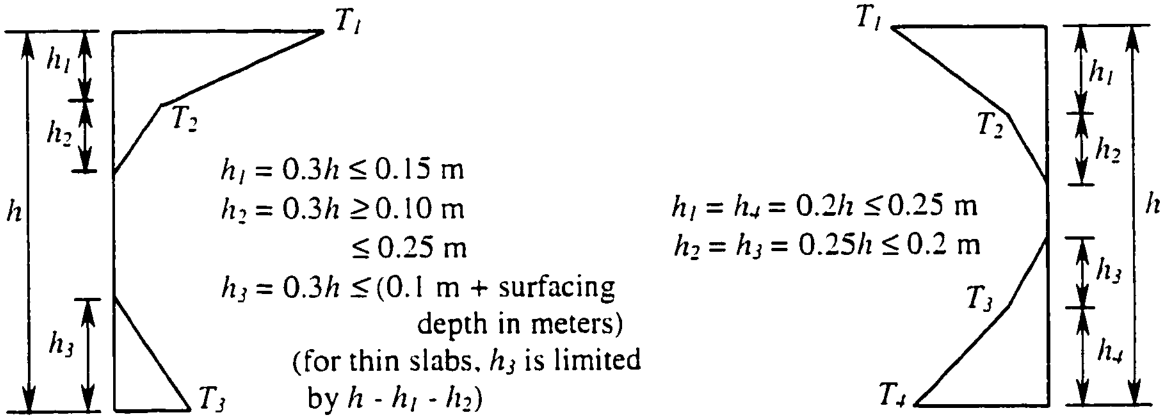

h (m)	T_1 °C	T_2 °C	T_3 °C
≤ 0.2	8.5	3.5	0.5
≤ 0.4	12.0	3.0	1.5
≤ 0.6	13.0	3.0	2.0
≥ 0.8	13.5	3.0	2.5

Deck Warming

h (m)	T_1 °C	T_2 °C	T_3 °C	T_4 °C
≤ 0.2	2.0	0.5	0.5	1.5
≤ 0.4	4.5	1.4	1.0	3.5
≤ 0.6	6.5	1.8	1.5	5.0
≤ 0.8	7.6	1.7	1.5	6.0
≤ 1.0	8.0	1.5	1.5	6.3
≥ 1.5	8.4	0.5	1.0	6.5

Deck Cooling
(Temperature is shown in absolute values)

(c) England

Figure 2.3 Design Thermal Gradient of Various Countries

Carbon fiber reinforced polymer. CFRP. for example. has a longitudinal coefficient of thermal expansion. $\alpha_L = -0.86 \pm 0.09 \times 10^{-6}$ /°C (Sayed-Ahmed and Shrive. 1998b).

- when the distribution of temperature over the cross section is nonlinear.

El-Badry and Abdalla (1998) explained the first case by considering a concrete prism symmetrically reinforced by FRP bars and subjected to uniform rise of temperature. T. They showed that the stresses in the reinforcements σ_f, and in the concrete, σ_c are given by:

$$\sigma_f = (\alpha_c - \alpha_f)\frac{TE_f}{(1+n\rho)} \qquad \text{and} \qquad \sigma_c = -\rho\,\sigma_f \tag{2.2}$$

where $\rho = A_f / A_c$ is the reinforcement ratio, with A_f and A_c being the cross-sectional areas of the reinforcement and the concrete, respectively; $n = E_f/E_c$ is the modular ratio, with E_f and E_c being the moduli of elasticity of the reinforcement and the concrete, respectively; α_f and α_c are the coefficients of thermal expansion of the reinforcement and the concrete, respectively.

The stresses due to nonlinear temperature distribution illustrated in Figure 2.4 arise from the incompatibility between the two following requirements that:

- plane section remain plane, and that
- individual fibers expand by an amount proportional to the local temperature rise.

In order to determine the magnitude of self-equilibrating stresses. a statically determinate prismatic member subjected to a nonlinear temperature shown in Figure 2.4 is considered. This member will undergo linear strain distribution given by:

$$\varepsilon = \varepsilon_0 + \psi y \tag{2.3}$$

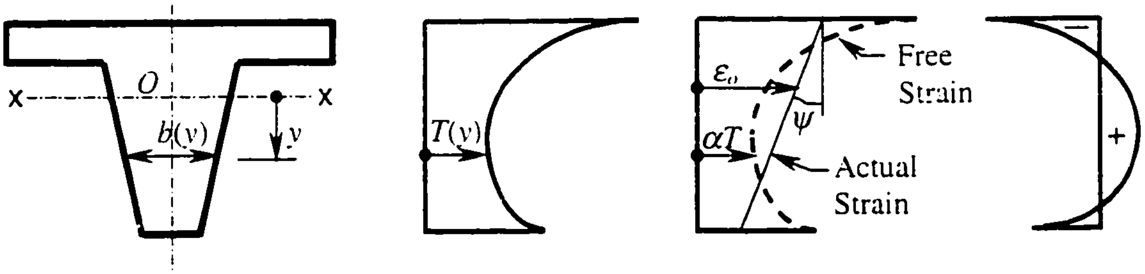

Cross section Temperature distribution Strain Stress

Figure 2.4 Typical Temperature Distribution and Corresponding Strain and Self-Equilibrating Stresses over a Concrete Section

where $$\varepsilon_o = \frac{\alpha_c}{A}\int T(y)b(y)dy \tag{2.4}$$

and $$\psi = \frac{\alpha_c}{I}\int T(y)b(y)dy \tag{2.5}$$

where $T(y)$ is the temperature rise at any fiber whose position is defined by coordinate y measured from the centroidal axis: $\psi = d\varepsilon/dy$ is the curvature when the end rotations of the member are free; ε_o is the strain at the centroid; $b(y)$ is the width of cross section at any fiber; y is the coordinate at any fiber; A and I are the area of the cross section and its moment of inertia about the x-axis.

If the individual fibers of the cross-section were not restrained against free expansion, the distribution of free thermal strains (ε_{free}) takes the same shape of the temperature distribution (dashed line in Figure 2.4). Therefore, the magnitude of the free strain is given by:

$$\varepsilon_{free} = \alpha_c T(y) \tag{2.6}$$

Because of the thermal strain at any fiber cannot occur freely, and also plane sections should remain plane, the final strain profile must be linear as shown in Figure 2.4 and given by:

$$\text{Final strain } \varepsilon_f = \varepsilon - \varepsilon_{free} = \varepsilon_O + \psi y - \alpha_c T(y) \tag{2.7}$$

Therefore, the restraint of thermal expansion produces stress given by:

$$\sigma_s = E_c \varepsilon_f = E_c[\varepsilon_O + \psi y - \alpha_c T(y)] \tag{2.8}$$

This is known as the self-equilibrating stress, because its resultants $N = \int \sigma_s \, dA$ and $M = \int \sigma_s y \, dA$, representing the internal normal force and bending moment, are zero. In the special case when $T(y)$ is linear $\sigma_s = 0$ at all individual fibers.

2.3.2 Continuity Stresses:

These stresses develop in indeterminate structures as a result of the external restraint to member deflections and rotations arising from temperature gradients. For a simply supported member subjected to temperature change that varies linearly over the cross section, the bending moment and reactions are equal to zero. On the other hand, if the rotations at the two ends of this member are prevented, a constant thermal bending moment will develop along the member length as shown in Figure 2.5. The magnitude of this moment and the corresponding stress are given by:

$$M = -EI\psi \qquad \text{and} \qquad \sigma = M\,y/I \tag{2.9}$$

The moment given by Equation (2.9) is just sufficient to eliminate the curvature and the deflection of the member. If the member is subjected to temperature rise with the end translation allowed but the end rotations prevented, the total stresses at any fiber due to the nonlinear temperature distribution are the sum of the self-equilibrating stress and the continuity stress produced by the moment M and are given by:

$$\sigma = \sigma_s + M\,y/I \tag{2.10}$$

The continuity thermal stresses are of greater magnitude than the self-equilibrating thermal stresses and play the major role in causing cracking and structural distress. The magnitude of a thermally induced moment is governed by the effective stiffness of the member. As cracks develop and propagate within the concrete, the member stiffness is reduced, thus causing relaxation in the thermal bending moments. The tensile strength of concrete at the cracked sections is zero. Equations (2.3) and (2.9) can be used to determine the strain and stress distributions taking into account the properties $A_2 = (A_c + n_f A_f)$ and I_2 of a cracked section, with A_c being the area of concrete in compression, while

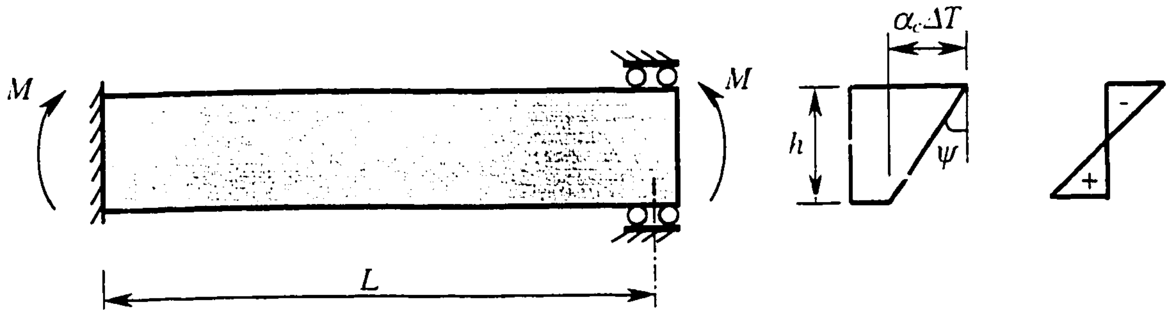

Restrained beam

Free thermal curvature

Stress

Figure 2.5 Continuity Thermal Stresses

the area of concrete in tension is ignored: A_f is the area of the FRP reinforcement: and $n_f = E_f / E_c$.

The stress at any fiber in a statically indeterminate concrete structure reinforced with FRP reinforcements and subjected to nonlinear temperature variation is the sum of the self-equilibrating stresses of Eqs. (2.2) and (2.8) and the continuity stresses of Eq. (2.9) (El-Badry and Abdalla. 1998).

2.4 Temperature Effects on Material Properties of FRP Bars

2.4.1 Coefficient of Thermal Expansion of CFRP Tendon

The coefficient of thermal expansion of the reinforcing bars in concrete members is one of the important parameters that affect the structural behaviors under temperature variations. Internal restraint to thermal deformations can occur when the reinforcement has a coefficient of thermal expansion different from that of concrete. Carbon Fiber Reinforced Polymer, CFRP, for example, has a coefficient of thermal expansion in the longitudinal direction, α_L close to zero while the concrete has $\alpha_c = 10\text{x}10^{-6}$ /°C.

Sayed-Ahmed and Shrive (1998b) conducted an experimental study to determine the coefficient of thermal expansion of CFRP. Leadline rods of 8mm diameter cut to length of 201 mm were used in the experimental program. Three threaded steel bars linked to circular steel plates to form a frame were used with MPE transducers fixed in two holes in the upper plate to determine the deformation of the specimens relative to the frame. The MPE transducers were linked to the data acquisition system. Two 201 mm long Invar bars with 36% Ni, providing a coefficient of thermal expansion of $1.4\text{x}10^{-6}$ /°C, were used to determine the deformation of the frame. The frame with the specimens was placed in an oven and the temperature changed between -23°C and +34°C. In order to establish repeatable readings, the temperature was changed 4 to 10 times for each test.

From their tests, the coefficient of thermal expansion of the CFRP using thermal compatibility is determined form:

$$\alpha_{CFRP} = \alpha_{invar} + [\Delta(MPE)_{invar} / l\,\Delta T] - [\Delta(MPE)_{CFRP} / l\,\Delta T] \qquad (2.11)$$

where, α is the coefficient of thermal expansion, l is the specimen length (201mm), and $\Delta(MPE)$ is registered by the MPE transducer corresponding to a change in temperature equal to ΔT. The subscripts *CFRP* and *Invar* refer to the CFRP specimen and Invar bar, respectively.

Using Equation (2.11), the average coefficient of thermal expansion was determined to be $(-0.86 \pm 0.09) \times 10^{-6}/^{\circ}C$ (average ± standard deviation).

The results obtained from the Equation (2.11) was compared with Daniel and Ishai's value ($-0.9\times10^{-6}/^{\circ}C$). This value was different from the value of $0.68 \times 10^{-6}/^{\circ}C$ obtained by Mitsubishi Kasei Corporation.

2.4.2 Transverse Thermal Expansion of FRP Reinforcement

In recent years, experiments have shown that the transverse coefficient of thermal expansion (CTE) of FRP reinforcing bars is much higher than its longitudinal CTE and can be 5 to 8 times higher than the CTE of concrete. The difference in the transverse thermal expansion may create significant bursting stresses within the concrete under a uniform temperature increase.

Matthys, Schutter and Taerwe (1996) developed a finite element model (FEM) to study the influence of the transverse thermal expansion of FRP reinforcements. Three different cases were considered to study the CTE of Arapree bars (ARAmid PREstressing Element) or strips embedded in concrete. Cases 1 and 2 were used to study the influence of the transverse thermal expansion of AFRP considering different ratios of the concrete cover to bar diameter c/ϕ while a noise barrier post was modeled in case 3. A maximum temperature increase $\Delta T = 60^{\circ}\text{C}$ applied both on the AFRP bar and the concrete was chosen. The following results were reported:

- The critical concrete cover equals 3.5 to 5 times the bar diameter of Arapree depending on the shape of the prestressing element and the concrete strength.
- A small concrete cover can be allowed when higher concrete strengths are used.
- The critical concrete cover to the bar diameter c/ϕ is needed to prevent splitting (crack through the total concrete cover) when:
  - the prestressing force is transferred to the concrete.
  - a uniform temperature $\Delta T = 60^{\circ}\text{C}$ is considered.
- the combined effects of the transverse thermal expansion and the Hoyer effect are very important to be considered when determining the critical concrete cover of FRP prestressing elements.

Abdalla and El-Badry (1997) studied experimentally the effects of high transverse thermal expansion of FRP rebars and explained that the stresses due to high transverse thermal expansion of GFRP induce radial cracking in the concrete around the rebars. These cracks may affect the bond of the reinforcement to the concrete as well as the effectiveness of the concrete cover to the reinforcements. Splitting strength tests were conducted on pre-heated concrete cylinders. A total of 45 concrete cylinders, 76 mm in diameter and 152 mm in height, reinforced with FRP bars of different diameters and materials shown in Table 2.1 were tested after being subjected to a uniform rise in temperature. Figure 2.6 shows the splitting strength of concrete cylinders reinforced with different reinforcing materials. The results are shown for concrete cylinder tested after being subjected to uniform rise of temperature up to 100°C and for cylinders tested at room temperature (20°C). The results of their tests can be summarized as follows:

- Increasing the temperature up to 100°C results in reduction in the splitting strength of all concrete cylinders.
- The highest reduction in the splitting strength was noted in the concrete cylinder reinforced with GFRP (Isorod).
- A crack through the full thickness of the concrete cover was observed at temperature value of 70°C in a cylinder reinforced with 25.4mm diameter GFRP (Isorod) as shown in Figure 2.7.

2.4.3 Tensile Strength of FRP Reinforcement

Most of FRP reinforcing bars are composed of organic binder and fibers that held together with epoxy resin which are considered to be less resistant to heat than steel reinforcement. Carbon fiber reinforced polymers, for example, can be expected to be very sensitive to elevated temperature. In order to estimate the heat resistance of FRP reinforcement, axial tensile strength of several types of FRP bars should be examined under high temperature and ordinary temperature after heating and cooling.

Kumahara et al. (1993) conducted an experimental program on several types of FRP bars. The aim of their study was to investigate the effect of temperature on FRP bars using hot tension test (i.e., tensile strength was tested while the specimen was heated), and postheating tension test (i.e., tensile strength was tested after the temperature of the

Table 2.1 Details of Test Specimens

Reinforcing Materials	Carbon Fiber Reinforced Polymers (CFRP) Rebars				Steel
	Isorod	C-Bar	Leadline	CFCC	
Diameter (mm)	9.5, 15.9, 19.1, 25.4	12, 15	8, 10	5, 15	6, 11, 20
Quantity	3 cylinders for each bar diameter and 6 plain concrete cylinders				
Heating Temperature	Room temperature(about 20°C), 50°C, 100°C				

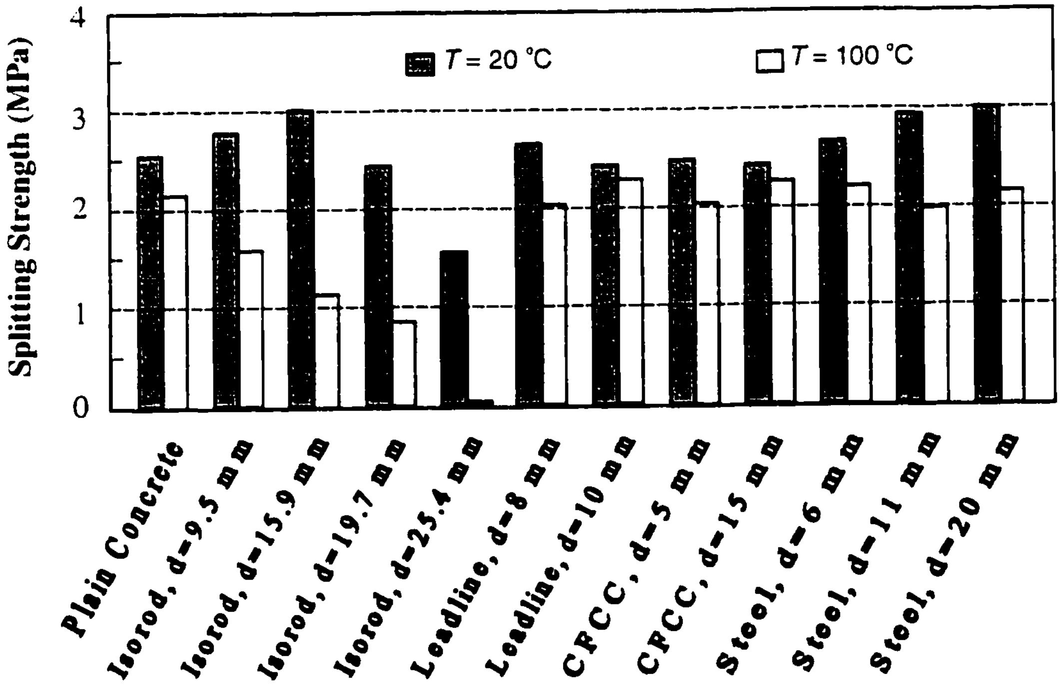

Figure 2.6 Splitting Strength of Cylinders Reinforced with Different Reinforcing Materials (El-Badry and Abdalla, 1998)

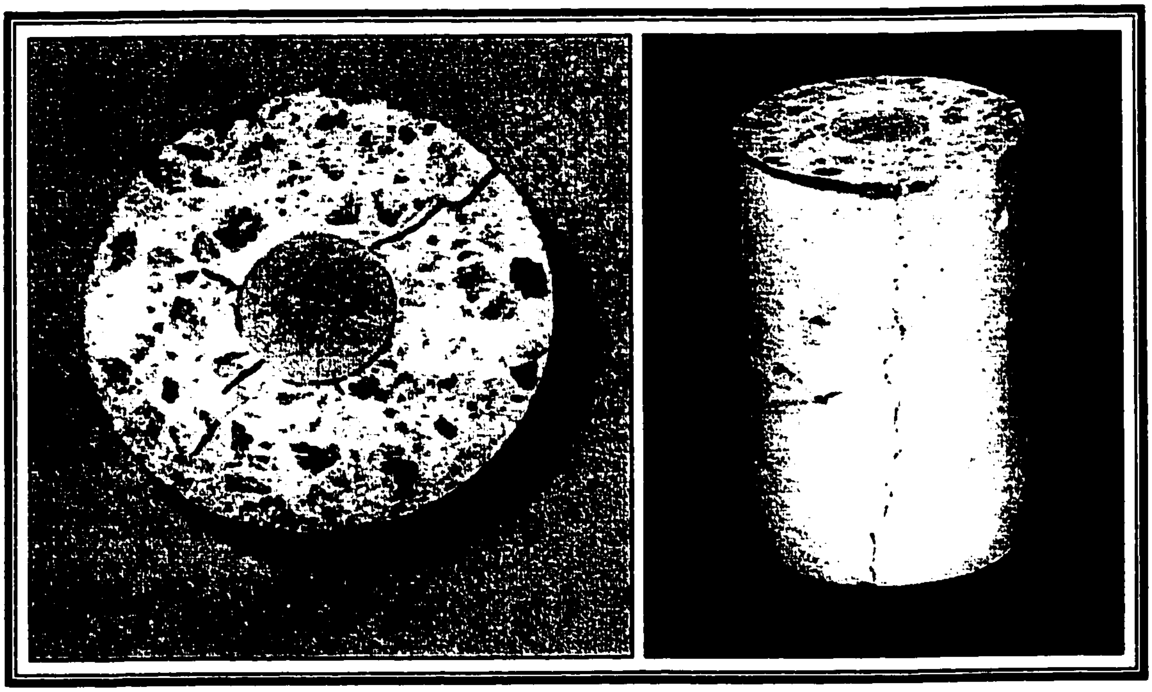

Plan Elevation

Figure 2.7 – Thermal Cracking due to Transverse Expansion of GFRP (El-Badry and Abdalla, 1998)

heated specimen was left to cool to room temperature). Specimens measuring 1000 mm in length were used in the tests. The details of testing specimens are shown in Table 2.2. A 50-ton universal-testing machine equipped with heating device consisting of a heating furnace and a temperature regulator was used for hot tension tests. In these tests, the specimens were heated for one hour at a required temperature shown in Table 2.2 and after that, loads were applied at 2-6 MPa per sec until a fracture occurred in the tested bar. In the postheating tension test, the specimens were heated for one hour and then allowed to cool to room temperature level. The loads were applied at 2-6 MPa per sec until a fracture occurred in the tested bar. The tensile strength of FRP reinforcing bars at high temperature and heating-cooling processes is shown in Tables 2.3 and 2.4.

Some conclusions of Kumahara et al. can be summarized as follows:

- The type of fibers and binders considerably affects the tensile strength of FRP reinforcing bars. For example, the bars whose tensile strength began to decrease at 60°C were made of pitch-based carbon and epoxy resin while PAN-based carbon and cement paste were used in the material whose tensile strength changed only slightly at 250°C or below.
- The tensile strength of continuous fiber bars was affected greatly by the surface configuration of formed bars.
- Very small influence of temperature was noted on Young's modulus at heating temperature of 250°C or below.
- Carbon and Glass fibers have more heat resistance than Aramid fiber.
- In organic binder bars, a little decrease of tensile strength was observed at high temperature and some recovers were note under ordinary temperature after heating

Table 2.2 Details of Test Specimens

Row material fiber	Carbon fiber	Aramid fiber	Glass fiber
Nominal Diameter (mm)	5, 7.5, 8	8	8, 10
Surface Configuration	twisted string, braided, spiral, straight		
Heating temp. (°C)	20, 100, 140, 200, 250, 300, 350, 400		
Quantity	each 2 specimens		

Table 2.3 Characteristics of FRP Bars at High Temperature (Kumahara et al., 1993)

Material	Symbol	Tensile Strength at Indicated Temperature (MPa)		
		60°C	250°C	400°C
Aramid Fiber		Dropped	Young's modulus decreased about 30% compared with that at room temperature	Decrease in tensile strength of more than 80% compared with that at room temperature
Glass Fiber	GR	Decreased at 60°C or above	Decreased about 40%	Decreased about 60%
Glass Fiber	GT		Did not change at 250°C or below*	
Carbon Fiber	Ca7 CaB CiB CiTE	Began to decrease		
Carbon Fiber	CaR CiTC		Changed only slightly at 250°C or below and fell sharply at higher temperature.	

* It was thought to be because the binder used in GT (PPS: thermoplastic resin) is more heat resistant than the one used in GR (vinyl ester).

Table 2.4 Characteristics of FRP Bars after the Heating-Cooling Process (Kumahara et al., 1993)

Material	Tensile Strength at Indicated Temperature (MPa)		
	150°C	250°C	400°C
Aramid Fiber	Recovered to the preheating level at 150°C or below	Recovered to about 50% of the preheating level at 250°C or above	Recovered to about 40% of the preheating level
Carbon and Glass Fibers	Recovered to the preheating level at 150°C or below	Recovered to the preheating level	Recovered little even after their temperature returned to room temperature level

and cooling in comparison with high temperature.

Sayed-Ahmed and Shrive (1998b) conducted an experimental program to examine the effect of temperature on the strength of CFRP tendons. Twenty-four specimens of 8 mm diameter Leadline tendon measuring 1000 mm in length were used in the test. Three specimens were placed in an oven for 24 hours at each of the following temperatures: 100°C, 200°C, 300°C, 400°C, and only one specimen was placed at 500°C. Before testing, all specimens were left for cooling at room temperature. One specimen was also placed at -60°C to determine the effect of extreme freezing. In addition to the above specimens, ten control specimens were tested to determine the average strength of the Leadline at room temperature (about 21°C). All direct tension tests were performed in a standard testing machine with 600 kN capacity. The test results are shown in Table 2.5. The following observations were made after the tests:

- The specimens exposed to temperature of -60°C and 100°C showed no physical changes visible to naked eye.
- Darker color due to evaporation of some of the epoxy resin was observed in the specimens subjected to 200°C and 300°C.
- Most of the epoxy resin evaporated from the tendon placed in the oven at 400°C and some of the fibers along the surface of the rod became loose. In addition, the failure of CFRP tendon occurred due to slippage of the anchorage rather than by failure in the tendon itself.
- The specimen subjected to 500°C could not be gripped due to evaporation of all the epoxy resin and reduction to merely fibers.

Table 2.5 Failure Load and Ultimate Strength of CFRP Specimens Tested in Direct Tension after Exposure to Different Temperatures (Sayed-Ahmed and Shrive, 1998b)

Temperature	No. of Replicas	Failure Load P_f (kN)	P_f (kN) (Av.) ± (S.D.)	Max. Strength[1] (MPa) (Av.) ± (S.D.)
-60°C	1	111.9	111.9	2427.3
Controls (+20°C)	10	105, 109, 108, 108, 107, 113, 109, 122, 113, 105	109.9 ± 5.1	2383.9 ± 110.6
+100 °C	3	114, 110, 98[2]	107.3 ± 8.3	2328.3 ± 180
+200 °C	3	104, 93, 102	99.6 ± 5.9	2160.5 ± 128.0
+300 °C	3	74, 73, 60[2]	69.0 ± 7.8	1496.7 ± 169.1
+400 °C	3	32[3], 26[3], 27[3]	28.3 ± 3.2	613.9 ± 69.4
+500 °C	1	-	-	-

[1] Nominal cross sectional area of an 8 mm diameter CFRP bar is 46.1 mm^2.

[2] Failure occurred in the anchorage zone.

[3] Failure occurred by slippage from the anchorage.

- The CFRP tendons retained about 90%, 63% and 26% of their strength at 200°C, 300°C, and 400°C respectively, compared to 94%, 78% and 52% for steel tendons at the same temperatures.

2.5 Studies on Temperature Effects on Concrete Members Reinforced with FRP Reinforcement

Due to lack of information on the temperature effects on concrete member reinforced with FRP reinforcing bar, very few investigations have been found in the literature.

El-Badry and Abdalla (1998) tested seven concrete slabs having 500mm x 250 mm rectangular cross-section and a length of 3350mm. The reinforcing material, reinforcement ratios, and numbers and diameter of FRP bars are given in Table 2.6. Ten infrared, 250 Watt heat bulbs, arranged in an insulated wooden box were used to produce a temperature heating over a testing length of 2000 mm on one vertical face of the slab, referred to as the hot face, while the opposite face of the slab, referred to as the cool face, was exposed to room temperature. The top and bottom faces of the slab were insulated. The temperature distributions through the cross-section depth (h=250mm) were monitored by five thermocouples at two locations for each slab. Two external thermocouples were also installed at the mid-length on the hot and cool faces of the slab. Four relatively rigid steel arms restrained end rotations produced by the temperature difference between the hot and cool faces. Because of this restraint, a bending moment developed along the tested length causing compression in the hot face and tension on the cool face. Two load cells were attached to the testing frame to measure the end moments ($M = PL$, where P is the absolute value of the axial force measured by each load cell; and

Table 2.6 Details of Test Specimens (El-Badry and Abdalla, 1998)

Beam	Reinforcing Material	On Tension Side				On Compression Side		
		Number of Bars	Nominal Diameter (mm)	A_s (mm^2)	ρ (%)	Number of Bars	Nominal Diameter (mm)	A'_s (mm^2)
G.4	ISOROD	3	12.7	380	0.4	3	9.5	200
G.6	ISOROD	5	12.7	630	0.6	3	9.5	200
G1.5	ISOROD	3	25.4	1520	1.5	3	9.5	200
C.4	C-Bar	4	12.0	450	0.4	2	8.0	100
C.8	C-Bar	5	15.0	880	0.8	3	12.0	340
L.2	Leadline	4	8.0	200	0.2	2	8.0	100
L.4	Leadline	6	10.0	470	0.4	3	8.0	150
S.2	Steel	2	11.3	200	0.2	2	11.3	200
S.4	Steel	2	16.0	400	0.4	2	16.0	400
S.6	Steel	3	16.0	600	0.6	2	16.0	400
S.8	Steel	4	16.0	800	0.8	2	16.0	400
S1.0	Steel	5	16.0	1000	1.0	2	16.0	400

L is the distance between the two axial forces) developed by the temperature gradient.

Before heating, two turnbuckles attached to load cells were used to provide the slab with initial equal end moments acting in the same direction as those produced by the temperature gradients. The reason for applying theses initial moments was to cause the cracking to occur at lower temperature gradient and to eliminate the need of high heating temperature. After that, the deflection at the midspan of the tested length with respect to its ends was recorded to keep the same initial curvature during the test. The temperature increase was applied in 10 to 12 increments for each slab. In each increment, the force, temperature, and strain were recorded after adjusting the initial curvature by using turnbuckles. In the last increment, the temperature difference between the hot and cool face was 120°C. Finally, the results were investigated and compared to results obtained from similar tests using slabs reinforced with conventional steel (Ariyawardena, Ghali and El-Badry, 1997).

The test results showed that the thermal behavior of the tested members reinforced with CFRP (Leadline) was better than those beams reinforced with GFRP and steel. A great reduction in tension stiffness of specimen G.6 reinforced with 0.6% of Isorod was noted at temperature over 80°C. In contrast, the specimens reinforced with Leadline had higher stiffness than those reinforced with steel especially at higher temperature. The deflection due to applied mechanical load in thermally cracked members reinforced with FRP was greater than that in beams reinforced with steel. It was also concluded that the spacing between cracks resulted from temperature difference was almost the same for all types of reinforcements of the same reinforcement ratio. Also, the ultimate strength of the thermally cracked specimens reinforced with CFRP was higher than that for the specimens reinforced with GFRP having the same reinforcement ratio.

Sayed-Ahmed and Shrive (1998b) studied experimentally the thermal effects on masonry walls post-tensioned with CFRP prestressing tendons. Thermal and flexural tests were carried out on diaphragm walls of 2 m and 3 m height. Temperature difference of up to 50°C was induced across the walls. Finite element analyses were also performed to confirm the obtained results using uniform or linear temperature variation across the wall thickness. Three cases were considered:

- Concentric tendon and uniform temperature.
- Eccentric tendon and uniform temperature.
- Eccentric tendon and nonuniform temperature change.

Case I: Concentric Tendon and Uniform Temperature

A diaphragm wall prestressed with concentric tendons is shown in Figure 2.8. The change in the force ΔP after applying the equilibrium and compatibility conditions can be obtained as:

$$\Delta P = \frac{1}{\frac{1}{E_m A_m} + \frac{1}{E_p A_p}} (\alpha_p - \alpha_m)\Delta T \qquad (2.12)$$

where the subscripts m and p refer to masonry and tendon respectively; α_m and α_p are the coefficients of thermal expansion for the masonry and the tendons; A_m is the cross sectional areas of the masonry wall stressed by n tendons and A_p is the cross sectional area of these n tendons; E_m and E_p are the elastic moduli of the masonry and the tendons materials, respectively.

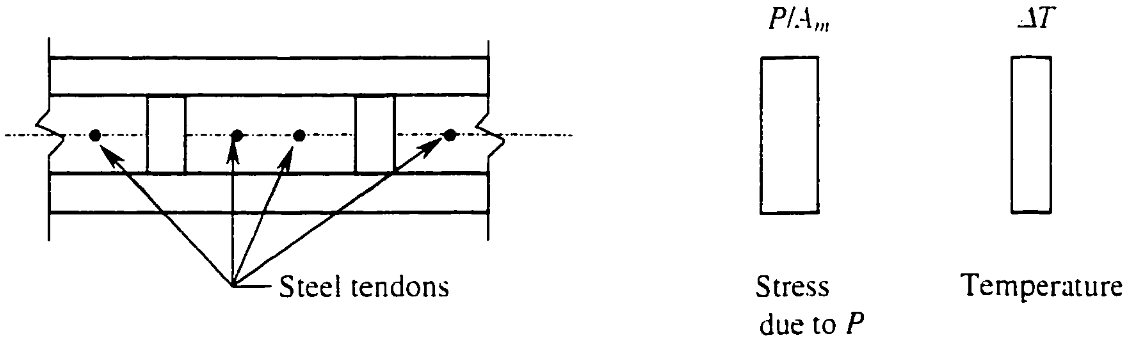

Figure 2.8 Diaphragm Cavity Wall Prestressed with Concentric Tendons and Subjected to Uniform Change of Temperature throughout the Thickness

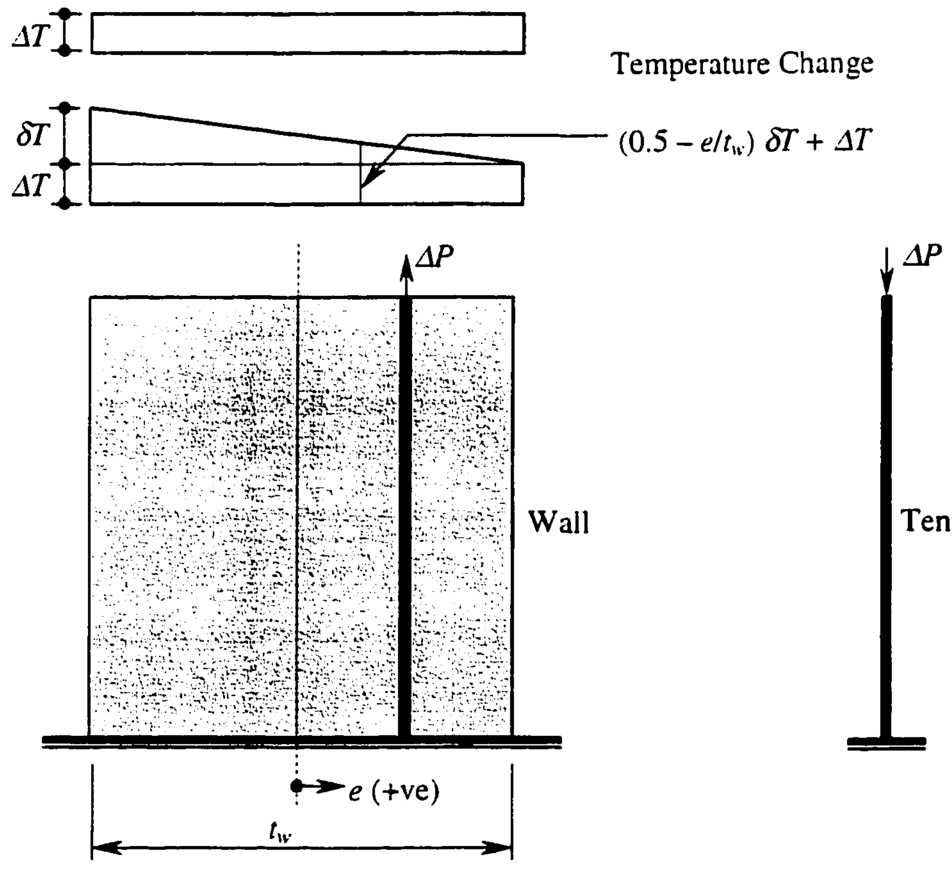

Figure 2.9 Diaphragm Wall prestressed with Eccentric Tendons and Subjected to either Uniform or Linearly Varying Temperature Change through the Thickness.

Steel and CFRP prestressing tendons were used in the experimental program. A diaphragm wall, having A_m = 0.414 m^2 and E_p = 20 GPa, prestressed with 4#25 steel tendons (f_u=1860 MPa, A_p = 0.0022 m^2 and E_p = 200 GPa) up to 70 % of the ultimate tensile strength was used. A second wall was prestressed with Leadline tendons (f_u = 2250 MPa and E_p = 142 GPa) stressed to the same level of prestressing as the steel. The findings of these tests can be summarized as follows:

- In the case where a uniform increase in the temperature of 35°C across the wall was used, a drop in the prestressing force of 58.5 kN was noted in the steel tendons. In contrast, the prestressing force in the CFRP tendon increased to 77.2 kN.
- At a 35°C drop in the temperature, the prestress level of the CFRP tendons decreased by 77.2 kN while steel tendons gained 58.5 kN.

It was thus concluded that because of the small coefficient of thermal expansion of CFRP with respect to concrete, the prestressing force in the Leadline tendons increases with the rise in temperature and decreased with the drop in temperature. The opposite holds true in the case of steel tendons.

Case II: Eccentric Tendon and Uniform Temperature

The analysis of change in strain and prestressing force resulting from eccentric tendon and uniform temperature shown in Figure 2.9 was performed as summarized below:

The change in the strain in both the masonry wall $\Delta\varepsilon_m$ and the prestressing tendons $\Delta\varepsilon_p$ was calculated from:

$$\Delta\varepsilon_p = \alpha_p \Delta T - \frac{\Delta P}{EpAp} \qquad (2.13)$$

$$\Delta\varepsilon_m = \alpha_m \Delta T + \frac{\Delta P}{E_m A_m} + \frac{\Delta P e^2}{E_m I_m} \tag{2.14}$$

where e is the tendon eccentricity measured from the centroid of the wall cross section; I_m is the second moment of area of the wall cross section.

The change in prestressing force ΔP after imposing strain compatibility between the tendon and the masonry is given by:

$$\Delta P = \frac{(\alpha_s - \alpha_m)\Delta T}{\left(\frac{1}{E_m A_m} + \frac{1}{E_p A_p}\right) + \frac{e^2}{E_m I_m}} \tag{2.15}$$

Case III: Eccentric Tendon and Nonuniform Temperature Change

A statically determinate system subjected to a linear variation of temperature across the wall was considered in this case. A uniform temperature of ΔT and a linearly varying change from zero to a maximum of δT was assumed. The uniform temperature causes a change in prestressing, $\Delta P_{\Delta T}$ defined by Equation (2.15). Using Equations (2.13) and (2.14), the change in prestress $\Delta P_{\delta T}$ becomes:

$$\Delta\varepsilon_p = \alpha_p \delta T \frac{(t_w/2 - e)}{t_w} - \frac{\Delta P}{E_p A_p} \tag{2.16}$$

$$\Delta\varepsilon_m = \alpha_m \delta T \frac{(t_w/2 - e)}{t_w} + \frac{\Delta P}{E_m A_m} + \frac{\Delta P e^2}{E_m I_m} \tag{2.17}$$

Strain compatibility between the tendon and the masonry leads to:

$$\Delta P = \Delta P_{\Delta T} + \Delta P_{\delta T} \tag{2.18}$$

$$\Delta P = \frac{\Delta T + [0.5 - (e/t)]}{\left(\frac{1}{E_m A_m} + \frac{1}{E_p A_p}\right) + \frac{e^2}{E_m I_m}} (\alpha_p - \alpha_m) \tag{2.19}$$

where e is positive when measured from the wall center line away from δT as shown in Figure 2.9.

The test results indicated that when uniform temperature distribution through the wall thickness was used, the eccentricity of the tendon has very little effect on the prestressing force. On the other hand, the eccentricity leads to a significant change if the temperature variation throughout the wall thickness was considered.

2.6 Summary

It can be seen from the above literature review that many factors can significantly affect the thermal behavior of concrete member reinforced with FRP reinforcements. Researchers have shown that temperature gradient is one of the important parameters that must be considered in the design calculations. They have also concluded that the magnitude of stress, crack spacing, crack widths and thermally-induced moment due to temperature effects depend upon the type and amount of reinforcement used.

Temperature variations have a major effect on the mechanical properties of FRP reinforcement. The transverse thermal expansion of GFRP bars, for example, may produce radial cracking in the concrete member under high temperature. In addition to the above factors, the following variables must be considered: the rate of temperature increase or decrease, the magnitude of initial temperature, the concrete thickness and the degree of restraint against deformation.

The experimental program of the present investigation into thermal behavior of concrete members reinforced or prestressed with FRP rebars under the effects of temperature gradients is described in the following chapter. The results of this experimental work are presented and discussed in chapter 4.

Chapter 3

Experimental Program

3.1 General

The experimental program conducted in the Structures Laboratory of Concordia University was planned to study the thermal behavior of concrete beams reinforced or prestressed with Fiber Reinforced Plastic (FRP) reinforcements. The primary objectives of this program were to:

1. examine the effects of thermal characteristics of different types of FRP reinforcement on the development of thermal stresses and on the control of thermal cracking in concrete members.
2. investigate the flexural behavior of thermally-cracked FRP reinforced concrete beams, in terms of crack pattern, spacing and widths of crack and deflection after cracking under thermal loading and mechanical moment as well as the different modes of failure under mechanical load.
3. study the effects of the reinforcement ratio (ρ) and the level of prestressing at the extreme tension fiber on the behavior of concrete members under temperature variations, particularly on the control of thermal cracking.

The experimental program consisted of testing a total of eleven concrete beams under the effects of temperature gradients across the depth, while restraining the end rotations of the beams, and thus, producing a constant thermal moment over the tested length of the beams. All beams had the same cross section dimensions. b = 500 mm and h = 250 mm. The eleven beams were divided into two series: Series A – Reinforced Concrete (RC), and Series B – Partially Prestressed Concrete (PPC). Series A consisted of six beams, each of length L = 3350 mm. This series was in turn subdivided into two groups, A1 and A2. Group A1 consisted of three beams reinforced with CFRP Leadline rods of different amounts. Three ratios, 0.6%, 0.8% and 1.0% were used. The results of testing these three beams along with those obtained from two specimens reinforced with 0.2% and 0.4% Leadline and tested by El-Badry and Abdalla (1998) provide a good insight into the effects of the reinforcement ratio (varying from 0.2% to 1.0% in this case) on the behavior of CFRP reinforced concrete members under thermal gradients. Group A2 consisted of three beams reinforced with GFRP grid type reinforcement known as NEFMAC. The three beams differed in terms of location of the NEFMAC grid within the cross section. One beam was reinforced with the grid placed near the extreme tension fiber of the cross section. The second beam had the grid placed at mid-depth of the cross section. In the third beam, two grids were used, one near the extreme tension fiber and one near the extreme compression fiber. Figures 3.1 to 3.3 give more details on the beams of series A.

The PPC Series B consisted of a total of five beams having the same concrete section dimensions of beams in Series A. The length of each beam in Series B was 4500 mm. This series included two groups, B1 and B2. Group B1 consisted of two beams pretensioned with CFRP Leadline rods whereas Group B2 included two beams post-tensioned with unbonded Leadline rods. One beam in each group had the prestressing rod at its center (i.e. concentric prestressing), whereas the second beam in each group had the prestressing rod at eccentricity of 50 mm from the cross-section centroid (i.e. eccentric prestressing). The fifth beam in Series B was post-tensioned with unbonded concentric conventional steel strand. The prestressing force in all five beams was of such magnitude that produced an average compressive stress of 0.5MPa in the concrete section. Figures 3.4 to 3.6 give more details on the beams of Series B.

All beams were tested in three steps: 1) under the effects of temperature gradients; 2) under the effects of constant mechanical moments; 3) under the effects of mechanical loads applied at the third points of the beam tested length. The results of the eleven beams were compared to those obtained from the tests conducted by Ariyawardena (1993) on similar beams reinforced or prestressed with conventional steel. A comparison is also made with the results obtained from analytical equations proposed by El-Badry and Ghali (1995) to predict the progressive reduction in stiffness as cracks develop under the effects of increasing the temperature gradient in reinforced concrete beams.

3.2 Design of Test Specimens

3.2.1 Geometry of Concrete Beams

The design of the test beams was controlled by flexural strength requirements in accordance with CSA Standard A23.3-94. The cross section of the test beams was selected a rectangular having 500 mm width and 250 mm depth. The purpose of using such small depth was to achieve stabilization of temperature readings across the depth of the tested beam in a relatively short time during the test.

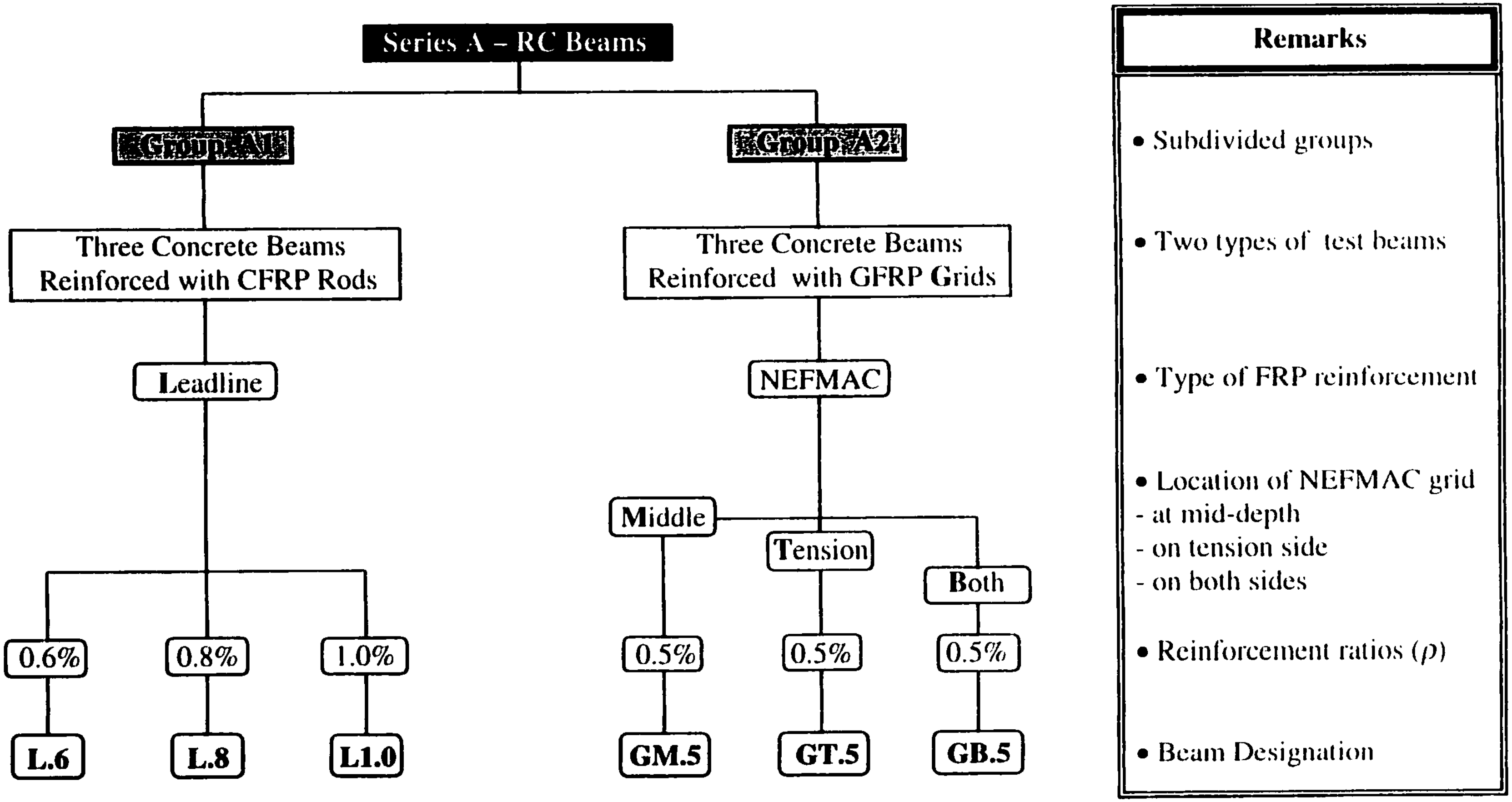

Figure 3.1 Experimental Program for Series A

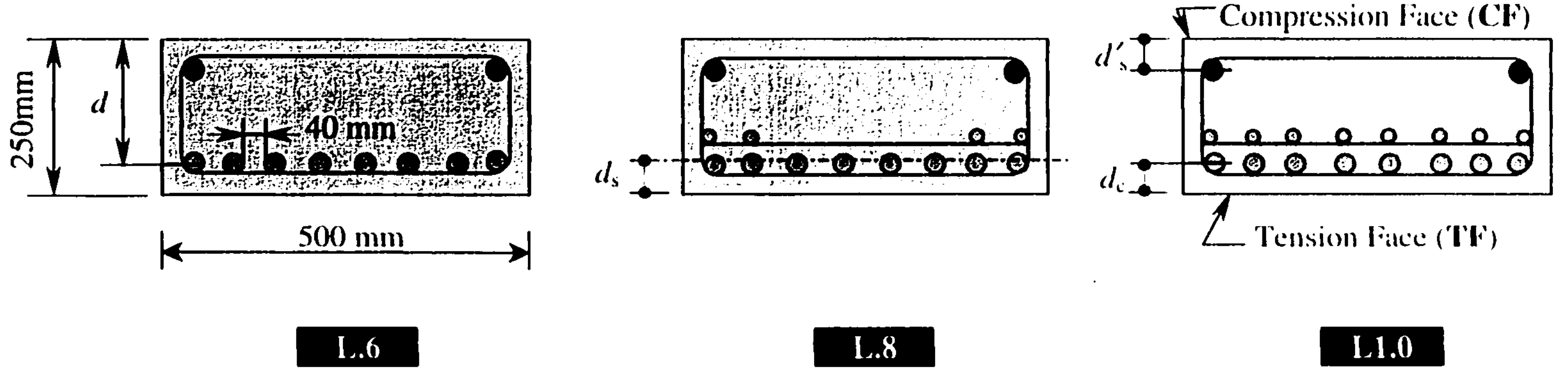

Side name	CF	TF		CF	TF		CF	TF	
Leadline rods		8φ10			8φ10	4φ8		8φ10	8φ8
Steel bars	2#10M			2#10M			2#10M		
Steel stirrups	At the two ends only			At the two ends only			At the two ends only		
d_c	50 mm			50 mm			50 mm		
d'_s	50 mm			50 mm			50 mm		
d_s	50 mm			56 mm			60 mm		
d	200 mm			194 mm			190 mm		

d_c = thickness of concrete cover measured from centroid of the bottom layer of tension reinforcement
d'_s = thickness of concrete cover measured from centroid of compression reinforcement
d_s = thickness of concrete cover measured from centroid of tension reinforcement
d = distance from compression face to centroid of tension reinforcement

Figure 3.2 Reinforcement Details for Beams Reinforced with Leadline (Group A1)

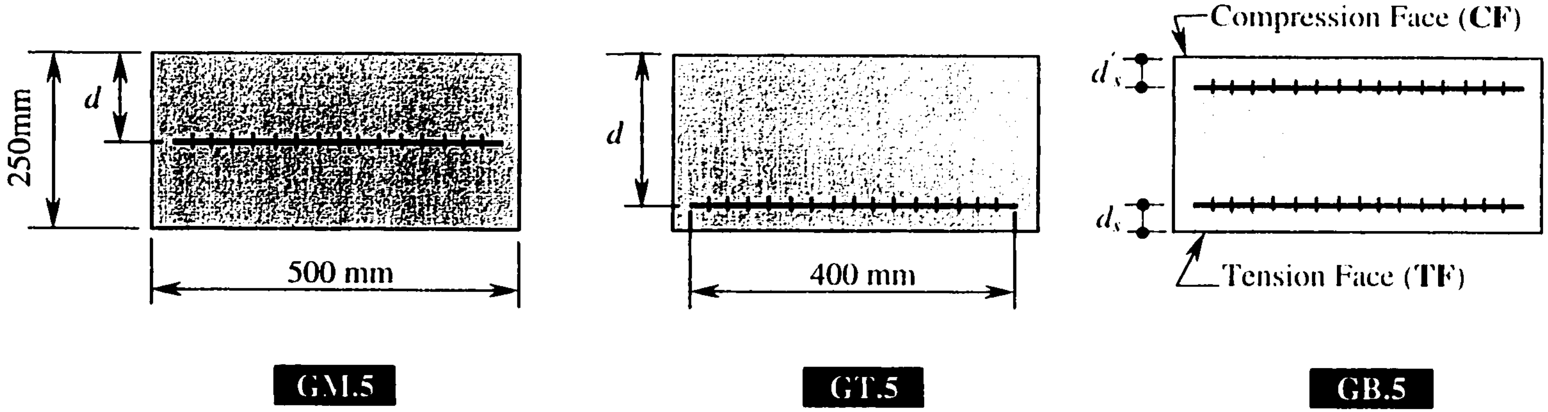

NEFMAC	400 mm x 3000 mm	400 mm x 3000 mm	400 mm x 3000 mm
Location	mid-depth of cross section	near tension face	on both sides
d_s		50 mm	50 mm
d'_s			50 mm
d	125 mm	200 mm	200 mm

Figure 3.3 Reinforcement Details for Beams Reinforced with NEFMAC (Group A2)

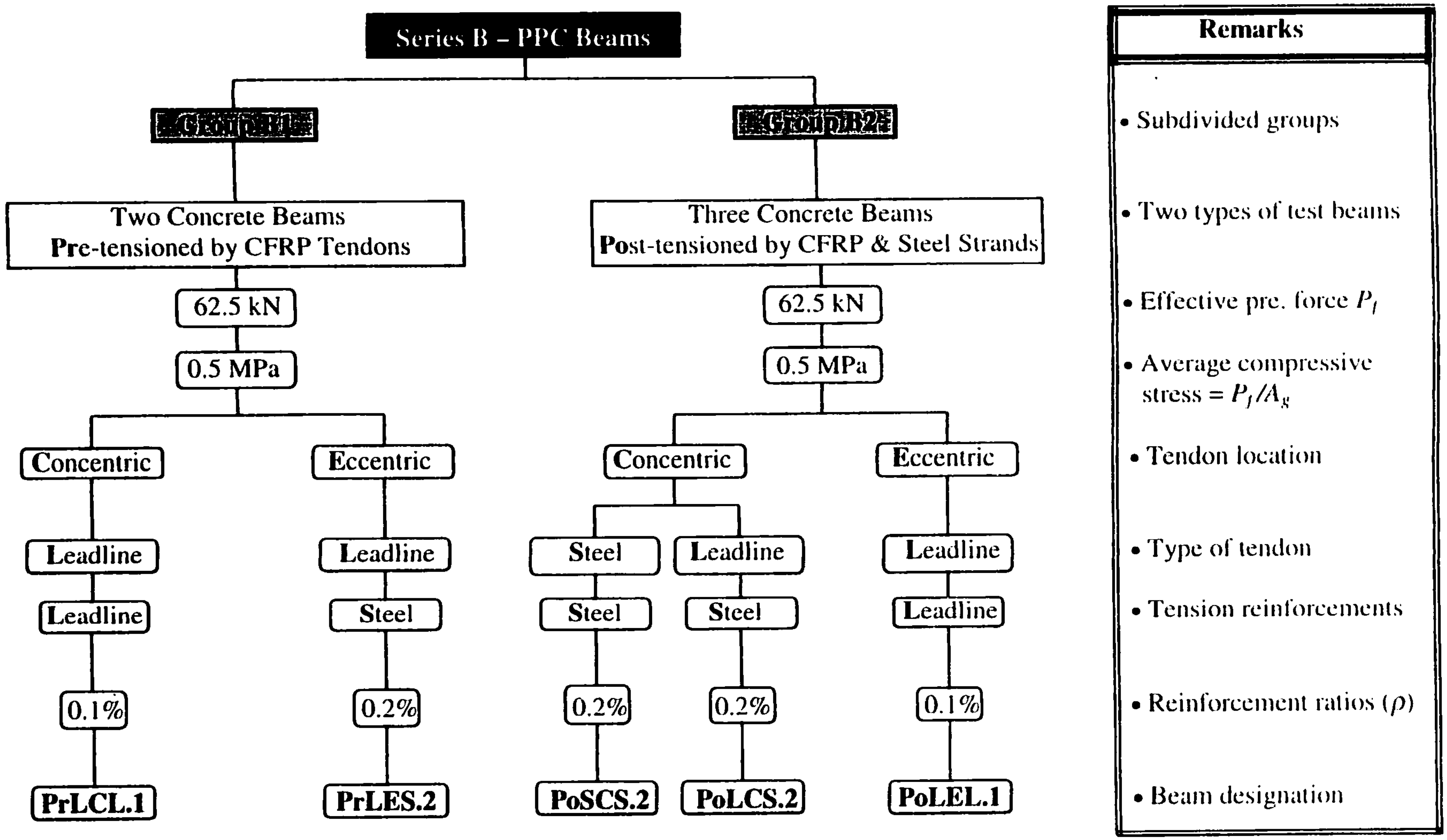

Figure 3.4 Experimental Program for Series B

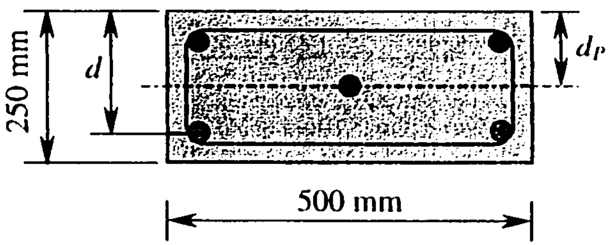

PrLCL.1

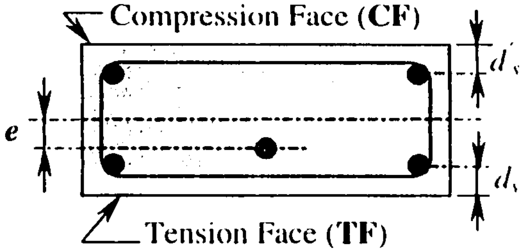

PrLES.2

Side name	CF	TF	CF	TF
Leadline rods		2ϕ8		
Steel bars	2#10M		2#10M	2#10M
Prestressing tendon	1- 8 mm Leadline		1 – 8 mm Leadline	
Tendon type	Concentric		Eccentric	
Steel stirrups	3/8in. @ 400 mm c/c		3/8in. @ 400 mm c/c	
d_s	50 mm		50 mm	
d'_s	50 mm		50 mm	
d_p	125 mm		175 mm	
d	200 mm		200 mm	
e	0		50 mm	

Figure 3.5 Reinforcement Details for Beams Partially Pretensioned by Leadline (Group B1)

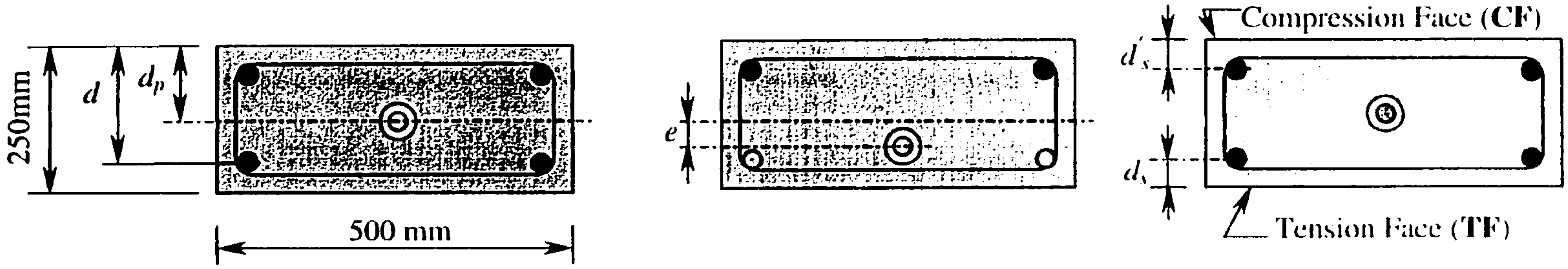

	PoLCS.2		PoLEL.1		PoSCS.2	
Side name	CF	TF	CF	TF	CF	TF
Leadline rods				2φ8		
Steel bars	2#10M	2#10M	2#10M		2#10M	2#10M
Prestressing tendon	1 – 8mm Leadline		1 – 8mm Leadline		1–9.5mm steel strand	
Tendon type	Concentric		Eccentric		Concentric	
Steel stirrups	3/8in. @ 400 mm c/c		3/8in. @ 400 mm c/c		At the two ends only	
d_s	50 mm		50 mm		50 mm	
d'_s	50 mm		50 mm		50 mm	
d	200 mm		200 mm		200 mm	
d_p	125 mm		175 mm		125 mm	
e	0		50 mm		0	

Figure 3.6 Reinforcement Details for Beams Partially Post-tensioned by Leadline and Steel Strands (Group B2)

The overall lengths of the beams were chosen 3350 mm and 4500 mm for the RC and PPC beams, respectively. The longer length used in the prestressed beams of PPC series was to allow for the transfer length of the pretensioning tendons as specified in C 12.9.1 of CSA Standard A23.3-94 and to minimizing the effect of anchor set losses in the post-tensioned tendons. Figures 3.2, 3.3, 3.5 and 3.6 show the reinforcement details of all the beams in the RC and PPC series.

3.2.2 Selection of Reinforcement

Two types of FRP reinforcements were used in the RC series A, namely, Leadline rods and NEFMAC-Grid type reinforcements as shown in Figures 3.7 and 3.8. The beams in group A1 were reinforced with different amounts of 8mm and 10mm diameter Leadline rods. Two deformed steel bars of size 10M with 11.3mm nominal diameter were also used as compression reinforcements in all test beams of group A1. The NEFMAC Grid reinforcement was chosen to reinforce beams of group A2.

In PPC series, two types of prestressing cables were used, namely, Leadline rods and steel strands. The Leadline rods of 8mm nominal diameter were used in both the pretensioned and the post-tensioned beams. A seven-wire steel strand of 9.25mm nominal diameter was provided only in one post-tensioned beam denoted as PoSCS.2. In addition, the beams were provided with sufficient Leadline rods and steel bars placed on tension and compression sides of the beam cross section. Both concentric and eccentric tendons were used to study their effects on the cracking behavior of the PPC beams.

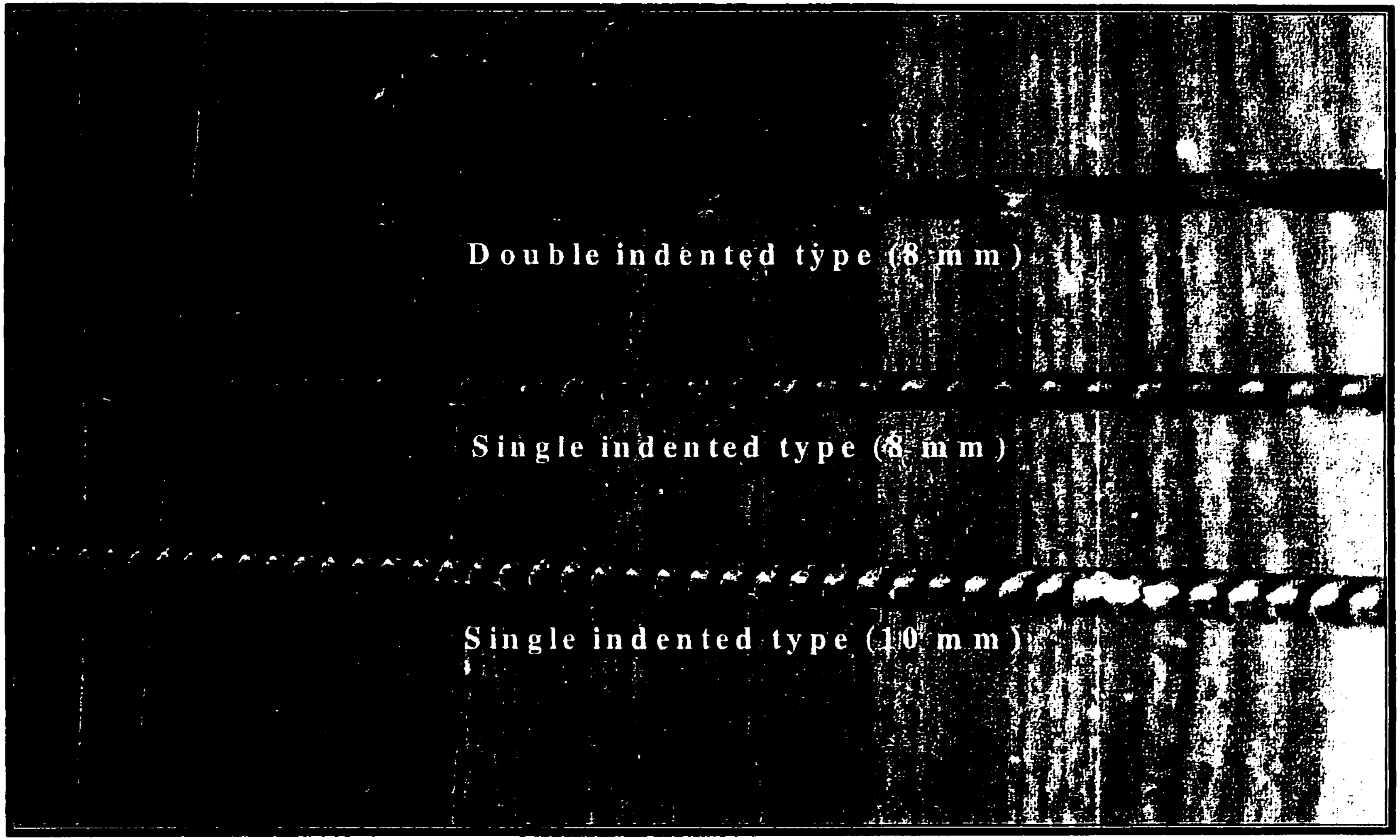

Figure 3.7 Different Types of Leadline Rods

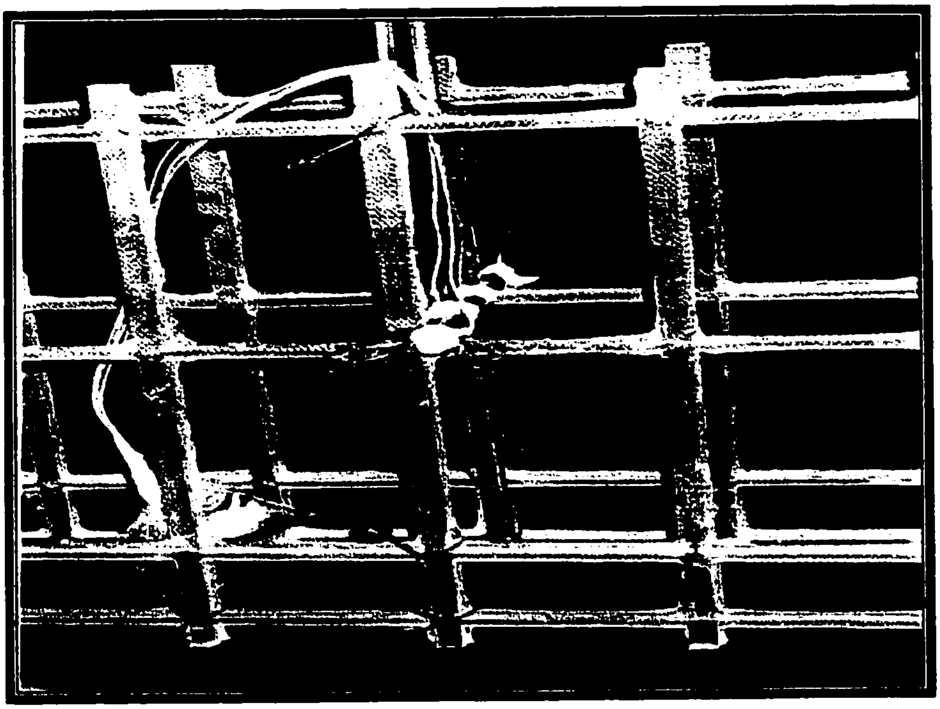

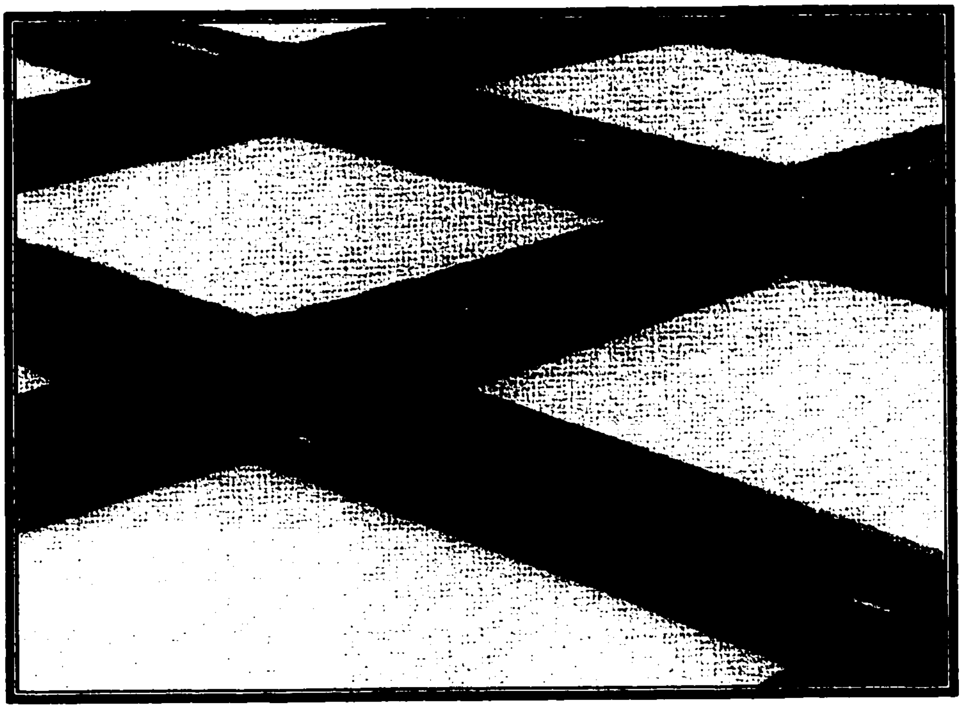

Intersections of a Grid

Figure 3.8 NEFMAC Grid Reinforcement

Table 3.1 provides description of the eleven test beams including beam designation, beam dimensions, types, numbers, and areas of tension and compression and prestressing reinforcements.

3.3 Test Set-up and Instrumentation

Two types of tests were performed:

1. Thermal loading test
2. Mechanical loading test of thermally cracked specimens

The purpose of the first test was to determine the flexural behavior of the concrete beams in terms of thermal stress development and crack formation under the effects of temperature gradient through the cross-section depth of the beams. The objective of the second type of test was to examine the load-deflection behavior of thermally cracked beams both at service load levels and up to ultimate failure. The set-ups used for the two tests are described below.

3.3.1 Set-up for Thermal Loading Test

The set-up used for this test was the same that was used by Ariyawardena (1993) and El-Badry and Abdalla (1998). Figures 3.9 and 3.10 show a schematic view and a photograph of the test set-up, respectively. During the test, the weight of the concrete specimen was supported on a roller bearing at point *A*, which allowed free expansion of the beam, and on a hinged bearing at point *B*. Details of the supports are shown in Figure 3.11. The distance between the two supports was 2500 mm. Teflon plates were placed between the bottom surface of the concrete beam and the top of each bearing to facilitate the rotation of the beam without any restraint caused by friction.

Table 3.1 Reinforcement Details in Test Beams

Beam Dimension	Beam Designation	Group Name	On Tension Side					On Compression Side			
			Reinforcing Material	Number of Bars	Nominal Diameter (mm)	A_s mm^2	ρ (%)	Reinforcing Material	Number of Bars	Nominal Diameter (mm)	A'_s mm^2
$b = 0.5$ m $h = .25$ m $L = 3.35$ m	L.6	A1	Leadline	8	10	600	0.6	Steel	2	11.3	200
	L.8	A1	Leadline	8	10	600	0.6	Steel	2	11.3	200
			Leadline	4	8	200	0.2				
	L1.0	A1	Leadline	8	10	600	0.6	Steel	2	11.3	200
			Leadline	8	8	400	0.4				

Beam Dimension	Beam Designation	Group Name	ρ (%)	On Tension Side	On Compression Side	At Mid-depth
$b = 0.5$ m $h = .25$ m $L = 3.35$ m	GM.5	A2	0.5			NEFMAC Grid (400 mm x 3000 mm)
	GT.5	A2	0.5	NEFMAC Grid (400 mm x 3000 mm)		
	GB.5	A2	0.5	NEFMAC Grid (400 mm x 3000 mm)	NEFMAC Grid (400 mm x 3000 mm)	

Beam Dimension	Beam Designation	Group Name	On Tension Side					On Compression Side			
			Reinforcing Material	Number of Bars	Nominal Diameter (mm)	A_s mm^2	ρ (%)	Reinforcing Material	Number of Bars	Nominal Diameter (mm)	A'_s mm^2
$b = 0.5$ m $h = .25$ m $L = 4.5$ m	PrLCL.1	B1	Leadline	2	8	100	0.1	Steel	2	11.3	200
	PrLES.2	B1	Steel	2	11.3	200	0.2	Steel	2	11.3	200
	PoLCS.2	B2	Steel	2	11.3	200	0.2	Steel	2	11.3	200
	PoLEL.1	B2	Leadline	2	8	100	0.1	Steel	2	11.3	200
	PoSCS.2	B2	Steel	2	11.3	200	0.2	Steel	2	11.3	200

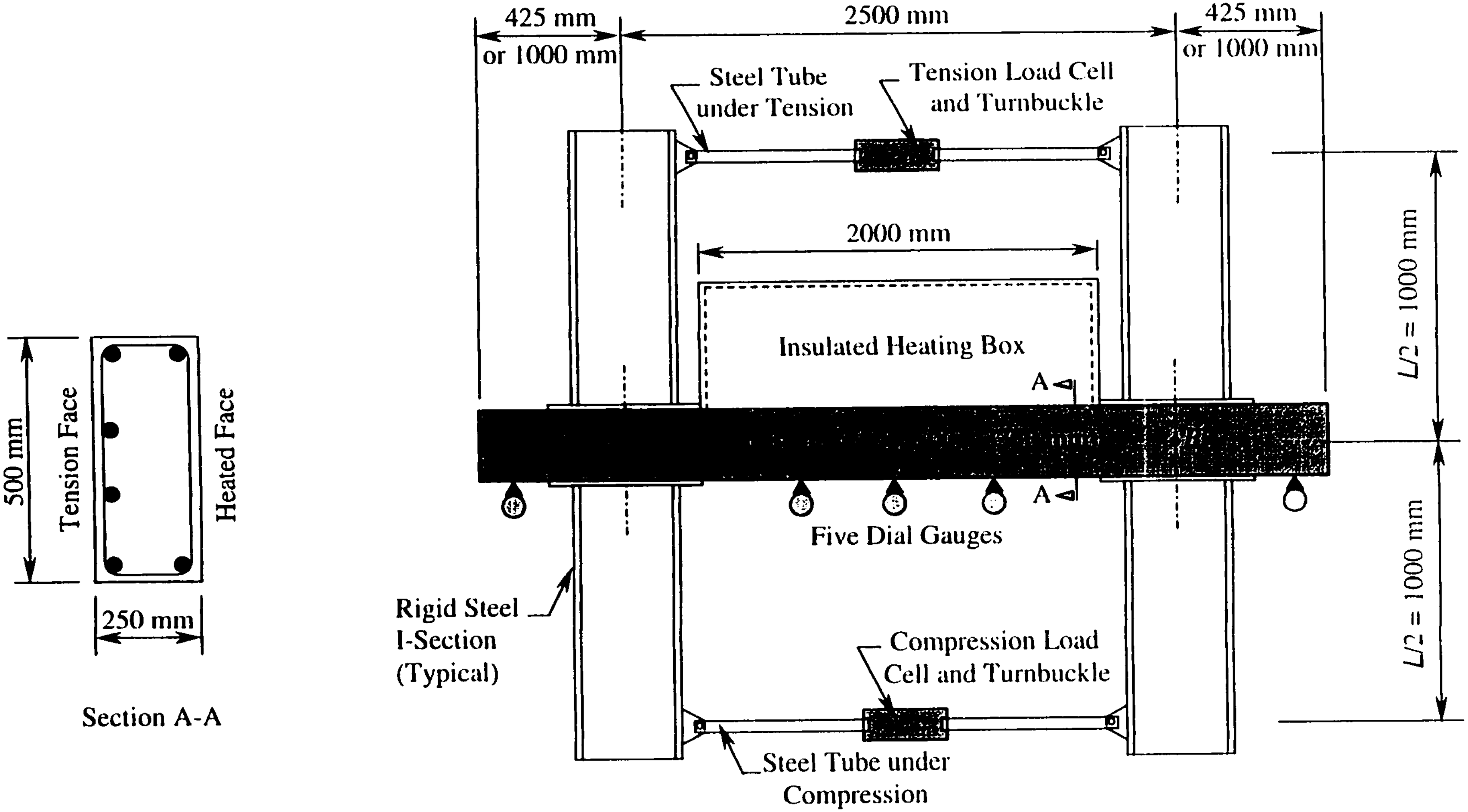

Section A-A

Plan View

Figure 3.9 Schematic View of Thermal Loading Test Set-up

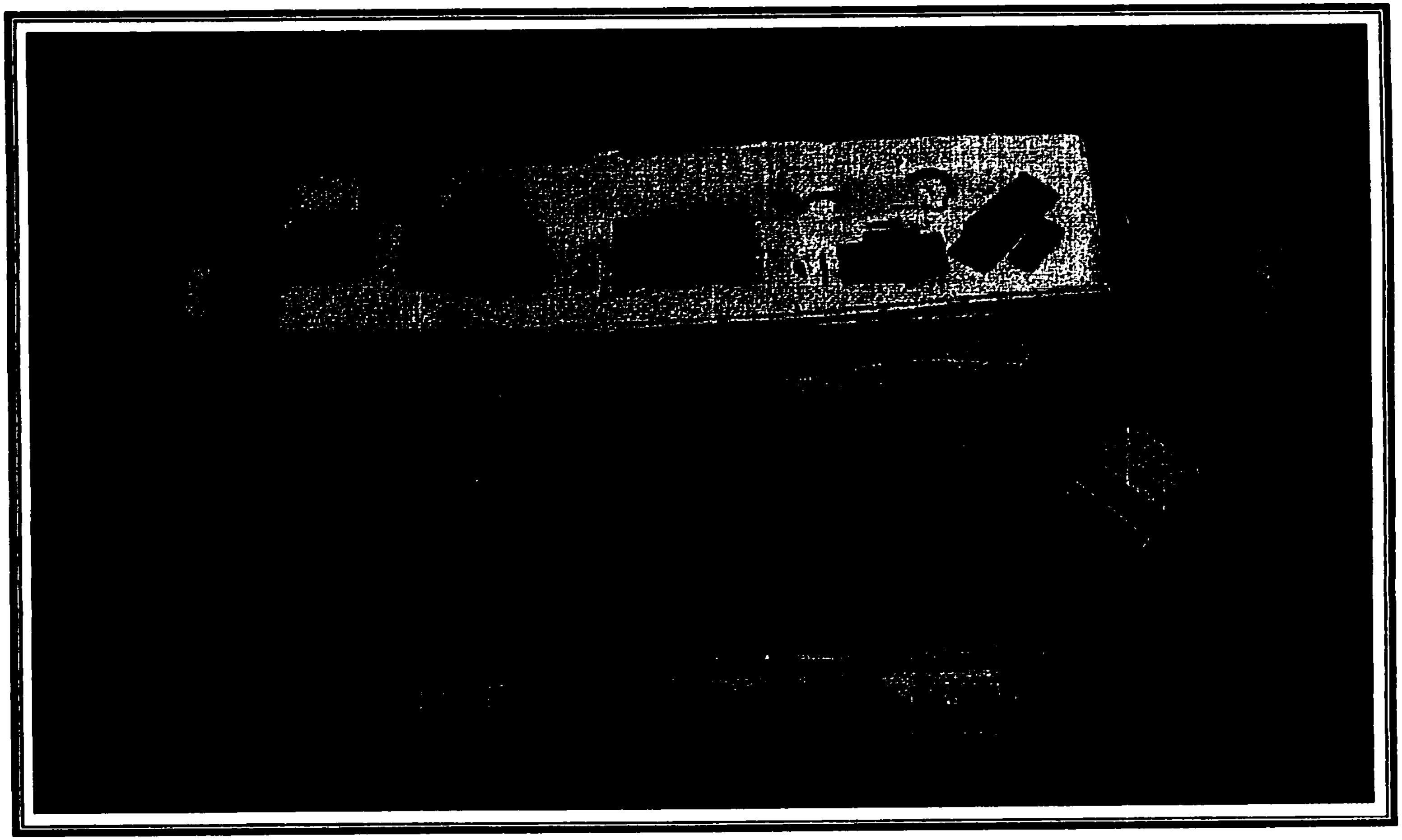

Figure 3.10 Test Set-up

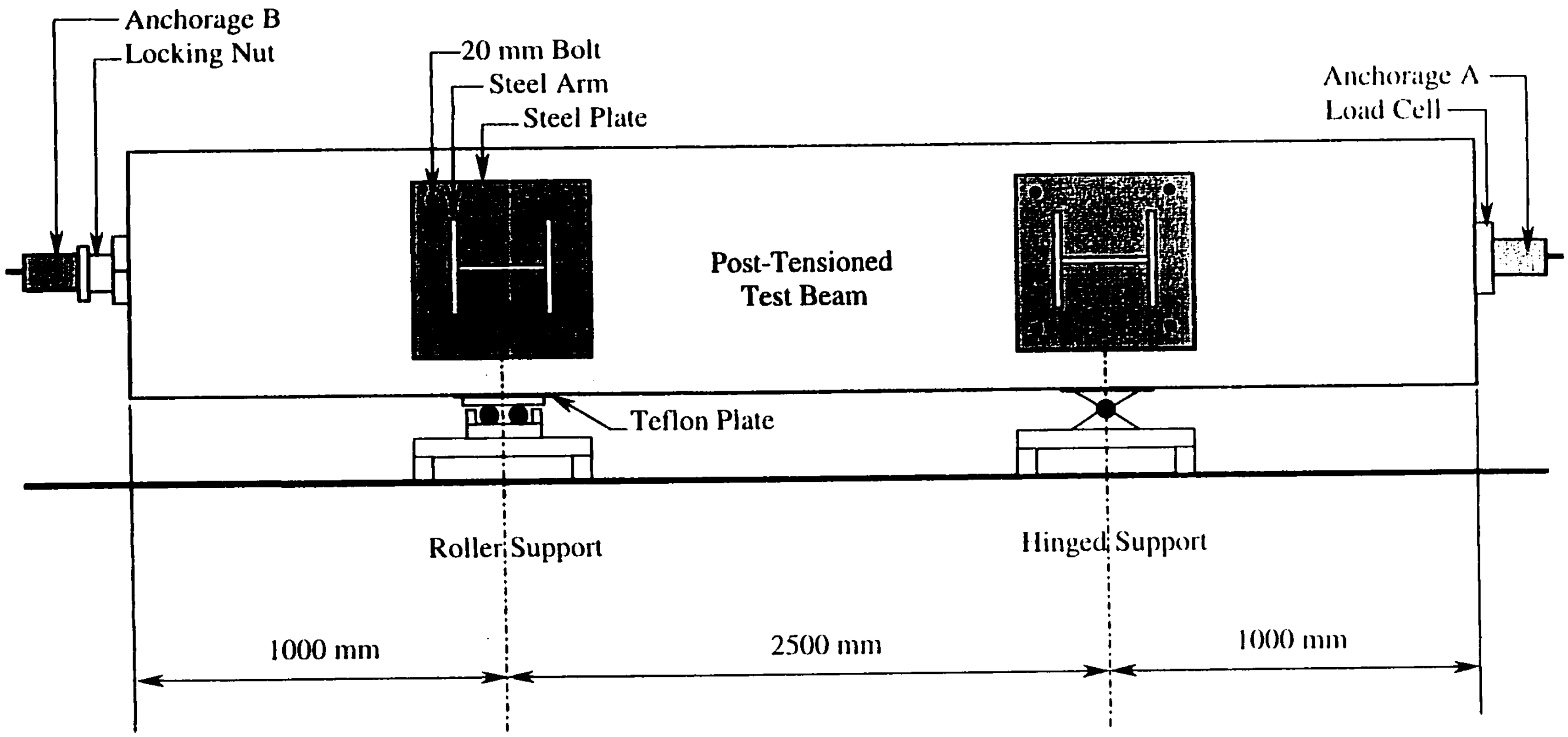

Figure 3.11 Details of Roller and Hinged Supports

For convenience and to eliminate the effect of self weight, the cross section was rotated 90° as shown in Figure 3.9. The test frame shown in the figures consists of four relatively rigid steel I beam section (steel arms) each having a cross-section depth, d = 354 mm, flange width, b = 205 mm and rigidity, $EI = 45 \times 10^6$ N-m. The steel arms were used to prevent the end rotations caused by the temperature difference between the two faces of the concrete beam. Four steel plates, each 500 x 250 x 20 mm, welded to the steel arms were connected to the concrete specimen using eight steel rods of 20 mm diameter with four rods at each end of the test beam. Two steel tubes of 60.3 mm diameter, 10 mm thickness and 2100 mm length provided with two load cells at their center were connected to the steel arms. The load cells shown in Figure 3.12 were employed to measure the end moments developed by temperature gradients ($M=PL$, where P is the axial force measured by each load cell, and L is the distance between the two axial forces created in the load cells).

To allow axial force only in the steel tubes, the joint that connects the steel arms with the steel tubes was designed as pin connection. The axial forces created in each load cell were monitored during the test by means of two indicators shown in Figure 3.12. The center line distance between the steel tube and the beam was kept at 1.0 m so that the two indicators displayed the forces in the load cells in Newton which directly represented the thermal moment in N-m. Two turnbuckles attached to the load cells as shown in Figure 3.12 were used to apply initial moments M_i to the test beam and to adjust the developing force due to temperature effects during the experiment. More details on the testing procedure are given in Section 3.7.

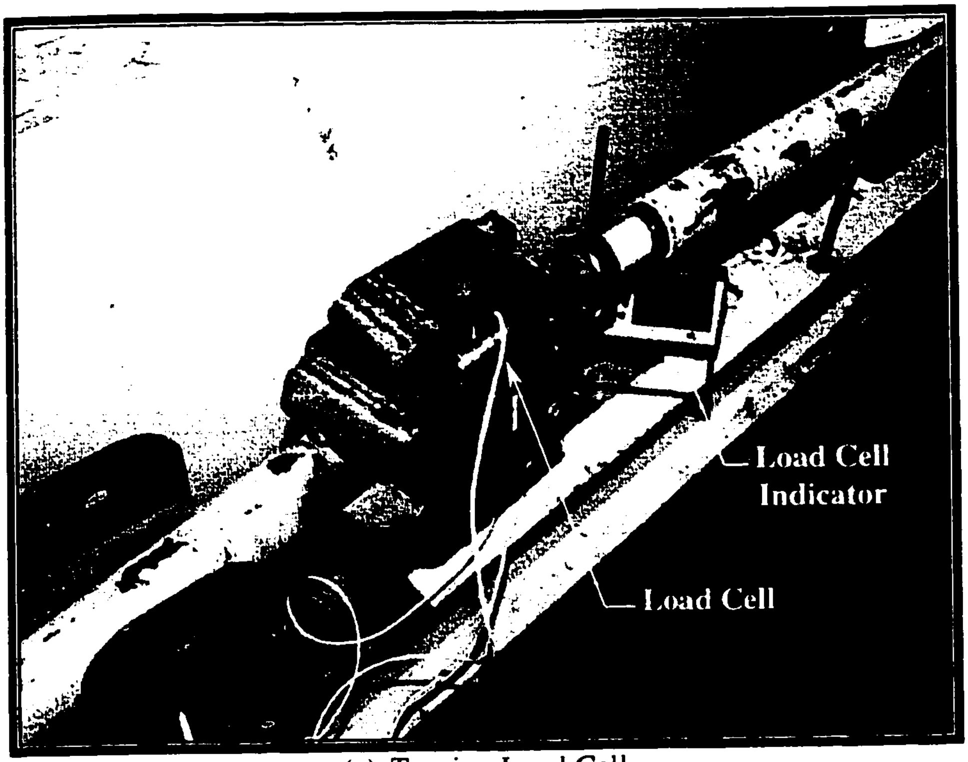

(a) Tension Load Cell

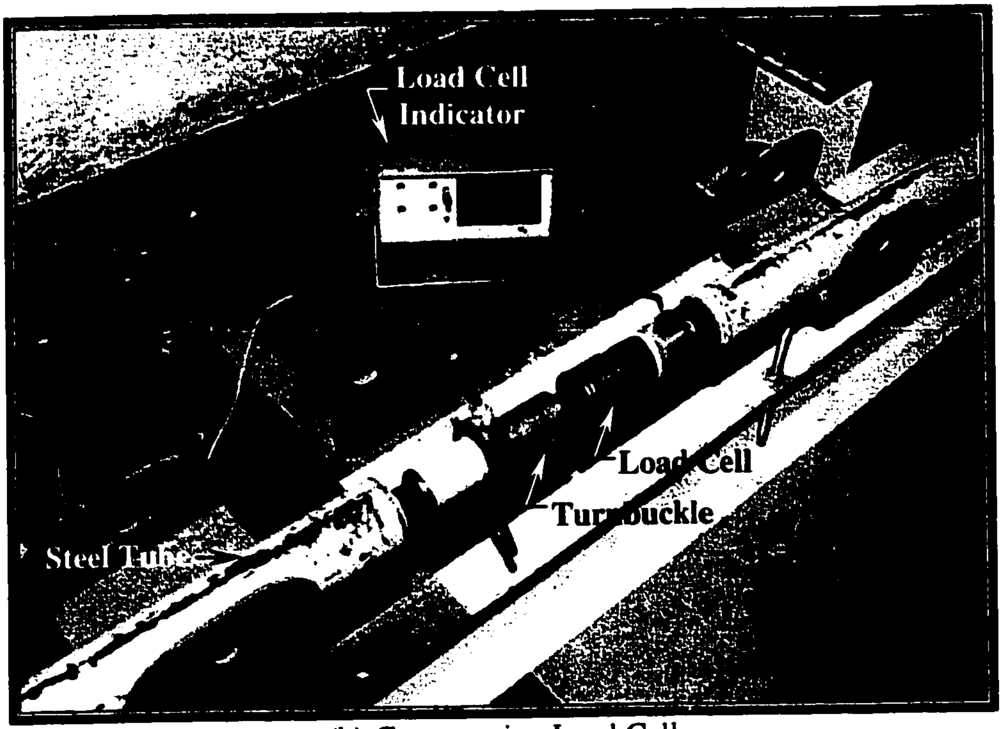

(b) Compression Load Cell

Figure 3.12 Load Cell Arrangements

3.3.1.1 Source of Heating

Thermal loading was applied to one vertical face of the beam (hot face), using ten infrared, 250 Watt heat bulbs. This system, which could produce temperature in excess of 200°C, was mounted in an insulated wooden box over a length of 2000 mm. The opposite face of the beam (cool face) was exposed to the room temperature while the top and bottom sides were insulated with 5 inches of AF 350-type sheet as shown in Figure 3.13. The heating box, 500 x 500 x 2000 mm, was manufactured from 12.5 mm thick wood plates and lined with aluminum foil (Fig. 3.14). The outside faces of the heating box were also insulated.

The temperature distribution over h = 250 mm was measured by means of four thermocouples at two locations (Fig. 3.22) within the heated length of each beam. Two external thermocouples were also installed on the hot and cool faces of the test beam. Figure 3.15 shows the temperature read-out unit, which were used to display temperature readings.

3.3.1.2 Deflection Gauges

Deflection of the test beam was measured using dial gauges with sensitivity of 0.01 mm at various locations. Five dial gauges were used for each concrete specimen; two gauges were placed at the two ends of the beam and the rest was uniformly spaced within the tested length of 2000 mm as shown in Figure 3.9. Each deflection device was supported during the test on a steel stand (I-Section).

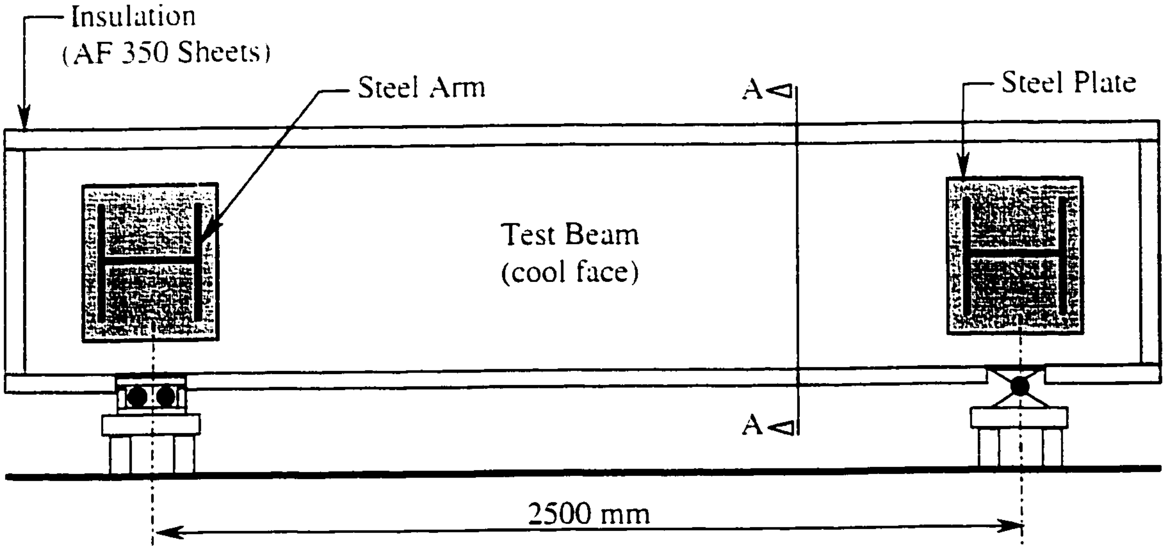

(a) Elevation Showing the Test Beam Insulation

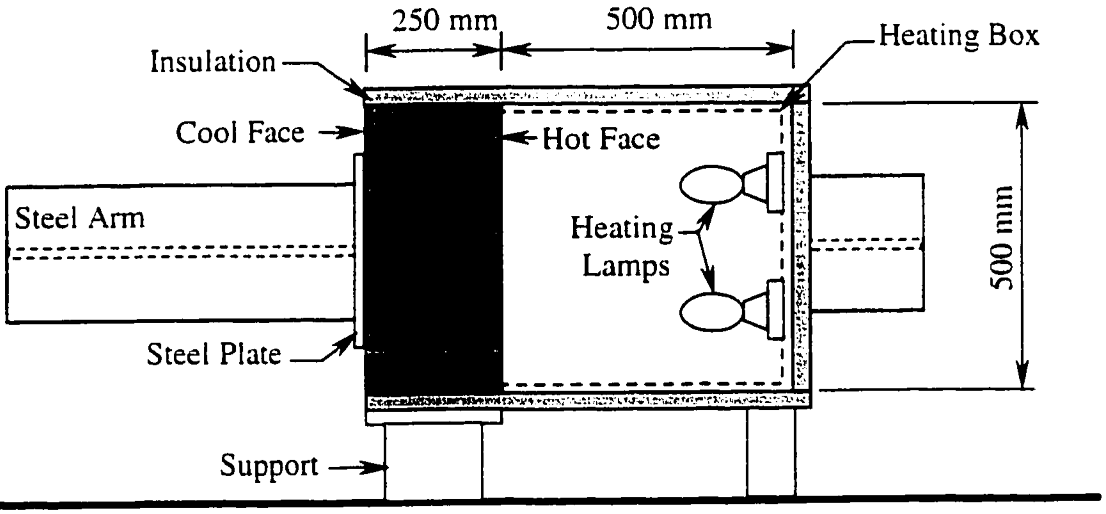

(b) Section A-A

Figure 3.13 Arrangements of Insulation on the Beam and the Heating Box

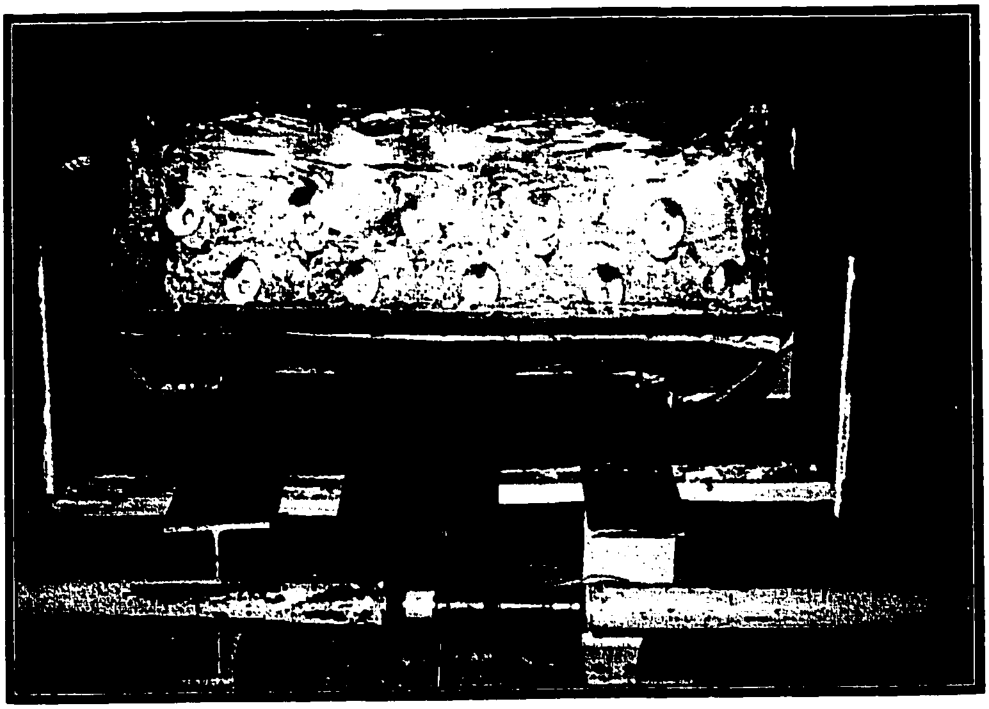

Figure 3.14 Heating Box

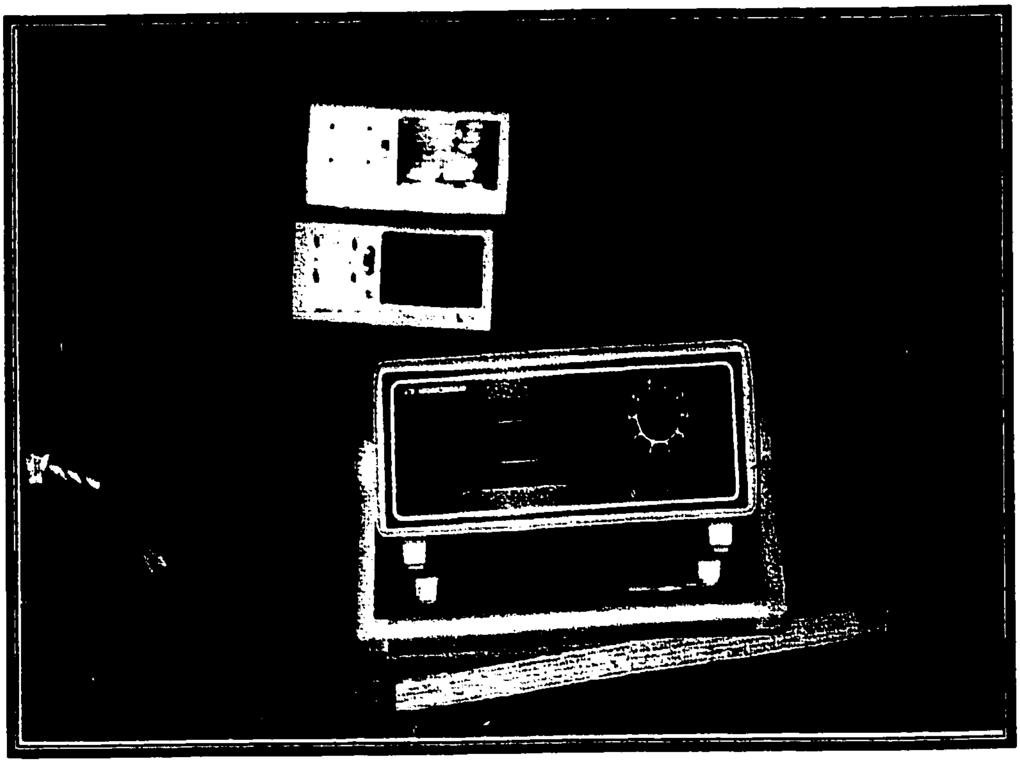

Figure 3.15 Temperature Read-out Unit

3.3.2 Set-up for Mechanical Loading Test

The mechanical loading tests were conducted following the end of thermal loading tests and after cooling the concrete beams down to the room temperature. The first mechanical test was done by applying constant moments to the two ends of the beam using the turnbuckle. The same testing frame of Figure 3.9 was used for this test. The second test was performed by applying two vertical loads to examine the load-deflection behavior of beams up to failure. Figure 3.16 shows a schematic view of the second mechanical test set-up. In this test, the beam was simply supported with a span of 2000 mm and a length of 667 mm and 1250 mm overhanging from each end for RC and PPC beams, respectively. All beams were subjected to two concentrated loads, each applied at one third of the 2000 mm tested length. The loads were increased monotonically with a rate of 3 kN/min.

A hydraulic jack of 500 kN capacity was used to apply the loads which were transmitted to the concrete beam by means of a steel spreader beam. Two pieces of rail spaced at 1/3 pint of the tested length were used to produce the two concentrated loads. A rubber pad was placed between the top surface of the beam and the bottom of each rail to provide a uniform bearing surface. Dial gauges were used to measure the deflection of the beam at three locations during the test. One gauge was placed at midspan, and the other two were placed directly under the two loading points as shown in Figure 3.16.

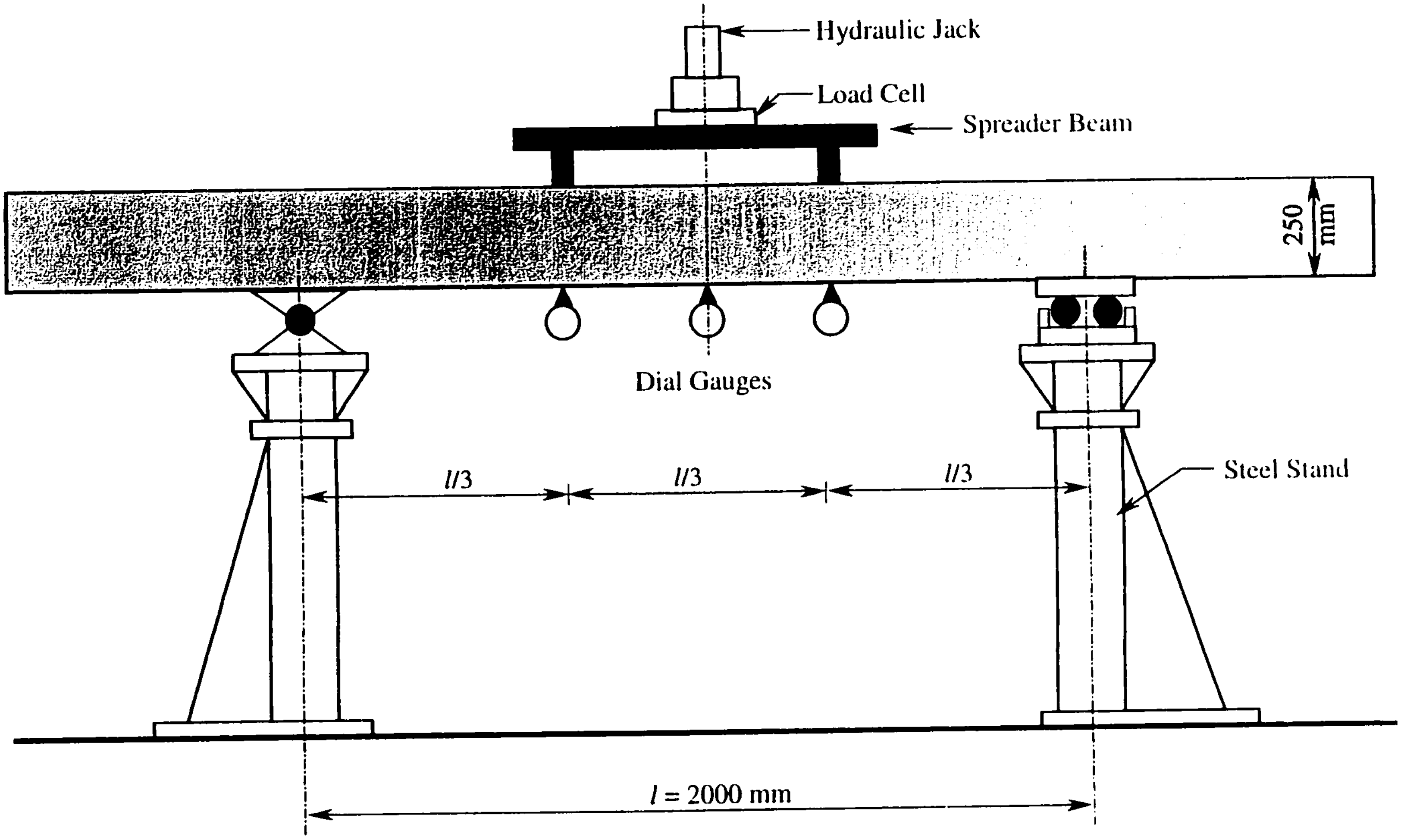

Figure 3.16 Schematic View of Mechanical Loading Test Set-up

3.4 Fabrication of Test Specimen

3.4.1 Preparation of Formwork

The specimen formwork was manufactured from 12mm and 25 mm thick wood plates. The formwork was fabricated in order to cast two beams at the same time. In order to prevent any lateral movement or change in beam dimensions during casting of concrete, bracings were used to fix the external sides of the formwork with the base using bolts to facilitate their stripping and reassembling. In addition, three ties were used at the top of the formwork. Holes were drilled at the ends of the formwork at premeasured locations for accurate placement of the prestressing tendons. The inner sides of the wood plates were covered by a plastic sheet to facilitate removal of the beams and cleaning of the formwork. Eight plastic tubes of 25 mm diameter were inserted through holes drilled in each plate to create 25 mm holes along the depth of the beam. These holes were used to connect the concrete beam with four steel arms used to restrain the rotations at the beam ends. Figure 3.17 shows details of the specimen formwork.

3.4.2 Preparation of the Reinforcing Cages

The reinforcing bars were cut in the laboratory to the required lengths. Steel bars, of 9.5mm diameter, were cut and bent forming rectangular stirrups. They were tied to the top and bottom of the longitudinal reinforcements. In the RC series A, no stirrups were used within the tested length (heated length) for all the concrete specimens. Stirrups were used only at the two ends of the beams at 200mm c/c spacing as shown in Figure 3.18. Extra U-Shaped steel bars of size 10M were added too at each end of the beams.

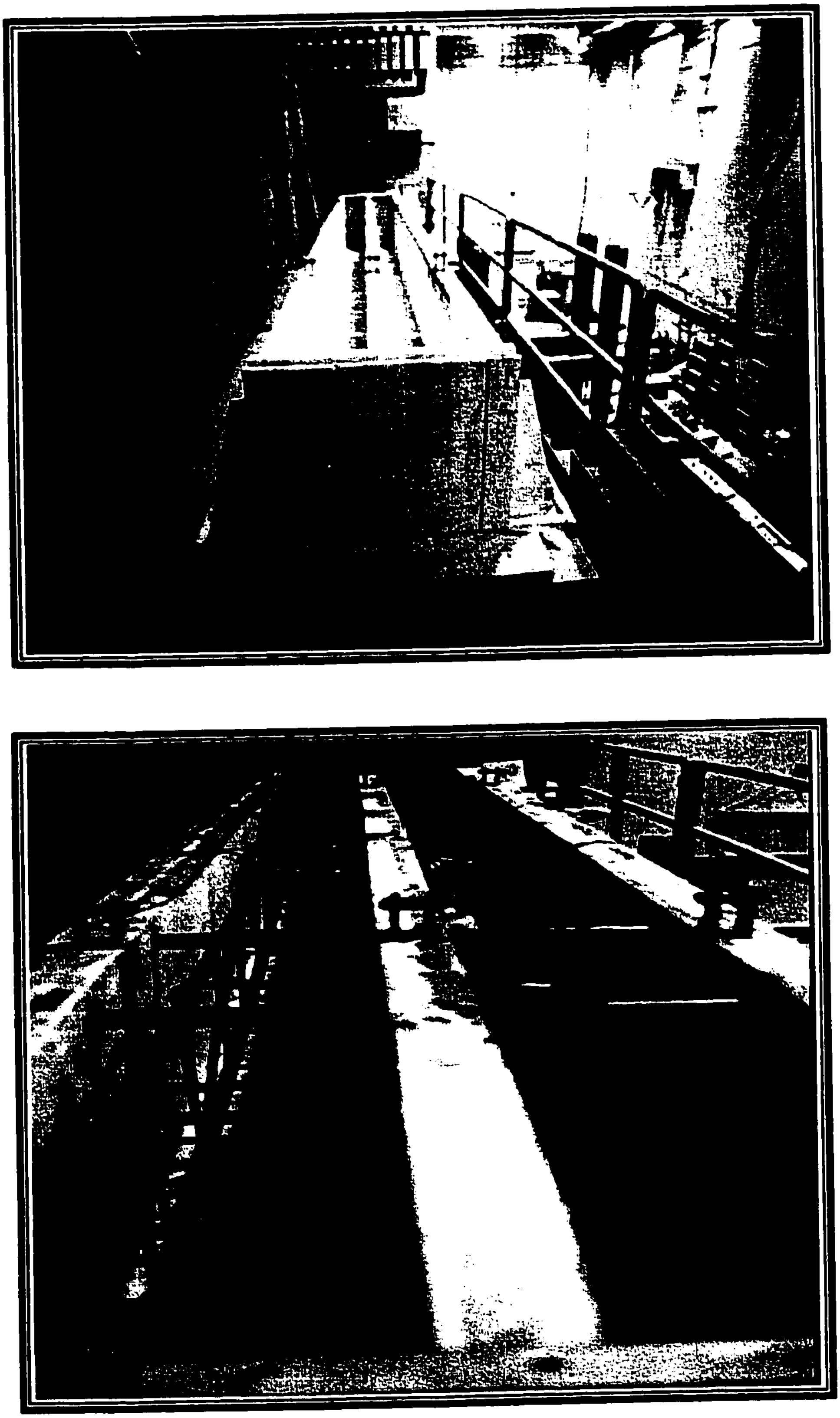

Figure 3.17 Details of the Specimen Formwork

The purpose of this extra reinforcement is to make a rigid connection between the concrete beam and the four steel arms placed at the two ends to prevent the end rotations due to thermal gradient.

In the PPC beams of Series B, with the exception of beam PoSCS.2 post-tensioned by steel strand, stirrups were uniformly spaced along the length of the test beams at 400 mm center of center as shown in Figure 3.19. The purpose was to study the effect of stirrups on locations and numbers of cracks occurred within the heated length. For beam PoSCS.2, stirrups were used only within the 1250mm length at the two ends of the beam. A plastic tube of 20mm diameter was fixed in the reinforcing cages of group B2 to make a duct along the beam length for post-tensioning operation.

The reinforcing cage was then placed inside the formwork. The bottom reinforcement was kept at its proper elevation using steel chairs (75 mm high). The purpose of using such concrete cover of 75 mm was to left the reinforcing cage above the lower plastic tubes. Photographs of reinforcing cages for beams L.6 and GB.5 are shown in Figures 3.20 and 3.21.

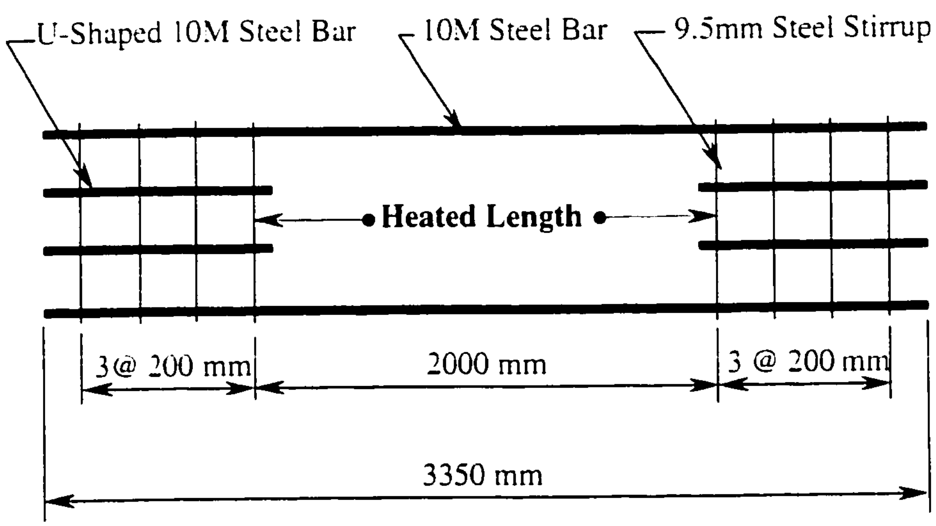

Figure 3.18 Reinforcing Cage for a Typical RC Beam in Series A

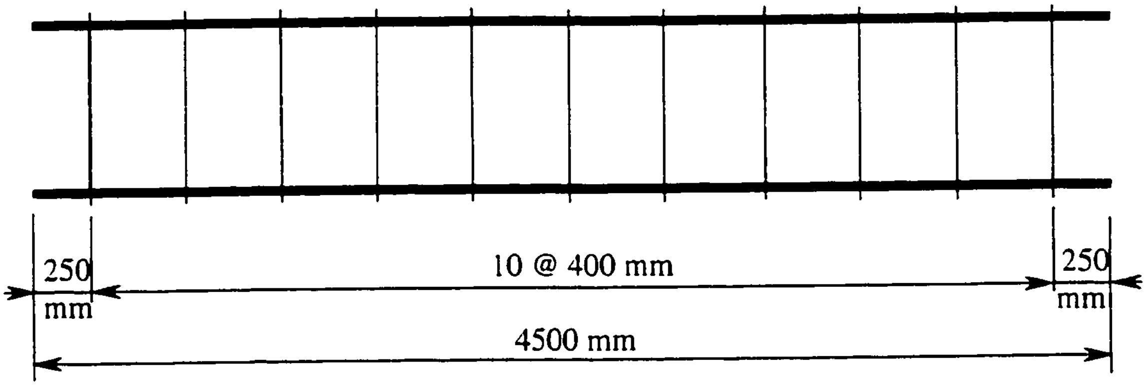

Figure 3.19 Reinforcing Cage for a Typical PPC Beam in Series B

Figure 3.20 Reinforcing Cage for Beam L.6

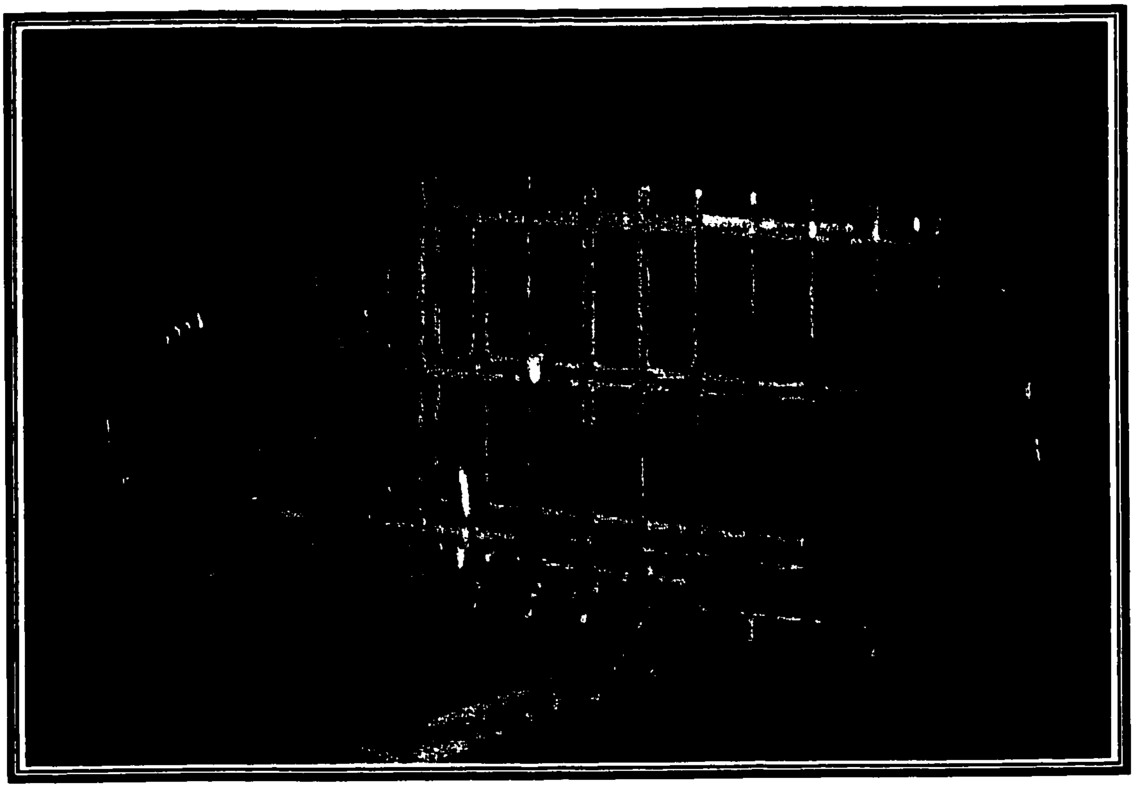

Figure 3.21 Reinforcing Cage for Beam GB.5

3.4.3 Installation of Thermocouples on Reinforcing Cage

The temperature distributions were monitored through the depth of each beam by means of thermocouples placed inside the concrete specimens. The thermocouples were installed during construction of the reinforcing cages. A total of eight Precision Fine Wire thermocouples were placed at two different locations with a 660mm distance from each other in the central part of the heated length. Four thermocouples were placed at each location as illustrated in Figure 3.22. Two external thermocouples were also placed, one on the hot face and one on the cool face. This arrangement of thermocouples allowed for determining the distribution of temperature over the concrete section depth and for ensuring the uniformity of temperature throughout the heated length. The ends of thermocouples were covered to avoid displaying any incorrect temperature readings due to moisture penetration into thermocouples. Photograph of the thermocouples inside the formwork is shown in Figure 3.23

3.4.4 Prestressing Procedure

3.4.4.1 New Anchorage System

The use of Carbon Fiber Reinforced Polymer (CFRP) tendons for prestressing of concrete structures has prompted the need for appropriate design of gripping system for pre- and post-tensioning applications. The CFRP tendons have very poor lateral and shear strength. They are very sensitive to transverse pressure in comparison to prestressing steel.

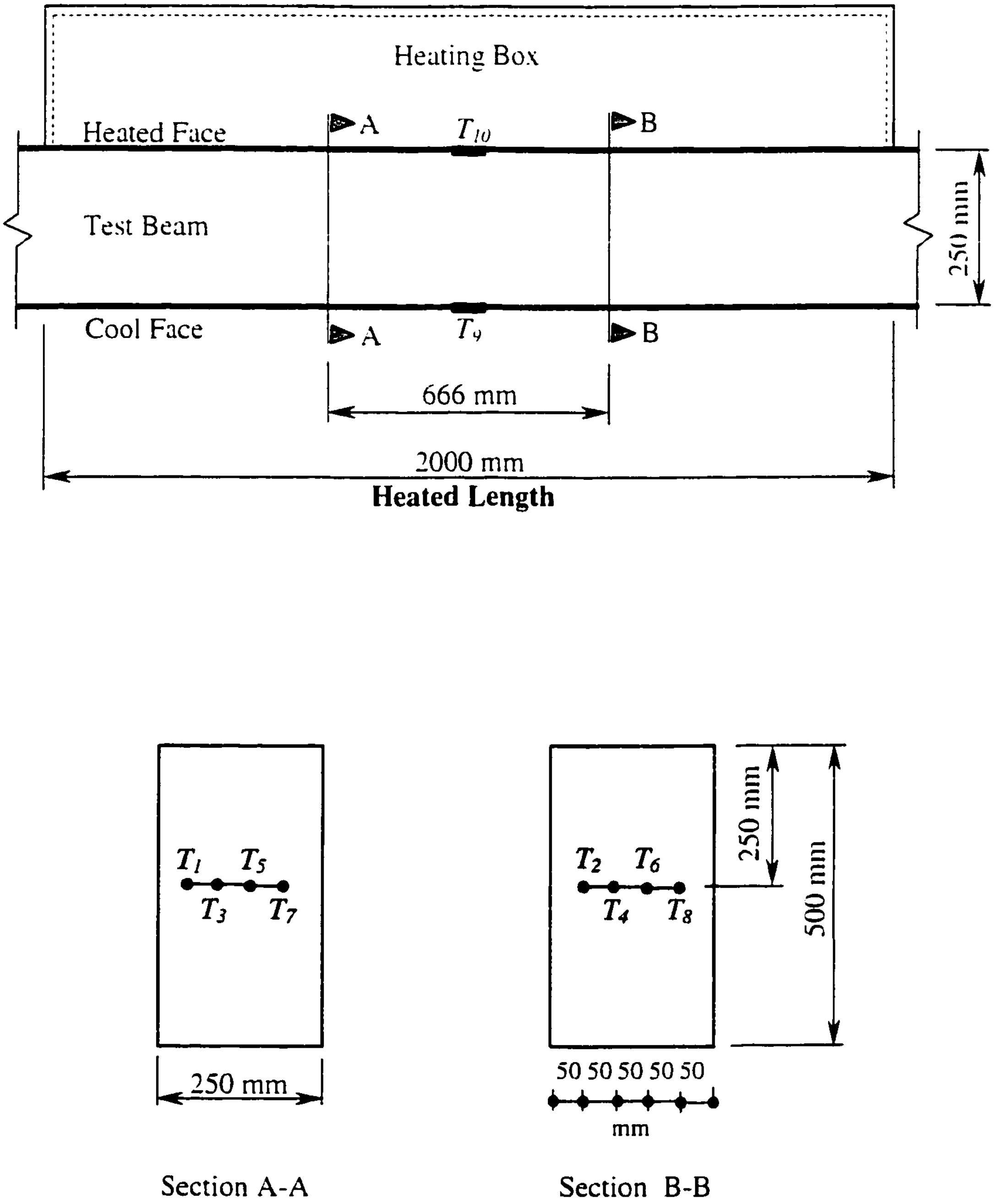

Figure 3.22 Locations of Thermocouples in a Typical Beam

Figure 3.23 One Location of Thermocouples installed on the Reinforcing Cage of a Prestressed Beam

In typical prestressing processes, steel anchorage systems are used for pre- and post-tensioning steel strands. However, when used for prestressing CFRP tendons, these conventional anchorage systems cause stress concentrations in the transverse direction around the edges of the wedge. These stress concentrations can be high enough to cause premature failure of the tendons. Thus, the steel wedge systems can not be used with the CFRP tendon. New anchoring devices for Leadline rods have been developed by Sayed-Ahmed et al. (1998) at the University of Calgary in order to get the best performance of the rods.

The new anchorage has been designed by merging concept form the plug-in, the split-wedge, and the soft-metal overlay anchorage systems (Sayed-Ahmed et al. 1998). It is resin-free and is very easy to manufacture or to put together during a prestressing operation. The new anchorage described here can be used in both post-tensioning and pretensioning applications. The main parts of the new system are:

1. An outer stainless steel cylinder (outer sleeve) with a conical hole as shown in Figure 3.24. The inside surface of the hole is made very smooth and grease is added to facilitate seating of the inner wedge inside the outer sleeve.
2. A four-piece wedge (spike). The wedge has a central hole and the internal surface is sand-blasted whereas the outer surface of the wedge is made smooth. To reduce the stress concentration on the tendon when the spike is seated in the outer sleeve, the edges of the four pieces at this hole are rounded. The angle of inclination of the outer surface of the spike is slightly larger than that of the inner surface of the outer sleeve. The inner hole of the spike is drilled to the outer diameter of the inner sleeve.
3. The inner sleeve is made of steel or cooper and has a small wall thickness. The inner

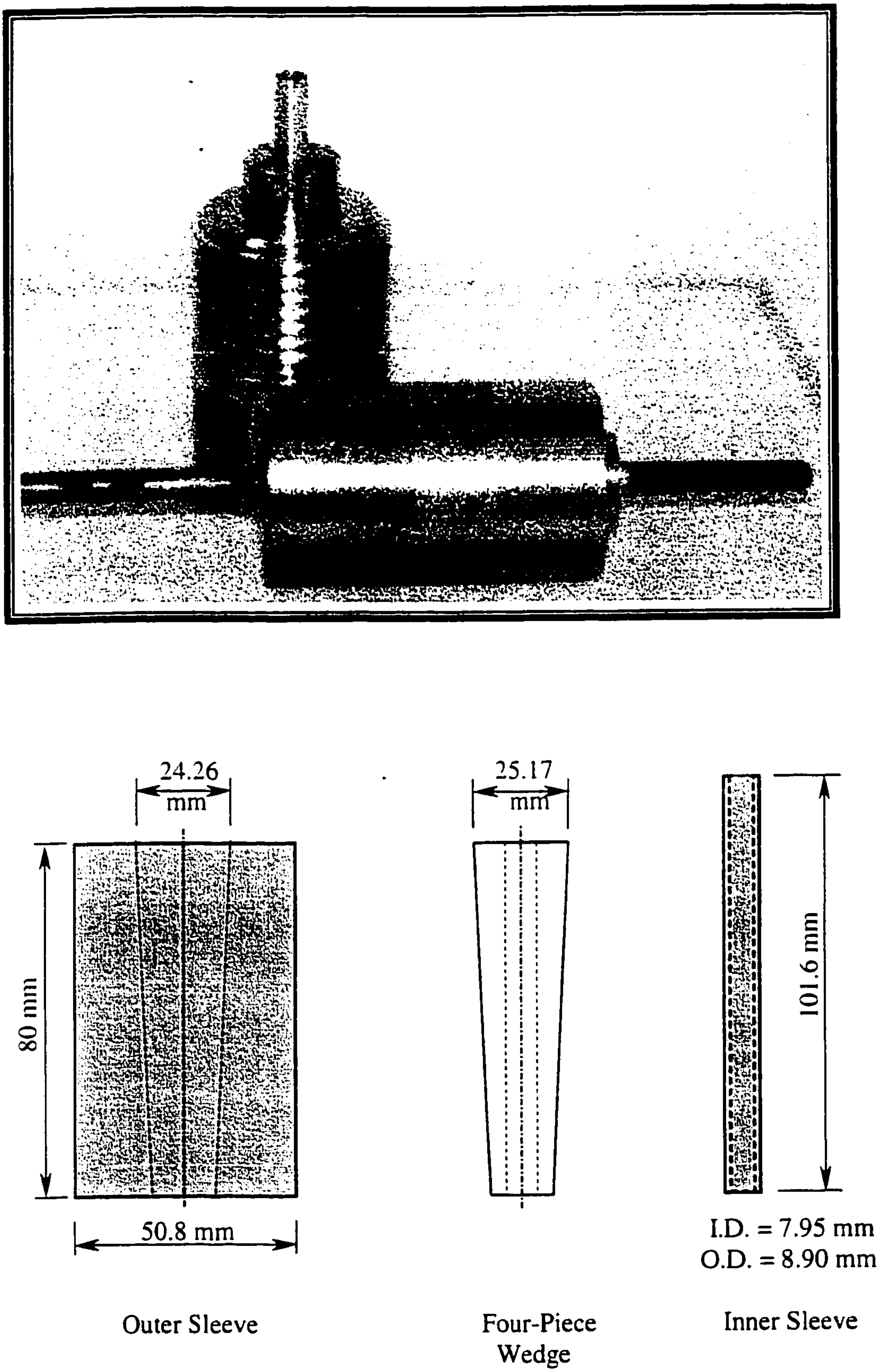

Figure 3.24 Components and Dimensions of the New Anchorage System

diameter of the sleeve is drilled to the diameter of the Leadline tendon. The outer surface of the sleeve is sand-blasted

3.4.4.2 Seating Operation for Leadline Tendons

In order to secure the four-piece wedge inside the outer steel cylinder and also to avoid slippage of the Leadline rod inside the anchorage, a seating process is necessary. For the purpose of the present investigation, a special frame, shown in Figure 3.25, has been developed for seating the dead and live anchorages in both pretensioning and post-tensioning operations. A 20-ton capacity hydraulic jack is used with an oil pump to provide the load required for seating the anchorage system, Figure 3.26. The seating force was monitored by means of a load cell. The seating force varied between 85 to 95 kN for the various tendons.

The seating procedure was done in steps as follows:

1. A cooper cylinder (inner sleeve), outside diameter = 8.9 mm, and inside diameter 7.95 mm, was drawn to appropriate spot on the CFRP tendon.
2. A thin layer of grease was put in the interior surface of the outer steel cylinder, which was then put in the front of the inner sleeve.
3. The sleeve was inserted inside the four-piece wedge, which was then seated by hand inside the outer steel cylinder.
4. The hydraulic jack was operated to provide the force required to seat the four-piece wedge inside the outer steel cylinder.

After seating, the cooper cylinder must be gripped with the four-piece wedge on the Leadline tendon to prevent any slippage between the anchorage system and the Leadline rod. The seating frame and the hydraulic jack were then completely removed from the

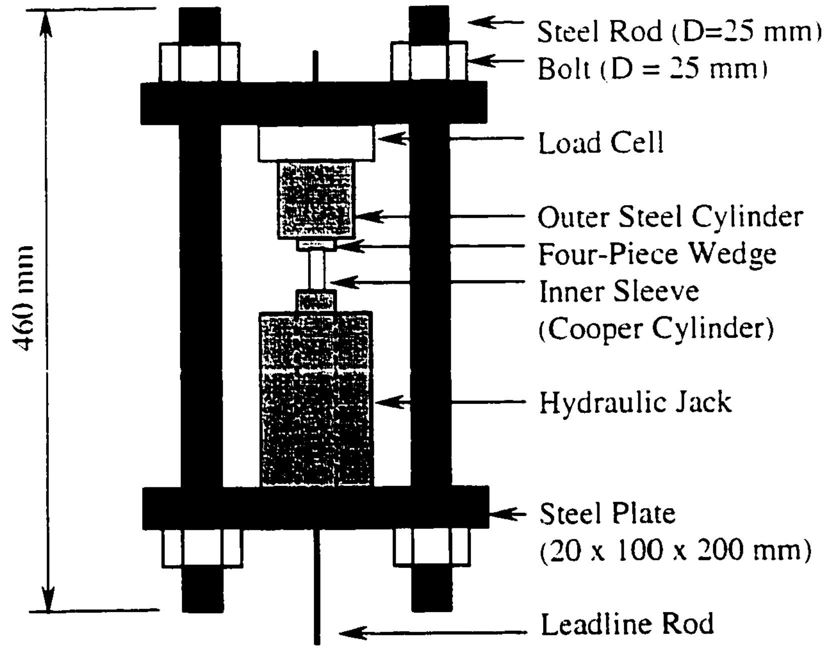

Figure 3.25 Schematic of the Seating Frame System

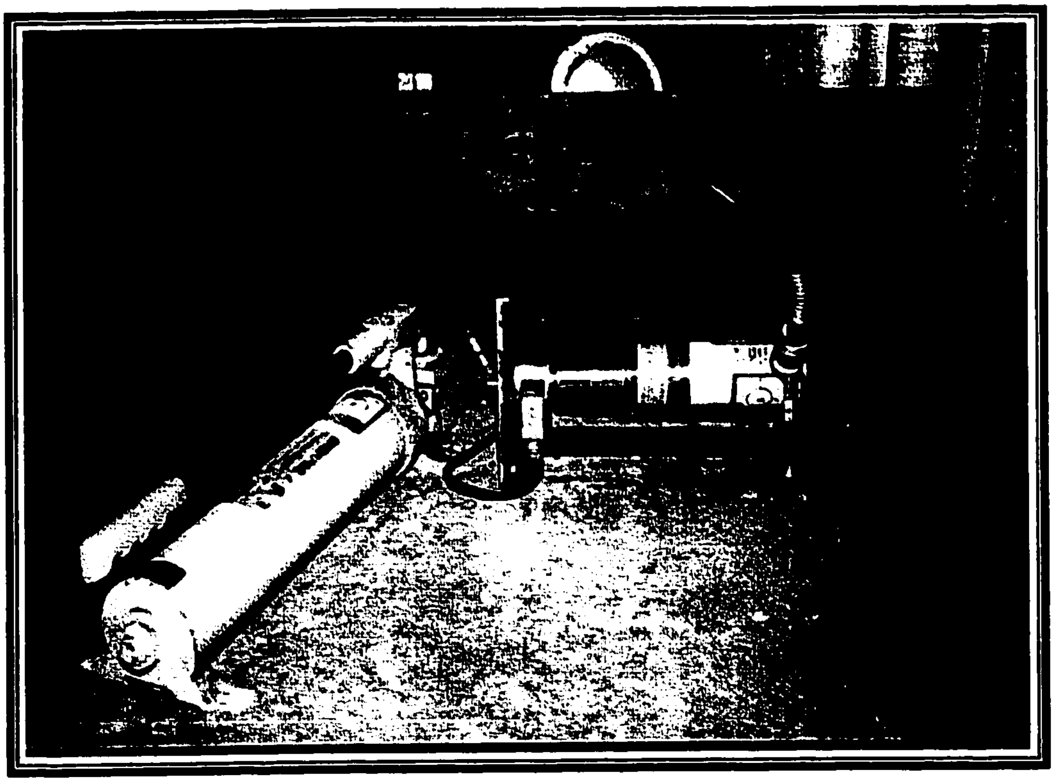

Figure 3.26 Seating of the Anchorage System

dead end of the tendon.

3.4.4.3 Pretensioning Operation

The jacking force, F_P, required for prestressing the Leadline tendon was calculated as follows:

- The guaranteed tensile strength, f_g = 1970 MPa, specified by Mitsubishi Chemicals Corporation based on tension test using steel wedge type anchorage was taken as the tensile strength of the Leadline tendon having a nominal cross-section A_P = 46.1 mm^2 for (8 mm diameter rods).
- The Leadline tendon was jacked up to 70% of the guaranteed tensile strength, thus, the allowable stress f_{all} = 1970 x 0.70 = 1379 MPa.
- The jacking force $F_p = f_{all} \times A_P$ = 1379 x 46.1 x 10^{-3} = 63.57 kN.
- The required concrete stress needed after transfer is 0.5 MPa.

  $F_{req.}$ = 0.5 x A_g = 0.5 x 250 x 500 x 10^{-3} = 62.5 kN < 63.57 kN O.K

The casting bed and the support system used for pretensioned the Leadline tendon for the prestressed beams in Series B are shown in Figure 3.27. Two beams, PrLCL.1 and PrLES.2, having concentric and eccentric Leadline tendons, respectively, were pretensioned to the same prestressing level producing an average compressive stress of 0.5MPa at any cross section of the beam. The 8 mm diameter straight tendons were pretensioned inside the formwork one day before casting of the concrete to reduce any losses that can take place due to relaxation of the Leadline tendon.

The anchorage system shown in Figure 3.24 was used for anchoring the prestressing tendons. The dead anchorage shown in Figure 3.28 was seated first using the seating

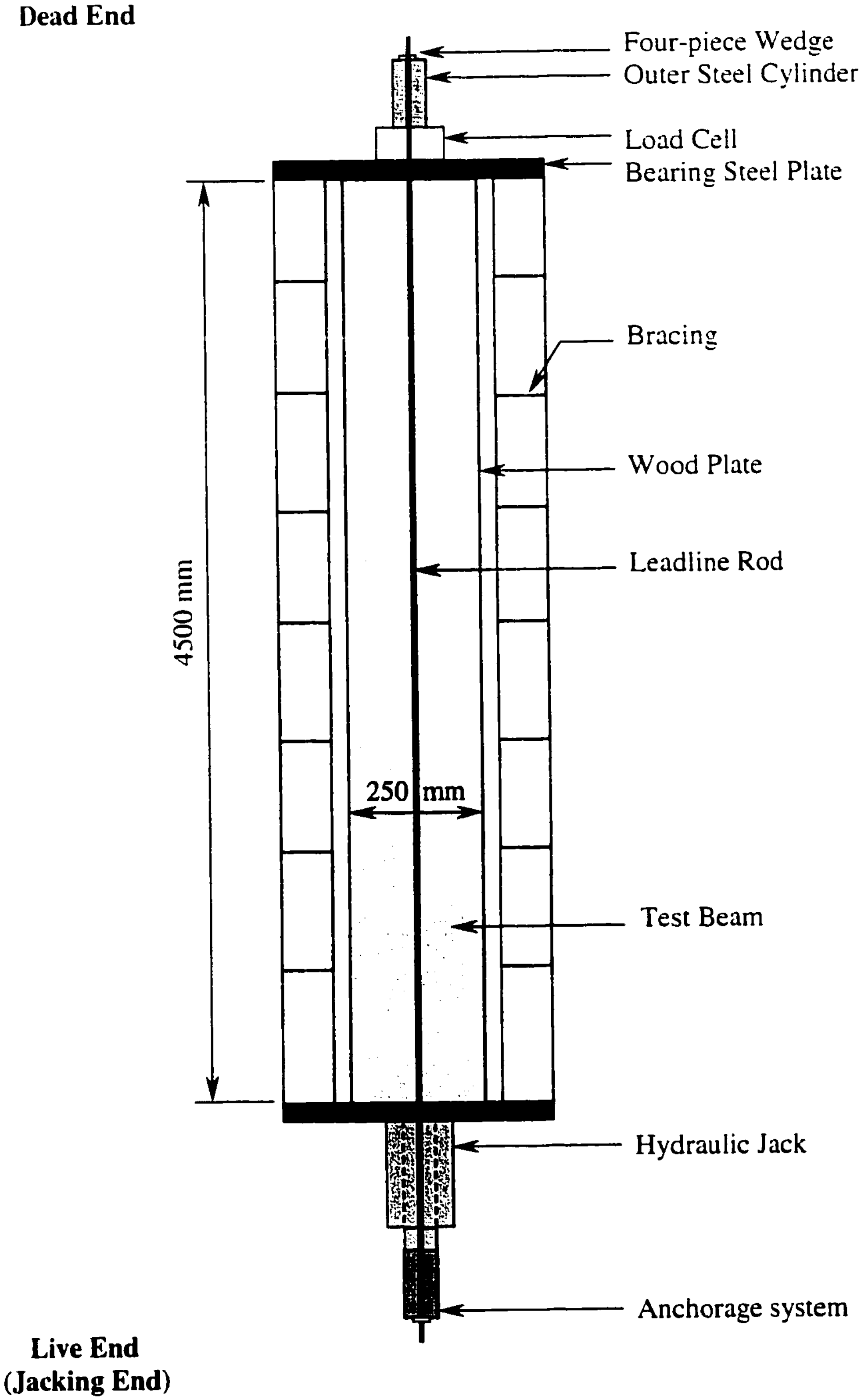

Figure 3.27 Schematic of the Pretensioning Set-Up

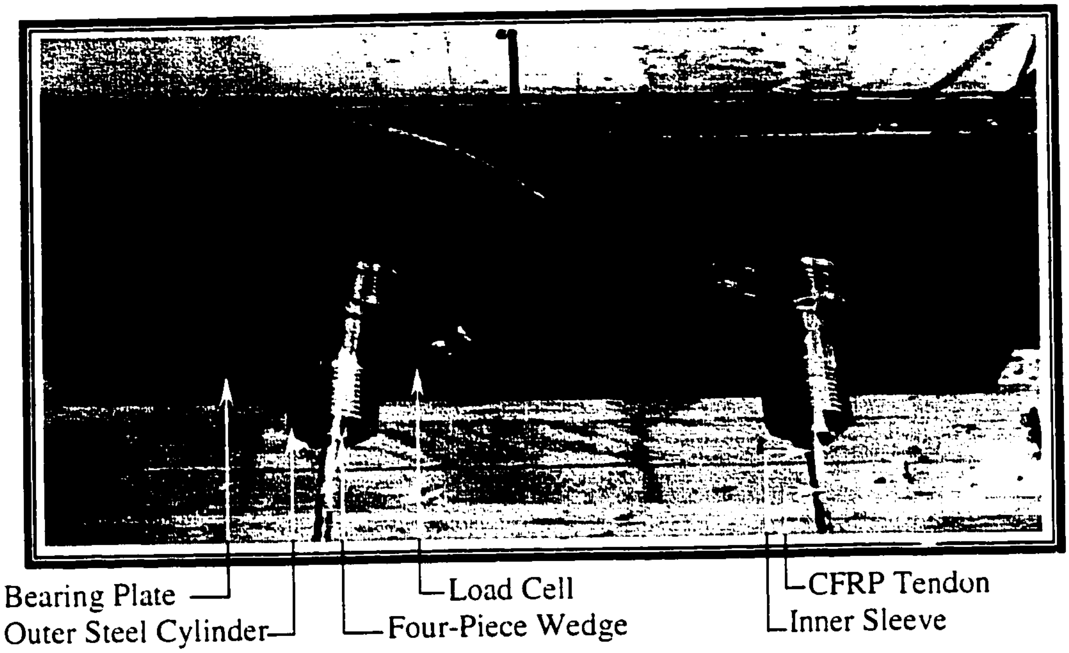

Figure 3.28 Anchorage System at the Dead End

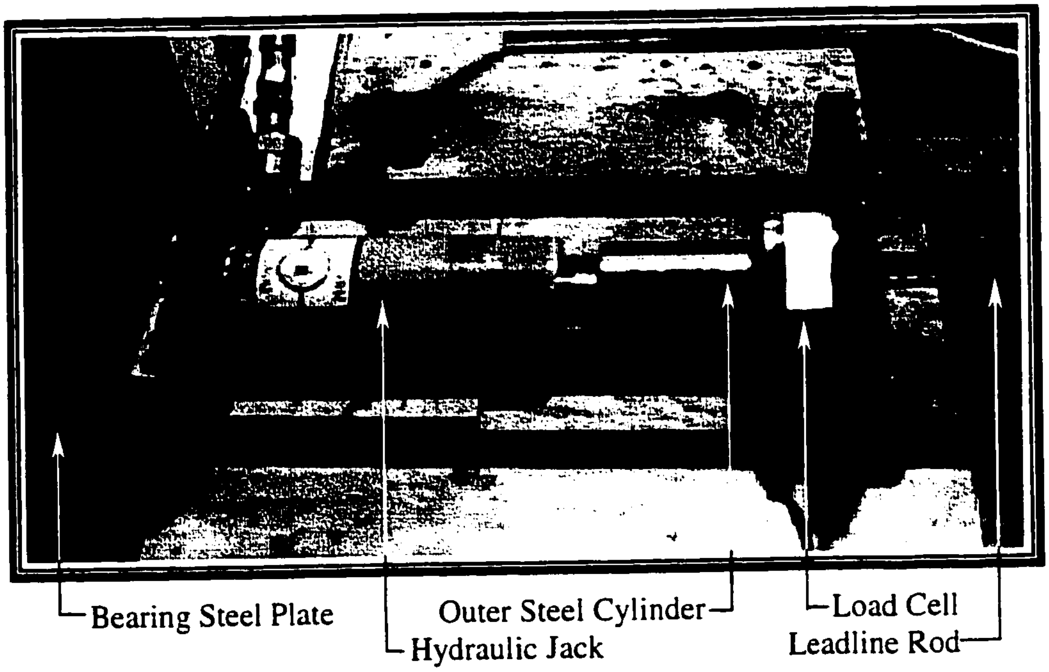

Figure 3.29 Seating Procedure for Live Anchorage System before Pull out of the Leadline Tendon

frame system of Figure 3.25 and then the tendon was fed through the beam bed. The live anchorage, shown in Figure 3.29, was then seated and the seating frame was then removed.

A 20-ton capacity hydraulic jack was used to create a tension force in the tendon by pushing out the live anchorage against the bearing plate attached to the live end of the beam formwork. The load was gradually increased in steps of 10kN until the desired prestressing force or higher was reached. The prestressing force was monitored by a load cell placed at the dead end. Prior to casting of the concrete beam, the prestressing force was checked and additional force was added when the force in the tendon decreased below 62.5kN. Four days after the casting of the concrete, the prestressing force was released gently by releasing the pressure of the jack.

3.4.5 Casting of the Concrete Specimens

A local ready-mix company supplied concrete with a minimum compressive strength of 30 MPa. Two beams of equal span of each group were cast at the same time. A concrete vibrator shown in Figure 3.30 was used for internal vibration of the concrete mix during casting of the concrete. A special care was taken to minimize any disturbance to the locations of thermocouples. Following the casting of the beams, concrete cylinders of size 75mm x 150 mm were cast from each patch.

After leveling the concrete surface, the specimens were left to cure in the formwork and covered with plastic sheet on the top surface for about 7 days. The beams were then stripped from the forms and left inside the laboratory until they were tested. Most of the beams were tested within 14 to 30 days after casting.

Figure 3.30 Casting of Concrete Specimens

3.4.6 Monitoring Concrete Temperature during Hardening

The aim was to study the effect of the heat of hydration of the concrete specimen at very early age. After pouring the concrete, four thermocouples were connected to read-out unit. Temperature data was collected during hardening for five days. Figure 3.31 shows a representative sample of the data collected on the beam PrLCL.1. This figure represents the temperature variation at one location shown in Figure 3.22 within the depth of the concrete beam. The maximum temperature reached in this beam was 62°C within an approximate duration of five days.

3.5 Material Properties

3.5.1 Concrete

The concrete used for casting the beams contained aggregate of maximum size of 14 mm. The slump of a typical mix was 80±20 mm. The design compressive strength of the concrete specimens ranged from 30 MPa to 35 MPa. The concrete mix proportions by weight were as given in Figure 3.32. The specified water/ cement ratio was 0.4 and the cement content was 450 kg/m^3. No superplasticizer was added to increase the concrete workability. High early strength and low temperature concreting type 30 cement was used. Six concrete cylinders, each 75 x 150 mm, were tested in compression before release of prestressing and at the same day of testing according to ASTM C39-86, and three cylinders were also tested for splitting strength according to ASTM C49-86. The results of the compressive and splitting strength tests are given in Table 3.2. Photographs of the compressive and splitting tests are shown in Figures 3.33 and 3.34.

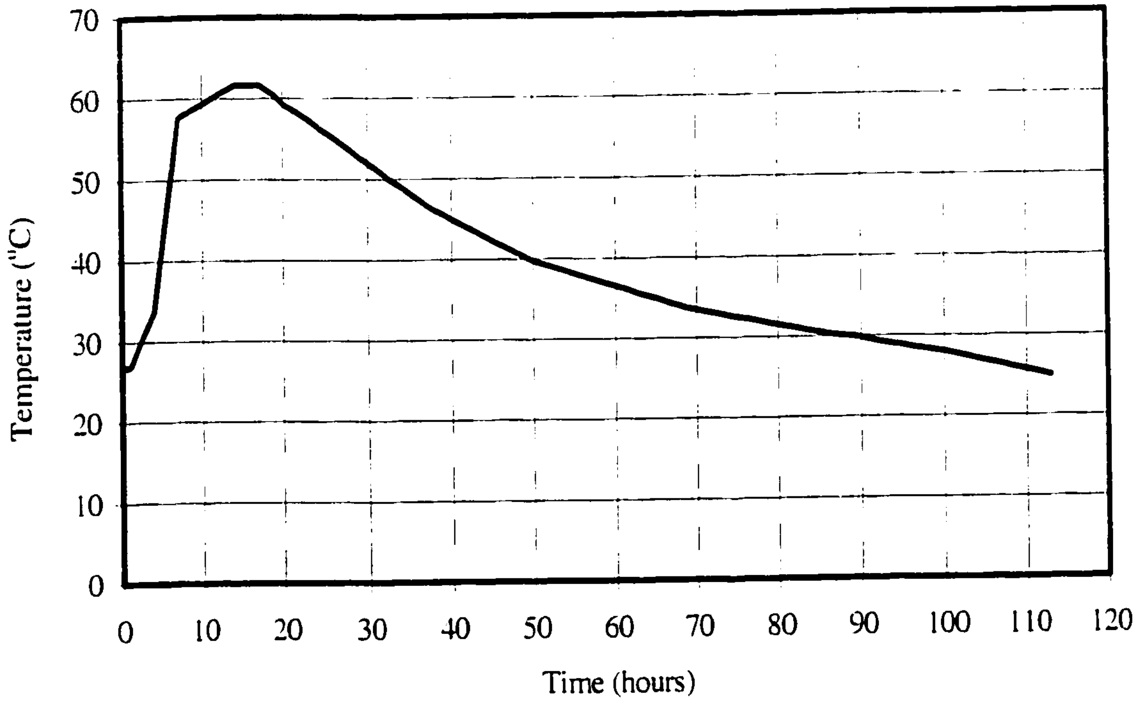

Figure 3.31 Temporal Variation of Temperature for Beam PrLCL.1 during the Curing Stage

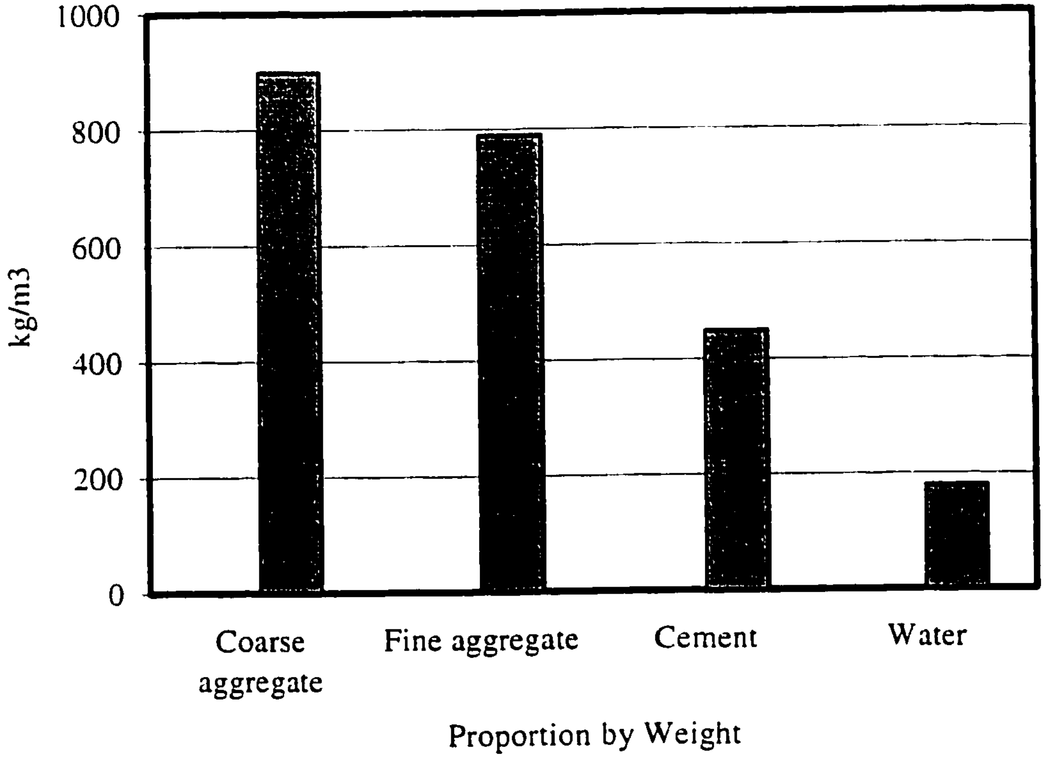

Figure 3.32 Composition of Typical Concrete

Table 3.2 Compressive and Splitting Strengths for Beam Specimens

Beam Designation	Group Name	Compressive Strength at the Time of Release				Splitting Strength at Testing Day				Compressive Strength at Day of Testing				Age at Testing (day)
		C1*	C2	C3	Average f'_c (MPa)	C1	C2	C3	Average f'_s (MPa)	C1	C2	C3	Average f'_c (MPa)	
L.6	A1					2.40	2.09	2.06	2.18	53	55	57	55.00	24
L.8	A1					2.50	2.46	-	2.48	52	53	-	52.50	17
L1.0	A1					2.53	2.86	-	2.69	58	53	-	55.50	22
GM.5	A2					1.94	1.99	-	1.97	55	49	-	52.00	10
GT.5	A2					2.14	1.73	-	1.96	52	45	-	48.50	14
GB.5	A2					2.90	2.30	2.60	2.60	50	52	57	53.00	12
PrLCL.1	B1	36	37	37	36.67	2.97	2.41	2.56	2.65	41	44	-	42.50	14
PrLES.2	B1	27	29	-	28.00	1.67	1.75	-	1.71	32	34	-	33.00	23
PoLCS.2	B2					1.67	1.75	-	1.71	32	34	-	33.00	23
PoLEL.1	B2					2.97	2.41	2.56	2.65	41	44	-	42.50	14
PoSCS.2	B2					2.65	2.30	-	2.48	52	53	48	51.00	8

* C1= Concrete Cylinder number 1 having an area of 4560 mm^2.

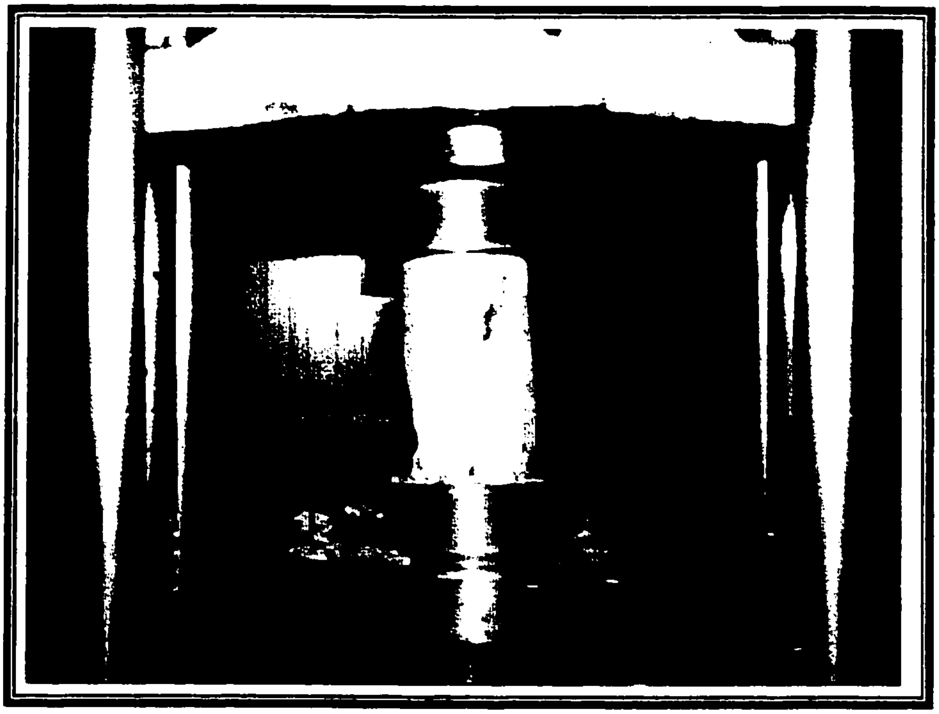

Figure 3.33 Compressive Strength Test

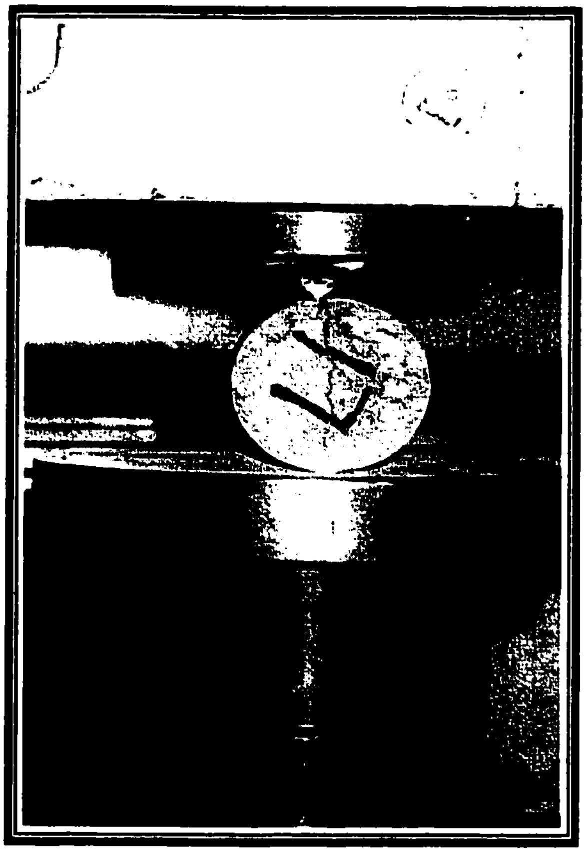

Figure 3.34 Splitting Strength Test

3.5.2 Reinforcing Steel (Bars)

Two different types of steel reinforcements were used in the concrete beams, namely, deformed and plain bars. The longitudinal bars used as compression reinforcements in the test beams were a deformed steel bar of size 10M. The steel bar of grade 60 (f_y = 400 MPa) has a nominal diameter of 11.3 mm and cross-section area of 100mm^2. Plain bars, each of 9.5mm diameter and area of 70 mm^2, with minimum yield strength of 275 MPa (Grade 40) were mainly used for stirrups.

3.5.3 Prestressing Steel

Low relaxation seven-wire strand, Grad 270 with ultimate strength of 1860 MPa was used for post-tensioning one beam denoted as PoSCS.2. The strand has a nominal diameter of 9.25mm (3/8 in.), a cross-sectional area of 54.8 mm^2 (0.085 in^2), and a modulus of elasticity of 200GPa. The strand consisted of seven individual wires and was made by tightly wrapping six of the wires around the seventh. The tensile strength of the steel strand was determined using 1.0m long specimen. Photograph of the testing machine is shown in Figure 3.35. The load-elongation curve for the prestressing strand is plotted in Figure 3.36.

3.5.4 FRP Reinforcement

In the present study, two types of FRP reinforcements were used: Leadline rods and NAFMAC-Grid type reinforcement. Three concrete beams denoted as L.6, L.8, and L1.0 were reinforced with Leadline rods with reinforcement ratios of 0.6%, .8%, and 1.0%, respectively. The two Leadline diameters used in these beams are 8mm single and double

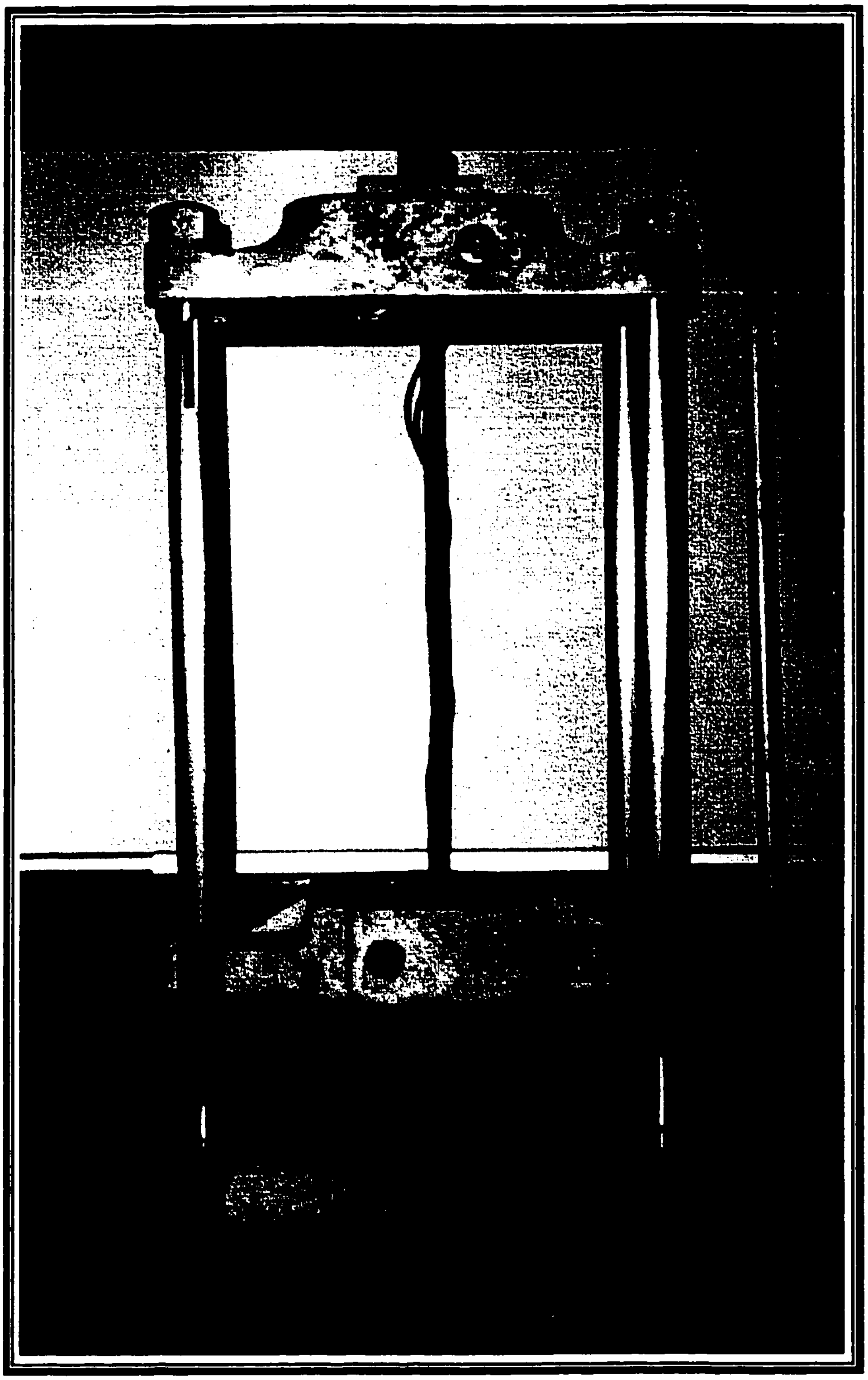

Figure 3.35 Tensile Testing of Prestressing Strand

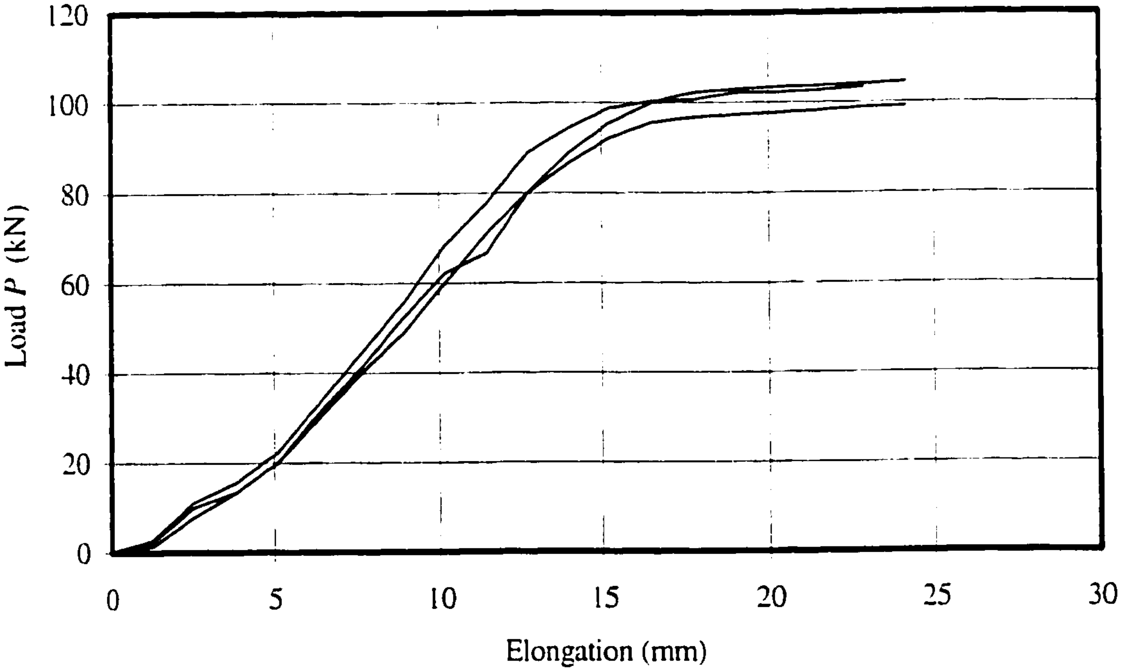

Figure 3.36 Load-Elongation Curves for Steel Strands under Tensile Loading

indented type and 10mm single indented type with cross-sectional areas of 46.1 mm^2 and 71.8 mm^2, respectively. Four prestressed concrete beams were constructed and tested using Leadline rods of 8mm single indented type. The mechanical characteristics of the Leadline rods in comparison to prestressing steel are given in Table 3.3. The two different types of the Leadline rods used in the experimental program are shown in Figure 3.7.

NEFMAC-Grid type reinforcement, glass fiber (GF) type with dimensions of 400 mm width and 3000 mm length, was used in all the beams of group A2. NEFMAC beams denoted as GB.5, GT.5 and GM.5 were reinforced with NEFMAC with the same reinforcement ratio of 0.5%. Standard specification of NEFMAC is provided in Table 3.4. The shape of the NEFMAC grid is shown in Figure 3.8.

3.6 Post-tensioning Procedure

3.6.1 Post-tensioning Operation for Leadline Tendon

A schematic view of the jacking arrangement used for post-tensioning the concrete specimens in Series B is shown in Figure 3.37. Three-anchorage systems: A, B, and C, shown in Figures 3.37 to 3.39 were used for each post-tensioning tendon. The dead anchorage (A) was seated first and then the tendon was passed through a plastic duct in the beam. A calibrated load cell was attached to the dead anchorage in order to measure the prestressing force. Using the same seating frame of Figure 3.25, the anchorages B and C were also seated. Figure 3.40 shows the seating operation for the anchorage B at the live end.

Table 3.3 Mechanical Characteristics of Leadline Tendon Compared to Prestressing Steel Strands (ISIS Canada, Project T4.4)

Property	CFRP	Steel
Minimum fiber volume ratio V_f	0.63	
Density (g/cm^3)	1.58	7.85
Longitudinal tensile strength (MPa)	2280	1860
Transverse tensile strength (MPa)	57	1860
Longitudinal modulus (GPa)	142	190
Transverse modulus (GPa)	10.3	190
In-plane shear strength (MPa)	71	
In-plane shear modulus (GPa)	7.2	73.1
Maximum longitudinal strain (%)	1.5	4.0
Maximum transverse strain (%)	0.6	4.0
longitudinal compressive Strength (MPa)	1440	1860
Transverse compressive strength (MPa)	228	1860
Longitudinal coefficient of thermal expansion (/°C)	-0.9×10^{-6}	11.7×10^{-6}
Transverse coefficient of thermal expansion (/°C)	27×10^{-6}	11.7×10^{-6}
Relaxation ratio (%)	2-3	8

Table 3.4 Standard Specification of NEFMAC (NEFCOM Corporation)

Type	Glass Fiber (GF) + Resin
Bar No.	G13
Sectional Area (mm^2)	131
Maximum Load (kN)	76.4
Tensile Strength (MPa)	588
Young's Modulus (GPa)	29.4
Weight (g/m)	220

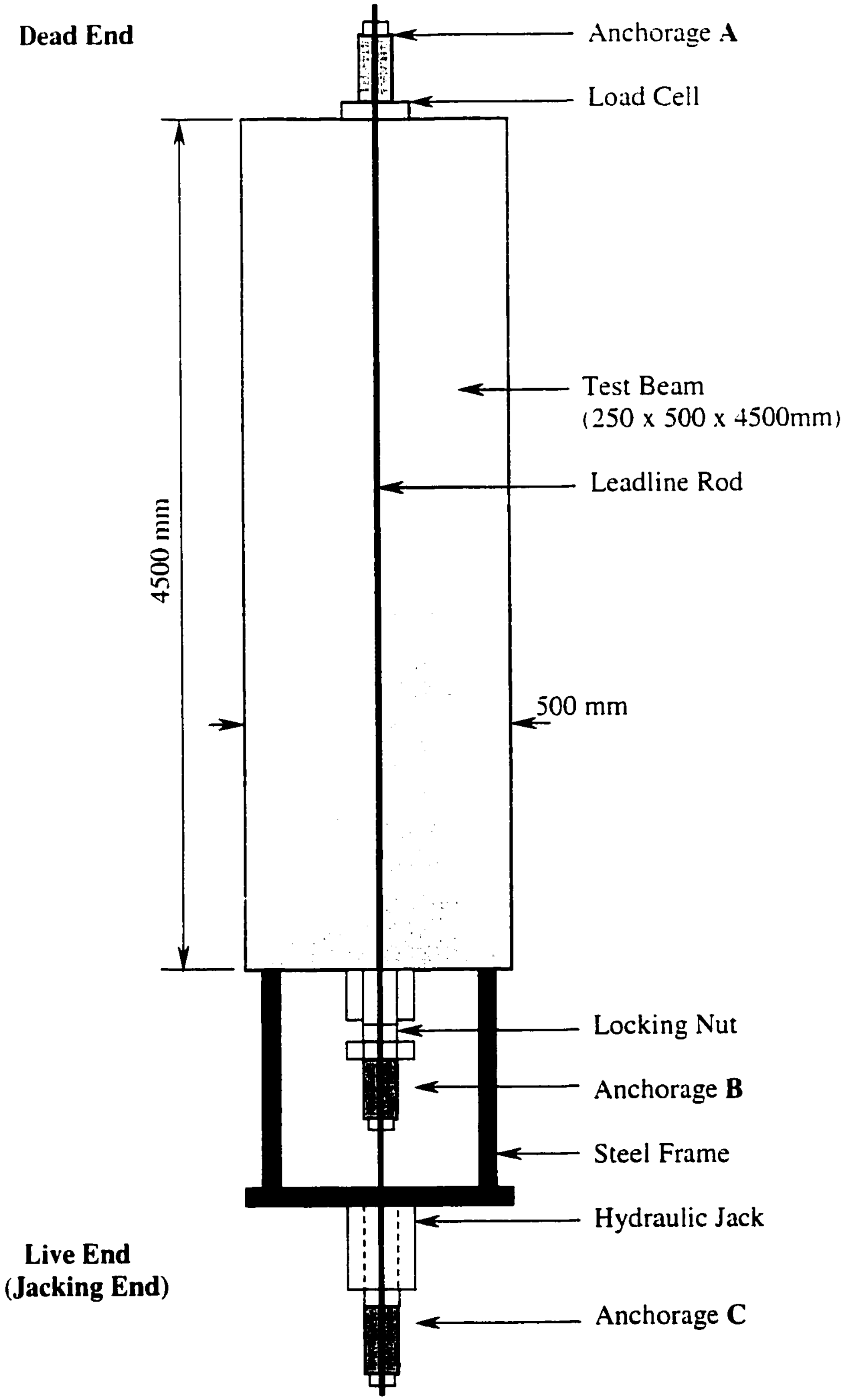

Figure 3.37 Schematic of the Post-tensioning Set-up

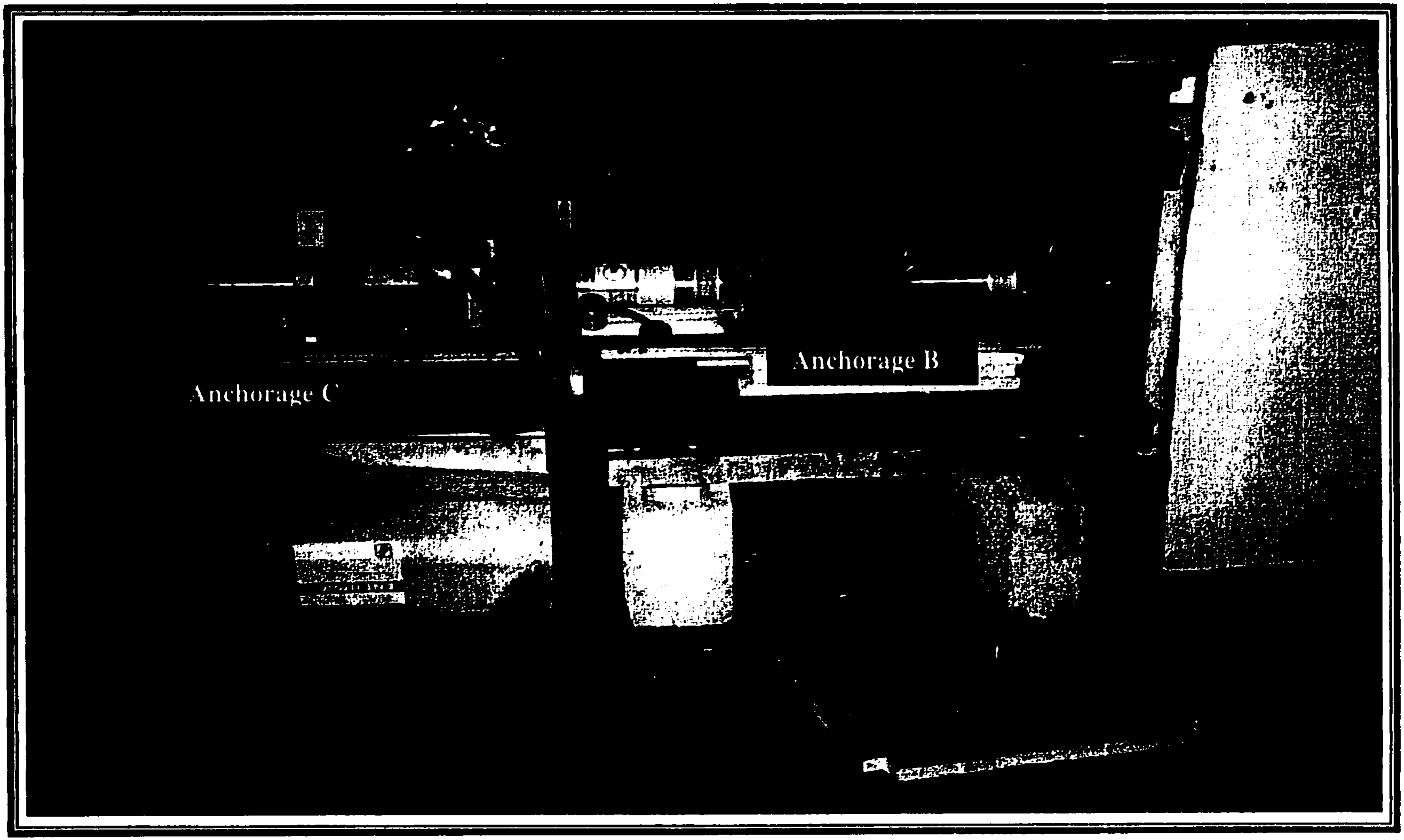

Figure 3.38 Anchorage Systems at the Live Jacking End

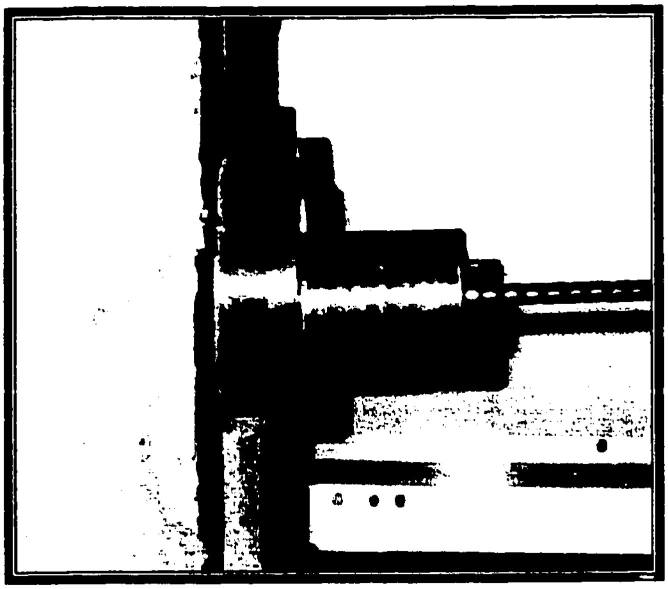

Figure 3.39 Anchorage A at the Dead End

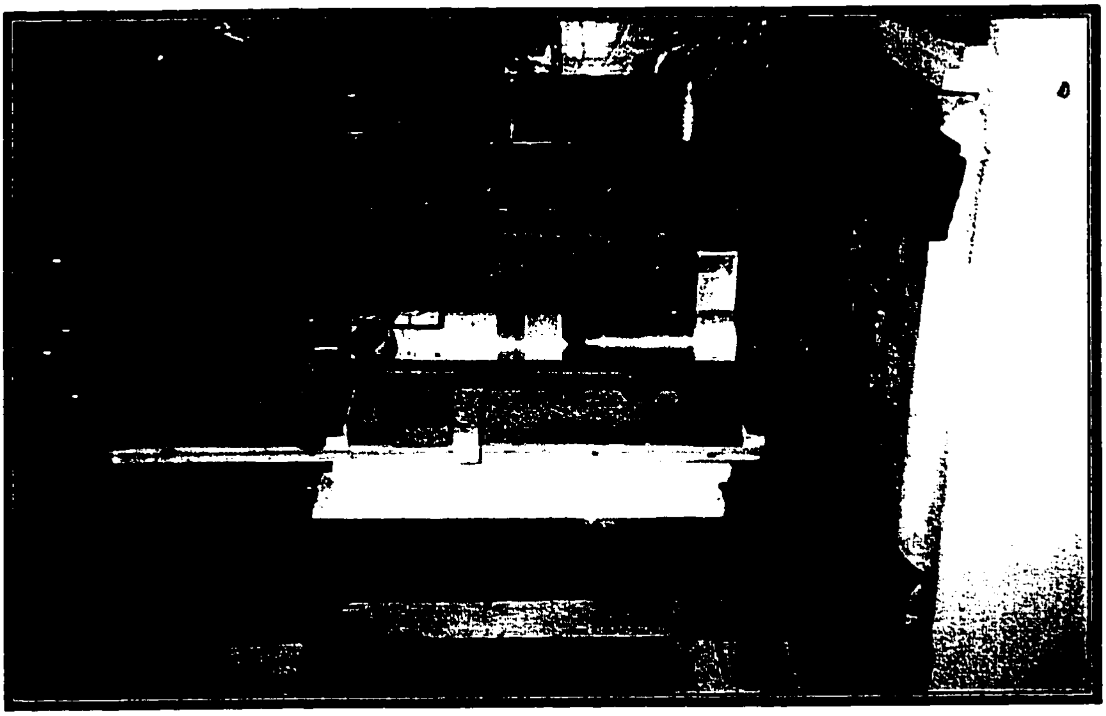

Figure 3.40 Seating Operation for Anchorage B

At the jacking end, a hydraulic jack was used to push anchorage C against a steel frame to create elongation in the tendon. When the desired prestressing force was reached, a locking nut placed between anchorage B and the beam end, was used to maintain the force after jacking and then the hydraulic jack at anchorage C was released. The prestressing force was monitored by the load cell. The post-tensioning operation was repeated two to three times within one hour for each beam to compensate for anchor set losses at the time of release and for relaxation of the tendon.

On the day of test, the prestressing force was checked and additional force was added when the prestressing force decreased below 62.5 kN. The tendon was cut between the two anchorages B and C and then the steel frame, the hydraulic jack, and anchorage C were completely removed.

3.6.2 Post-tensioning Operation for Steel Strand

The same procedure used for post-tensioning Leadline tendons was applied to beam PoSCS.2 post-tensioned with steel strand with the exception of the following two operations:

- No seating procedure was employed for anchorages A, B and C of the steel strand.
- The anchorages used to hold the prestressing strand were PSI Super Multiple use standard chucks 3/8in supplied by Prestress Supply Inc. USA, made for gripping 3/8in diameter 7-wires prestressing cables (Figure3.41).

Figure 3.42 shows anchorages A and B at the dead and live ends, respectively.

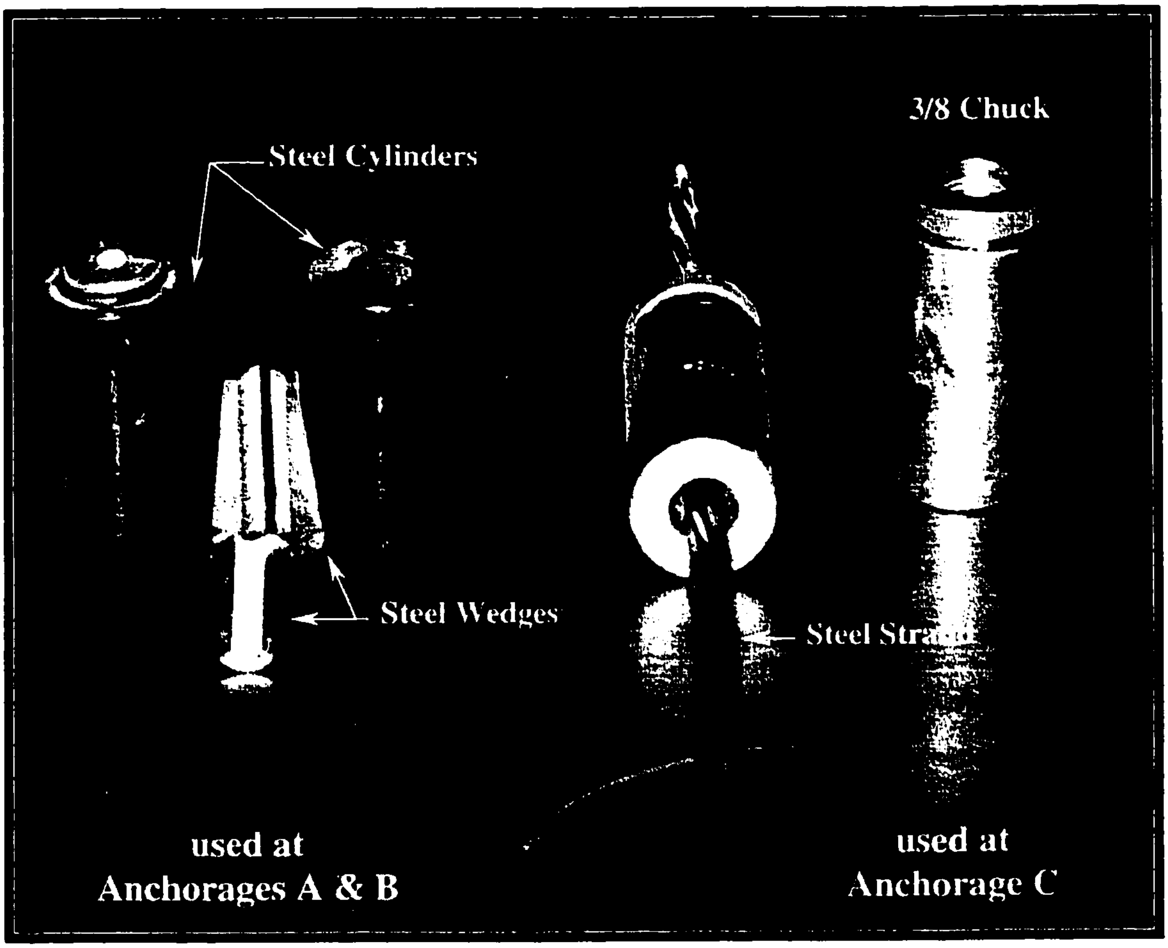

Figure 3.41 Components of the Anchorage Systems for Steel Strand

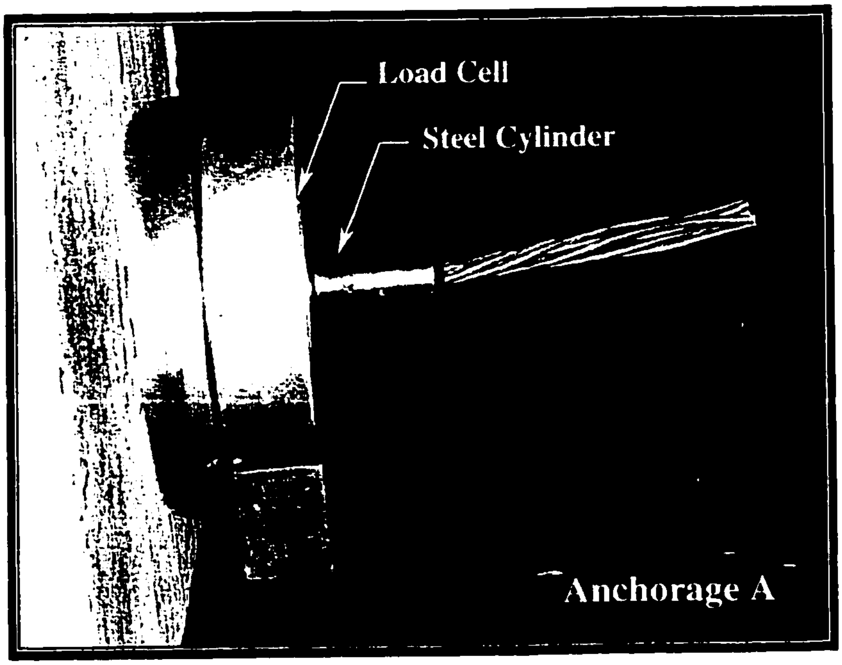

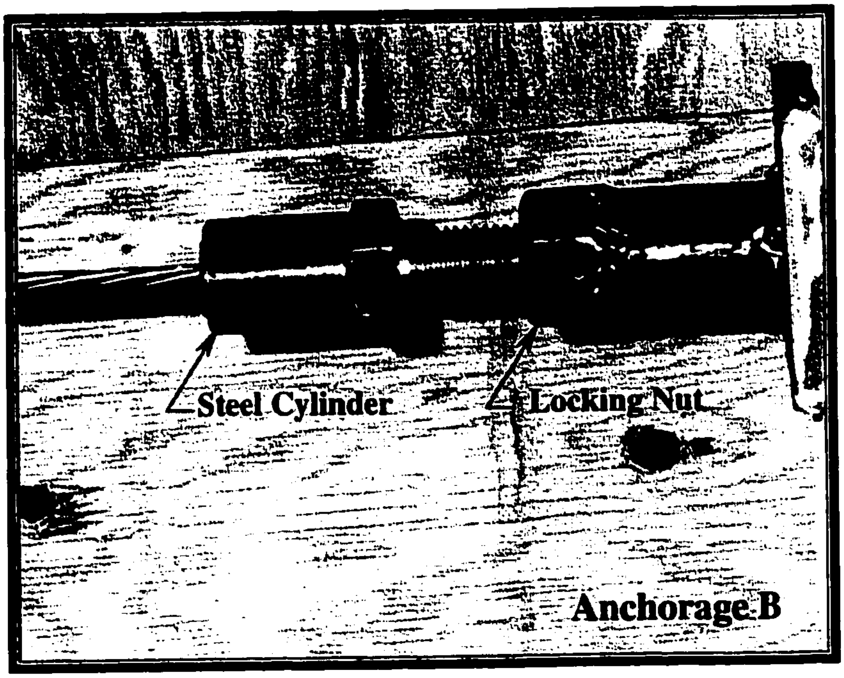

Figure 3.42 Anchorage Systems for Beam PoSCS.2

3.6.3 Avoiding the Risks during Prestressing and Testing

Failure of CFRP bars occurs suddenly and therefore, stressing and anchoring operations must be carried out with extreme care. In addition, the prestressing force must be monitored with a load cell to avoid any overloading of the tendons. At the failure, the CFRP bars release enormous amount of strain energy as they have a relatively low elastic modulus in comparison to steel reinforcements, and exhibit a liner stress-strain relationship up to their ultimate tensile strength.

To avoid breakage of CFRP tendons or detaching of the anchorage system during post-tensioning, a special arrangement was made to protect the two ends of the test beams. Photographs of the protection system are shown in Figure 3.43.

3.7 Testing Procedure

3.7.1 Pre-Testing Procedure

The following steps were carried out before the thermal loading test:

1. The concrete specimen was supported on hinge and roller bearings. Then the four steel arms were rigidly connected to the beam using 20 mm diameter bolts.
2. Two external thermocouples were installed on the hot and cool faces of the test beam using Fastweld^{TM}10 "Rapid setting epoxy structural adhesive". After that the ten thermocouples were then connected to the temperature read-out unit (Figure 3.15).
3. The cool face of the test beam was painted with white paint to facilitate visualization of the cracks.
4. The heating box was attached to the hot face as close as possible. The small space between the box and the heated length at the top and bottom was closed with

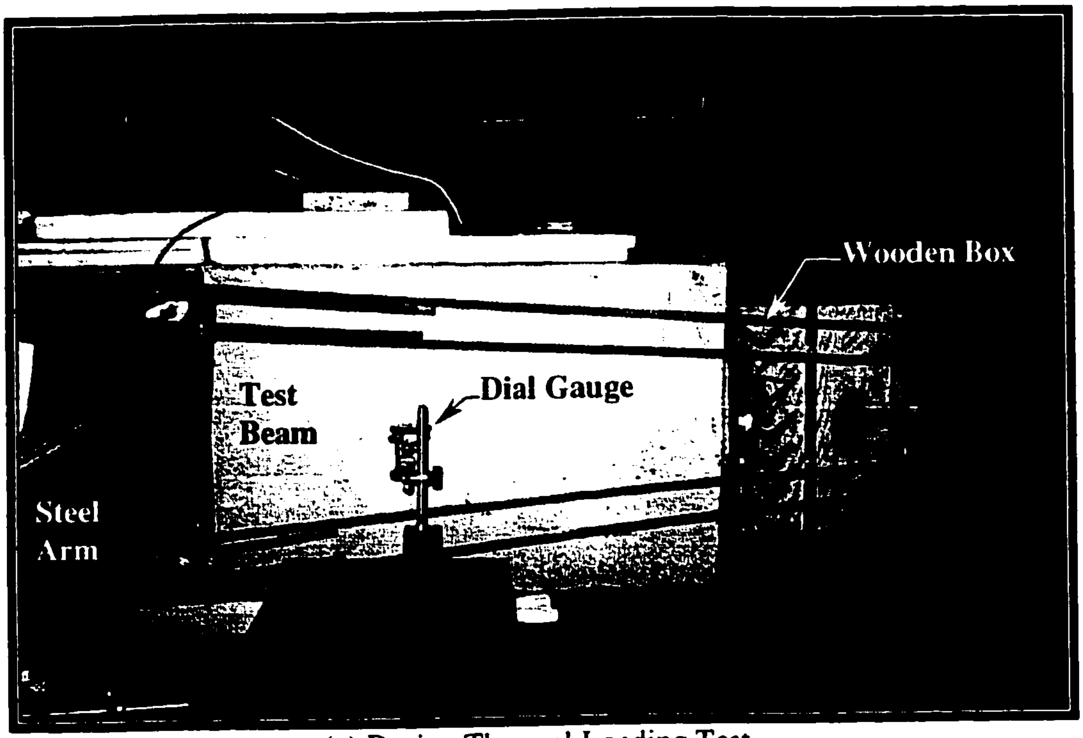

(a) During Thermal Loading Test

(b) During Mechanical Loading Test

Figure 3.43 Protection System at the Two Ends of the Test Beam

insulation sleets.

5. With the exception of the hot and cool faces, all sides of the concrete specimen were insulated using AF 350 sheets.

3.7.2 Thermal Loading Test

Before heating, the test beam was subjected to initial equal moments, M_o, at the ends of the 2000 mm heated length by rotating the two turnbuckles provided with load cells (Figure 3.12). These moments were acting in the same direction as the thermal moments produced by the temperature gradients. The purpose of applying these external moments was to:

- represent, in practice, the bending moments due to dead load on a concrete beam before applying the thermal loading.
- cause the cracking to occur at low temperature gradients in order to avoid heating the beam to very high temperatures.

The initial applied moment, M_o, for beams reinforced with FRP was 6 kN-m while higher initial moment of 16 kN-m was used for the PPC beams.

After application of the initial moments, the deflection at the center of the tested length relative to its ends was measured and the initial curvature was kept constant during thermal test. The temperature increase was applied in 10 to 12 increments for each beam; in each increment two to three hours were sufficient to reach a stable temperature distribution. A variable auto transformer connected to the heating box was used to provide temperature increase on the hot face. The increase in thermal moments was observed in each increment. The temperature distribution across the depth of the test beam will be provided in the following chapter.

After the temperature readings became stable in each increment, the turnbuckles (Figure 3.12) attached to the load cells were adjusted to satisfy the two following conditions:

1. eliminate any change in central deflection by maintaining the same initial curvature between the dial gauges placed along the cool face.
2. equalize the thermal forces produced by temperature difference in the two load cells.

This ensured that the 2000mm tested length was subjected to pure bending moment = $M_i + M_t$; where $M_t = L\ P$ = the value of the end moment produced by thermal loading. Readings of the thermal moments and the temperature in the 10 thermocouples were recorded. Then the next temperature increment was applied using the variable auto transformer.

The development of any crack was accompanied by a sudden change in the thermal moments. After cracking, the compressive force, which was created on the cracked face of the beam (cool face) was less than the tension force. This reduction in forces occurred because the cracked section centroid moved towards the hot face. Thus, the two load cells ended with different thermal moments in the four steel arms. Therefore, the forces were equally adjusted using the turnbuckles. The same readings mentioned above were recorded. The crack width was also measured using Crack Comparator. In the last increment, the temperature at the hot and cool faces was 160°C and 40°C, respectively, producing a temperature difference of 120°C between the two faces of the beam. Each beam specimen required 20 to 30 hours for completion.

3.7.3 Mechanical Loading Test

In the second sage of testing, the test beam was left for two days to cool down after the thermal loading test. After the ten thermocouples readings had returned to the room temperature, the beam was re-tested under mechanically applied moment. The moment was applied in steps by rotating the turnbuckles at both sides of the test beam simultaneously. The deflection, Δ, at mid-span was also measured. The mechanically applied moment led to additional cracks. The purpose of this test was to study the behavior of thermally cracked beam under the effect of dead and live loads.

Finally, the entire thermally cracked beam was re-tested up to failure under two concentrated loads as shown in Figure 3.16. The magnitude of the total load differed from one beam to another depending on the amount of reinforcement provided. The load was applied in small increments. All measurements, such as deflection, crack width, crack spacing and forces in the prestressing tendons were recorded during the test.

Chapter 4

Experimental Results

4.1 General

In the previous chapter, an experimental program to investigate the effects of thermal characteristics of CFRP Leadline rods and NEFMAC grid reinforcement on the development of thermal stresses and on the control of thermal cracking in concrete members was described. Eleven beam specimens including six reinforced concrete beams and five partially prestressed concrete beams were fabricated and tested. In the following sections, the results of the experimental investigation are reported and discussed. The variables in the tests are the type of reinforcement used, the reinforcement ratio, and the location of tendon (eccentric and concentric) for both pretensioned and post-tensioned concrete members. Plots of the variation of thermal moment with temperature difference for all the beam specimens during the thermal tests as well as the moment-deflection response of thermally cracked beam are presented. The results of tests on the Leadline and NEFMAC reinforced beams are compared to those obtained from tests conducted by Ariyawardena (1993) on beam specimens of the same dimensions but reinforced with conventional steel bars. The ultimate strength and modes of failure of thermally cracked beams under static loading conditions using two point loads are discussed.

Photographs showing the crack pattern and crack spacing during thermal and mechanical moment tests as well as deflection after cracking and failure mode under mechanical load for all beam specimens are given in appendix A.

4.2 Temperature Distribution

Temperature distributions over the 250mm depth have been recorded within the tested 2000mm length of each beam. Eight Precision Fire Wire Thermocouples were used at two locations (at 1/3 point) within the tested length. Four thermocouples at each section were placed with a 50mm distance from each other as illustrated in Figure 3.22. A maximum temperature difference of 130 to 145°C above ambient was observed. A nonlinear temperature distribution was observed over the depth of all the beams at different thermal load levels with a minor variation of temperature from one beam to another. The graph of Figure 4.1 shows the variation with time of all thermocouples readings in a typical beam. This graph can be used to plot the temperature distributions at the two beam sections where the thermocouples are located. Figure 4.2 shows the nonlinear temperature profile observed after 20 hrs of heating at the two locations of thermocouples for a typical beam.

4.3 Behavior of Test Beams under Thermal Loading

The temperature profiles shown in Figure 4.2 are similar to those recorded by Ariyawardena (1993) in the beams reinforced with steel rebars. Ariyawardena has shown that these temperature profiles can be approximated by a straight line variation between T_{top} and T_{bot}; where T_{top} is the temperature at the top face (measured by thermocouple

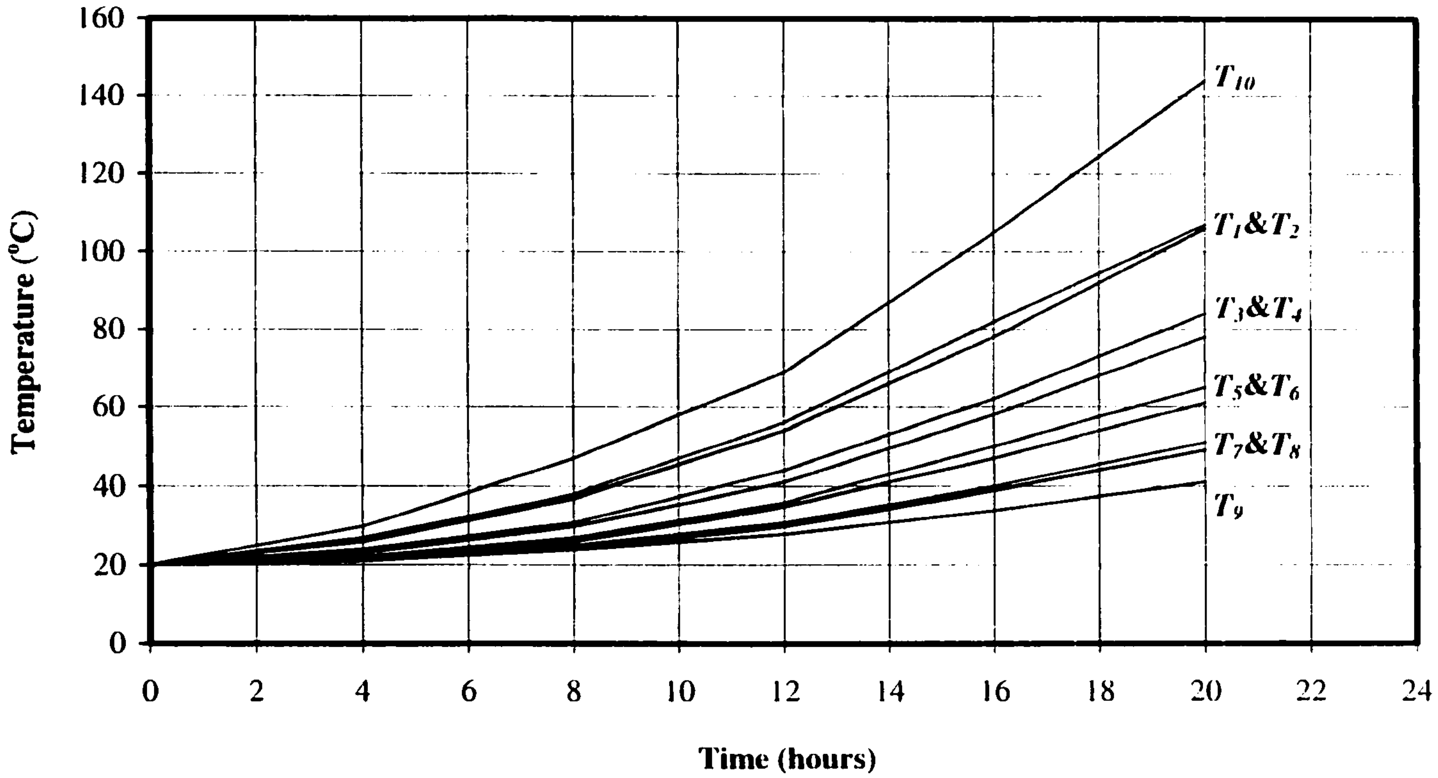

Figure 4.1 Nonlinear Temperature Profile in a Typical Beam

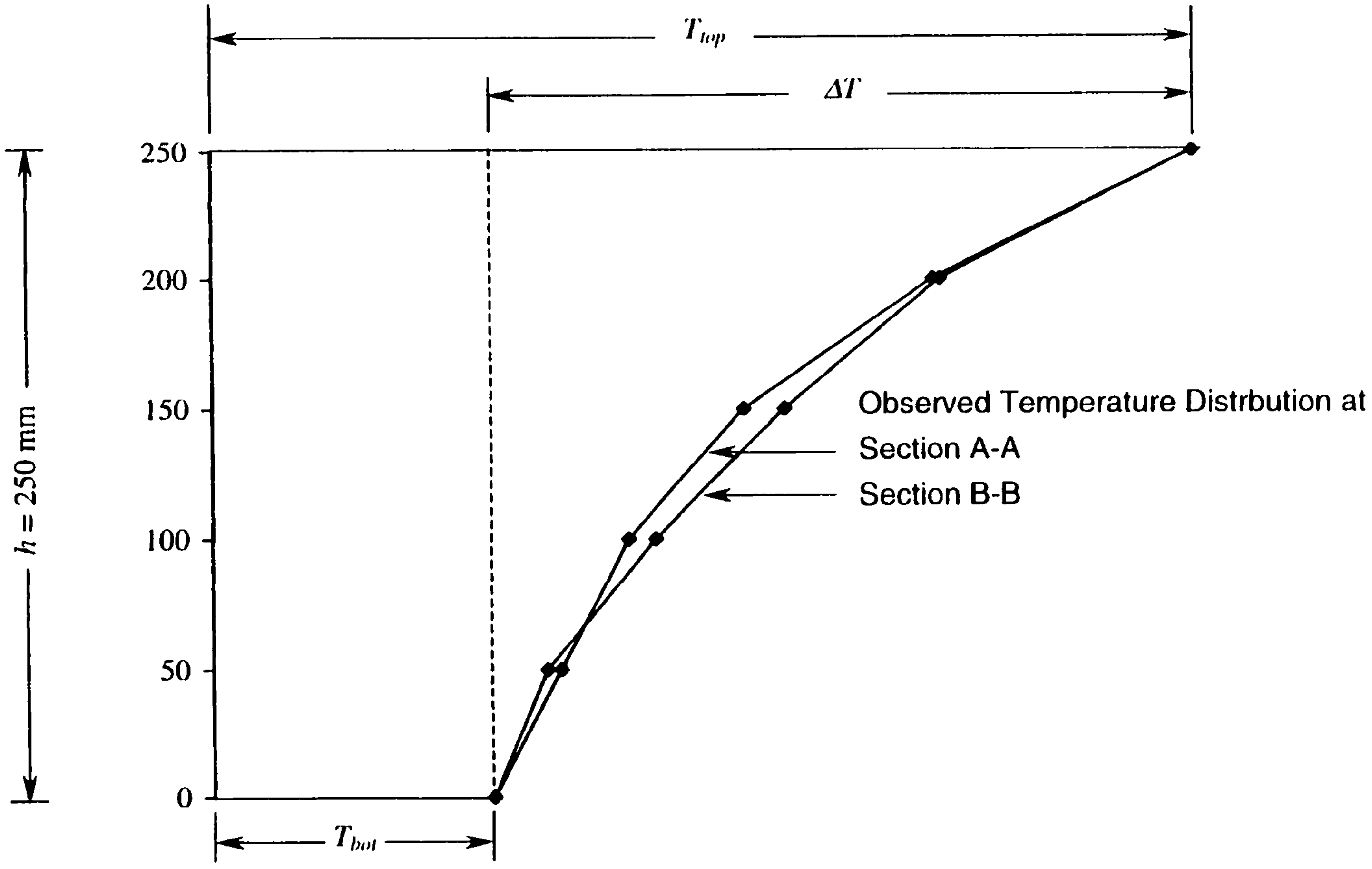

Figure 4.2 Observed Temperature Profile across the Beam Depth after 20 Hours of Heating

T_{10}), and T_{bot} is the temperature at the cool face (measured by thermocouple T_9). The restraint provided by the rigid steel arms to the rotation at the two ends of the beams produced by the temperature gradient causes a bending moment of constant magnitude along the tested length of the beam. Thus, the behavior of each beam can be described by the thermal moment-curvature relationship. The thermal curvature is given by:

$$\psi_{thermal} = \frac{\alpha_c \Delta T}{h} \tag{4.1}$$

where $\Delta T = T_{top} - T_{bot}$. The moment-curvature diagrams of all beams are presented and discussed in Subsections 4.3.1 to 4.3.3 for the beams reinforced with CFRP Leadline rods, the beams reinforced with NEFMAC mesh reinforcement and for the beams prestressed with the CFRP Leadline rods and steel strand, respectively.

The moment values plotted in the moment-curvature diagrams at $\psi_{thermal} = 0$ ($\Delta T = 0^{0}$C) represent the initial applied moment. Smaller values of this moment was chosen for beams reinforced with NEFMAC because cracking of these beams was expected to take place at a lower moment. A higher moment was used in partially prestressed beams to suppress the effect of the prestressing force, which increases the cracking moment.

4.3.1 Behavior of Beams Reinforced with Leadline

Figures 4.3 to 4.5 show the variation of thermal moment with thermal curvature for the three beams L.6, L.8, and L1.0 reinforced with Leadline of 0.6%, 0.8% and 1% reinforcement ratios, respectively. The results for the beams reinforced with the same ratios of steel rebars are also shown in the same figures 4.3 to 4.5. These steel reinforced beams are designed as S.6, S.8 and S1.0, respectively. It can be seen from the figures that a gradual increase in the thermal moment takes place with the increase in temperature

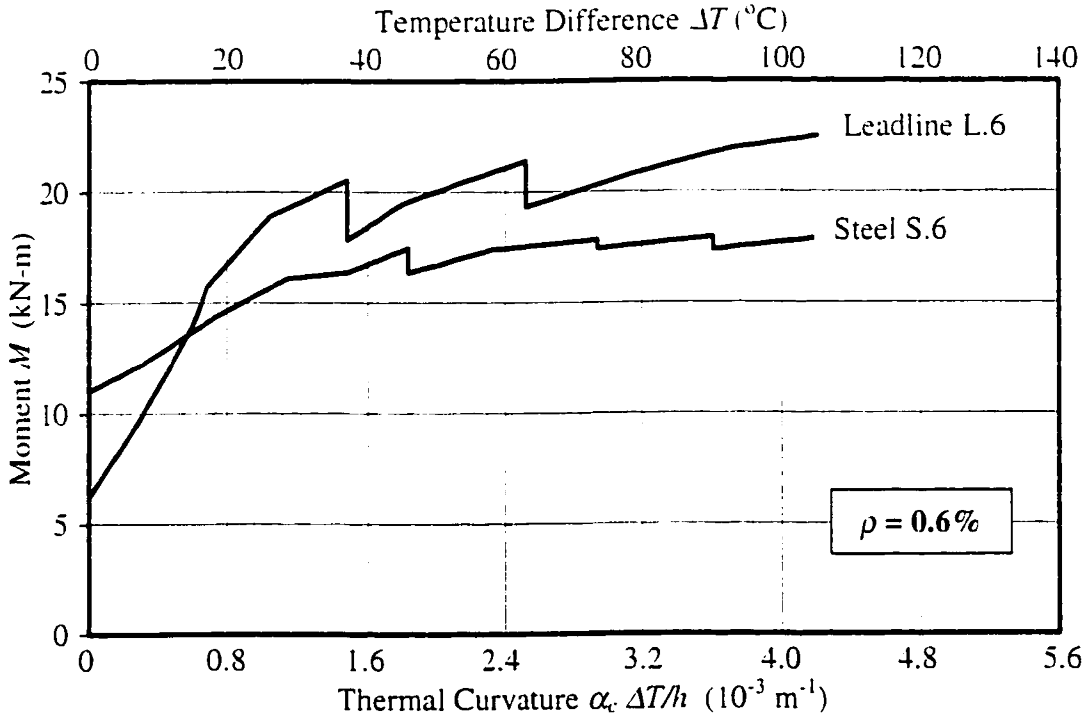

Figure 4.3 Bending Moment versus ΔT in Beams Reinforced with 0.6% Leadline or Steel

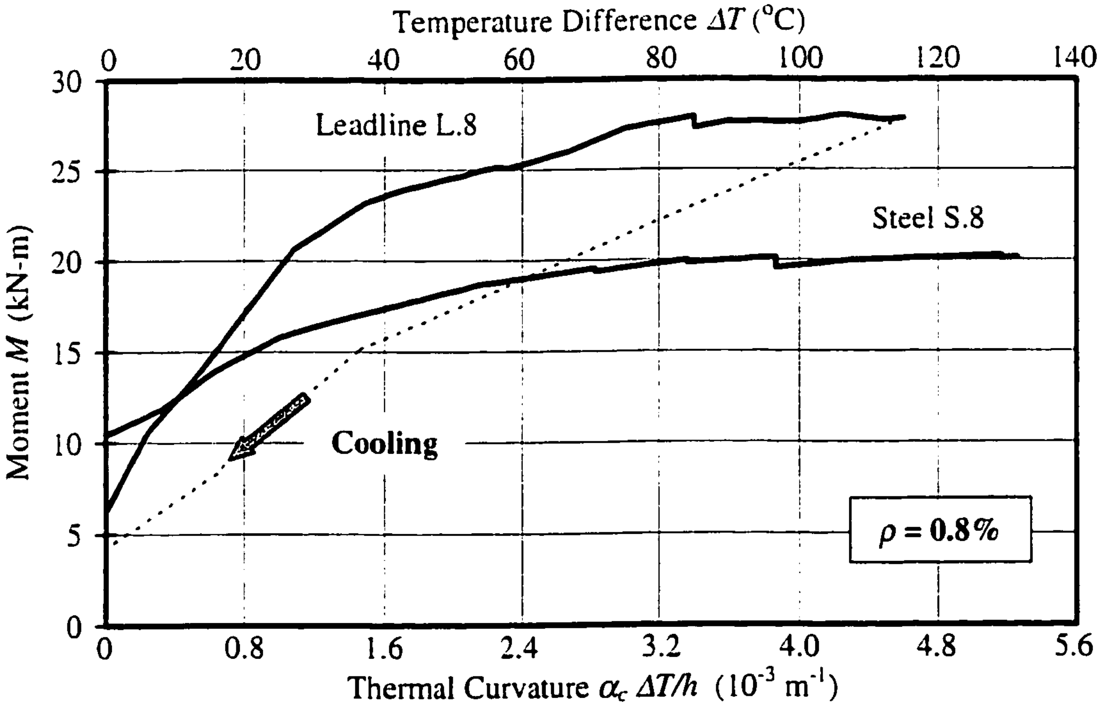

Figure 4.4 Bending Moment versus ΔT in Beams Reinforced with 0.8% Leadline or Steel

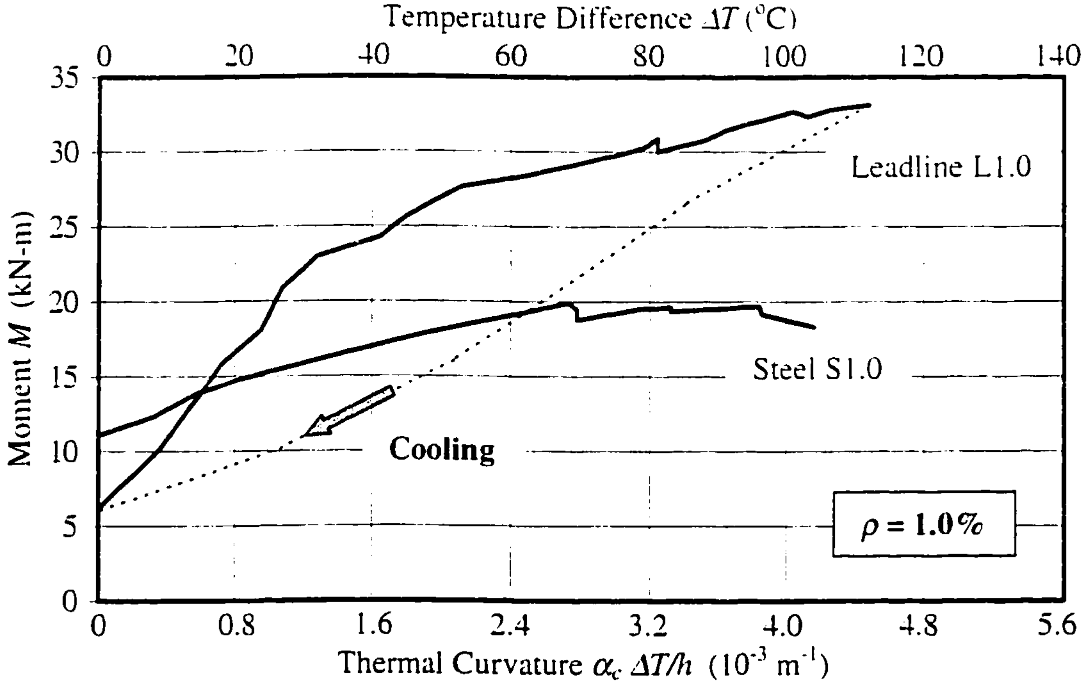

Figure 4.5 Bending Moment versus ΔT in Beams Reinforced with 1.0% Leadline or Steel

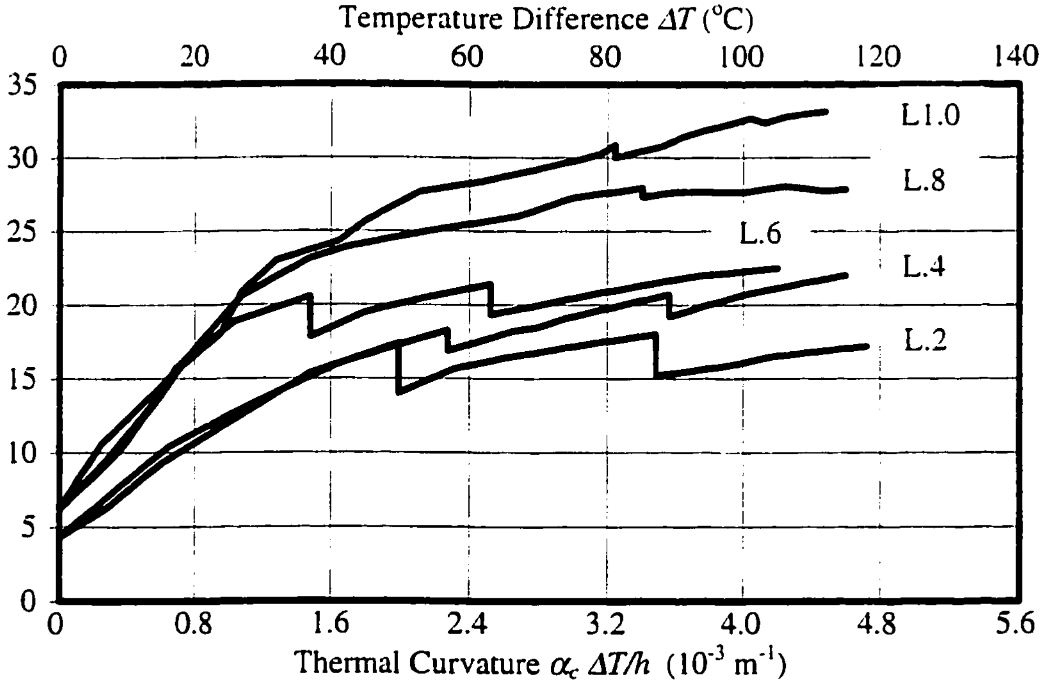

Figure 4.6 Bending Moment versus ΔT in Beams Reinforced with Leadline

difference for all the beams until the total moment (initial plus thermal) reaches the cracking moment and the first crack occurs at the weakest section. Since the bending moment is constant along the tested length of the beam, the first crack occurs randomly at the weakest section of the beam. Cracking reduces the stiffness of the beams, thus, a sudden drop in the thermal moment takes place after occurrence of the crack. The magnitude of the drop in the moment varies from one beam to another depending on the amount of reinforcement

In beam L.6, the increase in temperature gradient results in further increase in the thermal moment after the first crack until once again the cracking moment is reached and a second crack occurs at the next weakest section. The thermal moment at which the second crack took place is higher than the moment at the first crack. This is attributed to the fact that the tensile strength of concrete is not equal at all sections and that the longitudinal coefficient of thermal expansion, α_L, of CFRP is almost zero or small negative. As explained in Chapter 2, when temperature increases, the bond of the Leadline rod to the concrete restrains the large expansion of concrete relative to the reinforcement and creates compressive stresses that delays occurrence of the cracks due to thermal moment. The drop in thermal moment after the second crack is however smaller than that after the first crack. This is due to the further reduction in stiffness after occurrence of the second crack.

The three figures 4.3 to 4.5 show that for the same reinforcement ratio, the thermal moments of the Leadline reinforced beams are higher than those in the steel reinforced beams. This is despite the fact that the initial moment applied to the Leadline reinforced beams was smaller than that applied to the beams reinforced with steel. Beams L.6, L.8

and L1.0 continued to show an increase in the thermal moment up to the end of the test. On the other hand, the steel reinforced beams did not exhibit any significant increase in the thermal moment with the increase in thermal gradient as was noticed in the Leadline reinforced beams.

A comparison between the behavior of the three beams L.6, L.8 and L1.0 is shown in Figure 4.6. Included in the figure also are the thermal moment-curvature diagrams for beams L.2 and L.4 reinforced with 0.2% and 0.4% Leadline, respectively, and tested by El-Badry and Abdalla (1998). As the figure shows, increasing the reinforcement ratio from 0.2% to 1.0% improved the thermal behavior of the beams reinforced with Leadline.

The thermal behavior of beams L.8 and L1.0 during cooling is plotted in Figures 4.4 and 4.5. The thermal moment readings were recorded immediately after the heating source was terminated and until all the thermocouple readings reached the room temperature. It can be seen that the thermal moment decreased with the decrease in temperature gradient until it reached the value of the initial applied moment. When the temperature difference became zero (room temperature on both sides of the test beam), all the cracks that occurred during the thermal test closed.

4.3.2 Behavior of Beams Reinforced with NEFMAC

The thermal moment-curvature diagrams for the beams reinforced with NEFMAC grids are shown in Figures 4.7 to 4.9. In each of these figures, the diagrams for beams S.4 and S.6 reinforced with 0.4% and 0.6% steel are also shown for comparison.

Since beam GM.5 was reinforced with one layer of NEFMAC at mid-depth of the cross-section and there was no reinforcement provided close to the tension face of the beam, it was expected that cracking of this beam would take place at a lower moment

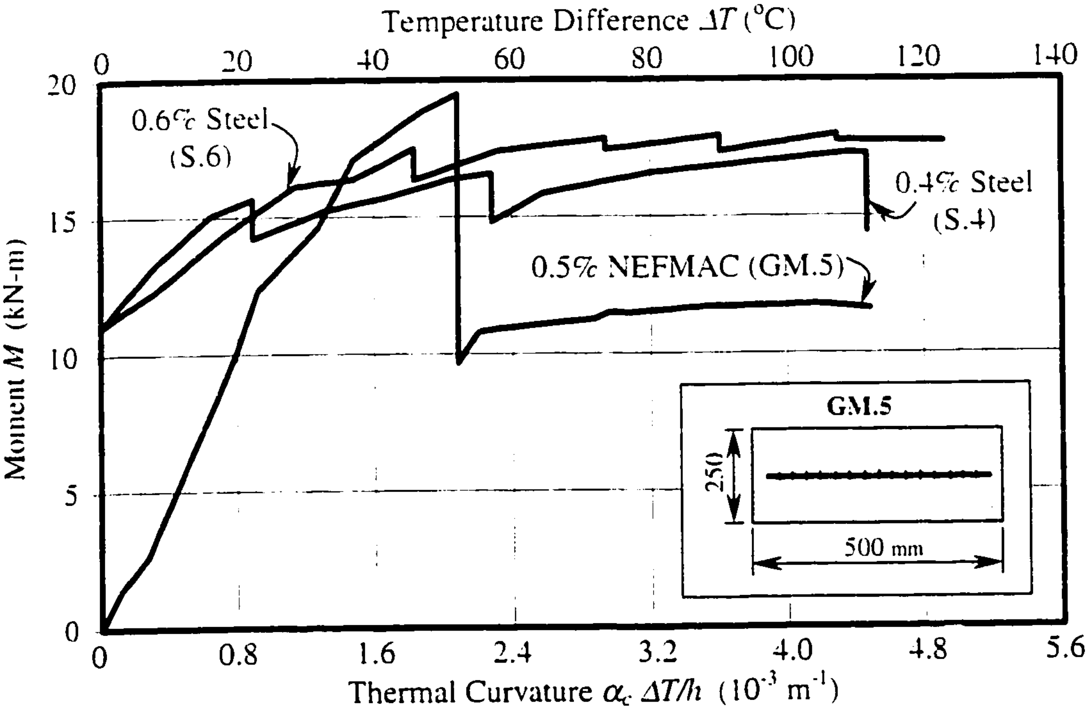

Figure 4.7 Bending Moment versus *ΔT* in Beams Reinforced with Steel or with NEFMAC at Mid-depth

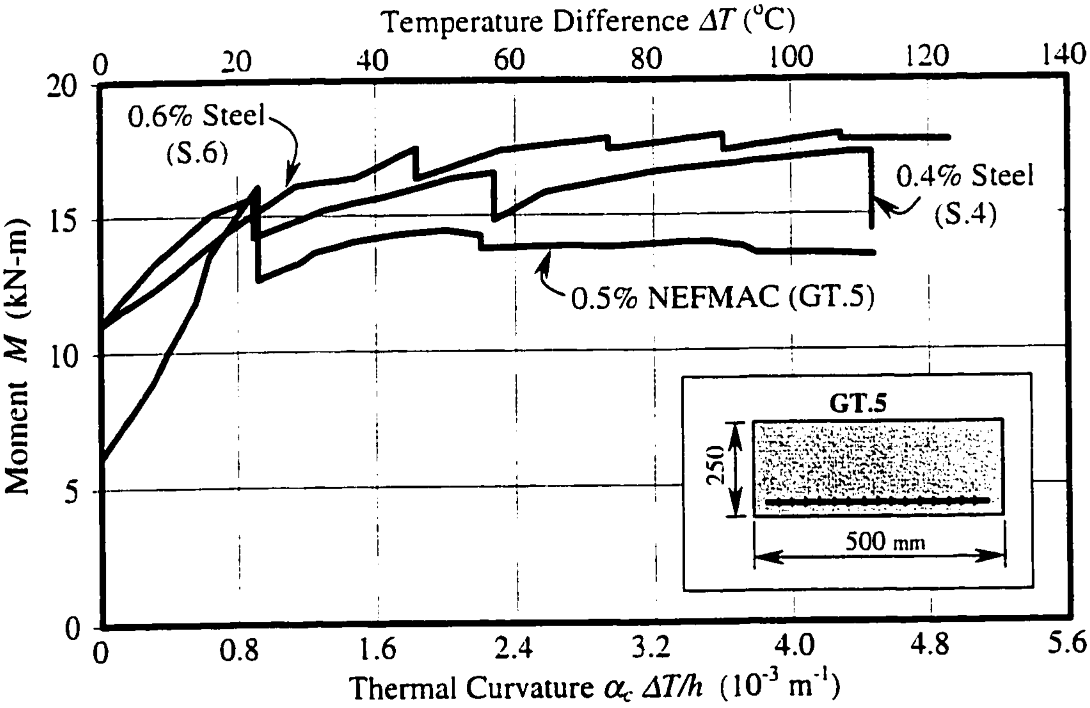

Figure 4.8 Bending Moment versus *ΔT* in Beams Reinforced with Steel or with NEFMAC on the Tension Face

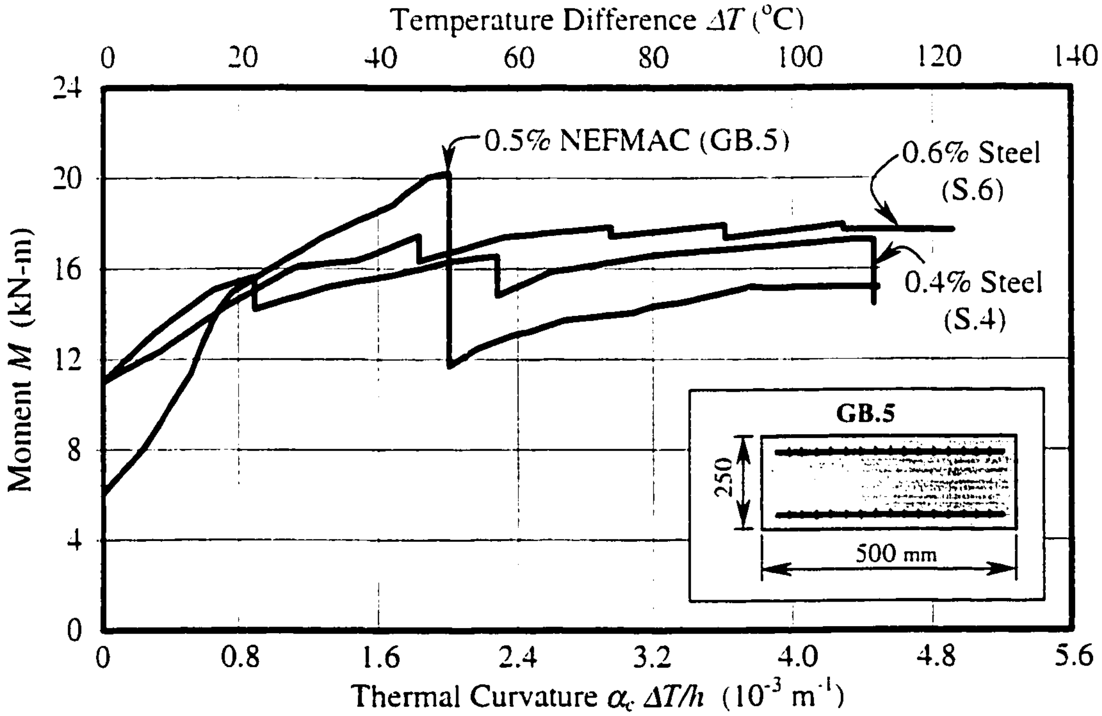

Figure 4.9 Bending Moment versus ΔT in Beams Reinforced with Steel or with NEFMAC on Both Sides

than beams GT.5 and GB.5, reinforced with NEFMAC close to the tension face and on both faces, respectively. Therefore, a zero initial moment was chosen for beam GM.5.

Figures 4.7 to 4.9 show that the thermal behavior of the beams reinforced with NEFMAC is completely different from the behavior of the beams reinforced with steel or with Leadline rods. As can be seen, the thermal moment gradually increased with the increase in temperature gradient until the total moment reached the cracking moment. Consequently, the first crack occurred accompanied with a drop in thermal moment. The drop in the thermal moment due to cracking was larger in these beams than in those reinforced with steel or Leadline. This may be attributed to the smaller elasticity modulus of the GFRP NEFMAC (29.4 GPa) than that of steel (200 GPa) or CFRP Leadline (142 GPa). After occurrence of the first crack, beams GM.5, GT.5 and GB.5 did not show any significant increase in thermal moment at higher temperature gradients. This was because only one major crack occurred in each of the three beams and with the increase in temperature all thermal deformations were concentrated at that single crack

4.3.3 Behavior of Beams Prestressed with Leadline and Steel Tendons

The variation of thermal moment with thermal curvature for the PPC beams of series B during the thermal tests is shown on Figures 4.10 to 4.14. Similar to other beams a gradual increase in thermal moment takes place with the increase in temperature gradient until the thermal moment reaches the cracking moment of the concrete section causing a crack and a sudden drop in the thermal moment. The magnitude of the drop in the moment was larger in beams with low reinforcement ratio of 0.1% as can be seen in the figures. Increasing the temperature after the first drop in the moment resulted in further increase in thermal moment but with slower rate, particularly in beams PrLCL.1,

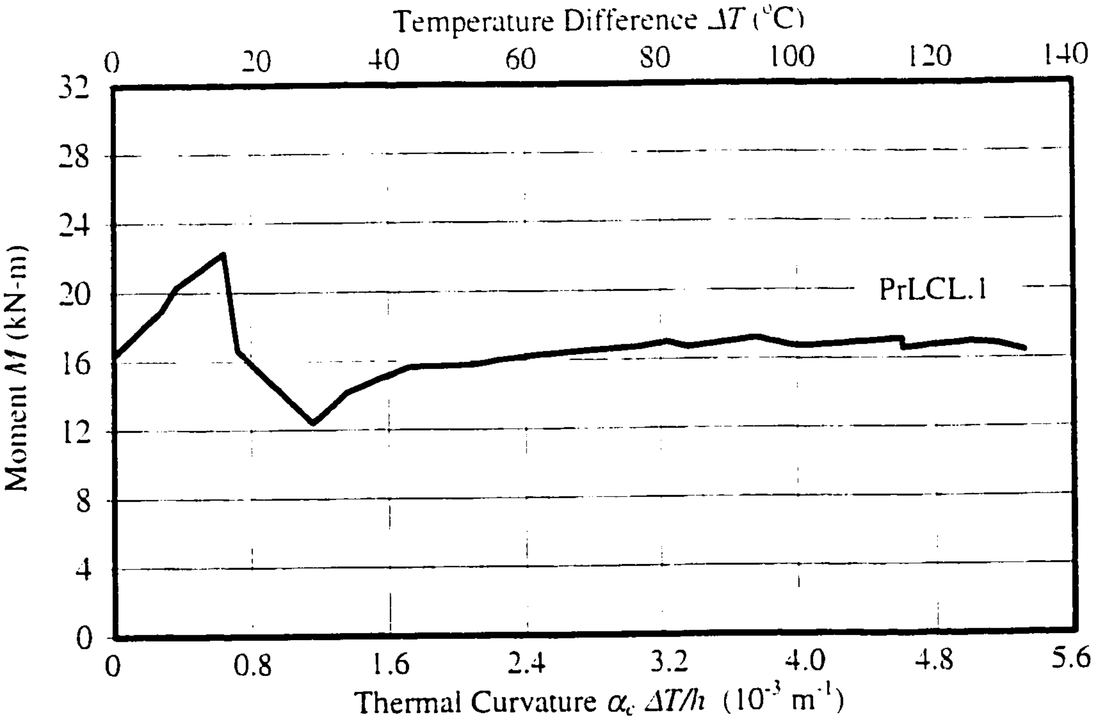

Figure 4.10 Bending Moment versus ΔT in Beam PrLCL.1 Pre-tensioned with Concentric Leadline Tendon

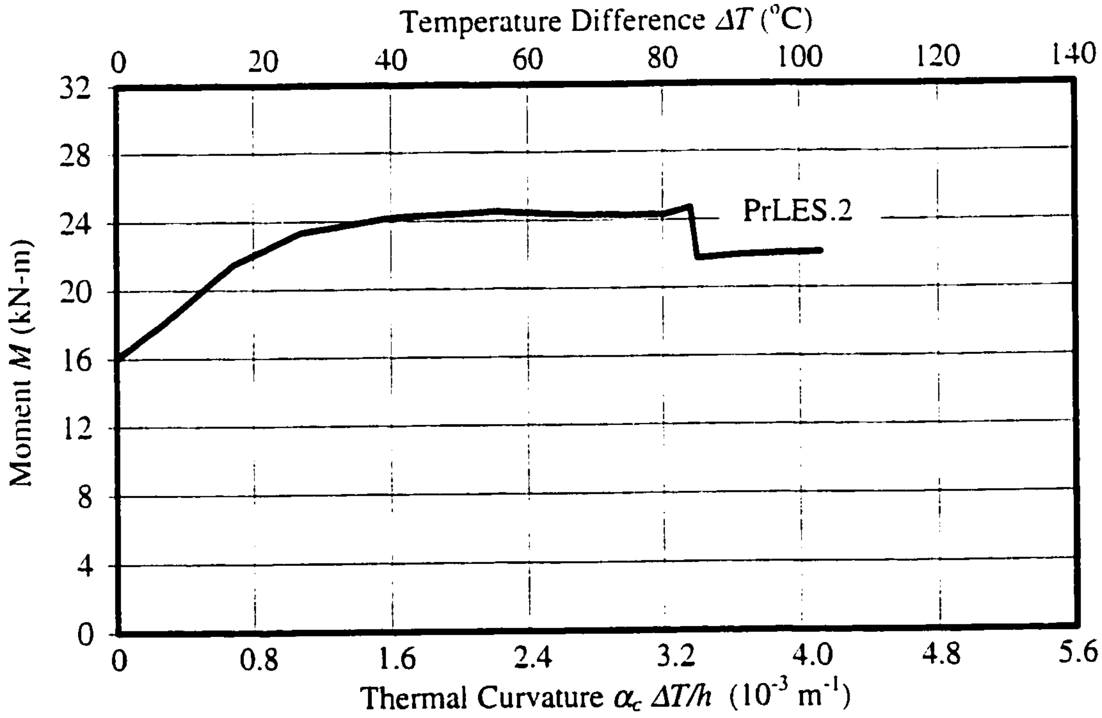

Figure 4.11 Bending Moment versus ΔT in Beam PrLES.2 Pre-tensioned with Eccentric Leadline Tendon

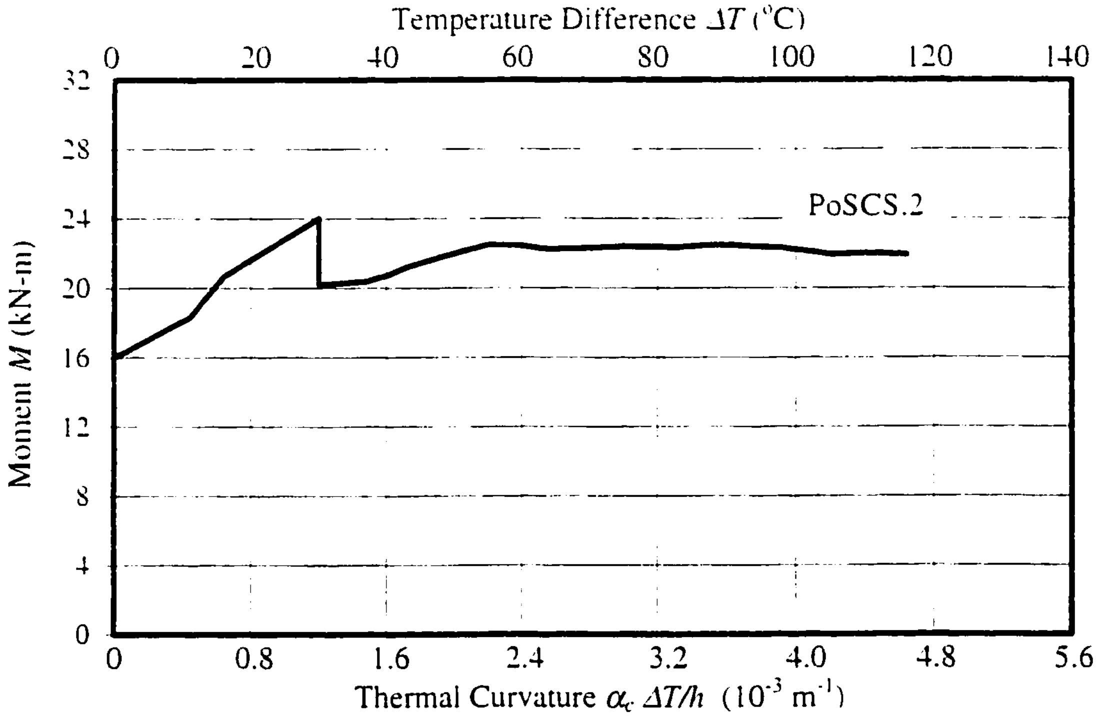

Figure 4.12 Bending Moment versus ΔT in Beam PoSCS.2 Post-tensioned with Concentric Steel Strand

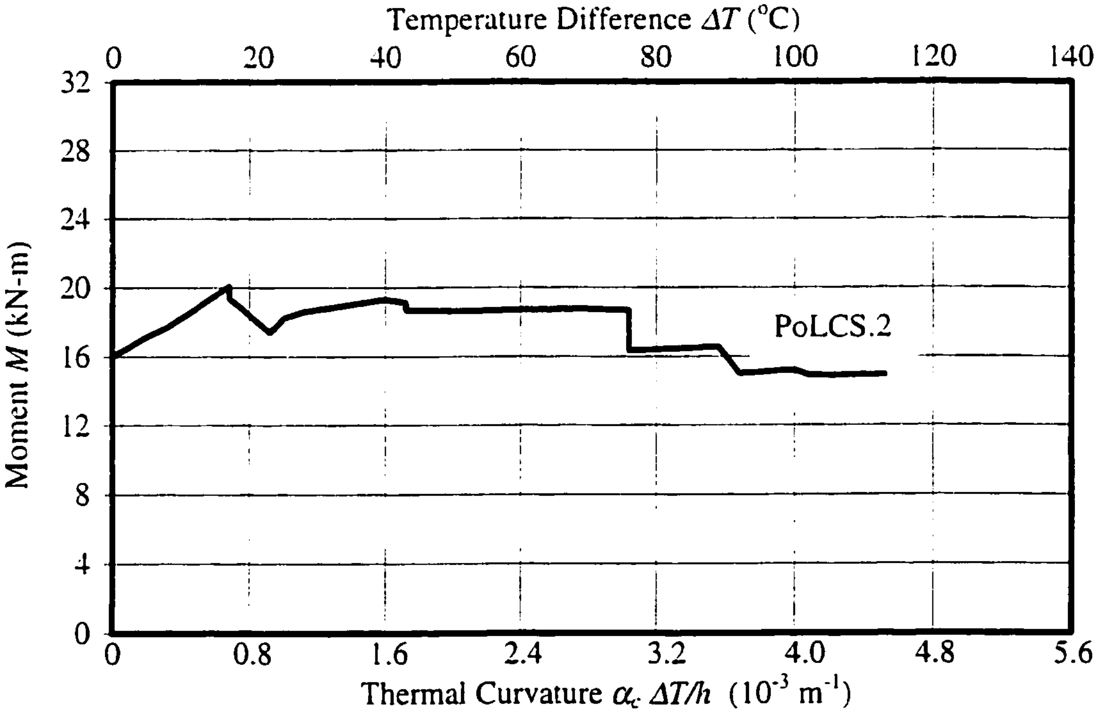

Figure 4.13 Bending Moment versus ΔT in Beam PoLCS.2 Post-tensioned with Concentric Leadline Tendon

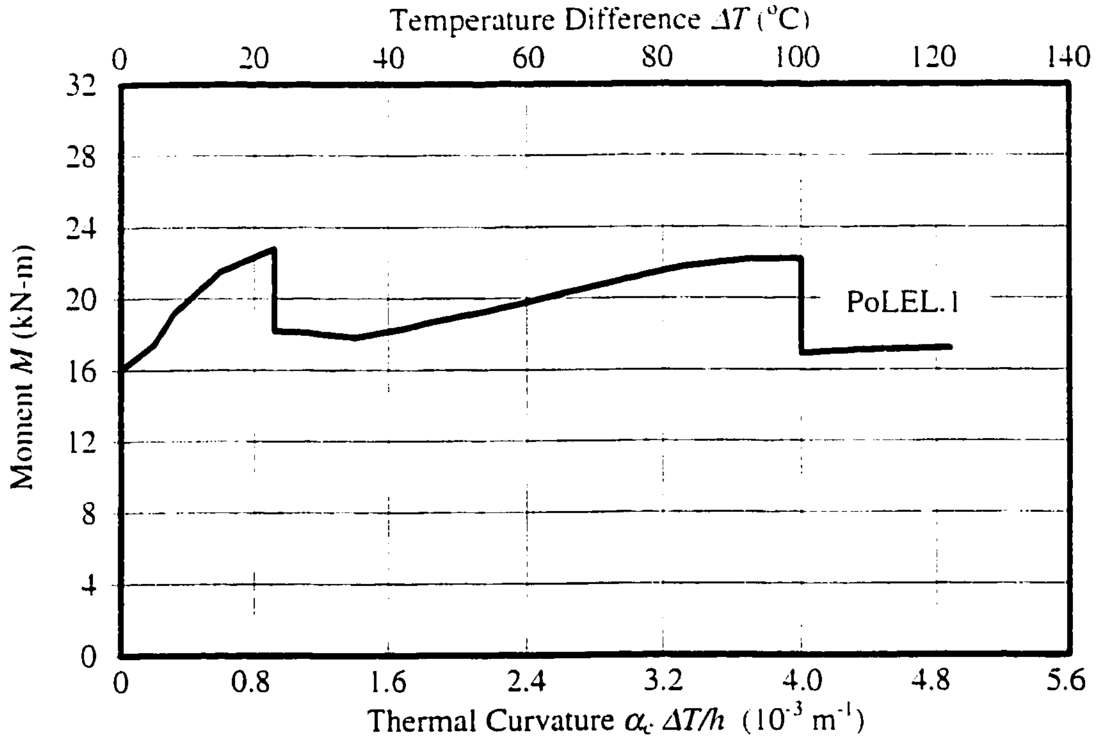

Figure 4.14 Bending Moment versus ΔT in Beam PoLEL.1 Post-tensioned with Eccentric Leadline Tendon

PoSCS.2 and PoLCS.2 prestressed with concentric tendons. These beams did not exhibit any increase in thermal moment above the moment at the first crack. It is clear that the eccentricity of the prestressing tendon improved the performance of the concrete beams under temperature gradient. This is due to the increase in tension in the eccentric tendon and hence the moment due to prestressing with the increase in temperature. Also, the pretensioned beams exhibit better performance than the post-tensioned beams. This is attributed mainly to the bond of the pretensioned tendons to the concrete. The beam PoSCS.2 post-tensioned with a concentric steel strand showed higher thermal moment than beam PoLCS.2 post-tensioned with the Leadline tendon.

4.3.4 Comparison of the M-$\psi_{thermal}$ Behavior of all Beams

Further to the graphs in Figure 4.3 to 4.14, Table 4.1 gives values of thermal moments developed at the first and second cracks for all beams, the temperature difference at which the two cracks took place and the drop in the thermal moment after occurrence of each of the two cracks.

As can be seen from the M-ψ graphs and the table, the thermal moment in beams reinforced with Leadline was higher than that in beams reinforced with NEFMAC and beams prestressed with Leadline. This indicates the higher stiffness of the CFRP reinforced beams than the rest of test beams. The smallest number of cracks and the largest drop in thermal moment were observed in the beams reinforced with NEFMAC grids.

Table 4.1: Thermal Moment at the First & Second Drops in all Beams

Beam Designation	Group Name	Initial Prestress (MPa)	Initial Applied Moment (kN-m)	Thermal Moment at the First Droop			Thermal Moment at the Second Droop		
				Thermal Moment (kN-m)	Drop in Moment (kN-m)	ΔT (°C)	Thermal Moment (kN-m)	Drop in Moment (kN-m)	ΔT (°C)
L.2*	-	-	4	17.35	2.77	50	17.99	2.77	87
L.4*	-	-	4	18.28	1.29	57	20.73	1.53	89
L.6	A1	-	6	20.55	2.72	37	21.40	2.07	63
L.8	A1	-	6	27.92	0.62	85	-	-	-
L1.0	A1	-	6	30.89	0.87	81	-	-	-
GM.5	A2	-	0	19.47	9.80	52	-	-	-
GT.5	A2	-	6	16.09	3.46	23	14.24	0.48	55
GB.5	A2	-	6	20.22	8.51	50	-	-	-
PrLCL.1	B1	0.5	16	22.26	5.63	16	17.11	0.54	115
PrLES.2	B1	0.5	16	24.69	3.00	84	-	-	-
PoLCS.2	B2	0.5	16	20.09	2.69	17	18.67	1.73	76
PoLEL.1	B2	0.5	16	22.80	3.45	23	22.21	5.28	100
PoSCS.2	B2	0.5	16	24.04	3.83	30	-	-	-
S.2**	-	-	10	16.41	3.20	28	16.84	4.11	79
S.4**	-	-	11	15.65	1.43	22	16.57	1.64	57
S.6**	-	-	11	17.48	1.13	46	17.84	0.40	73
S.8**	-	-	10	20.0	0.17	84	20.15	0.60	97
S1.0**	-	-	11	19.48	0.68	70	19.64	0.29	83

Note: ΔT = Temperature Difference (T_{top}-T_{bot})

* El-Badry and Abdalla (1998)

** Ariyawardena (1993)

4.4 Maximum Crack Width and Crack Spacing

General speaking, crack width and crack spacing depend on many factors, which include the reinforcement ratio, distribution of reinforcement in the concrete section, steel flexural stress, concrete cover and properties of the concrete. Cracks are caused by the difference in strain in the reinforcement and the concrete at the section considered. El-Badry and Ghali (1995) explained that a fully developed crack pattern is not normally attained in concrete structures subjected to temperature gradients produced by weather conditions. Only a few cracks may develop and widen under the increase of temperature.

A typical view of the crack patterns in the beams of Group A1 reinforced with Leadline rods and Group A2 reinforced with NEFMAC are shown in Figures 4.15 and 4.16, respectively. The number of cracks, crack spacing and the crack widths of all cracks under the maximum temperature difference are shown in Table 4.2 for all beams.

4.4.1 Maximum Crack Width and Crack Spacing of Beams Series A

Figure 4.17 presents plots of maximum measured crack width versus the temperature difference in beams of Group A1 reinforced with Leadline rods. A comparison with the behavior of beams S.6, S.8 and S1.0 reinforced with steel is shown in figures 4.18 to 4.20, respectively. As can be seen, for reinforcement ratios smaller than 1.0%, the beams reinforced with Leadline always exhibit larger crack width than the beams reinforced with steel. It can also be seen that increasing the reinforcement ratio reduced the crack width from 0.33 to 0.1 mm in beams L.6 and L1.0, respectively, (Fig. 4.17). It is seen that the crack width for beams L.8 and L1.0 increased at a very slow rate. This behavior is attributed to the fact that the Leadline rods have small positive or negative coefficient of

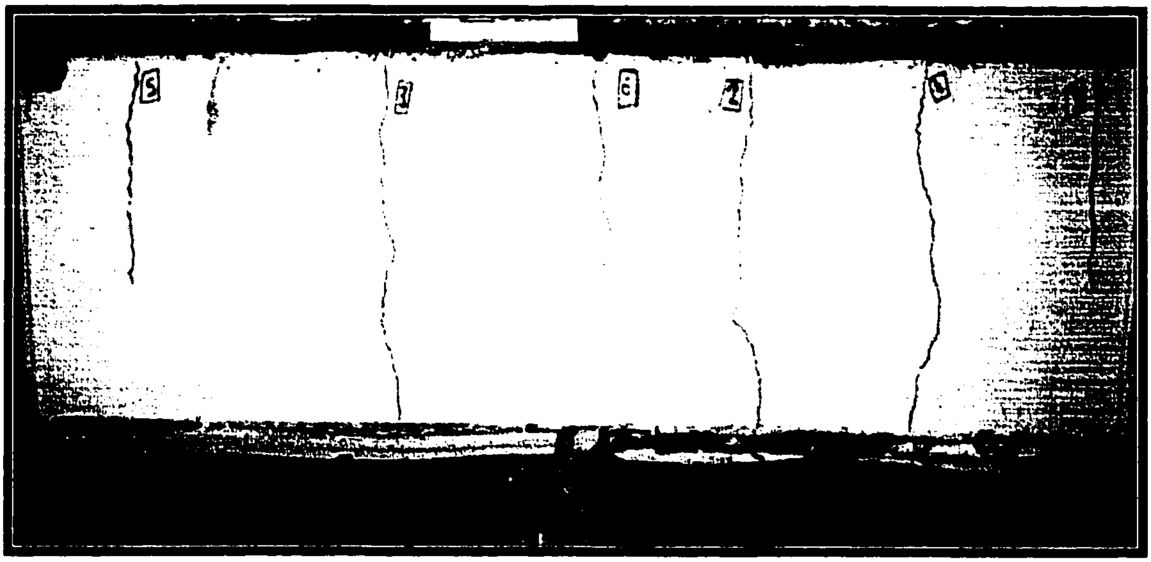

Figure 4.15 Crack Pattern in Beam L.8 due to Temperature Gradient

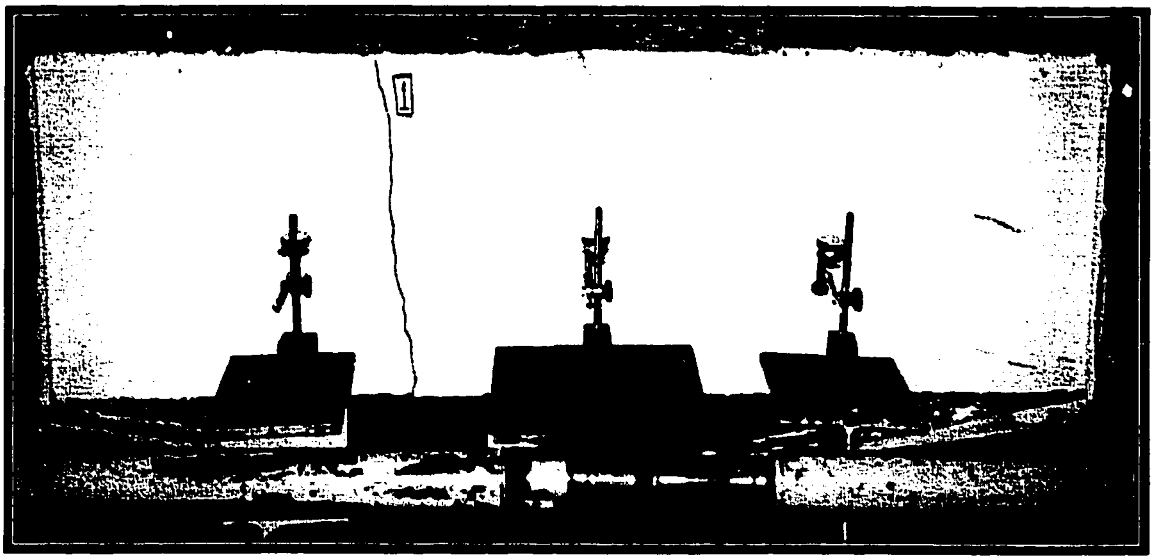

Figure 4.16 Crack Pattern in Beam GM.5 due to Temperature Gradient

Table 4.2: Maximum Crack Width and Crack Spacing for Prestressed and Nonprestressed Beams

Beam Designation	Group Name	Number of Cracks	Crack Width at the Maximum Temperature Difference (mm)									Measured Crack Spacings (mm)		
			C1	C2	C3	C4	C5	C6	C7	C8	C9	S_{max}	S_{min}	S_{avg}
L.6	A1	5	**0.33**	0.08	0.30	0.05	0.08					710	160	270
L.8	A1	6	**0.15**	0.08	0.10	0.08	0.15	0.15				450	270	340
L1.0	A1	4	**0.10**	0.05	0.08	0.05						540	370	460
GM.5	A2	1	**1.50**									at 1/3 span		
GT.5	A2	2	**1.70**	0.8								Close to the left end		
GB.5	A2	1	**1.50**									at 1/3 span		
PrLCL.1	B1	2	**1.00**	0.08								1200		
PrLES.2	B1	9	**0.33**	0.20	0.25	0.33	0.20	0.25	0.15	0.25	0.20	360	200	280
PoLCS.2	B2	4	**0.50**	0.33	0.30	0.30						730	400	510
PoLEL.1	B2	2	**1.50**	0.60								1570		
PoSCS.2	B2	1	**1.40**									at 1/3 span		

☐ Indicate the maximum measured crack width in each beam.

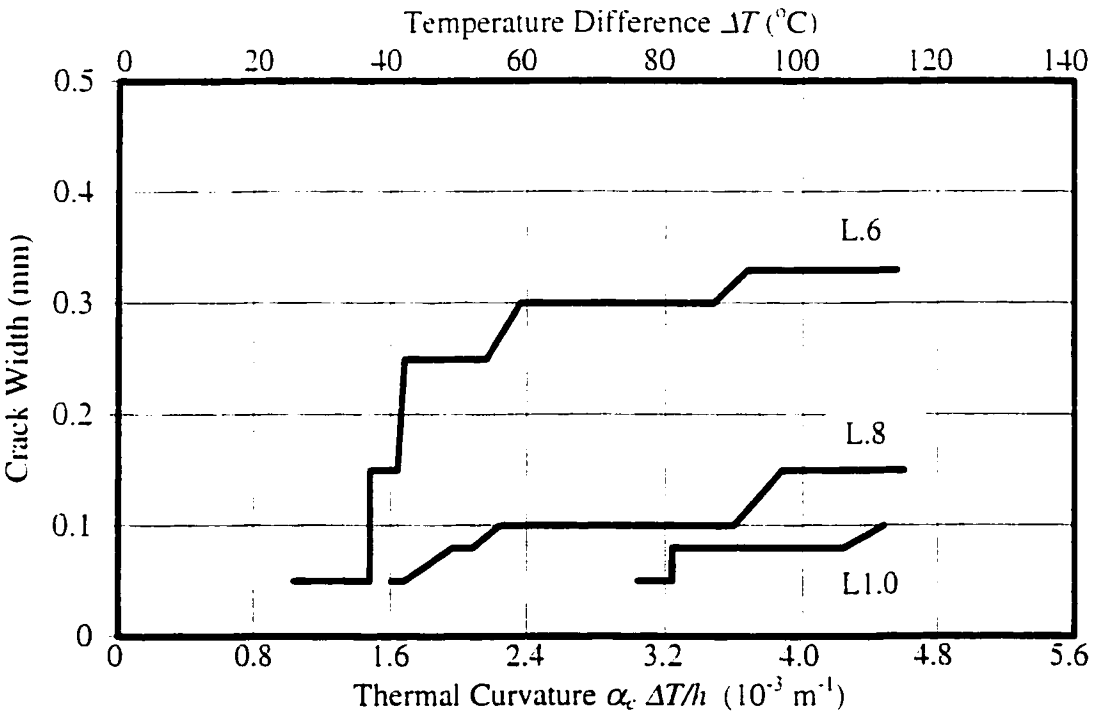

Figure 4.17 Maximum Crack Width for Beams Group A1 Reinforced with Leadline Rods

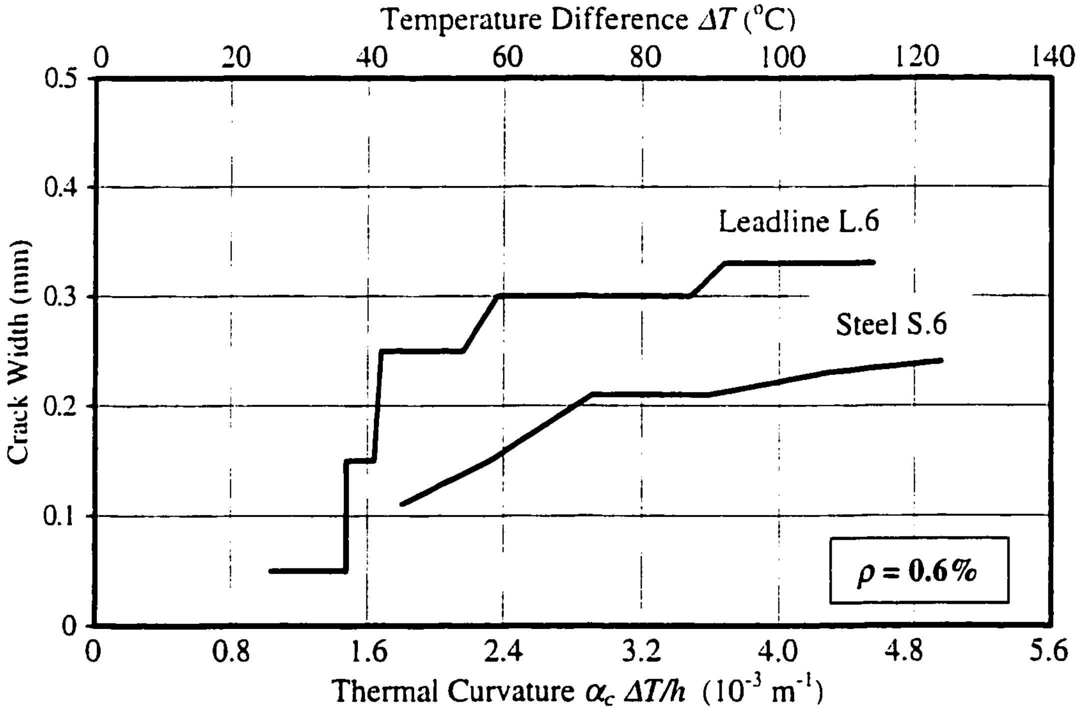

Figure 4.18 Maximum Crack Width for Beams Reinforced with 0.6% Leadline or Steel

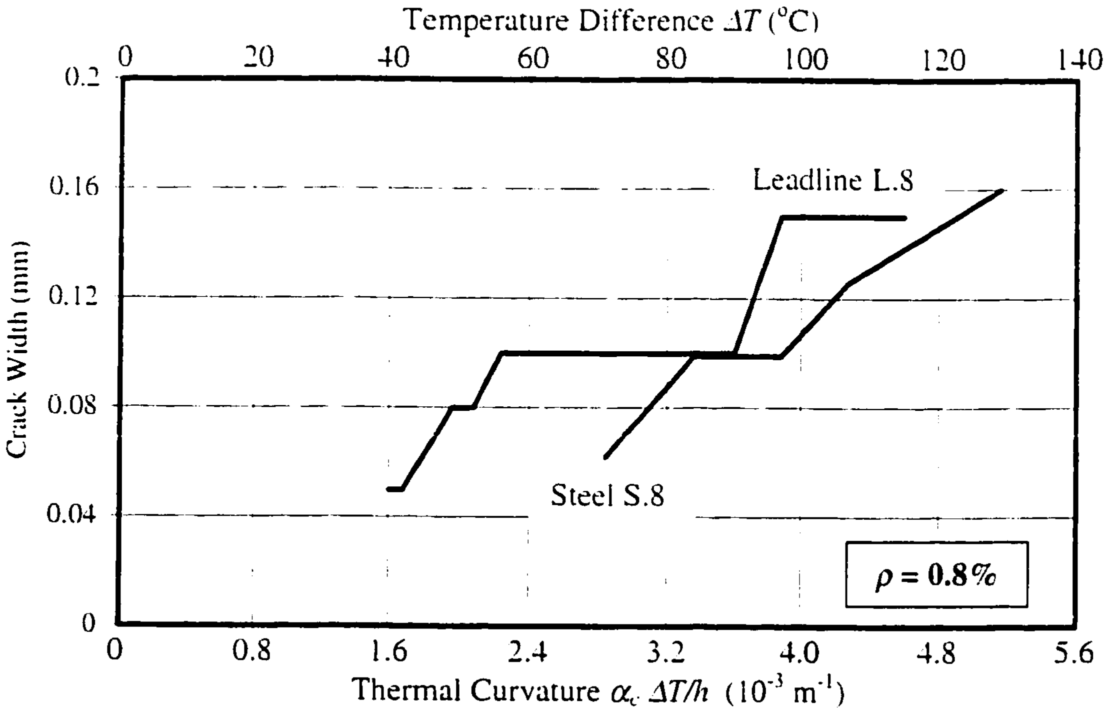

Figure 4.19 Maximum Crack Width for Beams Reinforced with 0.8% Leadline or Steel

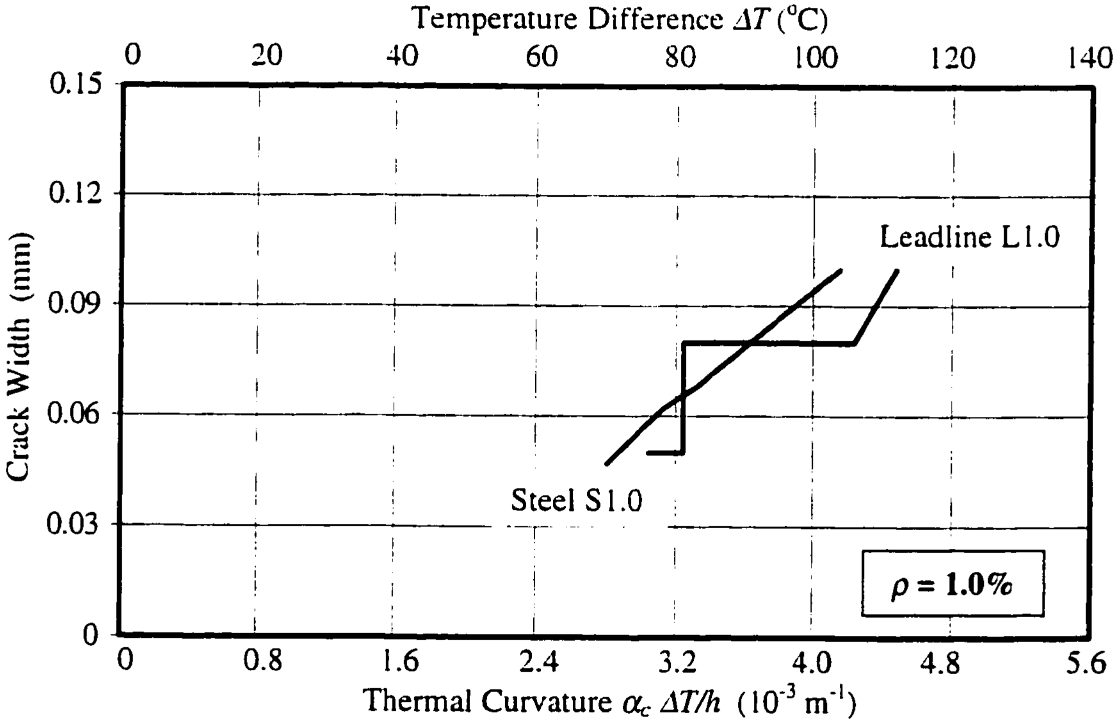

Figure 4.20 Maximum Crack Width for Beams Reinforced with 1.0% Leadline or Steel

thermal expansion relative to concrete and under temperature rise produce compression in the concrete reducing the crack width. The measured crack width in beams L.6, L.8 and L1.0 ranged from 0.1 to 0.33 mm, which satisfied the limiting crack width specified in Clause 10.6.1 of CSA-A23.3-94 Standard.

Figure 4.21 shows the variation of crack width with ΔT in beams GM.5, GT.5 and GB.5 reinforced with NEFMAC. These beams exhibited the largest crack width measured among all the tested beams. Figures 4.21 clearly shows the large difference in crack width between the NEFMAC reinforced beams and the steel reinforced beams. Only one crack developed in each of the beams reinforced with NEFMAC. The width of this single crack increased with the increase in temperature difference absorbing all thermal rotation of the beam. At $\Delta T = 50^{\circ}C$ the crack in each of the three beams was 0.6 mm wide and at the end of the test, at $\Delta T = 110^{\circ}C$, the crack width ranged from 1.5 mm in beam GM.5 to 1.7 mm in beam GT.5. At ΔT greater than 30°C, the crack width in any of the beams exceeded the 0.4 mm limit specified in CSA-A23.3-94 Standards.

Details of the measured maximum crack width, number of cracks and crack spacing in all beams reinforced with either FRP or steel reinforcement are given in Table 4.3.

4.4.2 Maximum Crack Width and Crack Spacing of Beams Series B

Figures 4.22 and 4.23 show the variation of the maximum measured crack width with temperature difference for beams of Series B partially prestressed with Leadline tendon or steel strand. As can be seen, the crack width in pretensioned beams is smaller than that in the beams post-tensioned with unbonded tendons. This confirms the effect of bond of reinforcement on the control of cracking in reinforced concrete beams with or without

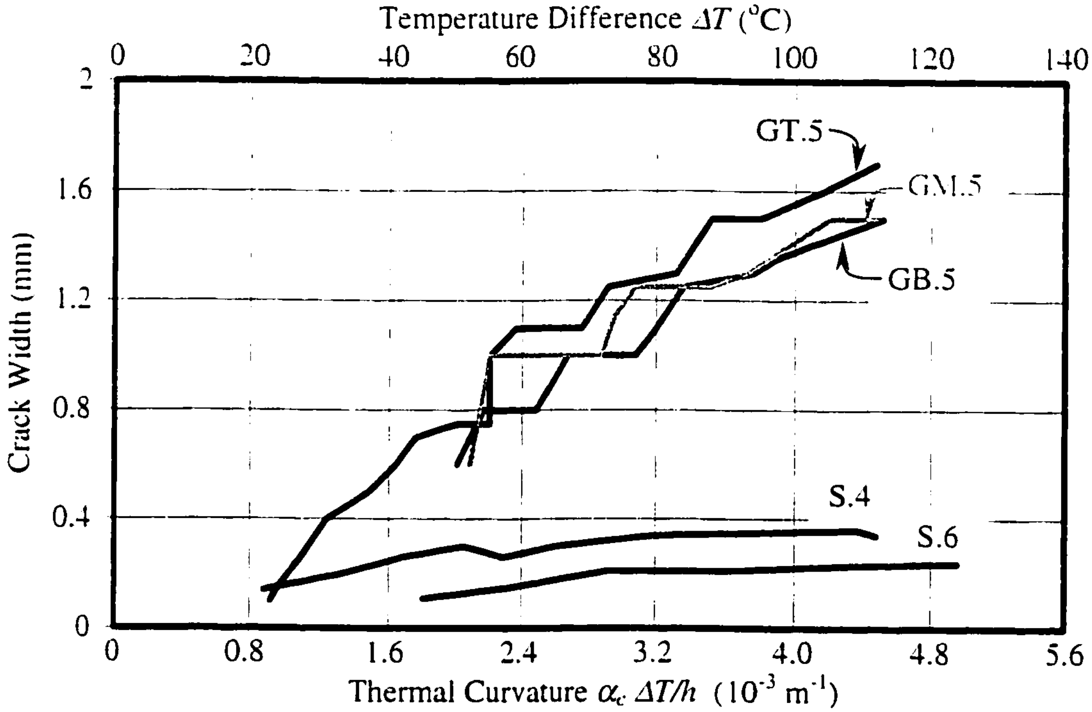

Figure 4.21 Maximum Crack Width for Beams Group A2 Reinforced with NEFMAC and Beams Reinforced with Steel

Table 4.3 Measured Crack Width and Number of Cracks Observed for all Reinforced Beams of Series A Compared with Beams Reinforced with Steel

Reinforcement Type		Beam Designation	Maximum Moment (kN-m)	Total Number of Cracks	Maximum Crack Width (mm)	Measured Crack Spacing (mm)		
						S_{max}	S_{min}	S_{avg}
FRP	Leadline	L.2*	17.99	4	0.65	400	400	400
	Leadline	L.4*	22.61	4	0.40	400	400	400
	Leadline	L.6	22.50	5	0.33	710	160	270
	Leadline	L.8	27.92	6	0.15	450	270	340
	Leadline	L1.0	32.78	4	0.1	540	370	460
	NAFMAC	GM.5	19.44	1	1.5			
	NAFMAC	GT.5	16.09	2	1.7	30		
	NAFMAC	GB.5	20.22	1	1.5			
Steel	Steel	S.2**	16.84		0.5			
	Steel	S.4**	17.29	3	0.36	850	570	710
	Steel	S.6**	17.98	5	0.24	530	345	407
	Steel	S.8**	20.25	5	0.16	470	325	404
	Steel	S1.0**	19.74	5	0.1	460	265	390

* El-Badry and Abdalla (1998)

** Ariyawardena (1993)

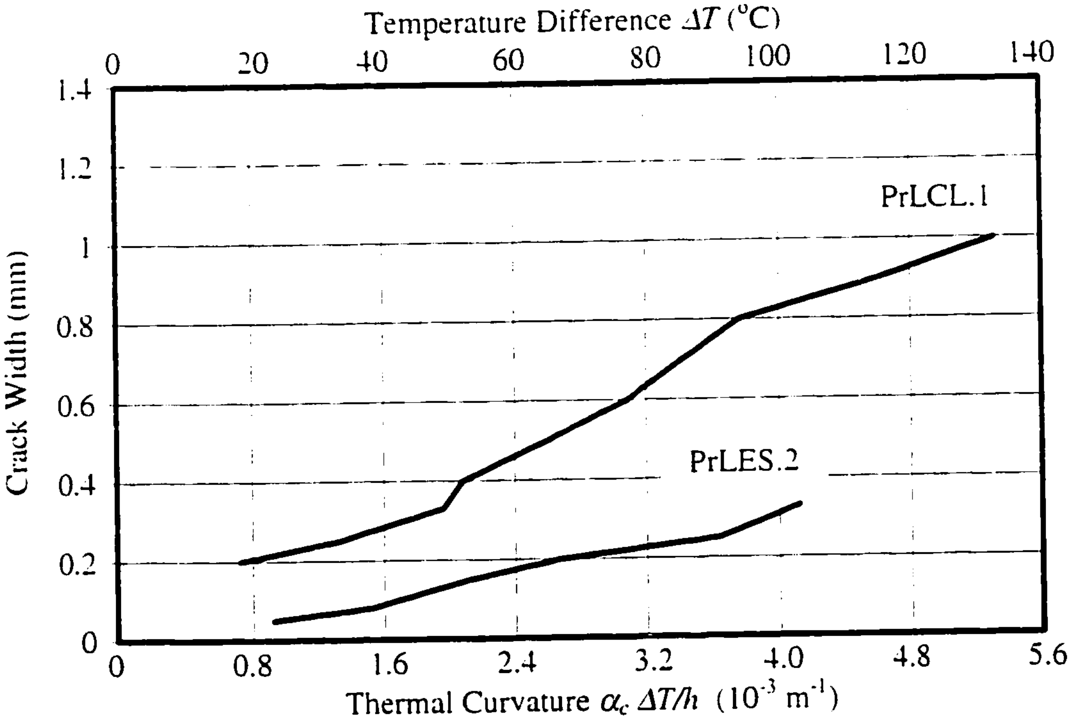

Figure 4.22 Maximum Crack Width for Beams Group B1 Pretensioned with Leadline Tendons

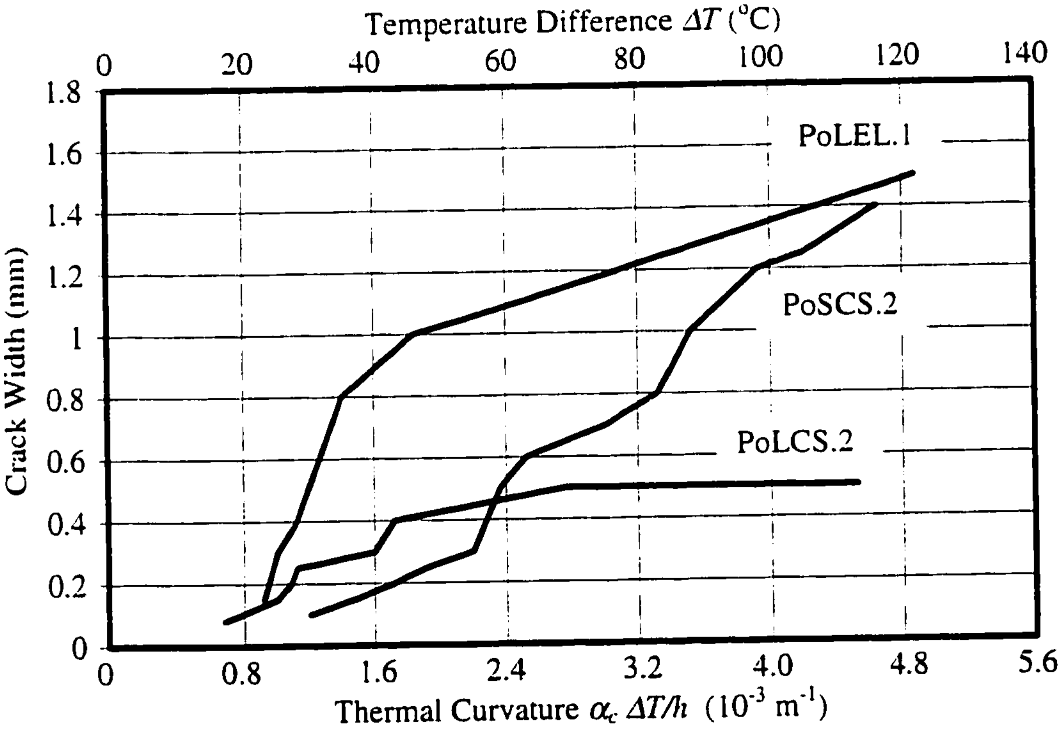

Figure 4.23 Maximum Crack Width for Beams Group B2 Post-tensioned with Leadline Tendons or Steel Strand

prestressing. Also, for the same type and amount of nonprestressed reinforcement on the tension face and for the same location of prestressing tendon, and for $\Delta T > 60^{\circ}C$, beam PoLCS.2 post-tensioned with Leadline tendon exhibited smaller crack width than beam PoSCS.2 post-tensioned with steel strand. This is attributed to the increase in the compressive stress induced by the Leadline tendon on concrete as the temperature increases. It is also evident from the graphs that the amount of nonprestressed reinforcement has a major role in reducing the width of cracks.

A well-developed crack pattern over the tested length in beams of Series B was clearly noted in beam PrLES.2 pretensioned with Leadline as shown in Figure 4.24. It can be also observed that the variation of the crack width and crack spacing is much lesser in beam PrLES.2 than in the other prestressed beams as indicated in Table 4.2.

In the present investigation of Series B, the maximum crack width measured at ΔT = 100°C in beams PrLCL.1, PoLCS.2, PoLEL.1 and PoSCS.2 ranged from 0.5 to 1.35 mm, exceeding the limiting crack width of 0.40 and 0.33 mm specified in Clause 10.6.1 of CSA A23.3-94 Standards. This could be related to reasons that a compressive stress of 0.5 MPa produced by prestressing in the test beams was not sufficient or the amount of nonprestressed reinforcement was too small to control cracking. Crack width can be minimized by provision of sufficient amount of nonprestressed steel in the tension zone and by selecting appropriate bar diameters and spacing.

Steel stirrups were provided only within the tested length of all beams pre- and post-tensioned with Leadline. It was noted that in these beams cracks took place at the stirrup locations uniformly spaced at 400 mm. This confirms that stirrups act as initiator for most of the flexural cracks regardless of the type of prestressing reinforcement and thus have

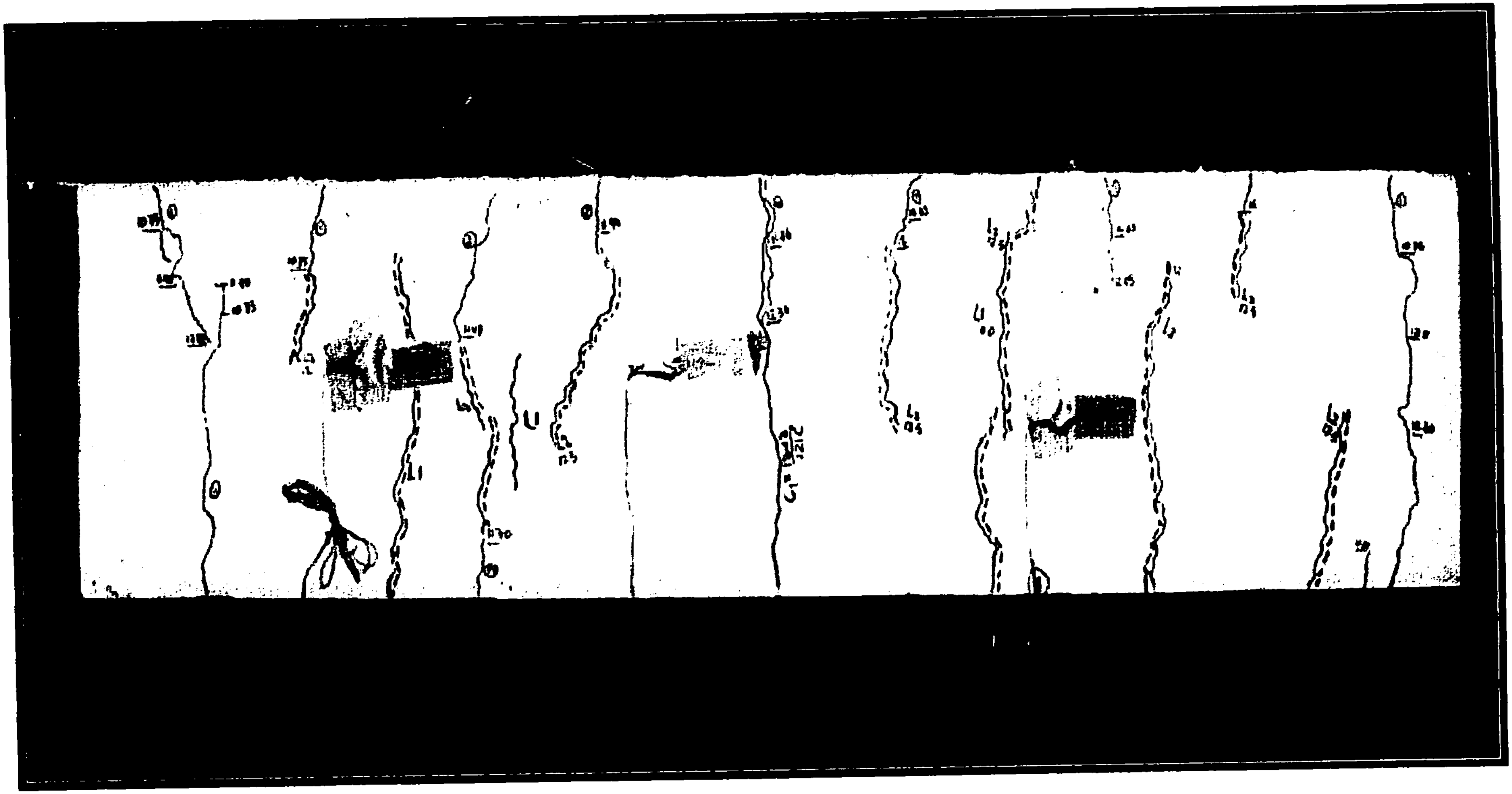

Figure 4.24 Crack Pattern in Beam PrLES.2

an effect on the spacing of cracks. The influence of stirrups on the location of cracks can be seen in Figure 4.25, which shows a typical cracked beam under temperature effects.

4.5 Force in Post-tensioned Tendon under Thermal loading

The variation of the measured force in the CFRP Leadline and steel tendons with the temperature difference over the entire thermal loading history is shown in Figures 4.26 to 4.28. As the figures show, only a slight increase of not more than 1 kN took place in the prestressing tendons with the increase in temperature.

4.6 Behavior of Thermally Cracked Beams under Mechanical Moment

The moment-deflection response of thermally cracked beams under mechanical moment was tested in order to examine the effects of cracking due temperature on the service load behavior of the beams. The test beams were first subjected to the thermal loading and then were left to cool down to room temperature. Subsequently, the specimens were reloaded in increments using the turnbuckles placed on both sides of the test frame and readings of midspan deflection were recorded at each moment increment. Also, the crack widths were measured after application of each increment. New cracks due to mechanically applied moment were marked, and the test beams were then unloaded.

The results of these tests are summarized in Table 4.4. Figure 4.29 shows the crack pattern in beam PrLCL.1 due to temperature effect and the new cracks (shown by dashed line) developed due to mechanically applied moment.

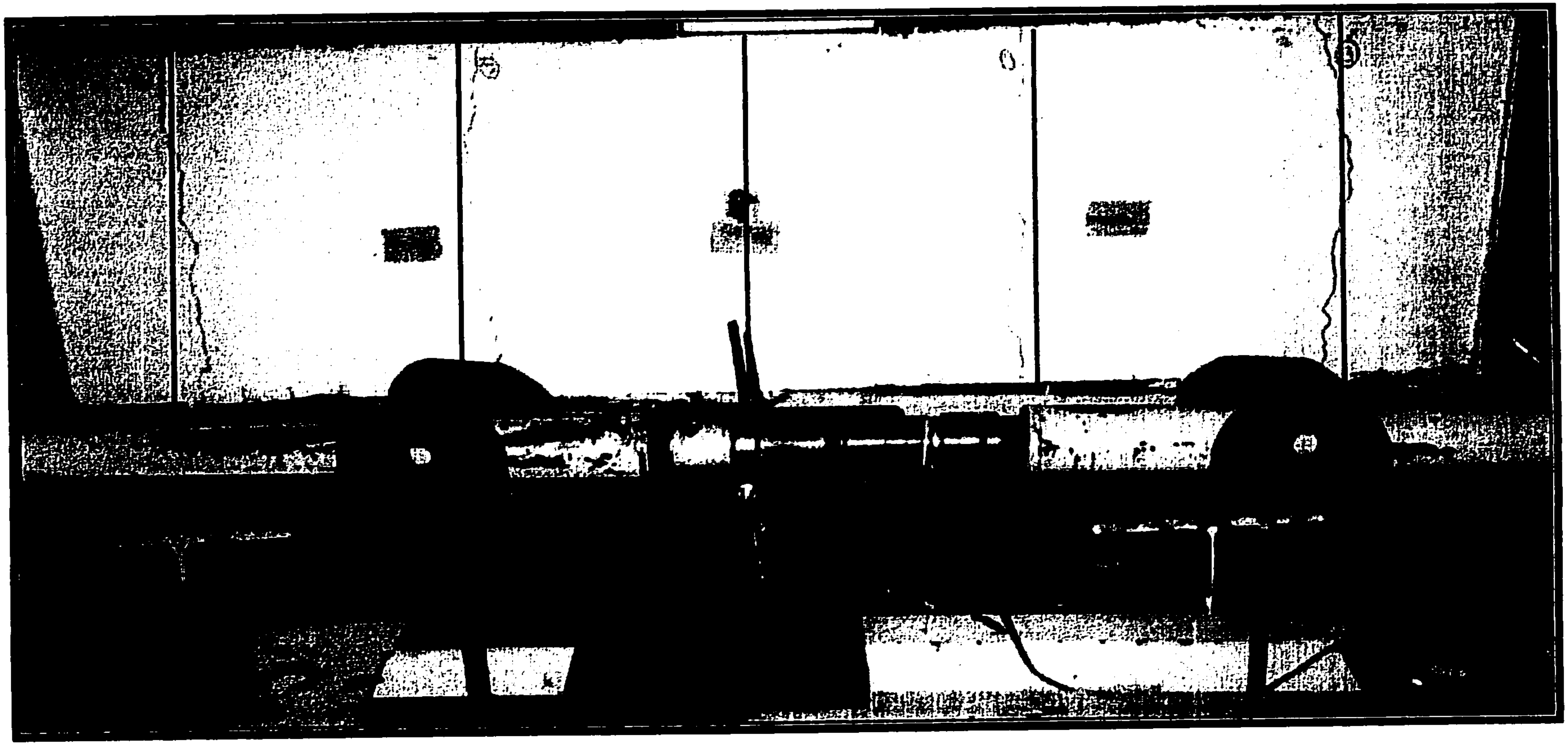

Figure 4.25 Location of Cracks and Stirrups in Beam PoLCS.2

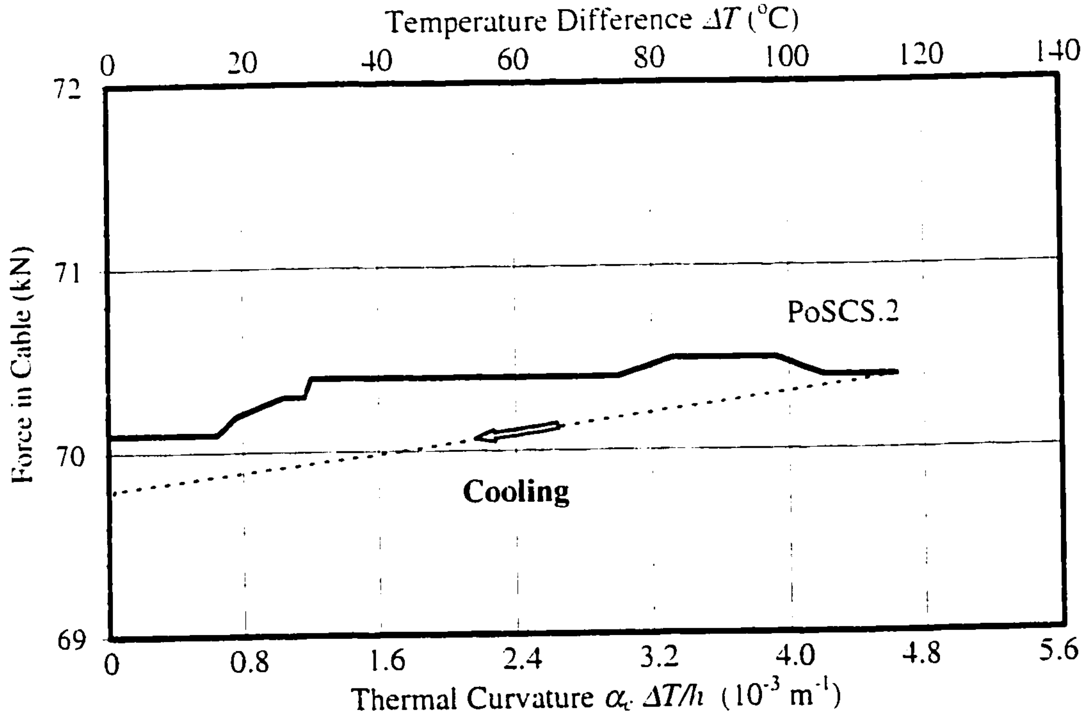

Figure 4.26 Variation of Force in Steel Strand for Beam PoSCS.2 due to Thermal Loading

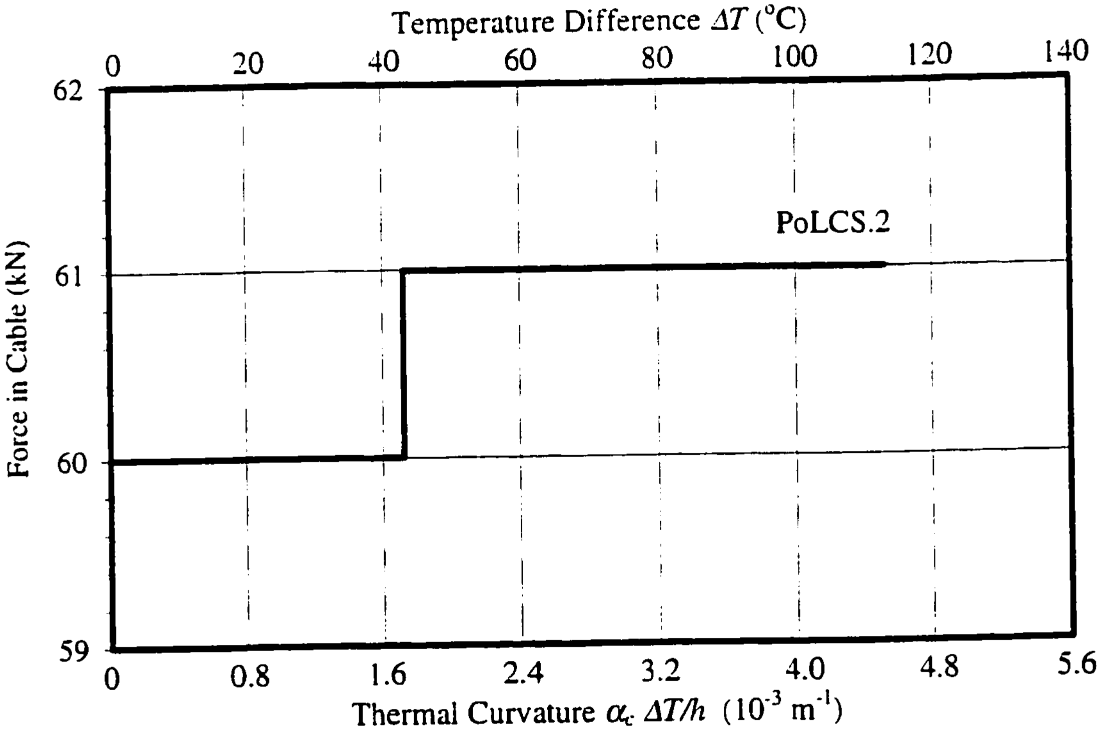

Figure 4.27 Variation of Force in Leadline Tendon for Beam PoLCS.2 due to Thermal Loading

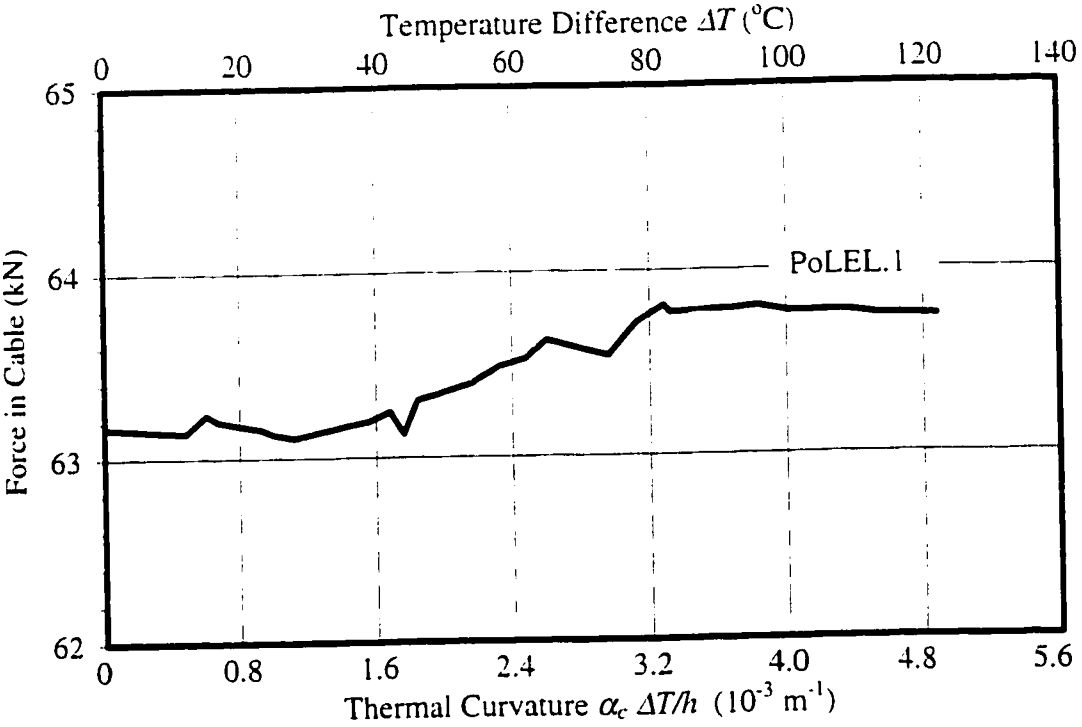

Figure 4.28 Variation of Force in Leadline Tendon for Beam PoLEL.1 due to Thermal Loading

Table 4.4: Maximum Moment and Mid-Span Deflection for Prestressed and Nonprestressed Beams

Beam Designation	Group Name	Thermal Test		Mechanical Moment Test			
		Maximum Moment (kN-m)	Number of Cracks	Maximum Moment (kN-m)	Observed New Cracks	Observed Drop in Moment	Mid-Span Deflection (mm)
L.2[*]		17.99	4	22.24	1	No	1.96
L.4[*]		22.61	4	20.00	1	No	1.74
L.6	A1	22.50	5	27.11	3	No	4.80
L.8	A1	27.92	6	32.34	6	No	4.32
L1.0	A1	32.78	4	30.14	3	No	2.91
GM.5	A2	19.44	1	13.47	-	No	4.68
GT.5	A2	16.09	1	15.08	1	Yes	3.57
GB.5	A2	20.22	1	18.52	1	Yes	4.91
PrLCL.1	B1	22.26	2	22.15	2	No	8.36
PrLES.2	B1	24.69	9	25.37	-	No	3.94
PoLCS.2	B2	20.09	4	16.13	1	No	2.48
PoLEL.1	B2	22.80	2	20.00	-	No	3.29
PoSCS.2	B2	24.04	1	21.75	3	No	3.40
S.2[**]		16.84					
S.4[**]		17.29	3	23.5		No	2.67
S.6[**]		17.98	5	27.0		No	2.48
S.8[**]		20.75	5	27.5		No	1.65
S1.0[**]		19.74	5				

[*] El-Badry and Abdalla (1998)

[**] Ariyawardena (1993)

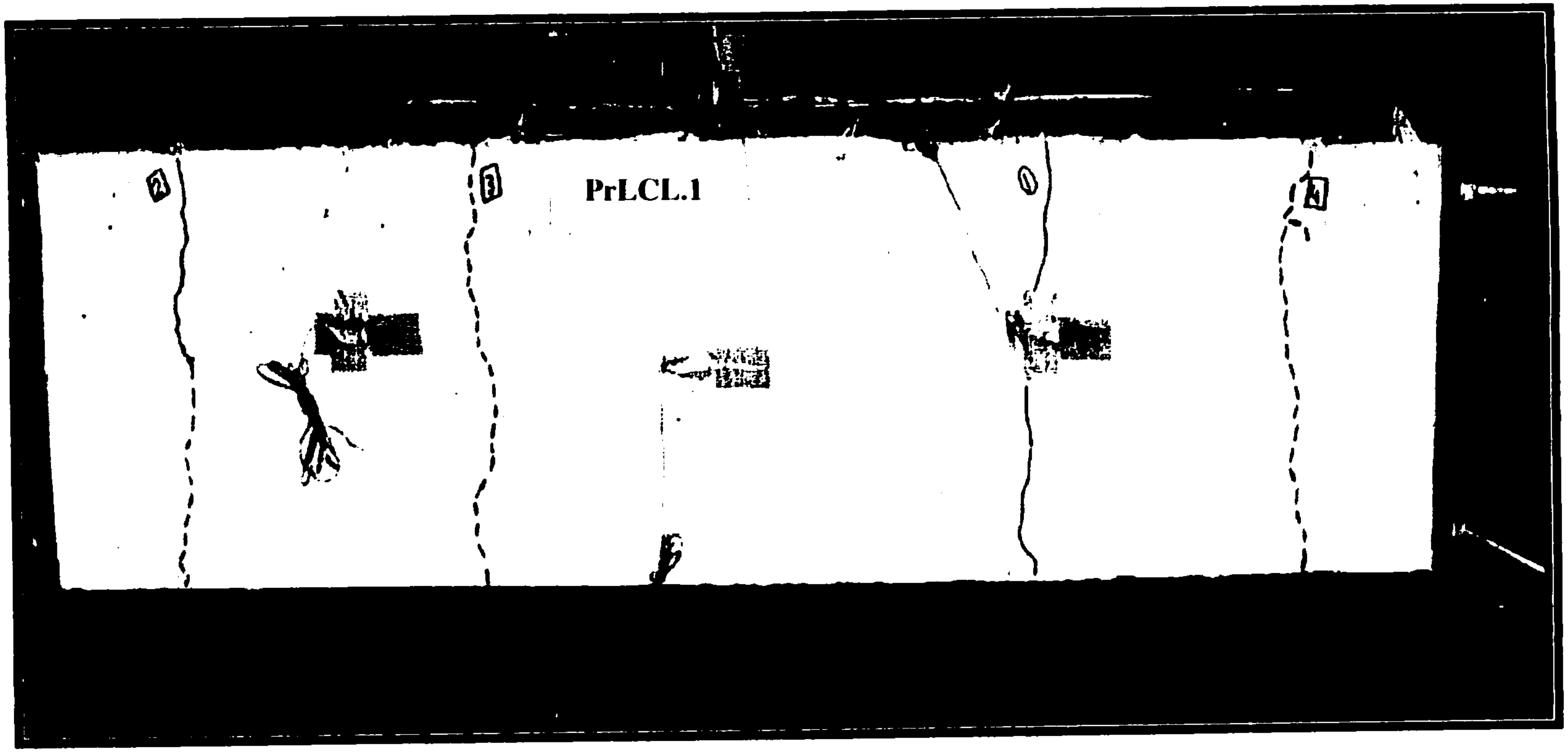

Note: —— due to Thermal Moments --- due to Mechanical Moment

Figure 4.29 New Cracks Developed in Beam PrLCL.1 under Mechanical Moment

Figure 4.30 presents plots of the mechanical moment, M, versus mid-span deflection, Δ, for beams Group A1 reinforced with Leadline rods. The maximum moments shown in this figure represent the largest moments that could be applied as the turnbuckles reach their maximum turning capacity. As expected, the figure shows that increasing the Leadline reinforcement ratio reduces the mid-span deflection under the effect of mechanical moment. A comparison is made in Figures 4.31 and 4.32 between the M-Δ behavior of beams L.6 and L.8 and that of beams S.6 and S.8 reinforced, respectively, with 0.6% and 0.8% steel bars (Ariyawardena, 1993). As can be seen, for the same magnitude of applied moment, the Leadline reinforced beams exhibit larger deflection than the beams reinforced with steel. For example, at M = 28 kN-m, beams L.6 and L.8 exhibit 47% to 60% larger deflection than beams S.6 and S.8. This behavior is attributed to the lower elastic modulus, E_f, of Leadline rods, which is about 25 – 29 percent less than that of steel (see Table 3.3).

Figure 4.33 gives the moment-deflection response of beams Group A2 reinforced with 0.5% NEFMAC grids. The graphs for beams S.4 and S.6 reinforced, respectively, with 0.4% and 0.6% steel are also shown in Figure 4.33 for comparison. As can be seen, the beams reinforced with NEFMAC showed much lower moment than the beams reinforced with steel even with a smaller reinforced ratio (0.4 percent). Because of the small modulus of elasticity of NEFMAC (42 GPa), beams GM.5, GT.5 and GB.5 exhibited much larger deflection than steel reinforced beams, for the same magnitude of moment.

The moment-deflection curves for beams of Group B1 and B2 are shown in Figures 4.34 and 4.35, respectively. The figures indicate the effects of bond of pretensioned beams, the eccentricity of the prestressing tendon, the increase in the amount of

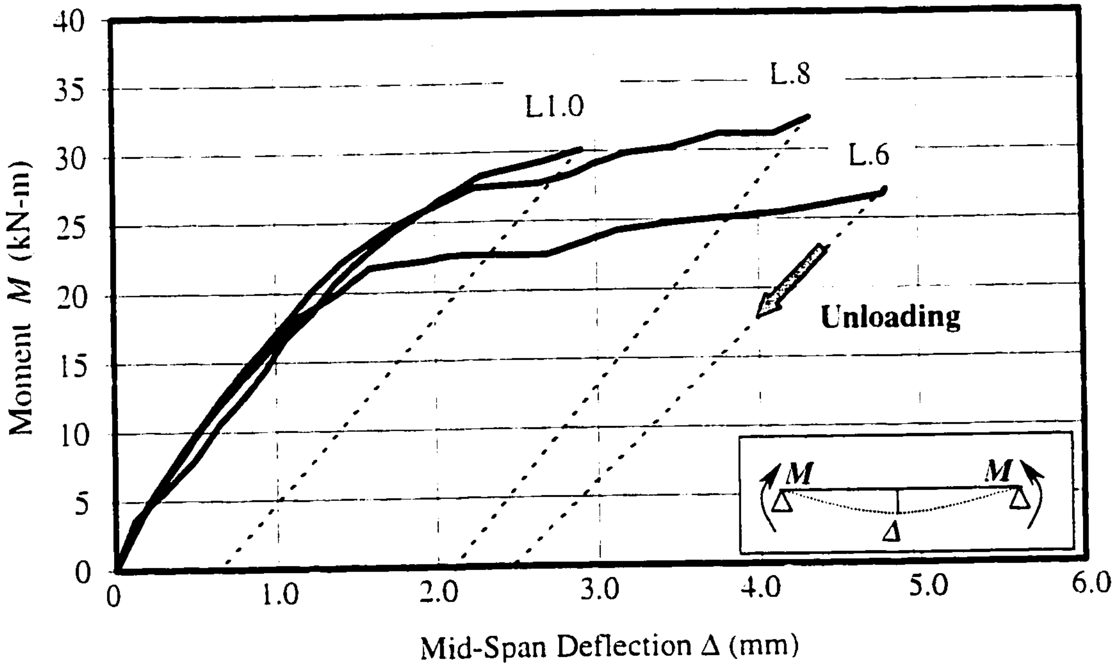

Figure 4.30 Mid-Span Deflection of Thermally Cracked RC Beams of Group A1 Subjected to Mechanical Moment

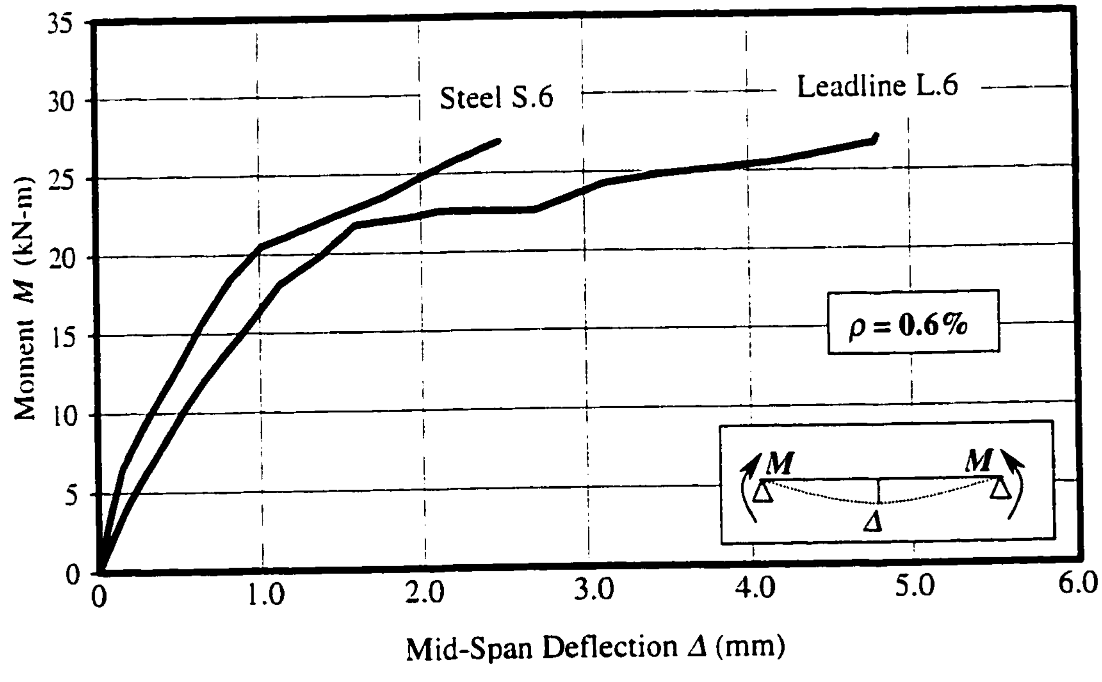

Figure 4.31 Mechanical Moment versus Mid-Span Deflection of Thermally Cracked Beams Reinforced with $\rho = 0.6\%$ Leadline or Steel

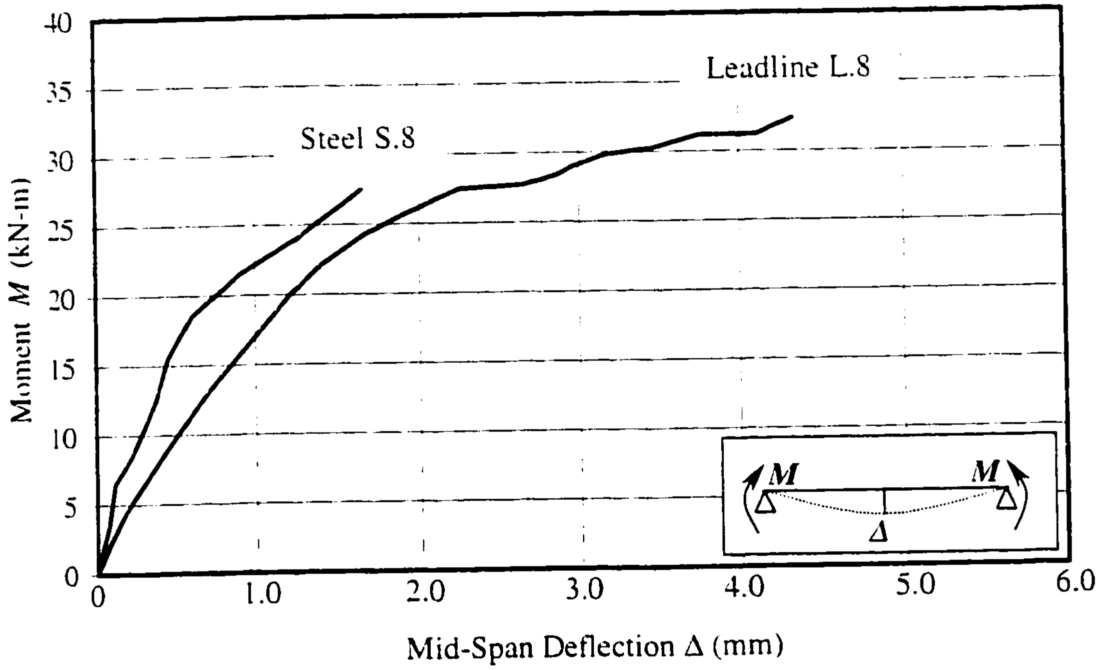

Figure 4.32 Mechanical Moment versus Mid-Span Deflection of Thermally Cracked Beams Reinforced with $\rho = 0.8\%$ Leadline or Steel

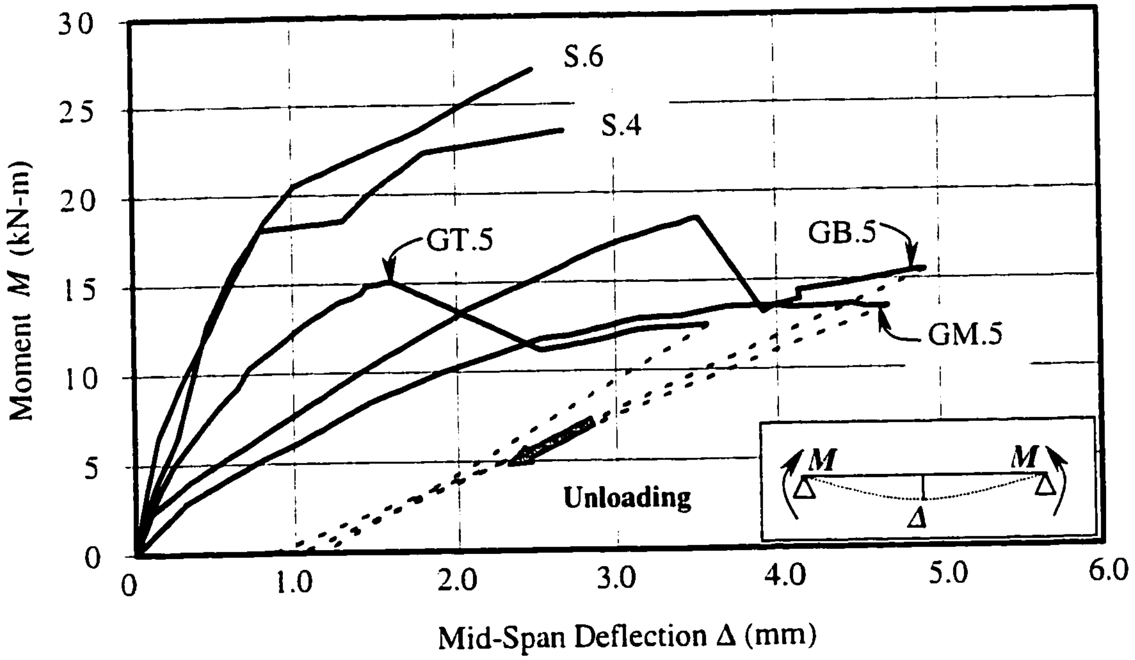

Figure 4.33 Mechanical Moment versus Mid-Span Deflection of Thermally Cracked Beams Reinforced with NEFMAC Grids (Group A2) or Steel Rebars

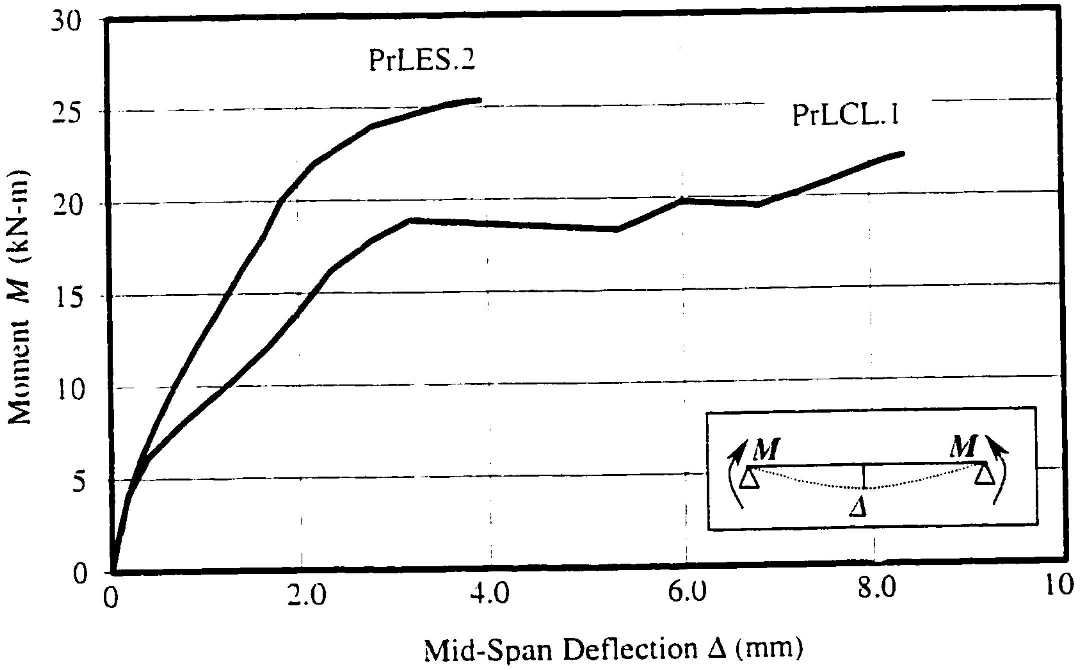

Figure 4.34 Mid-Span Deflection of Thermally Cracked Pretensioned Beams Group B1 Subjected to Mechanical Moment

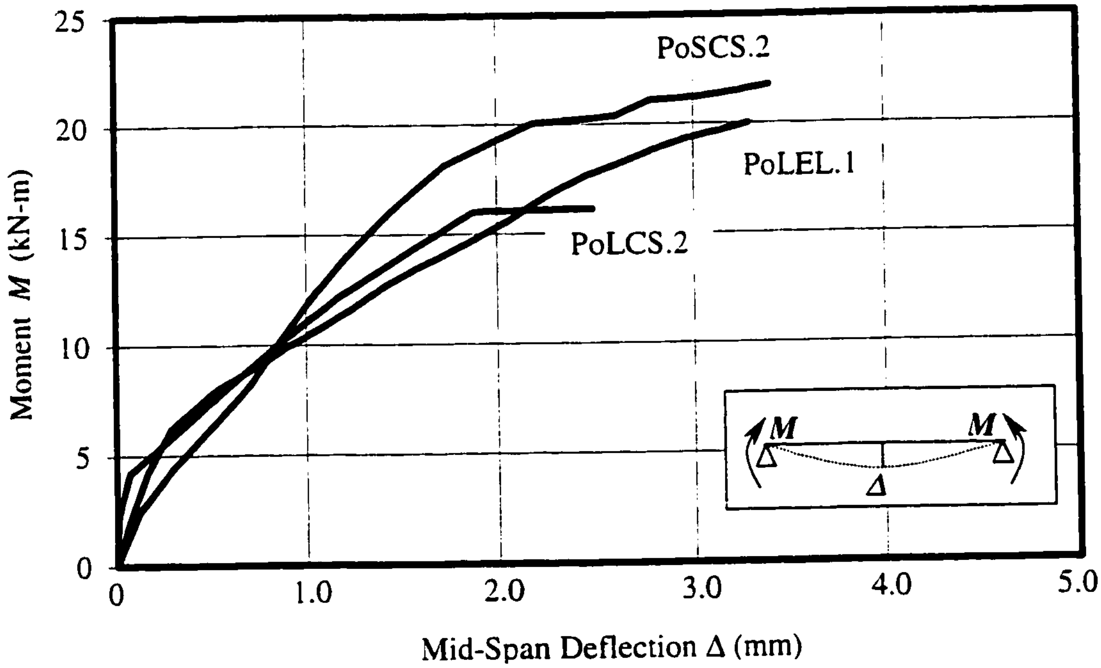

Figure 4.35 Mid-Span Deflection of Thermally Cracked Post-tensioned Beams Group B2 Subjected to Mechanical Moment

non-prestressed reinforcement in reducing the deflection of the tested beams. Once again, the beams reinforced or prestressed with Leadline rods exhibited larger deflection than those reinforced or prestressed with steel.

4.7 Force in Post-tensioned Tendons under Mechanical Moment

The prestressing force in beams PoLCS.2, PoSCS.2 and PoLEL.1 was measured by means of a load cell installed at the end of the tested beam. The prestressing force was recorded after each moment increment. The variation of the prestressing force in the post-tensioned tendons with the increase of applied mechanical moment is shown in Figures 4.36 to 4.38 for the three beams, respectively. As can be seen, the increase in applied moment increased the prestressing force only slightly (1 to 2 kN).

4.8 Ultimate Strength and Failure Modes of thermally cracked Beams

All the eleven beams cracked due to temperature gradients and due to the mechanical moments applied after the thermal loading tests were re-tested up to failure under static loading conditions using two point loads as shown in Figure 3.16. Each specimen was loaded in increments, and readings of mid-span deflection were recorded and crack widths were also measured after application of each load increment. In addition, variation of the prestressing force in the post-tensioned beams was recorded. In all beams, the ultimate load capacity was taken as the maximum load when the beam collapsed. Table 4.5 shows the ultimate load, deflection at ultimate, number of observed cracks, crack widths and modes of failure for all the tested beams. As can be seen, the beam reinforced

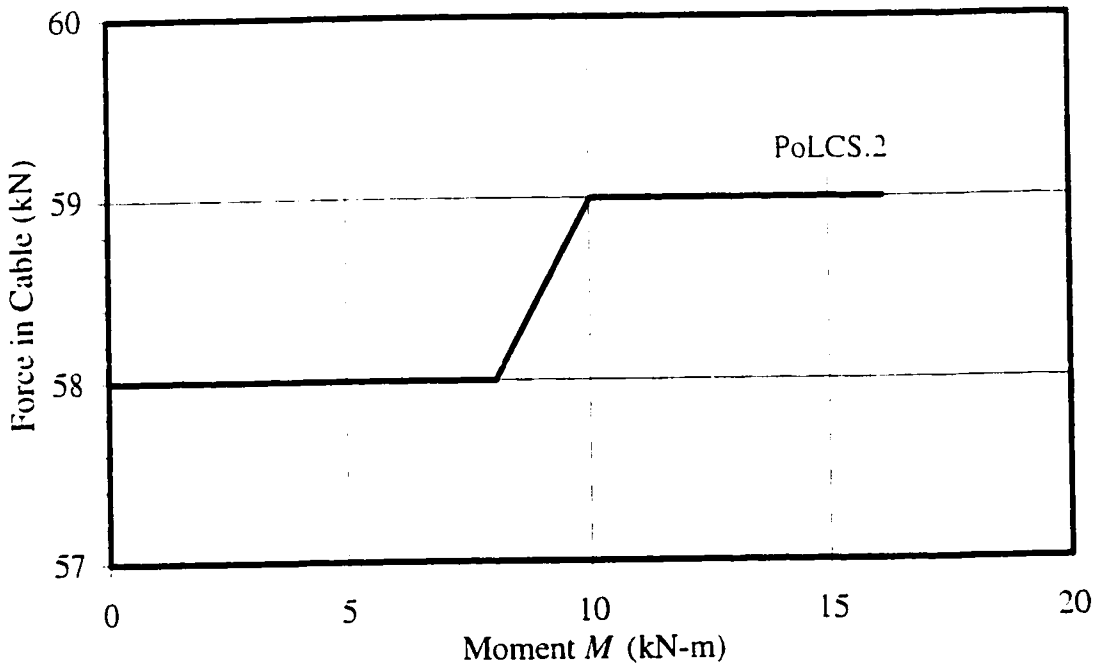

Figure 4.36 Variation of Force in Leadline Tendon for Beam PoLCS.2 due to Mechanical Moment

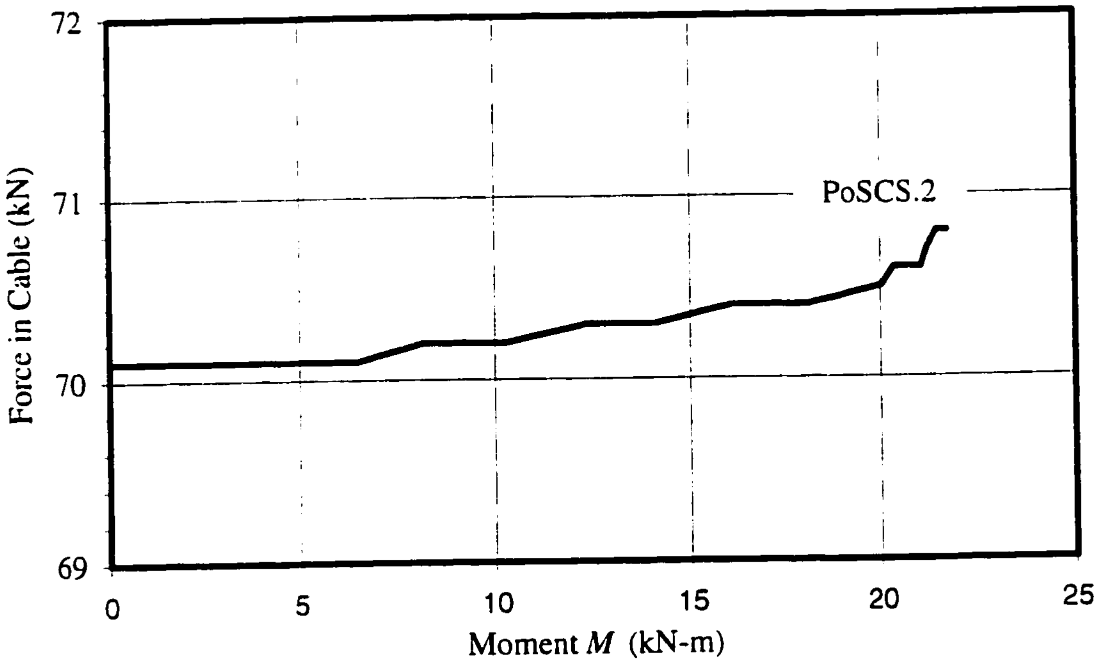

Figure 4.37 Variation of Force in Steel Strand for Beam PoSCS.2 due to Mechanical Moment

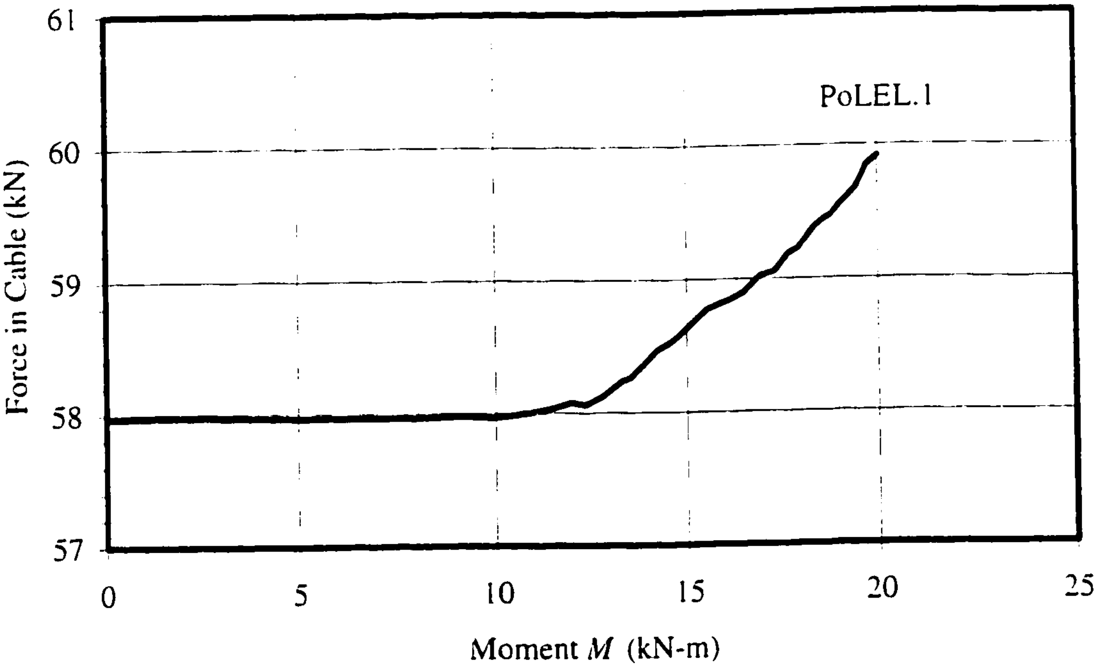

Figure 4.38 Variation of Force in Leadline Tendon for Beam PoLEL.1 due to Mechanical Moment

Table 4.5: Critical Results of Prestressed and Nonprestressed Beams and Their Modes of Failure

Beam Designation	Group Name	Number of New Cracks	Max. Crack Width (mm)	Max. Crack Spacing (mm)	Average Crack Spacing (mm)	Ultimate Load (kN)	Mid-Span Deflection at Ultimate (mm)	Force in Cable (kN)		Mode of Failure
								before Testing	at Failure	
L.6	A1	2	1.5	26	17	261	24	-	-	Shear Failure
L.8	A1	-	1.0	14	15	281	21	-	-	Shear Failure
L1.0	A1	5	0.9	16	11	300	22	-	-	Shear Failure
GM.5	A2	1	10	270	-	57	16	-	-	F.F. + L.C.
GT.5	A2	4	23	400	210	90	59	-	-	F.F. + L.C.
GB.5	A2	3	4	240	175	100	35	-	-	F.F. + L.C.
PrLCL.1	B1	1	10	420	298	109	46	-	-	F.F. at point load
PrLES.2	B1	-	6	250	191	152	33	-	-	Flexural Failure
PoLCS.2	B2	3	25	350	340	N/A	N/A	59.00	73	F.F. at point load
PoSCS.2	B2	1	23	280	248	113	132	69.80	102.4	F.F. at point load
PoLEL.1	B2	4	15	400	320	185	103	58.37	77.61	F.F. at point load

Note: N/A: Not Available F.F.: Flexural Failure L.C.: Longitudinal Crack with Leadline had the highest ultimate load and the smallest mid-span deflection at ultimate.

Figure 4.39 presents the complete load-deflection response of beams Group A1 reinforced with Leadline. The beams behaved almost linearly up to ultimate and with a much smaller stiffness up to failure (increase in deflection with no increase in load). This is attributed to the linear elastic characteristics of the Leadline rods. A web shear failure was observed in all beams. L.6. L.8 and L1.0. Prior to failure, a crack initiated at the support and extended diagonally up to the point load close to the support. A splitting failure was clearly noted on the resin surface of the Leadline rods in all beams while the carbon fibers were still carrying tensile stresses (see Appendix A, Figures A3 and A6). A close-up view of the web shear failure of beams L.8 is shown in Figures 4.40. The crack width of the three beams L.6, L.8 and L1.0 under mechanical load was not as extensive as the widths of cracks in the rest of the tested beams (Table 4.5).

The load versus mid-span deflection curves in beams of Group A2, reinforced with NEFMAC grids are shown in Figure 4.41. As expected the ultimate load of beam GM.5, reinforced with the NEFMAC grid located at mid-depth of the beam cross-section, was lower than that of beams GT.5 and GB.5. A flexural failure was observed in all the three beams. The failure of these beams was due to rupture of the NEFMAC grid as shown in Figure 4.42. Prior to failure, horizontal cracks developed in all the three beams at the level of the NEFMAC reinforcement. These horizontal cracks may have initiated due to the difference in transverse thermal expansion coefficient of the GFRP NEFMAC and the concrete. A close-up view of failure of beam GT.5 is shown in Figure 4.43.

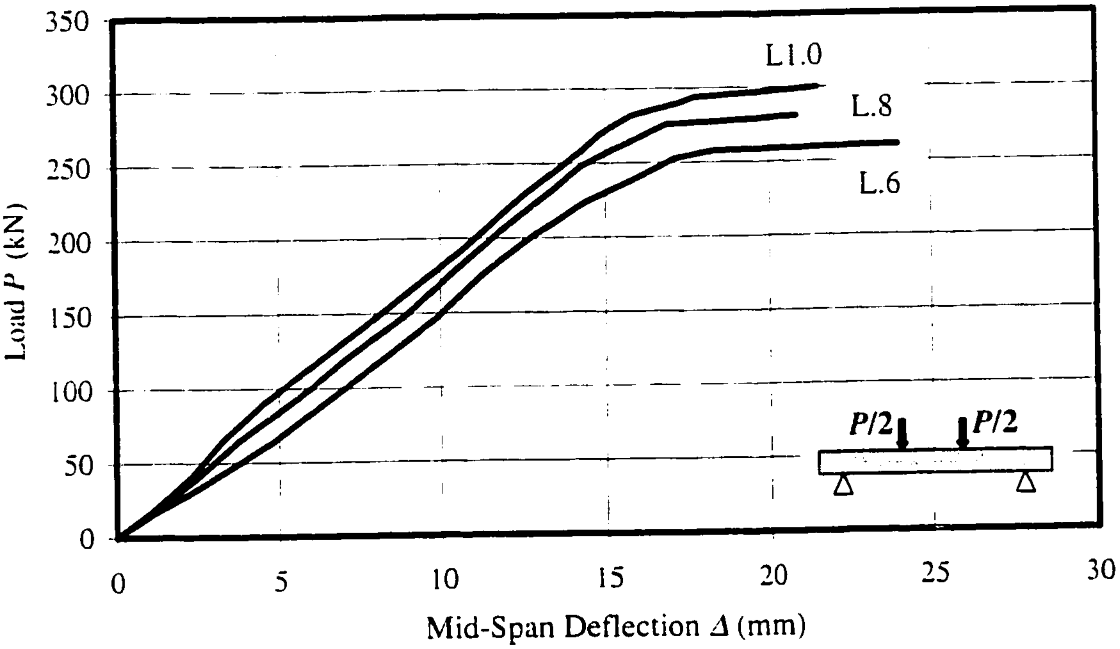

Figure 3.39 Load-Deflection Response of Thermally Cracked RC Beams (Group A1)

Figure 4.40 Close-up View of Web Shear Failure of Beam L.8 Reinforced with Leadline

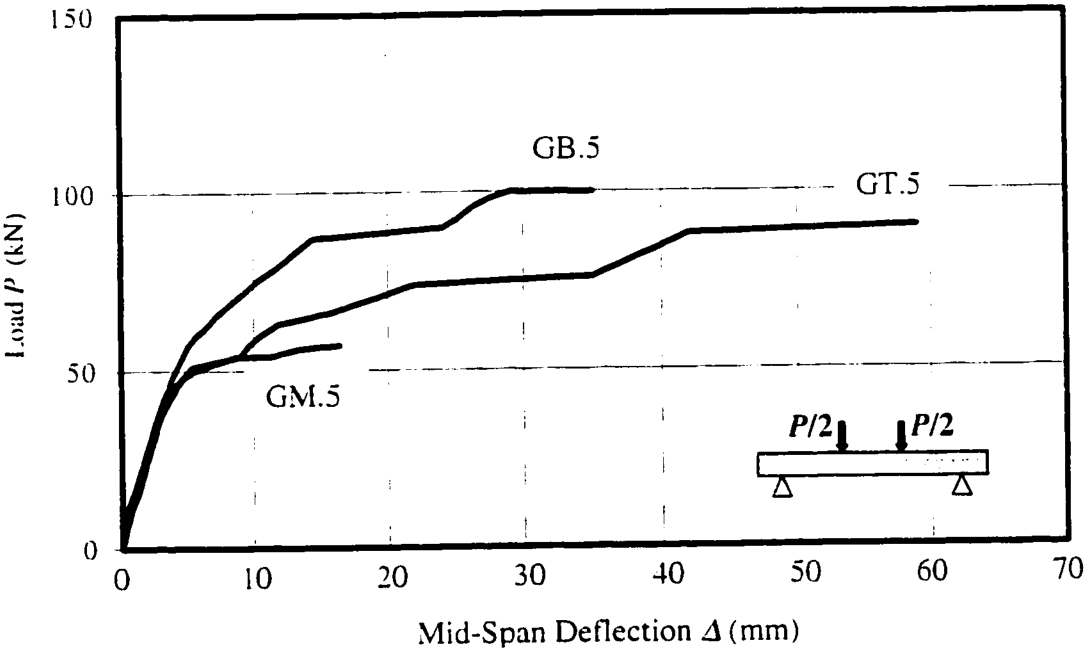

Figure 4.41 Load-Deflection Response of Thermally Cracked RC Beams (Group A2)

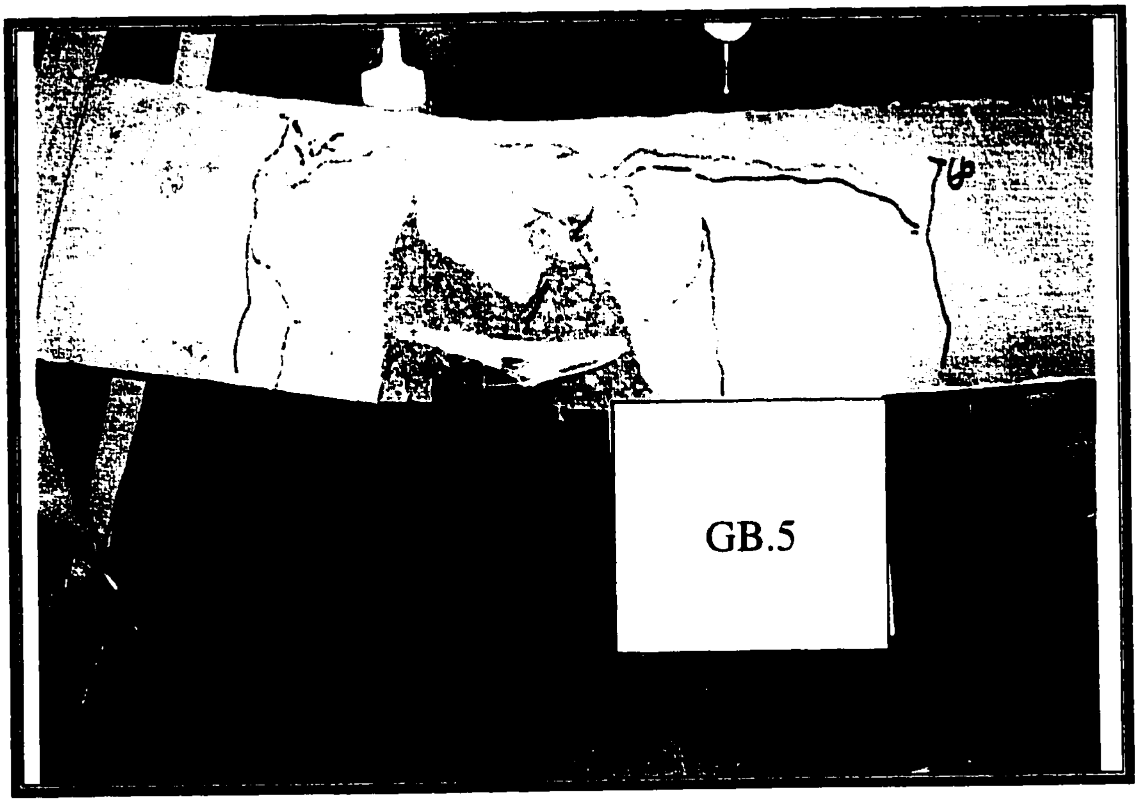

Figure 4.42 Flexural Failure of Beam GB.5 Reinforced with NEFMAC Grid Reinforcement

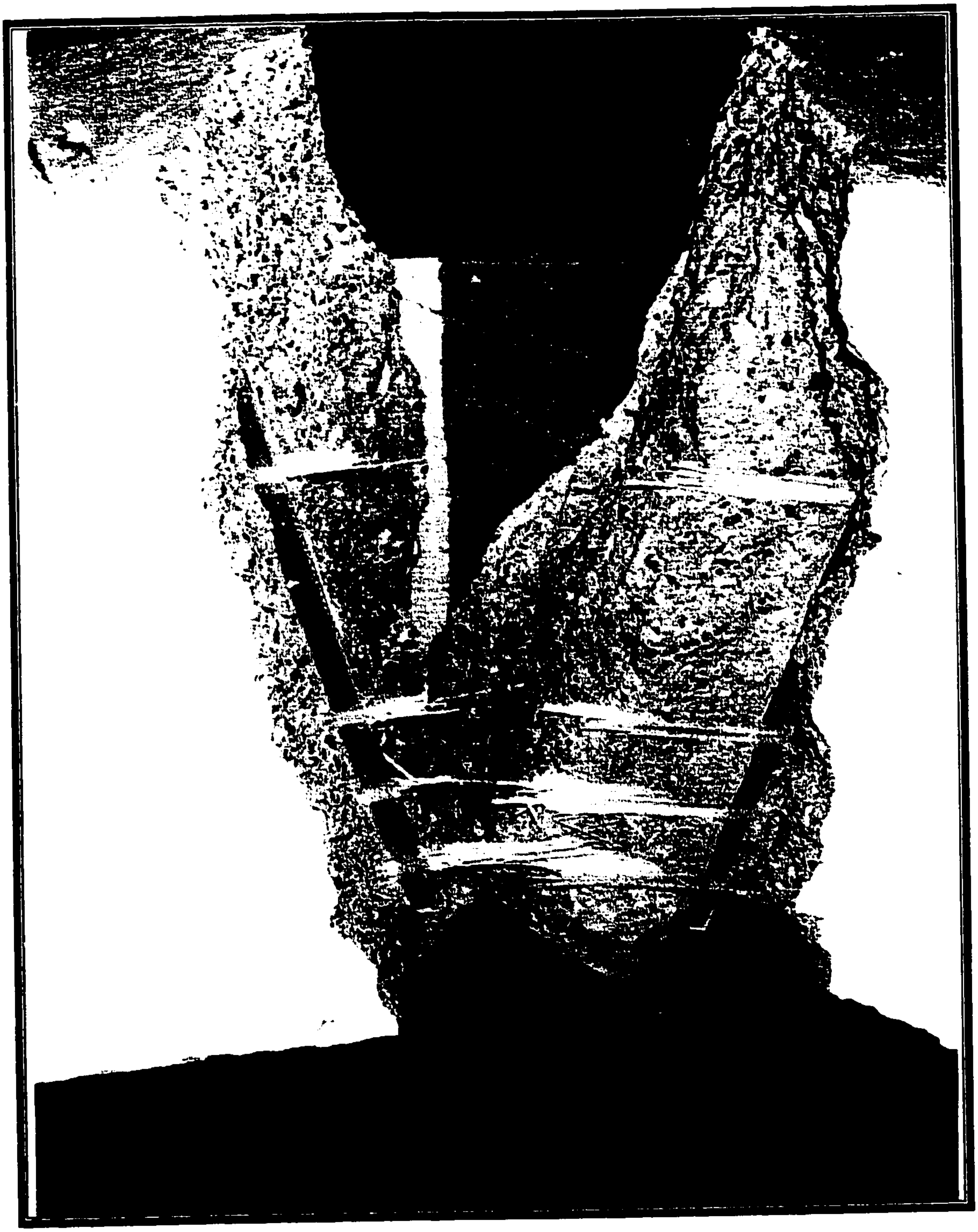

Figure 4.43 Close-up View of Failure of Beam GT.5

Figures 4.44 and 4.45 show the load-deflection curves for the partially prestressed beams of Series B. It should be mentioned here that the results for beams PoLCS.2 are not available since during the test, an error took place in the data acquisition system, which led to loss of the recorded data. Figures 4.44 and 4.45 indicate that under equal magnitude of applied load, the beams pretensioned with Leadline tendons exhibited much smaller deflection than the post-tensioned beams. Also, the eccentricity of the prestressing tendon led to an increase in the load and to a decrease in the mid-span deflection at ultimate.

Flexural failure was observed in all beams of Series B in the constant moment region between the two applied loads. Figure 4.46 shows beam PoSCS.2 at failure. This failure mode was typical for all the prestressed beams (see Appendix A). Failure of the post-tensioned beams was caused by rupture of the Leadline tendons (beams PoLEL.1 and PoLCS.2), see Figure 4.47, and the steel strand in beam PoSCS.2, see Figure 4.48. The rupture of the Leadline tendons occurred close to the anchorage system (Figure 4.47). No slip of the Leadline tendons at the anchorage was observed during the tests.

4.9 Force in Post-tensioned Tendons under Mechanical Load

The prestressing force was recorded after each load increment up to failure by means of a load cell. Variation of the prestressing force with the increase in applied load is shown in Figures 4.49 and 4.50 for beams PoLEL.1 and PoSCS.2, respectively. As can be seen, the prestressing force in these two beams increased by 33% and 43% at failure, respectively.

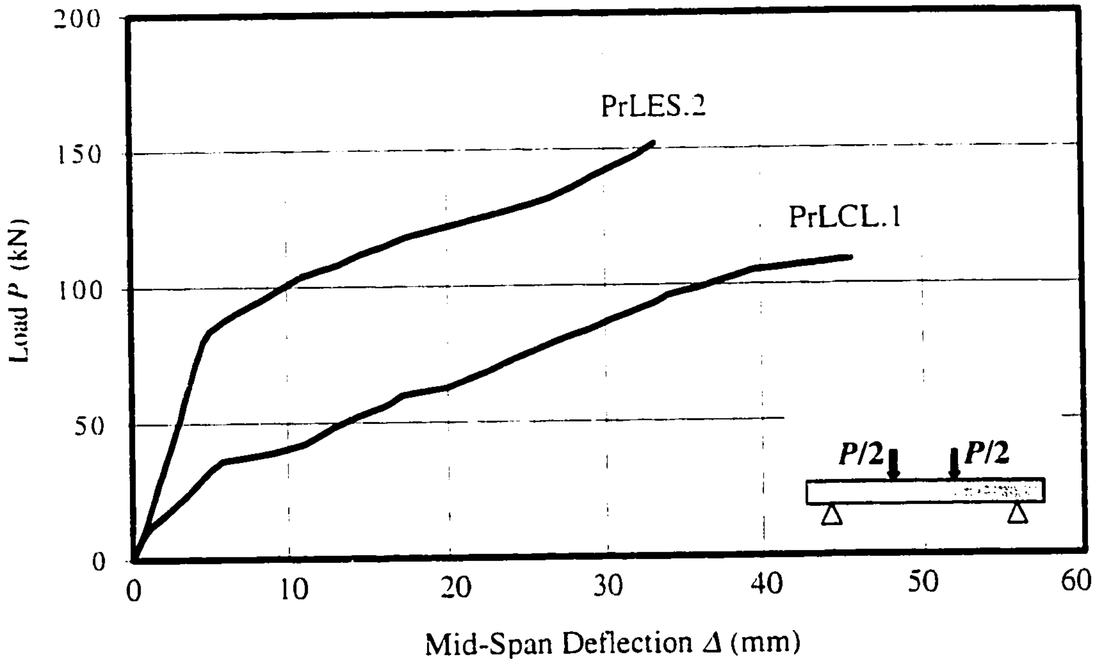

Figure 4.44 Load-Deflection Response of Thermally Cracked PPC Beams (Group B1)

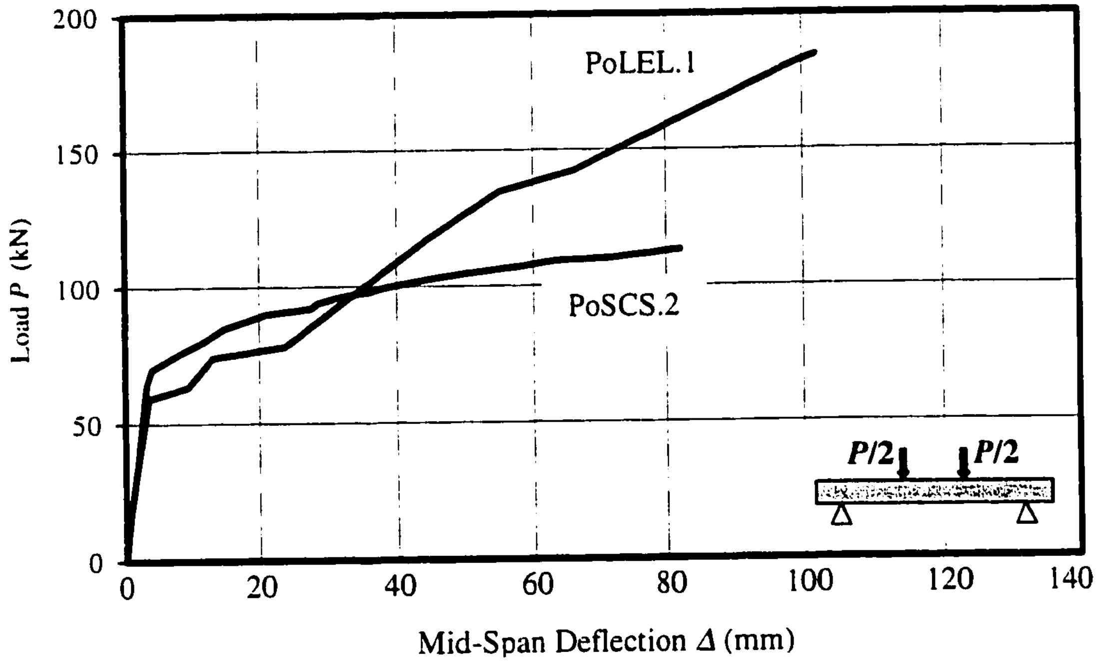

Figure 4.45 Load-Deflection Response of Thermally Cracked PPC Beams (Group B2)

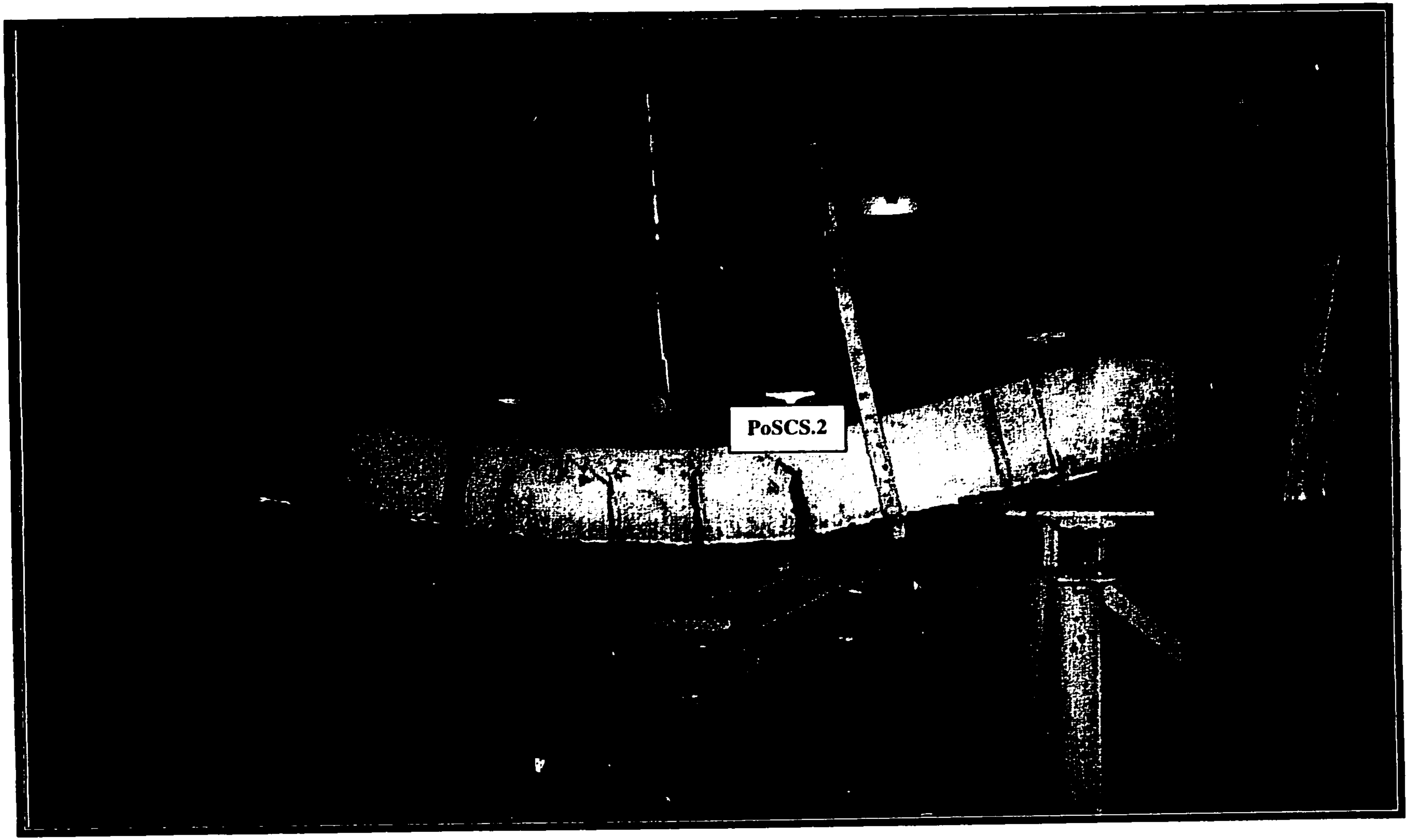

Figure 4.46 Flexural Failure of Beam PoSCS.2

Figure 4.47 Leadline Tendon of Beam PoLEL.1 after Rupture

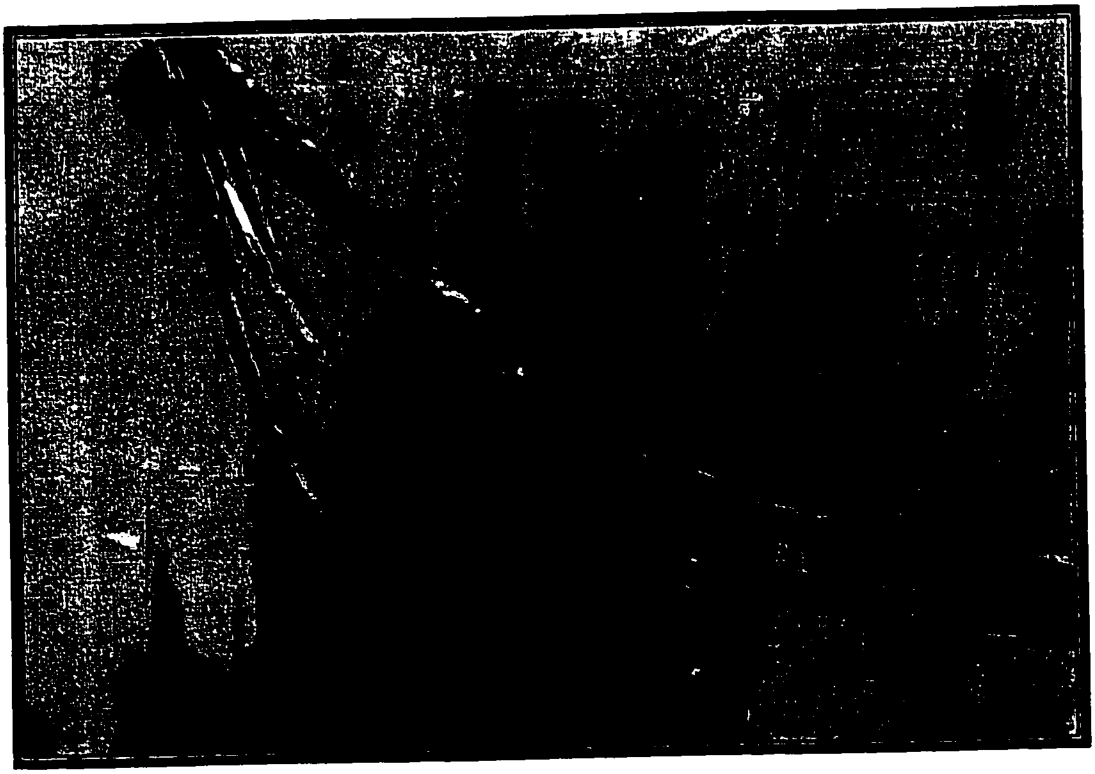

Figure 4.48 Steel Cable of Beam PoSCS.2 after Breakage

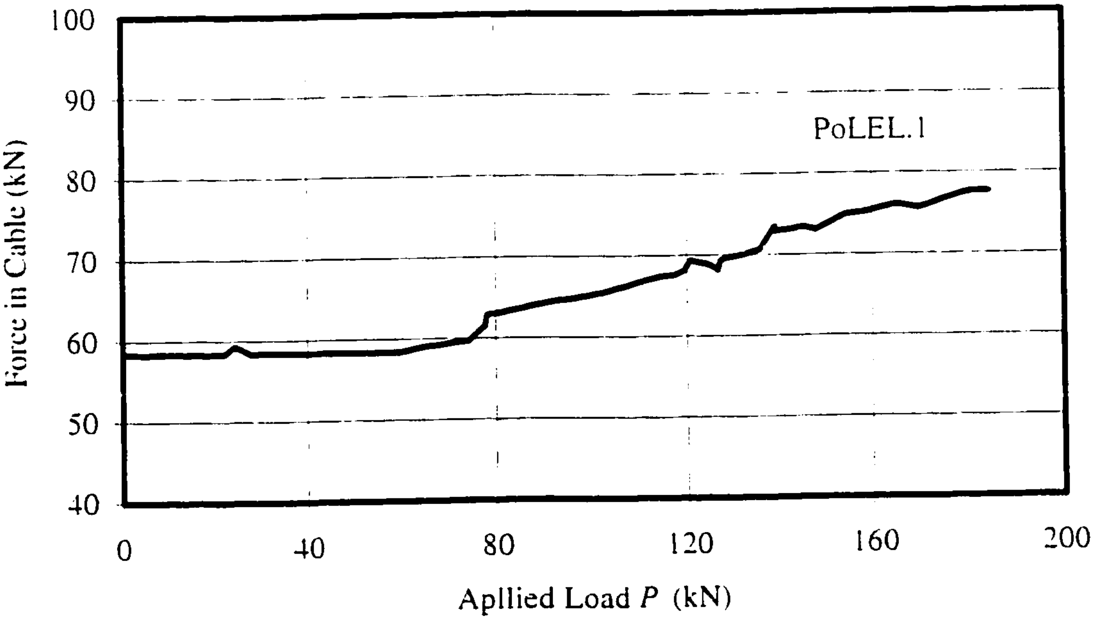

Figure 4.49 Variation of Force in Leadline Tendon for Beam PoLEL.1 due to Mechanical Load

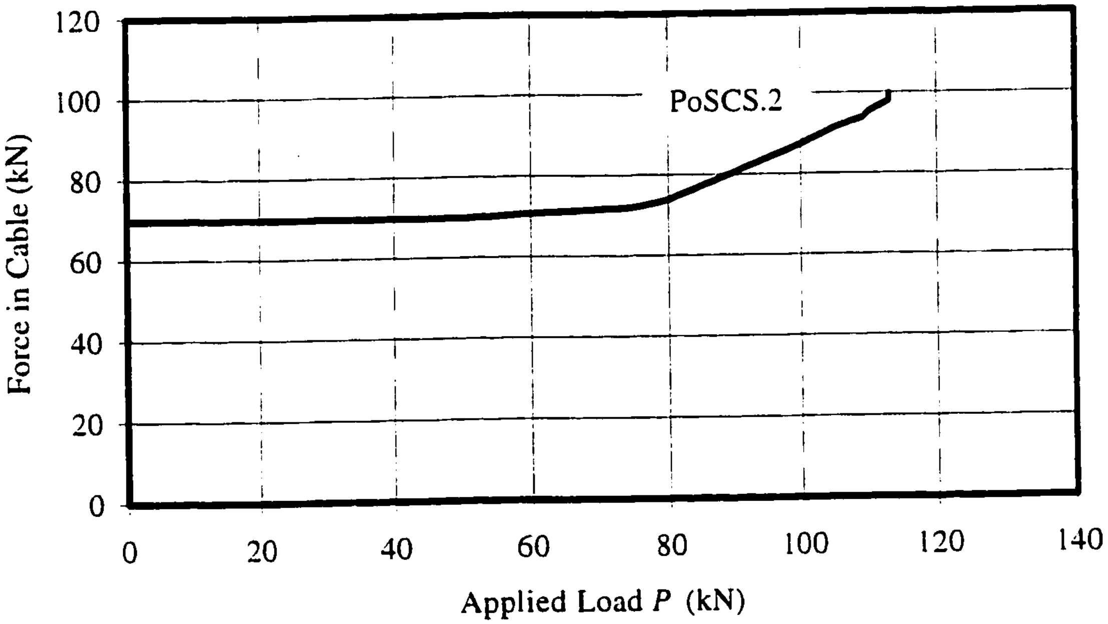

Figure 4.50 Variation of Force in Steel Strand for Beam PoSCS.2 due to Mechanical Load

The critical results of all the test specimens during the three stages of testing are summarized in Table 4.6 for easy understanding and comparison.

Table 4.6 Comparison of the Critical Results of Test Specimens during Three Stages of Testing

Beam Designation	Group Name	due to Thermal Test			due to Mechanical Moment Test			Due to Mechanical Load Test		
		Max. Moment (kN-m)	No. of Cracks	ΔT at First Crack (°C)	Max. Moment (kN-m)	No. of New Cracks	Max. Mid-Span Deflection (mm)	Ultimate Load (kN)	Total No. of Cracks	Max. Mid-Span Deflection (mm)
L.6	A1	22.50	5	37	27.11	3	4.80	261	10	24
L.8	A1	27.92	6	85	32.34	6	4.32	281	12	21
L1.0	A1	32.78	4	81	30.14	3	2.91	300	12	22
GM.5	A2	19.44	1	52	13.47	-	4.68	57	2	16
GT.5	A2	16.09	2	23	15.08	1	3.57	90	6	59
GB.5	A2	20.22	1	50	18.52	1	4.91	100	5	35
PrLCL.1	B1	22.26	2	16	22.15	2	8.36	109	5	46
PrLES.2	B1	24.69	9	84	25.37	-	3.94	152	9	33
PoLCS.2	B2	20.09	4	17	16.13	1	2.48	N/A	8	N/A
PoSCS.2	B2	24.04	1	30	21.75	3	3.40	113	5	132
PoLEL.1	B2	22.80	2	23	20.00	-	3.29	185	6	103

Note: N/A: Not Available

Chapter 5

Comparison with Analytical Results

5.1 General

In the previous chapter, the results obtained from the tests conducted on concrete beams reinforced with CFRP Leadline rods and Glass fiber NEFMAC grids were compared to the results from tests conducted by Ariywardena (1993) on the same scale beams but reinforced with steel bars. In this chapter, the analytical equations proposed by El-Badry and Ghali (1995) for prediction of the moment-curvature behavior of reinforced concrete members under thermal gradients are reviewed. The equations account for the progressive reduction of stiffness of the concrete members with the formation of cracks under the increase of thermal gradient. The equations are modified to account for the effects of difference in thermal expansion coefficients between the concrete and the CFRP Leadline rods. A comparison is made between the experimental results and the theoretical prediction.

5.2 Assumptions

The analysis presented in this chapter is based on the following assumptions:

1. Temperature is assumed to vary linearly over the cross-section depth of the concrete member.

2. The effects of temperature on creep and shrinkage of concrete and on the coefficient of thermal expansion and moduli of elasticity of both the concrete and the Leadline reinforcement are neglected.
3. Based on the results shown in Table 4.2, an average crack spacing S_{ave} = 330mm can be assumed under the effect of thermal loading. Thus, the maximum number of cracks that can develop in this stage is l / S_{ave} = 6 cracks; where l = 2000mm is the tested length of the member.
4. Since the tensile strength of concrete, f_{ct}, can vary from section to section in the concrete member, all cracks do not form at the same level of M. Thus, in this study, the values of tensile strength $f_{ct1}, f_{ct2}, \ldots\ldots, f_{ct6}$, at which successive cracks develop are calculated from the following equation (Ariyawardena et al., 1997):

$$f_{cti} = f_{ct(i-1)} \left(1+\gamma\right) \quad \text{MPa} \tag{5.1}$$

where γ = 0.02 is a coefficient giving the percentage of increase of tensile strength from one crack to another.

$$f_{ct1} = 0.6\lambda \sqrt{f_c'} \quad \text{MPa} \tag{5.2}$$

with f_c' being the compressive strength of concrete taken from tests (see Table 3.2), λ is a factor accounting for concrete density, λ = 1.0 for normal weight concrete.

5.3 Analytical Moment-Curvature Relationship of CFRP Reinforced Concrete Member under Temperature Gradient

First, consider the effect of difference in thermal expansion coefficient between the concrete and the CFRP reinforcement. Figure 5.1a depicts a concrete section reinforced

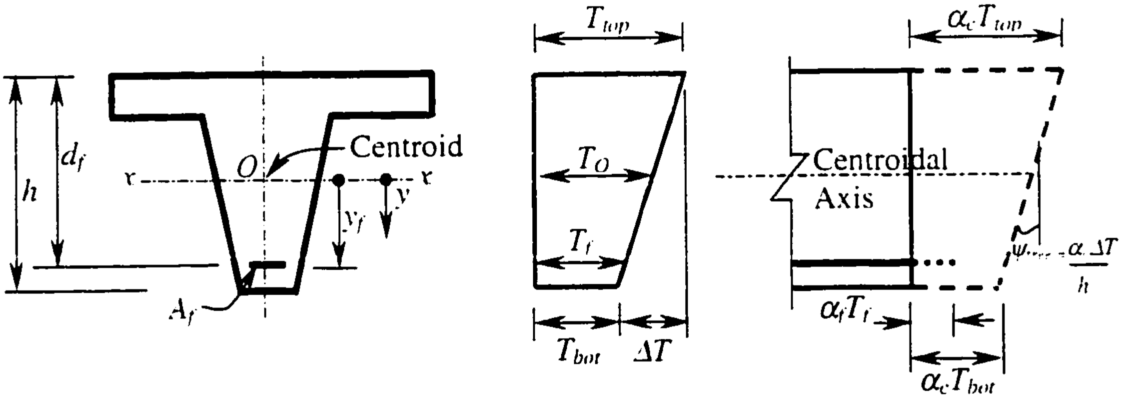

a) Cross-Section

b) Temperature Distribution

c) Free Strain

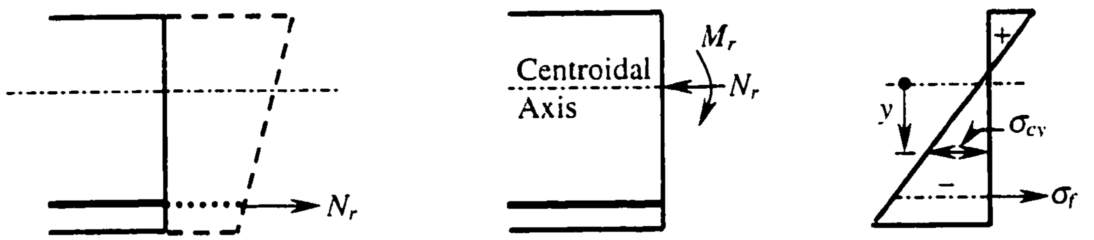

d) Restraining Force

e) Elimination of Artificial Restraint

f) Stress Distribution

Figure 5.1 Thermal Stresses due to Difference in Thermal Expansion of Concrete and CFRP

with one layer of CFRP reinforcement and subjected to a linear temperature distribution (Figure 5.1b). The CFRP layer has a cross-sectional area A_f and its position is defined by a coordinate y_f from the centroid O of the reinforced concrete section: y is positive when measured downward of O. The value of temperature T_f at the level of the CFRP layer is given by:

$$T_f = T_O + \frac{\Delta T}{h} y_f \tag{5.3}$$

where T_O and ΔT are, respectively, the temperature at the centroid and the difference in temperature between the top and bottom fibers of the cross-section: h is the height of the concrete section. The temperature value T_f can also be calculated as

$$T_f = T_{bot} + \Delta T\left(\frac{h - d_f}{h}\right) \tag{5.4}$$

where d_f is the depth of the CFRP layer from the top fiber.

Figure 5.1c shows the distribution of free strain due to temperature had the concrete section and the CFRP layer been free to expand separately. Figure 5.1d shows the force, N_r which if applied on the CFRP reinforcing layer would restrain the expansion of the CFRP layer to be equal to $\alpha_f T_f$. This restraining force, N_r is given by:

$$N_r = (\alpha_c - \alpha_f)T_f E_f A_f \tag{5.5}$$

where E_f is the elasticity modulus of CFRP. The restraining stress σ_r is given by:

$$\sigma_r = (\alpha_c - \alpha_f)T_f E_f \tag{5.6}$$

The restraining force is equivalent to a normal force N_r applied at the centroid O and a moment $M_r = N_r \, . \, y_f$ about an axis x-x passing through O.

In order to eliminate this artificial restraint, the forces N_r and M_r must be applied in a reversed direction on a transformed section composed of the concrete area plus the area A_f of the CFRP reinforcement multiplied by the modular ratio $n_f = E_f / E_c$ (Figure 5.1e). The corresponding strain ε_O at O and the curvature ψ are given by:

$$\varepsilon_O = -\frac{1}{E_c A}\left[(\alpha_c - \alpha_f)T_f E_f A_f\right] \tag{5.7}$$

$$\psi = -\frac{1}{E_c I}\left[(\alpha_c - \alpha_f)T_f E_f A_f y_f\right] \tag{5.8}$$

where A and I are, respectively, the area of the transformed section and its moment of inertia about an axis through O; E_c is the modulus of elasticity of concrete.

The stresses σ_f in the CFRP reinforcement and σ_c in the concrete at any fiber at coordinate y are given by:

$$\sigma_f = E_f\left[\varepsilon_O + \psi\, y_f + (\alpha_c - \alpha_f)T_f\right] \tag{5.9}$$

$$\sigma_c = E_c(\varepsilon_O + \psi\, y) \tag{5.10}$$

These stresses are shown in Figure 5.1f.

El-Badry and Ghali (1995) described the crack formation process in members of statically indeterminate reinforced concrete structures subjected to temperature gradients. They developed an analytical model to predict the relation between the thermal moment, M, and the temperature difference, ΔT, for such members. An example of M-ΔT diagram is shown in Figure 5.2 for concrete member having a rectangular cross section and reinforced with steel rebars. The end rotations of the member are restrained while its elongation is free.

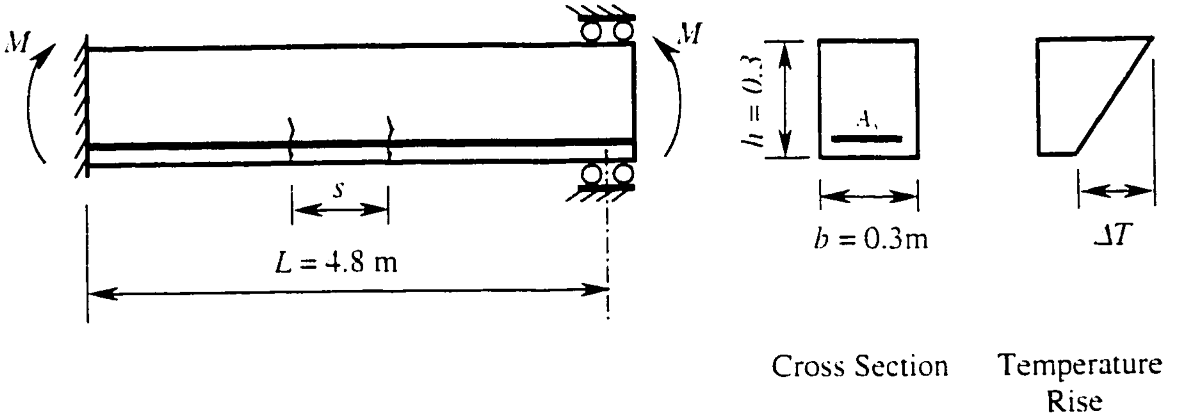

a) A Reinforced Concrete Member with End Rotations Restrained and Subjected to Temperature Rise

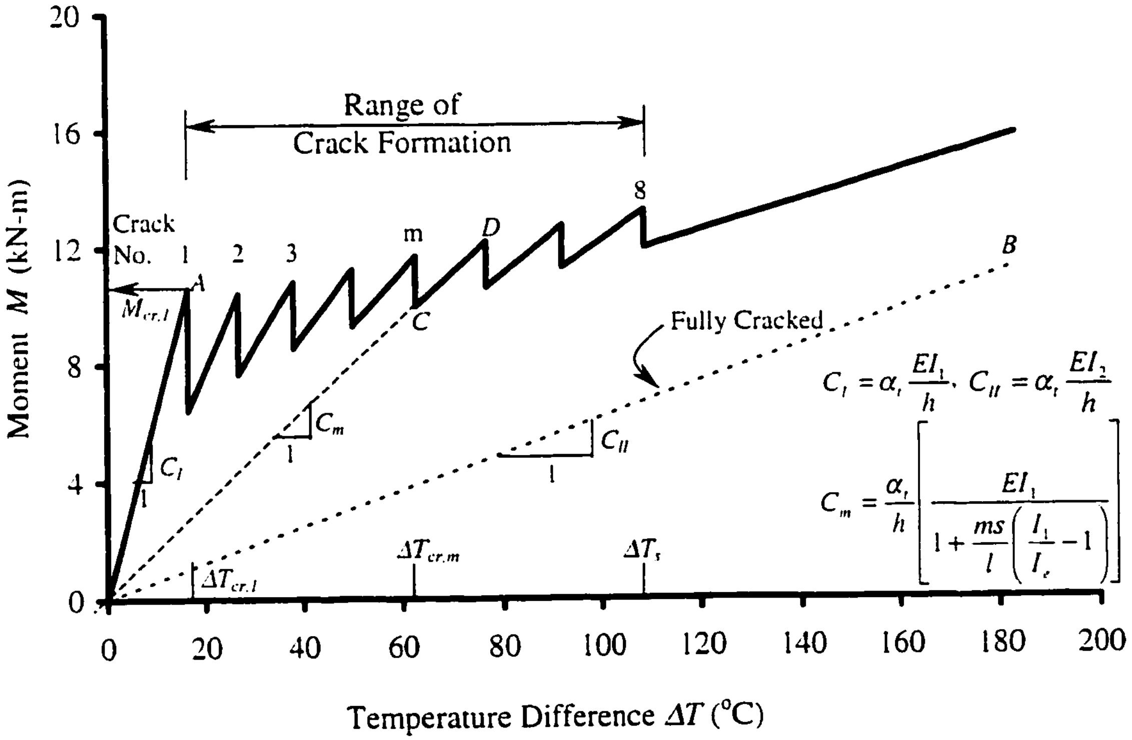

b) Variation of M with ΔT

Figure 5.2 Development of Cracks and Continuity Moments due to Temperature Gradient in a Statically Indeterminate Beam. (El-Badry and Ghali, 1995)

According to El-Badry and Ghali's model, the first crack occurs at the weakest section, when the stress in concrete reaches its tensile strength, f_{ct1}. The corresponding end moment is equal to the cracking moment, M_{cr1}, and develops at $\Delta T = \Delta T_{cr1}$. Cracking reduces the member stiffness; consequently, a drop in the end moment takes place just after occurrence of the first crack. The moment increases with the increase in ΔT until the second crack develops at the second weakest section, when the stress reaches a value f_{ct2}, which is slightly greater than f_{ct1}. The distance between the two cracks can not be smaller than the crack spacing s. This process of crack formation continues until a so-called *stabilized crack pattern* is developed, when no further cracks can develop. The maximum number of cracks n that can form in a member of length l is equal to the integer part of the quotient (l/s). The temperature gradient when cracking reaches the stabilized state is ΔT_s. Further increase of ΔT beyond ΔT_s causes widening of the existing cracks.

The model considers a member having m cracks consist of two parts, an uncracked part of length (l-ms) and moment of inertia I_l, and a cracked part of length ms and effective moment of inertia I_e. The moment of inertia I_l, is about an axis through the centroid of a noncracked transformed section composed of the area of concrete plus the area of the reinforcement multiplied by E_r/E_c; where E_r is the elasticity modulus of the reinforcement (in the present investigation, $E_r = E_f$). For the cracked part, the effective moment of inertia, I_e is used to account for the effects of tension stiffening of concrete between cracks; I_e is given by

$$I_e = \frac{I_1 I_2}{\zeta\, I_1 + (1-\zeta) I_2} \tag{5.11}$$

where I_2 is the moment of inertia of a transformed fully cracked section composed of the area of concrete in the compression zone plus the area of reinforcement multiplied by E_r/E_c; ζ is an empirical interpolation coefficient given by:

$$\zeta = 1 - 0.5\beta\left(\frac{f_{ct}}{\sigma_{c\,\max}}\right)^2 \tag{5.12}$$

where $\sigma_{c\,max}$ is the stress that would exist in the concrete at the extreme tension fiber assuming no cracking; $\beta = 0.5$ assuming non-deformed bars. Thus, at cracking, when $\sigma_{c\,max} = f_{ct}$, the value ζ can be taken as 0.75.

The value of M at which the mth crack occurs is given by:

$$M_{cr,m} = f_{ct,m} Z_1 \tag{5.13}$$

where Z_1 is the section modulus of the transformed noncracked section, and $f_{ct,m}$ is given by Equation (5.1). For the purpose of the present investigation, to account for the effects of the initial moment applied prior to the thermal loading test and for the effects of different thermal expansion coefficients of concrete and CFRP [see Equations (5.7) to (5.10)], Equation (5.13) must be modified to calculate the thermal moment just before occurrence of the mth crack as

$$M_{cr,m} = \left(f_{ct,m} - \sigma_{ci} - \sigma_{c\alpha}\right) Z_1 \tag{5.14}$$

where σ_{ci} is the stress at the extreme tension fiber due to the initial moment M_i,

$$\sigma_{ci} = \frac{M_i}{Z_1} \tag{5.15}$$

The value $\sigma_{c\alpha}$ is the stress at the extreme tension fiber due to the effects of difference between α_f and α_c; $\sigma_{c\alpha}$ is calculated from Equation (5.7), (5.8) and (5.10), substituting $A = A_1$, $I = I_1$ and y = coordinate of the extreme tension fiber from the centroid of the transformed section; A_1 and I_1 are the area and moment of inertia of the transformed noncracked section.

Before cracking, i.e. in the range $0 < \Delta T < \Delta T_{cr,1}$, the bending moment due to temperature is given by:

$$M = \alpha_c E_c I_1 \frac{\Delta T}{h} \tag{5.16}$$

Setting $M = M_{cr,1}$ and $\Delta T = \Delta T_{cr,1}$ in Equation (5.16), and solving, gives the value of $\Delta T_{cr,1}$ at which the first crack occurs.

$$\Delta T_{cr,1} = \frac{h}{\alpha_c} \frac{M_{cr,1}}{E_c I_1} \tag{5.17}$$

or

$$\Delta T_{cr,1} = \frac{h}{\alpha_c} \frac{(f_{ct,1} - \sigma_{ci} - \sigma_{ca}) Z_1}{E_c I_1} \tag{5.18}$$

After occurrence of the *m*th crack and before formation of the next crack, the value of M is represented by (line CD in Figure 5.2)

$$M = \frac{\alpha_c \Delta T}{h} E_c I_1 \left[1 + \frac{m\,s}{l} \left(\frac{I_1}{I_e} - 1 \right) \right]^{-1} \tag{5.19}$$

(with $\Delta T_{cr,m} \leq \Delta T \leq \Delta T_{cr,m+1}$)

Substituting $\Delta T_{cr,m}$ for ΔT and $m-1$ for m in Equation (5.19), the value of $\Delta T_{cr,m}$ at which the *m*th crack occurs, is given by:

$$M_{cr,m} = \frac{\alpha_c \Delta T_{cr,m}}{h} E_c I_1 \left[1 + \frac{(m-1)\,s}{l} \left(\frac{I_1}{I_e} - 1 \right) \right]^{-1} \tag{5.20}$$

In the derivation of the above equation, it was assumed, for simplicity, that the beam does not lose symmetry about the center of the span as a result of crack formation. This assumption makes the structure statically indeterminate to the first degree, with the indeterminate force being a bending moment M whose magnitude is constant over the span (El-Badry and Ghali, 1995).

Equations (5.14) and (5.18) give $M_{cr,1}$ and $\Delta T_{cr,1}$. Substituting the value of $\Delta T_{cr,1}$ in Equation (5.19) gives the lower ordinate of M.

Setting $m = 2, 3, \ldots, 6$ and solving Equations (5.2), (5.14) and (5.20) for $\Delta T_{cr,m}$, then substituting in Equations (5.14) and (5.19), gives all the values necessary for plotting the graphs in Figures 5.3 to 5.5 for beams L.6, L.8 and L1.0, respectively. The values of $\Delta T_{cr,m}$ and the corresponding M-ordinates for the three beams are listed in Table 5.1. More details on the above equations can be found in El-Badry and Ghali (1995).

Also plotted in Figures 5.3 to 5.5 are the experimental M-ΔT diagrams obtained from the thermal load tests. As can be seen, a reasonable agreement between the analytical and the experimental results is obtained, particularly for beams L.8 and L1.0

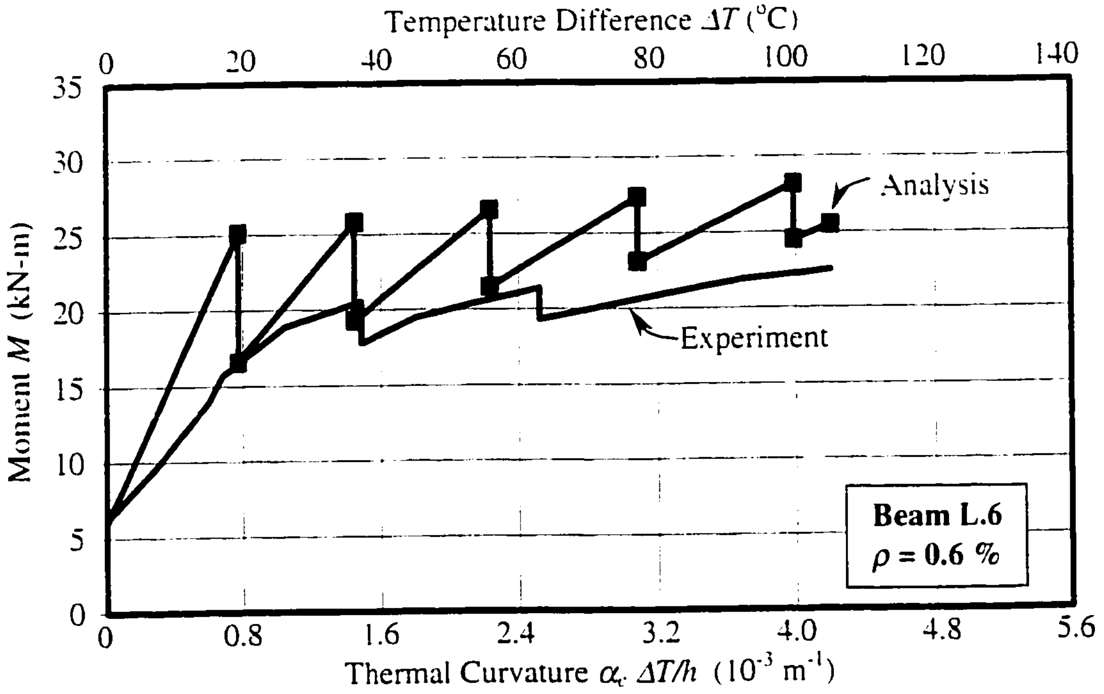

Figure 5.3 Bending Moment versus ΔT in Beam L.6 Reinforced with 0.6% Leadline

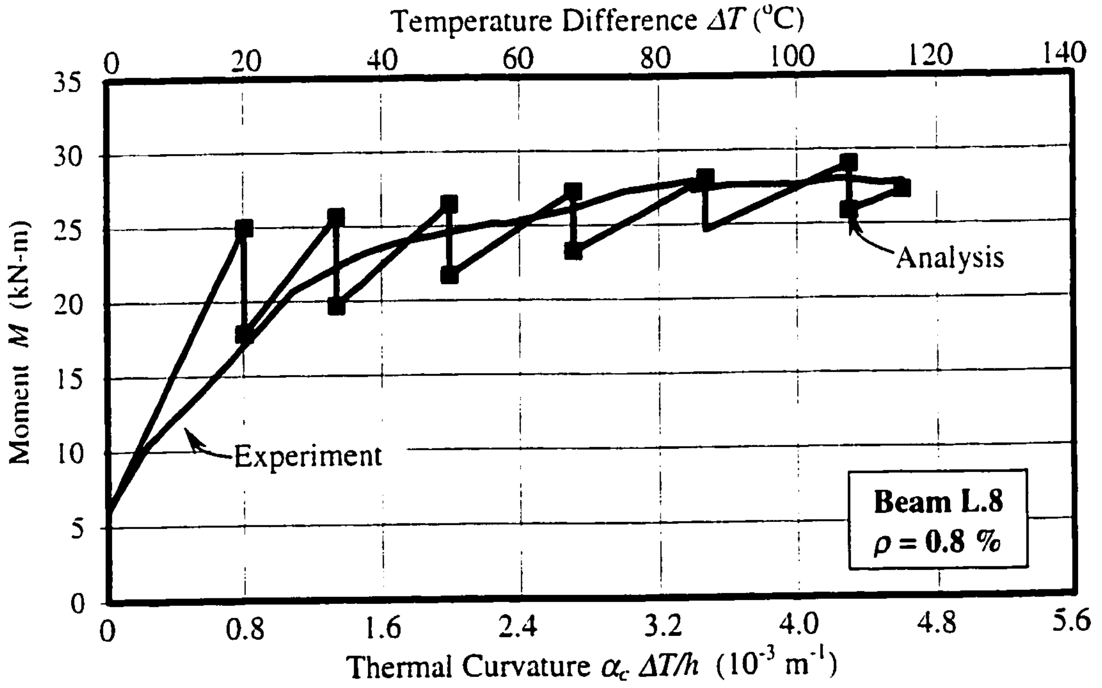

Figure 5.4 Bending Moment versus ΔT in Beam L.8 Reinforced with 0.8% Leadline

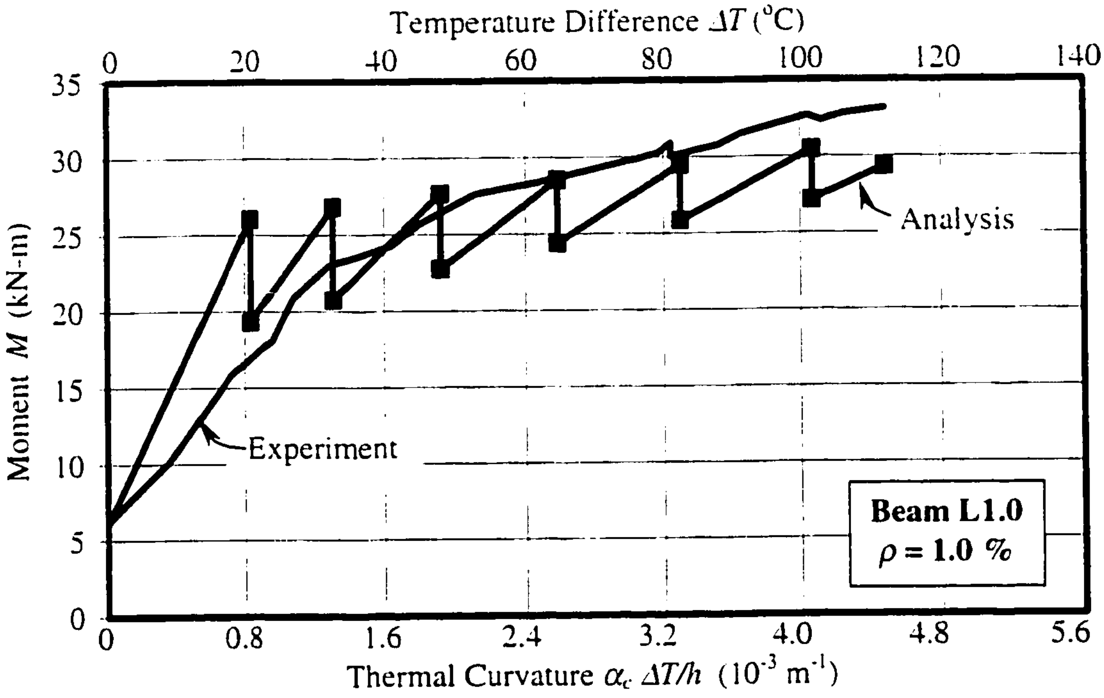

Figure 5.5 Bending Moment versus ΔT in Beam L1.0 Reinforced with 1.0% Leadline

Table 5.1 Values of M versus ΔT Plotted in Graphs of Figures 5.3 to 5.5

Beam Designation	Crack Number m	1	2	3	4	5	6
L.6	Temperature Difference $\Delta T_{cr,m}$ (°C)	19.33	36.12	55.84	77.01	99.71	124.04
	Moment at Cracking $M_{cr,m}$ (kN-m)	25.14	25.84	26.60	27.38	28.20	29.04
	Reduced Moment M, Lower Ordinate, (kN-m)	16.62	19.32	21.50	23.14	24.52	25.77
L.8	Temperature Difference $\Delta T_{cr,m}$ (°C)	20.09	33.39	49.92	67.72	86.87	107.45
	Moment at Cracking $M_{cr,m}$ (kN-m)	24.97	25.68	26.46	27.28	28.13	29.02
	Reduced Moment M, Lower Ordinate, (kN-m)	17.84	19.69	21.69	23.25	24.61	25.86
L1.0	Temperature Difference $\Delta T_{cr,m}$ (°C)	20.92	32.73	48.05	64.58	82.40	101.60
	Moment at Cracking $M_{cr,m}$ (kN-m)	26.07	26.82	27.67	28.56	29.49	30.47
	Reduced Moment M, Lower Ordinate, (kN-m)	19.31	20.76	22.79	24.41	25.84	27.18

Chapter 6

Summary, Conclusions, and Recommendations

6.1 Introduction

The major emphasis of the experimental program presented in this thesis was to investigate and examine the behavior of concrete members under the effects of temperature gradients. The investigation focuses on concrete beams reinforced with different types of Fiber Reinforced Polymer (FRP) reinforcement and partially prestressed by Carbon Fiber Reinforced Polymer rods.

Summary and conclusions of the project are presented in this chapter. Recommendations are also given for further research in the area of the thermal behavior of FRP reinforced concrete structures.

6.2 Summary

The main objective of this research was to investigate the behavior of FRP reinforced and partially prestressed concrete beams when subjected to temperature variations. The focus of this experimental program was on the use of carbon fiber and glass fiber reinforced polymer reinforcement in lieu of conventional steel bars. More specifically, the objective was to determine the effects of thermal characteristics of different types of FRP on the development of thermal stresses and on the control of thermal cracking. Another major objective was to study the effects of important parameters such as the reinforcement ratios, ρ, and the level of prestressing produced by both concentric and eccentric tendons on the thermal behavior of the concrete members.

A total of eleven reinforced concrete (RC) and partially prestressed concrete (PPC) beams using FRP reinforcements were tested. The test program consisted of two series: Series A (RC) and Series B (PPC). The beams in both series had 500 x 250mm rectangular cross section. The beams of Series A were 3350 mm long and the beams of Series B were 4500 mm long. Beams of Series A were divided into two groups, A1 and A2. Each group consisted of three beams of the same dimensions, 250 x 500 x 3350mm, but reinforced with different type of FRP rebars. In Series B, five beams were constructed into two groups: two partially pretensioned concrete beams and three partially post-tensioned concrete beams.

The FRP rods used in the experimental program for Series A were 8mm single-indented and 10mm-double indented rods made of carbon fibers (Leadline), and NEFMAC-Grid type reinforcement made of glass fibers. Two types of tendons were used in Series B: one was a prestressing steel strand (low-relaxation seven wire, Grade 270) and the other was 8mm single-intended rod made of carbon fibers (Leadline). The FRP rebars were produced and supplied by Mistubish Kasei Corporation and the NEFMAC were supplied by NEFCOM Corporation in Japan. In the PPC beams, the tendons were stressed in small increments using a hydraulic jack until the desired prestressing force was reached. The target effective prestressing force in the tendons was 63.5 kN (0.5MPa) or about 70% of its guaranteed tensile strength.

All the beams were tested in three satges: under temperature loading, under mechanically applied moment and finally under mechanical load. In the thermal loading tests the specimens were subjected to thermal gradients on one side using infrared lamps. End rotations were restrained to produce thermal moment along the tested length. The bending moment and the cracks developed by thermal gradient were monitored and the crack widths and spacing were recorded. The behavior of the thermally cracked beams was also investigated under the effects of mechanically applied moment. Finally, the beams were tested statically as simply supported and subjected to two concentrated loads, each applied at one third of the 2000 mm test length. The load was increased monotonically in increments of 3kN each.

The experimental results were compared to those results obtained from tests carried out on beams with the same dimensions but reinforced with conventional steel (Ariyawardena, 1993). An analytical model was also employed in this project to calculate the thermal moment versus temperature difference. The equations proposed by El-Badry and Ghali (1995) were used. Theoretical predictions were then compared to the experimental results obtained from this investigation.

6.3 Conclusions

The results of the behavior of FRP reinforced and prestressed concrete beams under the effects of temperature gradients were presented and discussed in Chapters 4 and 5 and Appendix A. The following conclusions can be drawn from the present investigation:

1. The temperature distribution measured across the depth of the beam cross section was nonlinear. However, because of the shallow depth of the cross section, the temperature distribution could be approximated to a linear distribution.
2. The large difference between the longitudinal coefficient of thermal expansion of the CFRP Leadline rods and the concrete ($\alpha_{fL} = -0.9\times10^{-6}\,^{\circ}C^{-1}$ to $0.68\times10^{-6}\,^{\circ}C^{-1}$ compared

to $\alpha_c = 10\text{x}10^{-6}\ ^{\circ}C^{-1}$) produces compressive stresses in the concrete and tensile stresses in the Leadline rods under increasing temperature.

3. The maximum end moment produced by temperature gradient in the tested beam is equal to the cracking moment. Cracking of concrete produces a drop in the end moment because of the reduction in beam stiffness.
4. The thermal behavior of the beams reinforced with CFRP (Leadline) rods was better than that of the beams reinforced with steel or those reinforced with GFRP NEFMAC grids. The CFRP reinforced beams continued to show an increase in the thermal moment with the increase in temperature up to the end of the test.
5. The test results demonstrated that increasing the reinforcement ratio from 0.6% to 1.0% improved significantly the thermal moment of the CFRP reinforced beams, and reduced the crack width from 0.33 mm to 0.1 mm.
6. The NEFMAC reinforced beams under the effects of temperature gradients showed the largest drop in thermal moment at cracking. This led to a great reduction in the stiffness of the concrete beam, and consequently relaxation of the induced thermal moment in the beam.
7. For the same reinforcement ratio, the crack width in the beams reinforced with Leadline and steel ranged between 0.1mm and 0.33mm, which is considered to be within the service load limits. However, for the beams reinforced with NEFMAC, the crack width ranged between 1.5 mm and 1.7 mm, which greatly exceeds the allowable limits.
8. Since the modulus of elasticity of NEFMAC and CFRP are about 20% and 70% that of steel, respectively, the deflection of NEFMAC and CFRP reinforced beams due to

mechanically applied moment in thermally cracked concrete beams are larger than those beams reinforced with steel bars.

9. The new anchorage system used in this investigation is effective for prestressing applications using CFRP Leadline rods.
10. The PPC beams pretensioned with Leadline rods showed better behavior under thermal and mechanical loading than the unbonded post-tensioned beams. This is mainly because of the bond between the pretensioned tendons and concrete. Also, the eccentricity of the prestressing tendon improves the behavior in terms of thermal moments, crack width and mid-span deflection.
11. The load-deflection response of thermally cracked concrete beams showed that the ultimate strength of the CFRP reinforced or prestressed beams was higher than that the NEFMAC reinforced beams. This is attributed to the fact that the tensile strength of the Leadline is about 1.25 and 4 times higher than that of steel and NEFMAC, respectively.
12. The PPC beams and the NEFMAC reinforced beams failed in flexure whereas the beams reinforced with Leadline failed in shear, accompanied by splitting on the resin surface of the Leadline rods while the carbon fibers continued to carry tensile stresses.
13. After modifying the analytical model of El-Badry and Ghali (1995) to account for the effects of difference in the coefficient of thermal expansion of CFRP and concrete, the model proved to be efficient in predicting the thermal moment-curvature relationship for beams reinforced with CFRP reinforcement.

6.4 Recommendations for Further Research

The present investigation was limited to some but important parameters that affect the behavior of concrete members reinforced or prestressed with FRP and subjected to temperature variations. Further research is needed to investigate the effects of other parameters and to provide a comprehensive understanding of the thermal behavior of concrete structures. Some of the investigations needed in this area are recommended below:

1. Tests needed to be carried out to study the effect of temperature on creep of concrete.
2. In the present investigation, only one straight-CFRP tendon with small reinforcement ratios and one value of prestressing force was used. The effects of other profiles such as curved and more than one tendon with different reinforcement ratios and values of prestressing need to be investigated under the effect of temperature.
3. More research is required to investigate the thermal behavior of concrete members using Leadline rods and steel bars together in the same section.
4. The effects of transverse thermal expansion coefficient of FRP rebars on concrete members when subjected to temperature variation need to be investigated.
5. Research is needed to study the behavior of beams of different cross section shapes and depths reinforced with FRP reinforcement under the effects of temperature gradients.

References

Ariyawardena, T.M., (1993), "Behavior of Concrete Structures Subjected to Thermal Stresses," M.Sc. Thesis, the University of Calgary, Alberta, Canada, 1993, 212 pp.

Ariyawardena, T.M., Ghali, A. and El-Badry, M.M., (1997), "Experimental Studies on Thermal Cracking in Reinforced Concrete Members," ACI Structural Journal, Vol. 94, No. 4, July-August 1997, pp. 432-442.

Abdalla, H.A. and El-Badry, M.M., (1997), "Temperature Effects on Concrete Members Reinforced with FRP Reinforcement," the 25th Annual Conference of the Canadian Society for Civil Engineering, Sherbrooke, Canada, May 1997, pp. 171-180.

CSA Standard CAN3-A23.3-94, (1994), *Design of Concrete Structures for Buildings*. Canadian Standard Association, Rexdale, December 1994.

Daniel, I.M. and Ishai, O., (1994), *Engineering Mechanics of Composite Material*, Oxford University Press., Inc.

Erik, M.A. and Rizkalla, S.H., (1993a), "FRP Reinforcement for Concrete Structures," ACI Concrete International Journal, Vol. 15, No. 6, June 1993, pp. 48-53.

El-Badry, M.M. and Ghali, A., (1983), "Temperature Variation in Concrete Bridge," Journal of Structural Engineering, ASCE, Proceedings, Vol. 109, No. 10, October 1983, pp. 2355-2374.

El-Badry, M.M. and Ghali, A., (1995), "Control of Thermal Cracking of Concrete Structures," ACI Structural Journal, American Concrete Institute, Vol. 92, No. 4, July-August 1995, pp. 435-450.

El-Badry, M.M. and Abdalla, H.A., (1998), "Experimental Studies on Thermal Cracking in Concrete Member Reinforced with FRP," the First Conference on Durability of Fiber Reinforced Polymer Composites for Construction, (CDCC98), August 1998, Sherbrooke, Canada, pp. 669-680.

Gentry, T.R. and Hudak, C.E., (1996), "Thermal Compatibility of Plastic Composite Reinforcement and Concrete," the Second International Conference on Advanced Composite Materials in Bridges and Structures, Montreal, Canada, August 1996, pp. 149-156.

ISIS Canada, Project T4.4, "A New Anchorage System for Carbon Fiber Reinforced Plastic (CFRP) Tendons," http://www.enci.ucalgary.ca/~isis/new_anch.html, Canada.

ISIS Canada, Project T4.4, "Properties of GFRP, AFRP, and CFRP Compared to Prestressing Steel Tendons." http://www.enci.ucalgary.ca/~isis_prop.html, Canada.

Kumahara, S., Masuda, Y., Tanano, H. and Shimizu, A., (1993), "Tensile Strength of Continuous Fiber Bar Under High Temperature," International Symposium on Fiber-Reinforced-Plastic Reinforcement for Concrete Structures, ACI Publication SP 138-52, Nanni A. and Dolan C.W., (Editors), Deteroit, Michigan, USA, 1993, pp. 731-742.

Matthys, S., De Schutter, G. and Taerwe, L., (1996), "Influence of Transverse Thermal Expansion of FRP Reinforcement on the Critical Concrete Cover," the Second International Conference on Advanced Composite Materials in Bridges and Structures, Montreal, Canada, August 1996, pp. 665-672.

Mitsubishi Kasei Corporation, (1992), "Leadline Carbon Fiber Rods," Technical data, Japan, 1992, 40 pp.

NEFCOM Corporation, "NEFMAC Reinforcement," Technical Report Data, http://www.iijnet.or.jp/NEFCOM/NEFCHTM/EFCOM0.HTM, Japan.

Podolny, J.W., (1985), "The Cause of Cracking in Post-Tensioned Concrete Box Girder Bridges and Retrofit Procedures," PCI Journal, Vol. 30, No. 2, March-April 1985, pp. 82-139.

Priestley, M. J. N., (1978), "Design of Concrete Bridge for Temperature Gradients," ACI Journal, Vol. 75, No. 5, May 1978, pp. 209-217.

Sayed-Ahmed, E.Y. and Shrive, N.G., (1998a) "A New Steel Anchorage System for Post-Tensioning Application Using Carbon Fiber Reinforced Plastic Tendons" Canadian Journal of Civil Engineering, Vol. 25, No. 1, February 1998, p. 113-127.

Sayed-Ahmed, E.Y. and Shrive, N.G., (1998b) "CFRP Post-Tensioned Masonry Diaphragm walls," Proceedings of the Annual CSCE Conference, Halifax, June 10-13, 1998, pp. 571-582.

Bibliography

American Concrete Institute. (1996), "Fiber Reinforced Plastic Reinforcement." ACI Compilation C-33. 1996. 72 pp.

ACI Committee 435. (1985), "State-of-the-Art Report on Temperature-Induced Deflections of Reinforced Concrete Members." ACI 435.7R-85, 1985, 14 pp.

ACI Committee 224. (1990), "Control of Cracking In Concrete Structures." ACI 224R-90, 1990. 42 pp.

ACI Committee 224, (1993), "Causes, Evaluation and Repair of Cracks in Concrete Structures," ACI 224.1R-93, Detroit, 1993, 22 pp.

ACI Committee 605, (1988),"Recommended Practice for Hot Weather Concreting," ACI 605-59, American Concrete Institute, Detroit, 1988, 10 pp.

Annual Book of ASTM Standards, (1987), Section 4, Vol. 04.02, Concrete and Aggregate, 1987, pp. 348-352.

Abdalla, H.A., El-Badry, M.M. and Rizkalla, S.H., (1996), "Deflection of Concrete Slabs Reinforced with Advanced Composite Materials," the Second International Conference on Advanced Composite Materials in Bridges and Structures, Montreal, August 1996, pp. 201-208.

Abdelrahman, A.A. and Rizkalla, S.H., (1995a), "Behavior of Concrete Beams Prestressed by Carbon Fiber Reinforced Plastic Reinforcement," Second Annual Conference in Engineering Materials Symposium, Canadian Society for Civil Engineering, CSCE, Ottawa, Ontario, June 1-3, 1995, pp. 585-594.

Abdelrahman, A.A. and Rizkalla, S.H., (1995b), "Serviceability of Concrete Beams Prestressed by Carbon Fiber Reinforced Plastic Rods," Proceedings of the Second International RILEM Symposium (FRPRCS-2), "Non-Metallic (FRP) Reinforcement for Concrete Structures," Taerwe L. (Editor), Chapman and Hall Publisher, 1995, pp. 403-412.

Beeby, A.E., (1971), "An Investigation of the Cracking on the Side Faces of Beams," Cement and Concrete Association, Technical Report No. 42.466, December 1971.

Beeby, A.E., Keyder, E. and Taylor, H.P.G., (1972), "Cracking and Deflection of Prestressed Concrete Beams," Cement and Concrete Association, London, Technical Report, January 1972.

Bertero, V.V. and Polvika, M. (1972), "Influence of Thermal Exposure on Mechanical Characteristics of Concrete," Concrete for Nuclear Reactors, ACI Special Publication SP-34, Paper SP 34-28, Vol. 1, 1972, pp. 505-519.

Benmokrane, B. and Rahman, H., (Editors), (1998), *First Conference on Durability of Fiber Reinforced Polymer Composites for Construction*, CDCC 98, Sherbrooke, Canada, July 18, 1998, 692 pp.

Church, J.G. and Clark, L.S., (1988), "the Effect of Combined Thermal and Force Loads on the Behavior of Reinforced Concrete Beams," the Structural Engineer, Vol. 66, No. 16, August 1988, pp.262-267.

Clark, L.A. and Church, J.G., (1987), "Thermal Curvatures and Strains in Cracked Reinforced Concrete Beams," Proceedings, Institute of Civil Engineering, Part 2, Vol. 83, March 1987, pp. 197-212.

Cooke, N., Priestley, M.J.N. and Thurston, S.J., (1984), "Analysis and Design of Partially Prestressed Concrete Bridges Under Thermal Loadings," PCI Journal, May-June 1984, pp. 94-113.

CHBDCT Technical Subcommittee No. 16, (1996), "Design Provisions for Fiber Reinforced Structures in the Canadian Highway Bridge Design Code," Second International Conference on Advanced Composite Materials in Bridges and Structures, ACMB II, CSCE Publication, El-Badry M.M., (Editor), Montreal, Canada, August 11-14,1996, pp.391-406.

Collins, M.P. and Mitchell, D., (1991), *Prestressed Concrete Structures*, Prentice Hall, Englewood Cliffs, 1991, 766 pp.

Dilger, W.H., Ghali, A., Cheung, M.S. and Maes, M.A., (1983), "Temperature Induced Stresses in Composite Box-Girder Bridges," Journal of Structural Engineering, ASCE, Vol. 109, No. 6, June 1983, pp. 1460-1478.

Emersion, M., (1973), "the Calculation of the Distribution of Temperature in Bridges," TRRL Report LR 561, Transport and Rod Research Laboratory, Crowthrone, Berkshire, 1973, 33 pp.

England, G.L. and Ross, A.D., (1962), "Reinforced Concrete Under Thermal Gradients," Magazine of Concrete Research, Vol. 14, No. 40, March 1962, pp. 5-12.

Erik, M.A. and Rizkalla, S.H., (1993b) "Anchorages for FRP Reinforcement," ACI Concrete International Journal, Vol. 15, No. 6, June 1993, pp. 54-59.

El-Badry, M.M., (1982), " Thermal Response of Concrete Box-Girder Bridges," M.Sc. Thesis, The University of Calgary, Calgary, Alberta, Canada, 1982.

El-Badry, M.M. and Ghali, A., (1986), "Thermal Stresses and Cracking of Concrete Bridges," Journal of the American Concrete Institute, ACI Proceedings, Vol. 83, No. 6, November-December 1986, pp. 1001-1009.

El-Badry, M.M., (Editor), (1996), *Advanced Composite Materials in Bridges and Structures*, ACMBS-II, Second International Conference, Montreal, Canada, August, 11-14, 1996, 1027 pp.

Freskakis, G.N., (1980), "Behavior of Reinforced Concrete at Elevated Temperatures," Proceedings, ASCE Conference on Civil Engineering and Nuclear Power, Vol. 1, Knoxvilla, Tennessee, September 1980.

Farhang, A.A., (1998), Plain and Steel Fiber Reinforced Concrete Beams Subjected to Combined Mechanical and Thermal Loading, TRITA-KN, Bulletin 38, 1998, 300 pp.

Gere, J.M. and Timoshenko, S.P., (1991), Mechanics of Materials, Chapman & Hall, UK, Third SI Edition, 1991, 807 pp.

Ghali, A. and Faver, R., (1994), *Concrete Stresses: Stresses and Deformations*, Chapman and Hall, London and New York, Second Edition, 1994, 352 pp.

Hannant, D.J. and Pell, P.S., (1962), "Thermal Stresses in Reinforced Concrete Slabs," Magazine of Concrete Research, Vol. 14, No. 41, July 1962, pp. 91-98.

Harada, T., Takeda, J., Yamane, S. and Furumura, F., (1972), "Strength Elasticity and Thermal Properties of Concrete Subjected to Elevated Temperatures," ACI Special Publication SP-34, Paper SP34-21, Vol. 1, 1972, pp. 377-406.

Hunt, B. and Cooke, N., (1975), "Thermal Calculations for Bridge Design," Journal of The Structural Division, ASCE, Vol. 101, No. ST9, Proc. Paper 11545, September 1975, pp.1763-1781.

Imbsen, R.A. and Vandershaf, D.E, (1985), "Thermal Effects on Concrete Bridge Structures," Second Bridge Engineering Conference, Transportation Research Record 950, TRB Transportation Research Board, National Research Council, Vol. 2, 1985, pp. 101-113.

Inino, K., Ikoma, T. and Yamazaki, N., (1983), "Studies on Thermal Stress Design Method for Reinforced Concrete Members of Nuclear Power Plants," 7th SMIRT Conference, Chicago, August 1983, Paper J4/5, pp. 209-217.

Irving, J. (1975), The Effects of Elevated Temperatures on Concrete and Concrete Structures, First Edition, Wexham Springs, 1975, 25 pp.

Kar, A.K., (1997), "Thermal Effects on Concrete Members," 4th Conference on Structural Mechanics in Reactor Technology, San Francisco, August 1997, paper J4/4, 11 pp.

Leonhartdt, F., (1987), "Cracks and Crack Control at Concrete Structures," IABSE Proceedings P-109/87, International Association for Bridge and Structural Engineering, February 1987, pp. 25-44.

Maher, D.R.H., (1970), "The effects of Differential Temperature on Continuous Prestressed Bridges," Australia, Institution of Engineers, Civil Engineering Transactions, Vol. CE. 12, No.1, Paper 233, April 1970, pp. 29-32.

Mentes, G.A., Bhat, P.D. and Ranni, A.I., (1980), "Thermal Effects on Reinforced Concrete Structures," Proceedings, ASCE Specialty Conference on Civil Engineering and Nuclear Power, Knoxville, American Society of Civil Engineers, New York, Vol. 1, Paper No. 3-5, September 1980.

Mallic, P.K., (Editor), (1998), *Fiber-Reinforced Composites: Materials, Manufacturing, and Design.* Marcell Dekker, INC. 470 pp.

Neville, A.M., (1981), *Properties of Concrete*, 3rd Edition, Pitman, London, 1981, 779 pp.

Nanni A., (Editor), (1993), *Fiber-Reinforced-Plastic (FRP) Reinforcement for Concrete Structures: Properties and Applications.* Developments in Civil Engineering, 42, Published by Elsevier Science. Amsterdam 1993, 450 pp.

Pillai, S.U. and Kirk, D.W., (1988), *Reinforced Concrete Design*, 2nd Edition, Mcgraw-Hill Ryerson Limited, Toronto, Canada, 1988, 641 pp.

Priestley, M. J. N., (1972), "Thermal Gradients in Bridge - Some Design Considerations," New Zealand Engineering (Wellington), Vol. 27, No. 7, July 1972, pp. 228-233.

Priestley, M. J. N., (1976), "Design Thermal Gradients for Concrete Bridges," New Zealand Engineering (Wellington), Vol. 31, No. 9, September 1976, pp. 213-219.

Ross, A.D. and England, G.L, (1962), "Reinforced Concrete Under Thermal Gradients," Magazine of Concrete Research, Vol. 14, No. 40, March 1962, pp. 5-12.

Ross, A.D., England, G.L and Suan R.H., (1965), "Prestressed Concrete Beams Under a Sustained Temperature Cross Fall," Magazine of Concrete Research, Vol. 17, No. 52, September 1965, pp. 117-126.

Rao, D.S.P., (1986), "Temperature Distributions and Stresses in Concrete Bridges," ACI Journal, July-August 1986, pp. 588-596.

Shibasaki, N., Yoshida, H., Sugawara, Y., Itabashi, H., Furukawa, S., Isobata, O., Yamazaki, N. and Irino, K., (1983), "An Experimental Study on Thermal Stresses on Reinforced Concrete Members under Short-Term Loading," 7th SMIRT Conference, Chicago, August 1983, Paper J 4/4, pp. 199-207.

Sugita, M., (1993), "NEFMAC-Grid Type Reinforcement," Fiber-Reinforced-Plastic (FRP) Reinforcement for Concrete Structures: Properties and Application, Nanni A. (Editor), Development in Civil Engineering Volume 42, Elsevier Science Publishers B.V. 1993, pp. 355-385.

Thurston, S.J. and Priestley, M.J.N., (1978), "Thermal Stresses in Concrete Structures", Research Report 78.21, Dept. of Civil Engineering, University of Canterbury, New Zealand, 1978.

Thurston, S.J., (1978), "Thermal Stresses in Concrete Structures," Ph. D Thesis, University of Cantebury, New Zealand, 1978.

Thurston, S.J. and Priestley, M.J.N., (1984), "Influence of Cracking on Thermal Response of Reinforced Concrete Bridges," Concrete International, Vol. 6, August 1984, pp. 36-43.

Vecchio, F.J. and Sato, J.A., (1990), "Thermal Gradients Effects in Reinforced Concrete Frame Structures," ACI Structural Journal, Vol. 87, No. 3, May-August 1990, pp. 262-275.

Zuk, W., (1965), "Thermal Behavior of Composite Bridges-Insulated and Uninsulated," Highway Research Record, No. 76, 1965, pp. 231-253.

Appendix A

Crack Pattern and Failure Mode in the Test Beams

The crack distribution and the failure mode for each beam specimen are presented in Figures A.1 to A.29. The first photograph for each beam represents the crack pattern under thermal loading which are marked in the picture by solid lines. The cracks produced by mechanically applied moment are shown by dotted lines in the same photograph. The crack distribution and a close up view of failure of each beam specimen under mechanical load are illustrated in the second photograph for each beam.

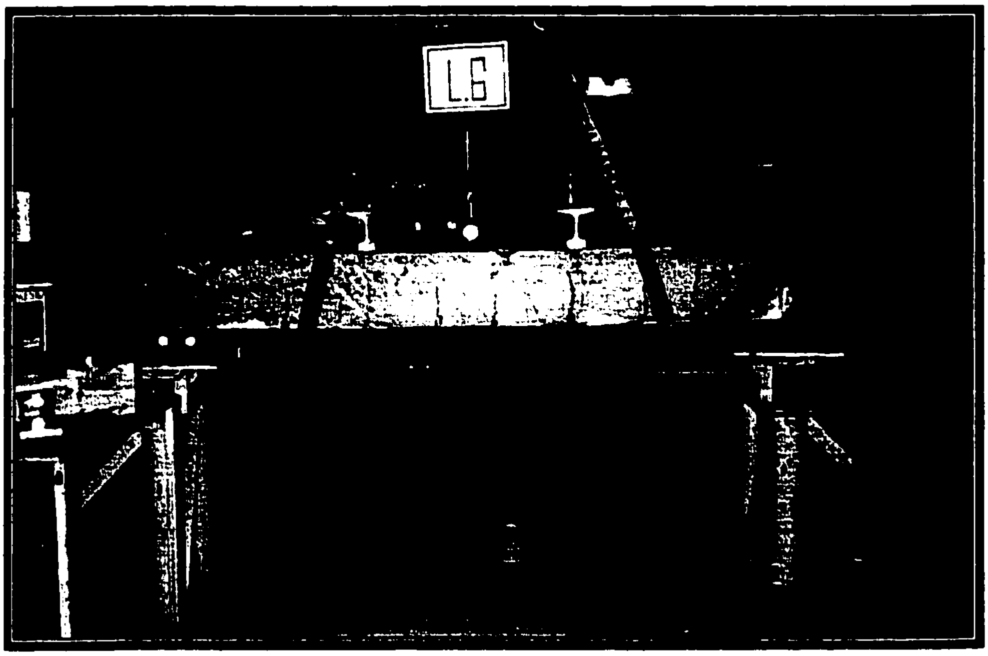

Figure A.1 Cracking due to Mechanical Load in Beam L.6

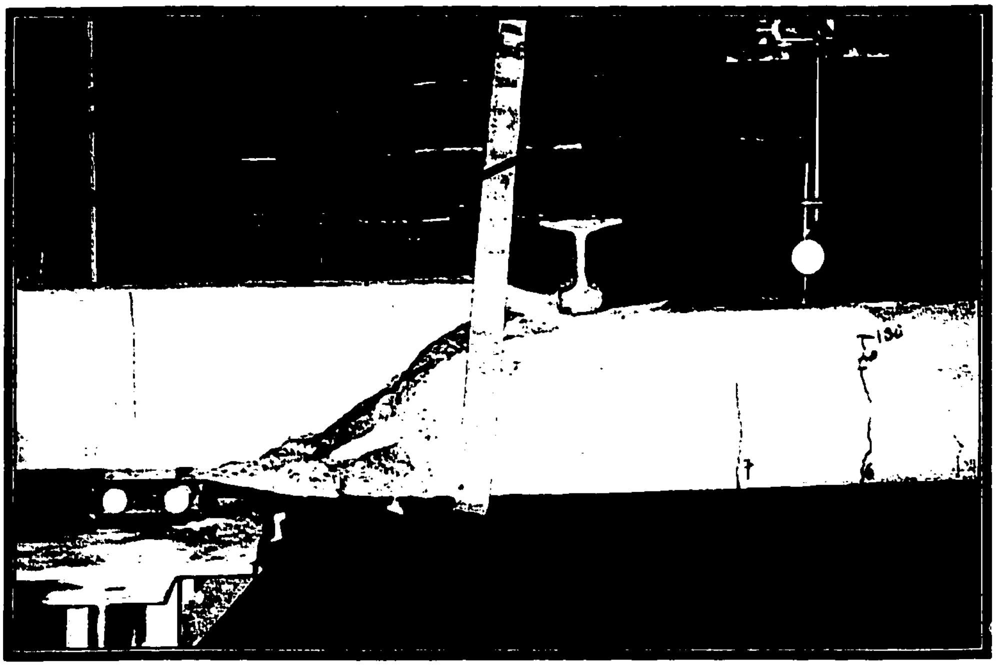

Figure A.2 Beam L.6 at Failure

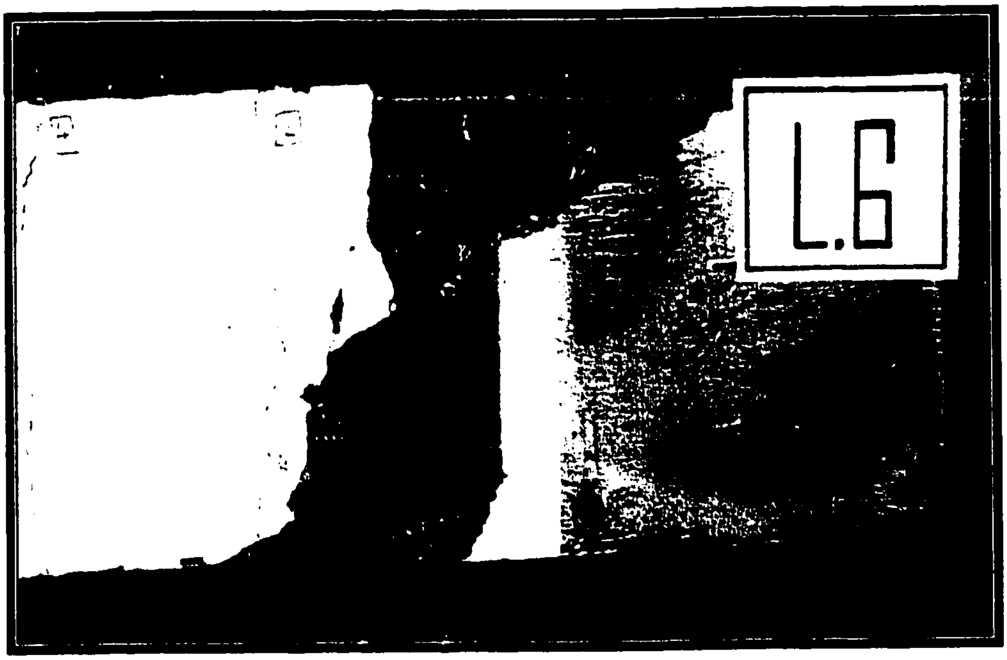

Note: Splitting failure was noticed on the resin surface of the Leadline rods for beam L.6 while the carbon fibers were still carrying tensile stress.

Figure A.3 Close-up View of Failure of Beam L.6

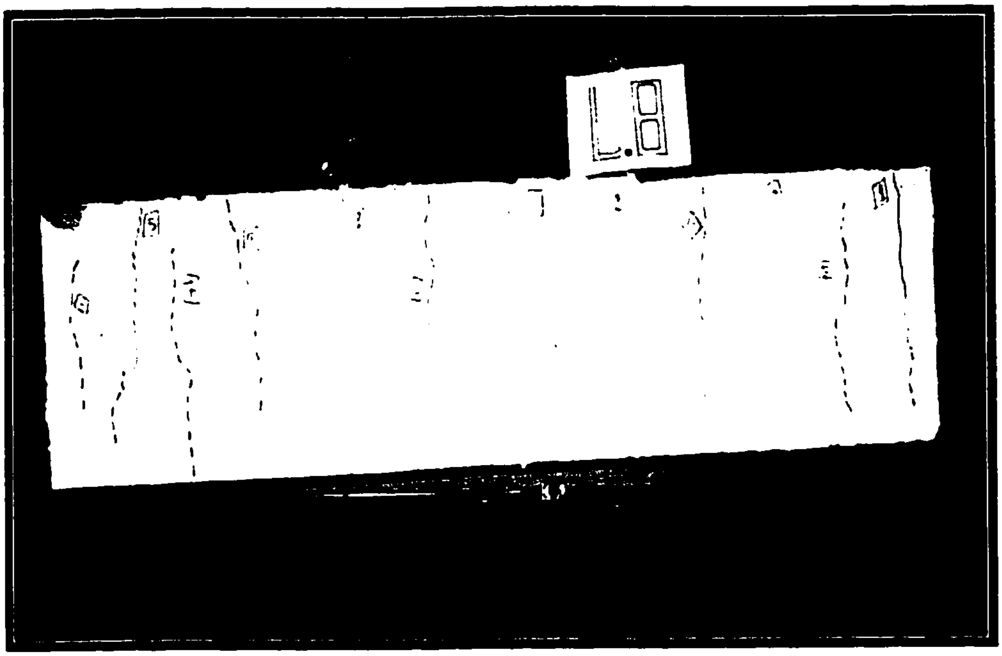

Figure A.4 Cracking due to Thermal Gradient and Mechanically Applied Moment in Beam L.8

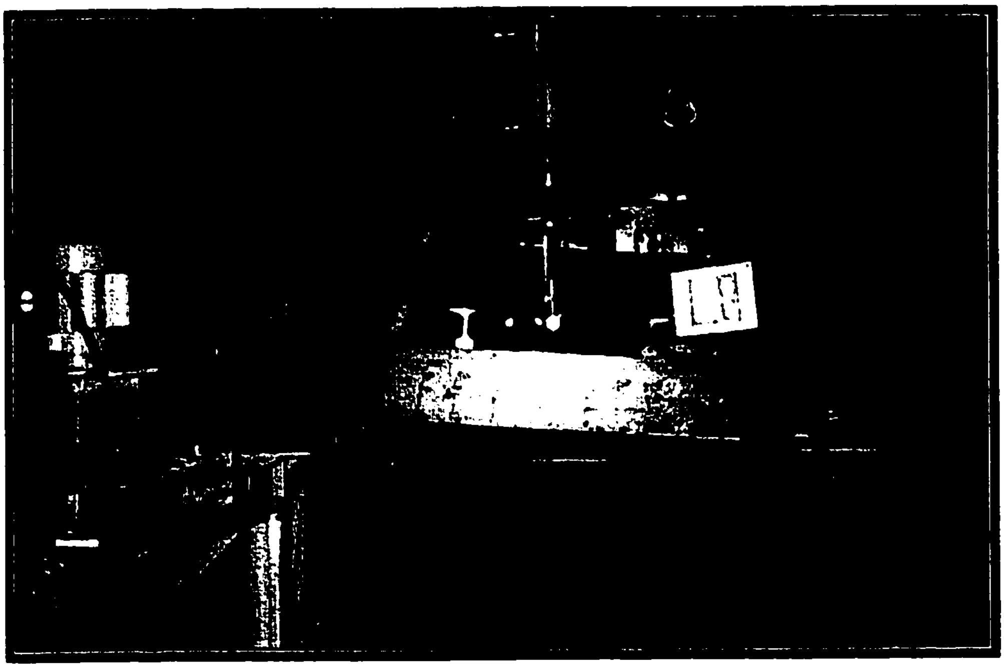

Figure A.5 Beam L.8 at Failure

Note: Splitting failure was noticed on the resin surface of the Leadline rods for beam L.8 while the carbon fibers were still carrying tensile stress.

Figure A.6 Close-up View of Failure of Beam L.8

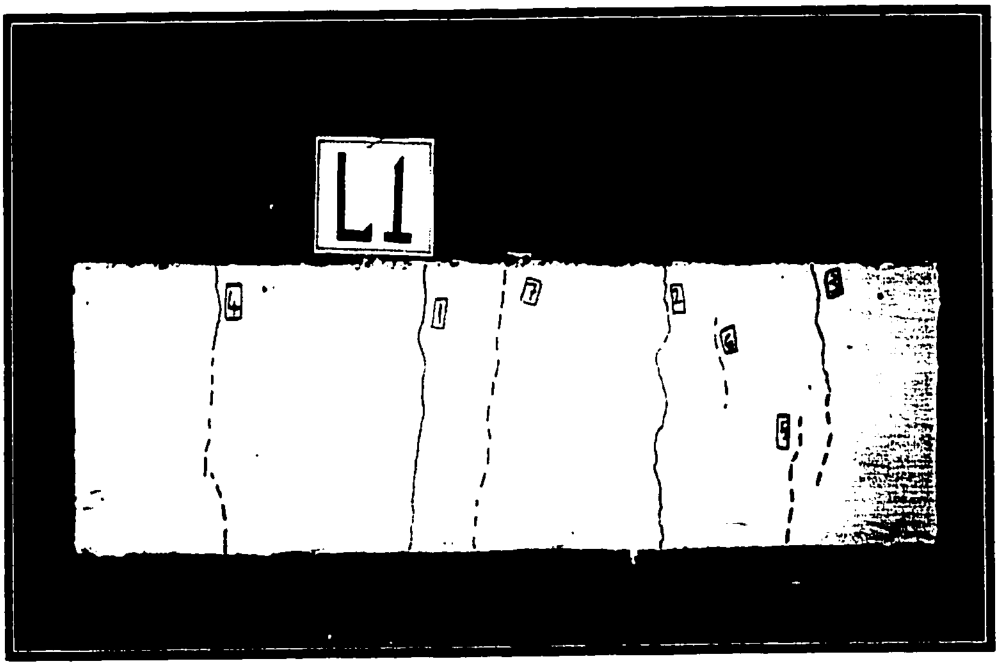

Figure A.7 Cracking due to Thermal Gradient and Mechanically Applied Moment in Beam L1.0

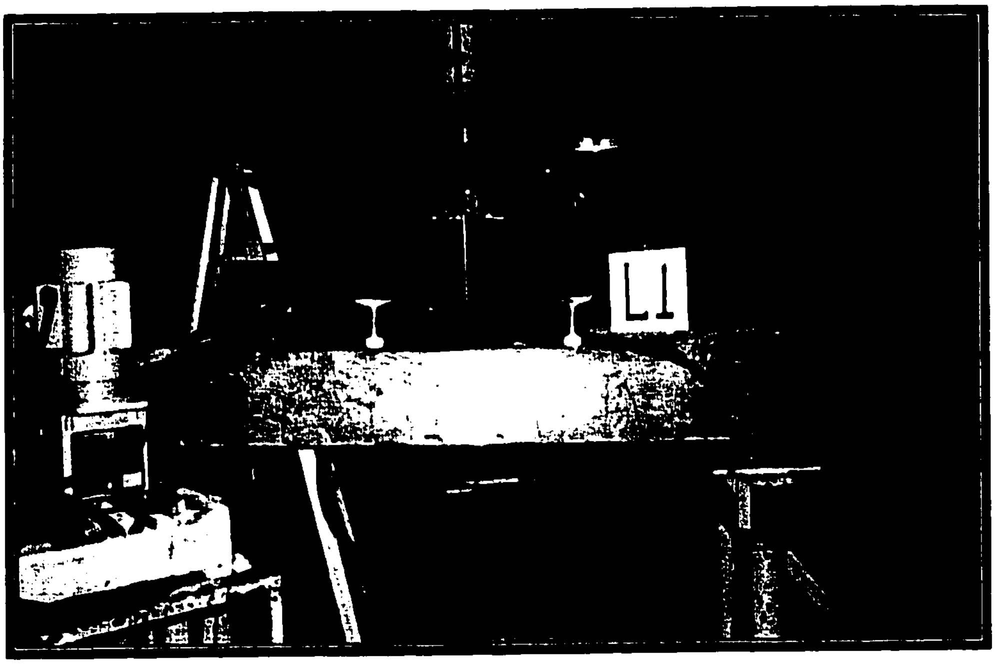

Figure A.8 Beam L1.0 at Failure

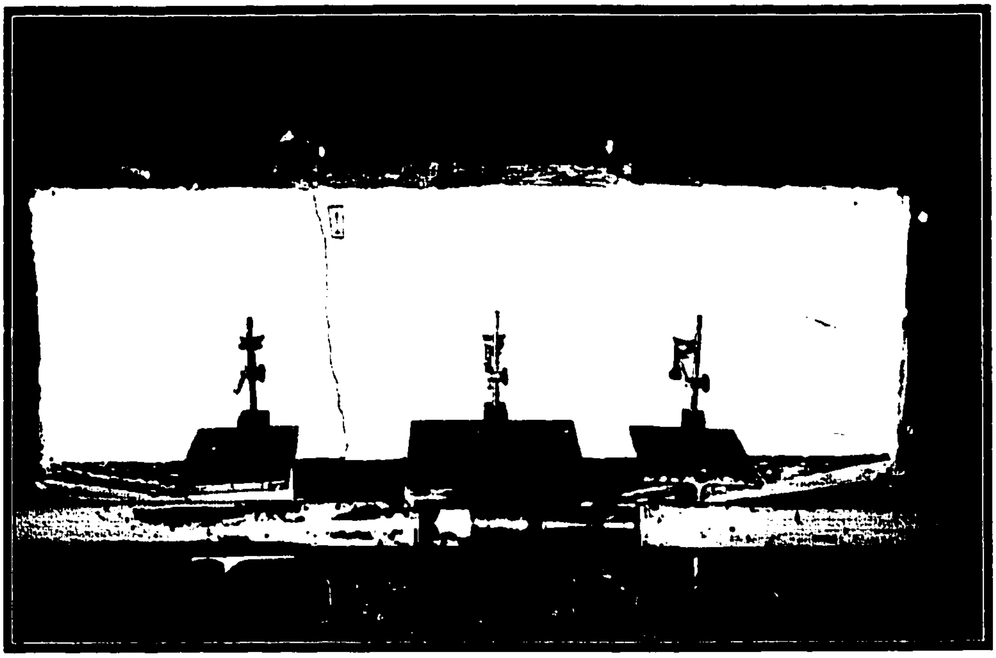

Figure A.9 Cracking due to Thermal Gradient in Beam GM.5

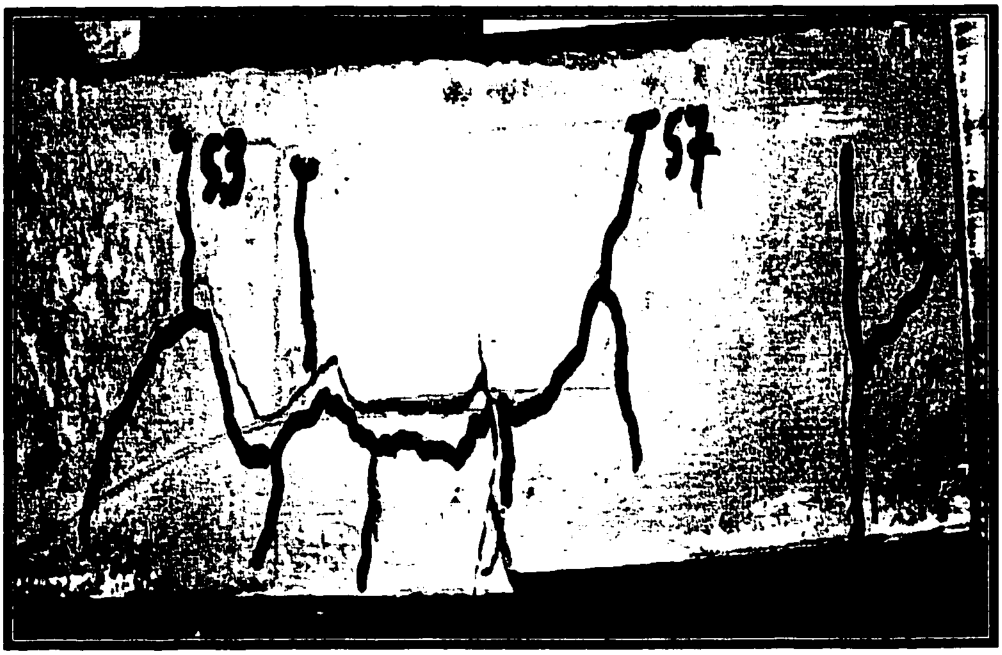

Figure A.10 Close-up of Failure of Beam GM.5 under Mechanical Load

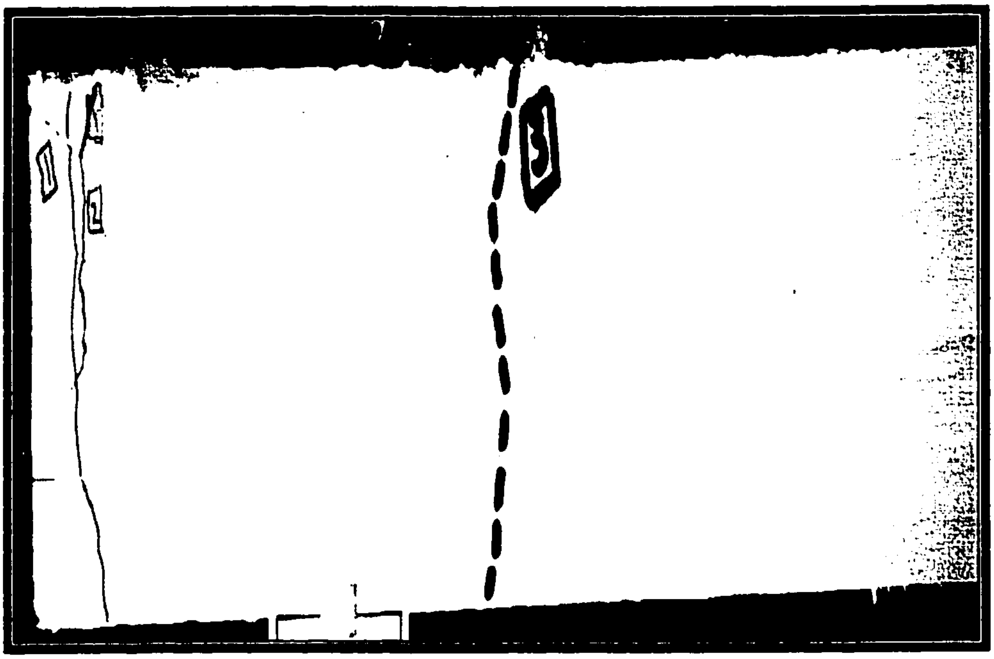

Figure A.11 Cracking due to Thermal Gradient and Mechanically Applied Moment in Beam GT.5

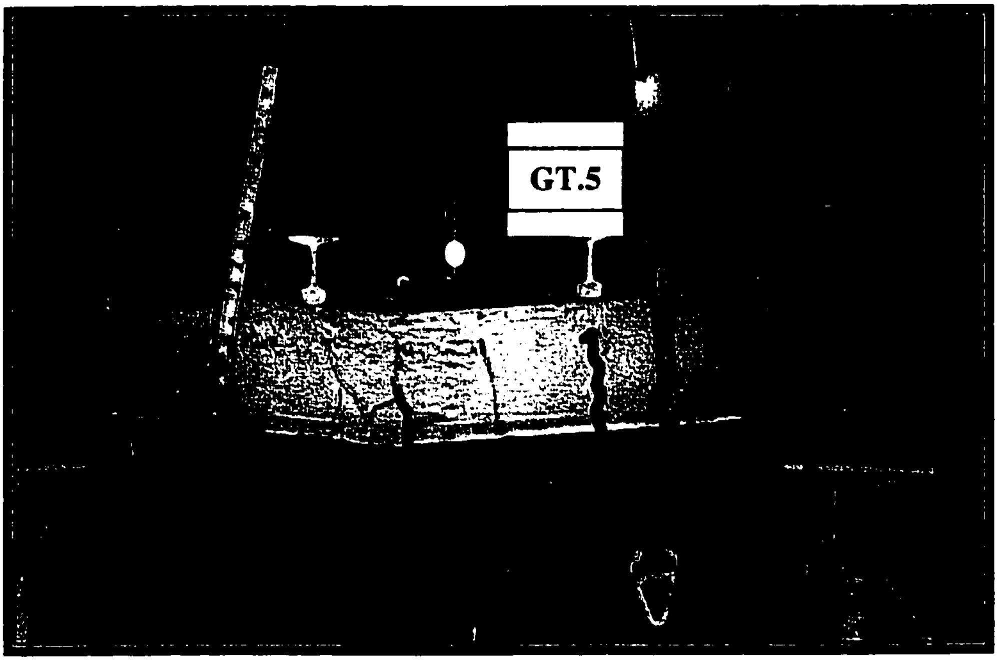

Figure A.12 Beam GT.5 at Failure

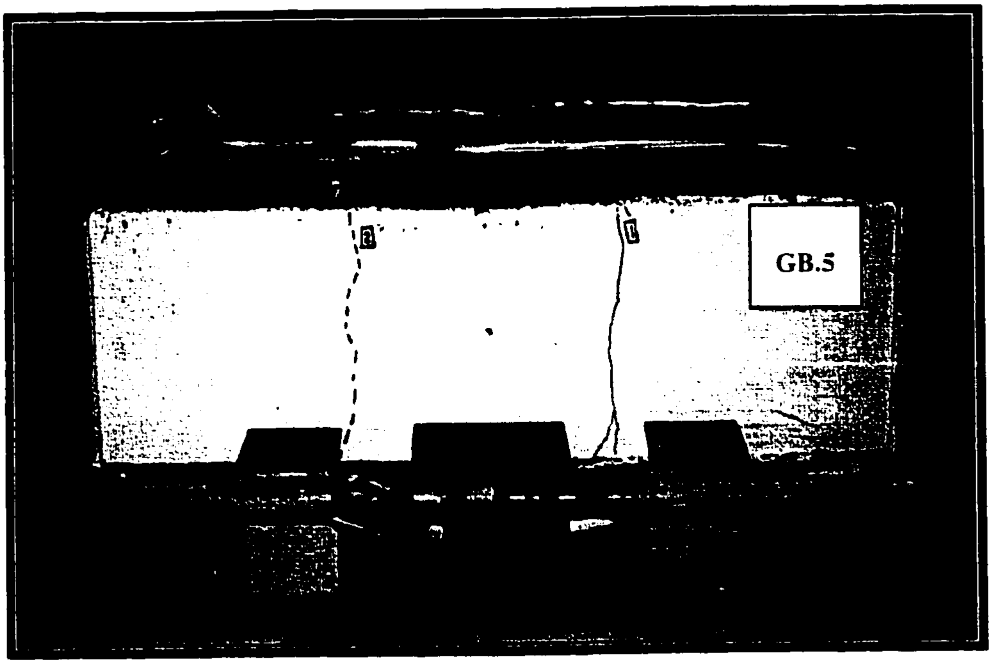

Figure A.13 Cracking due to Thermal Gradient and Mechanically Applied Moment in Beam GB.5

Figure A.14 Beam GB.5 at Failure

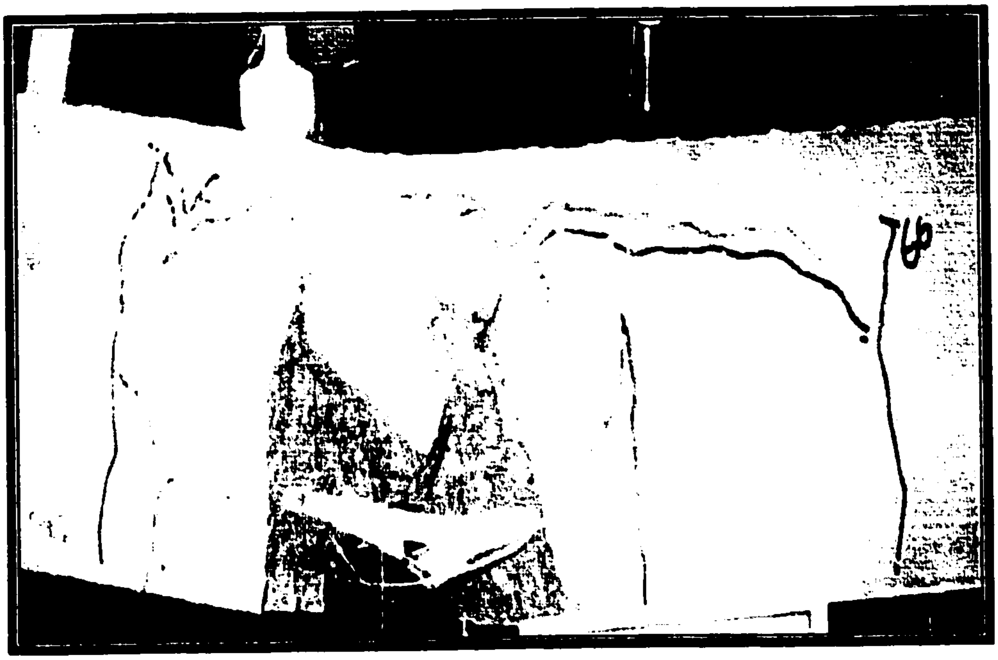

Figure A.15 Close-up of Failure of Beam GB.5 under Mechanical Load

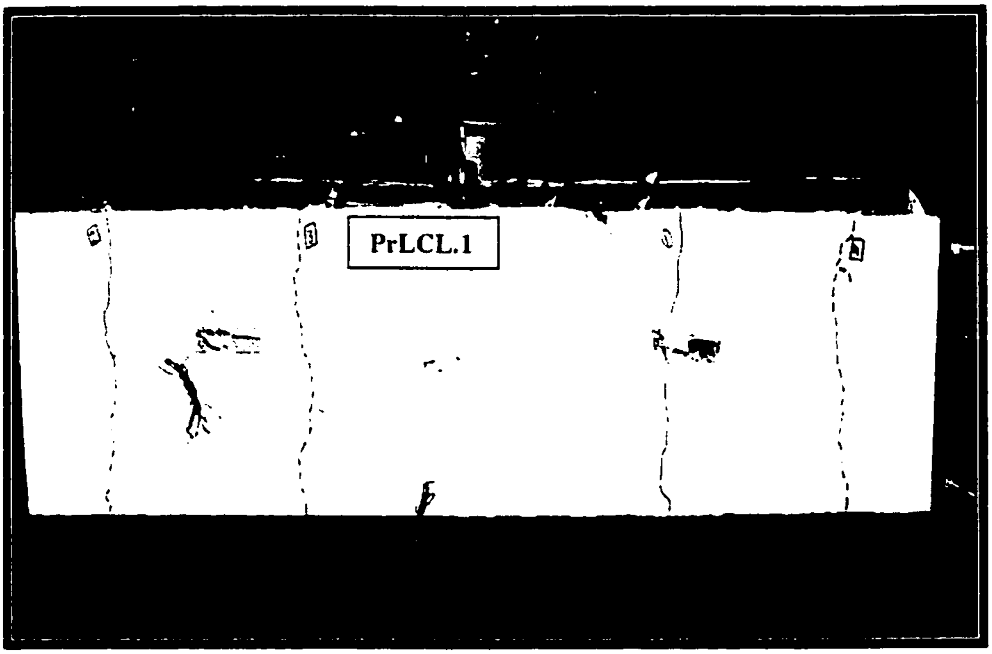

Figure A.16 Cracking due to Thermal Gradient and Mechanically Applied Moment in Beam PrLCL.1

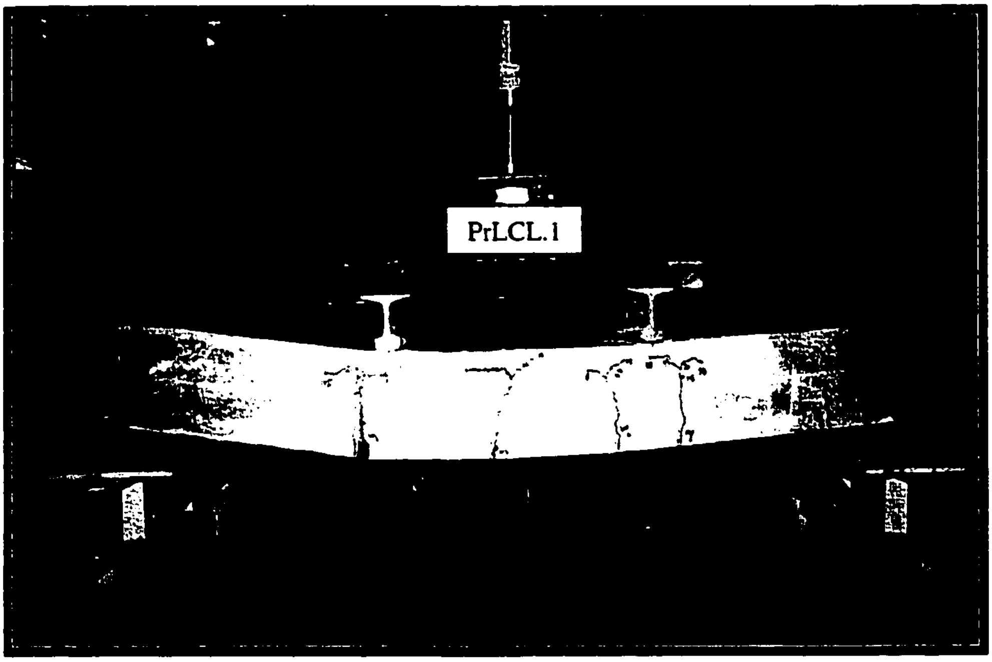

Figure A.17 Beam PrLCL.1 at Failure

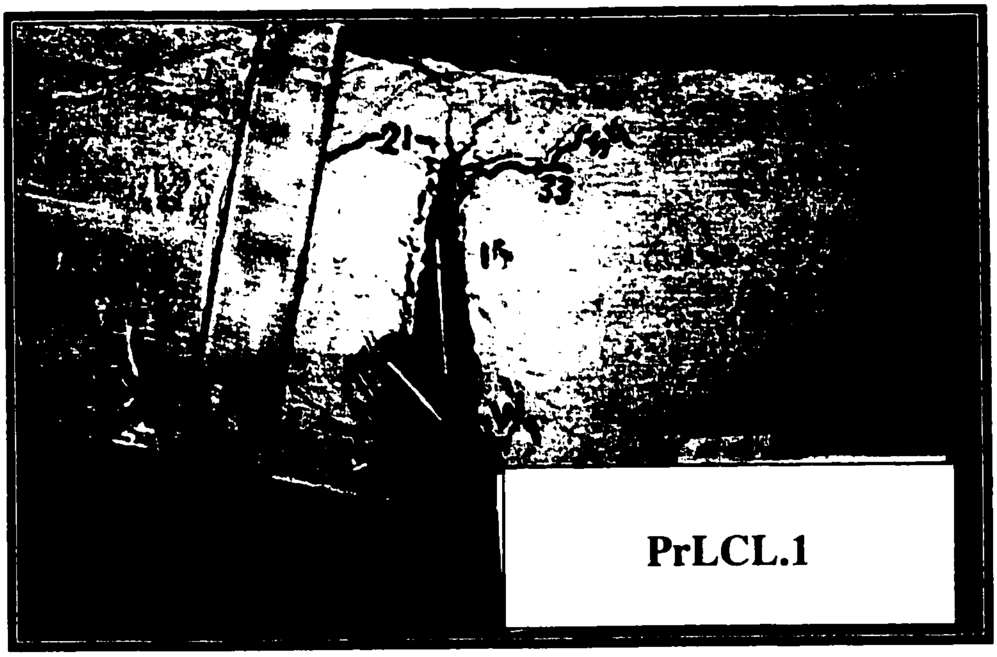

Figure A.18 Close-up of Failure of Beam PrLCL.1

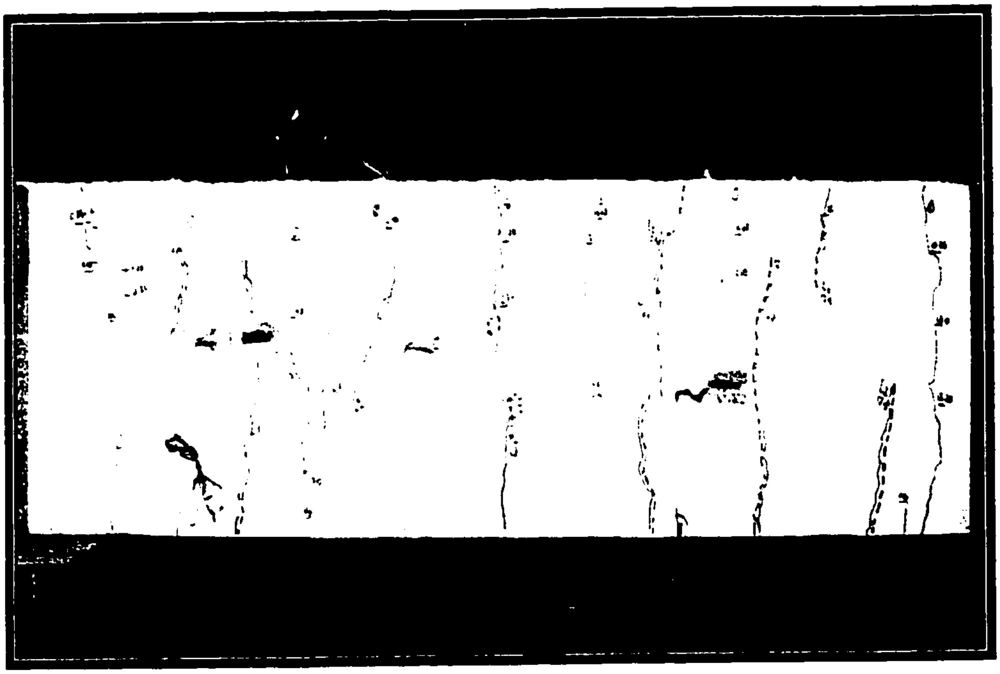

Figure A.19 Cracking due to Thermal Gradient and Mechanically Applied Moment in Beam PrLES.2

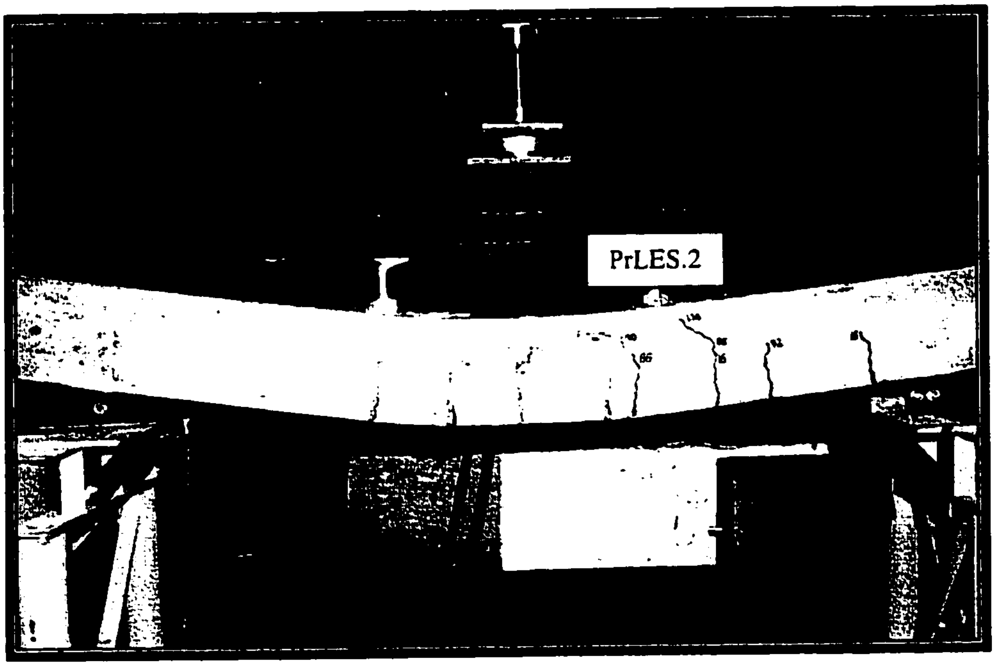

Figure A.20 Beam PrLES.2 at Failure

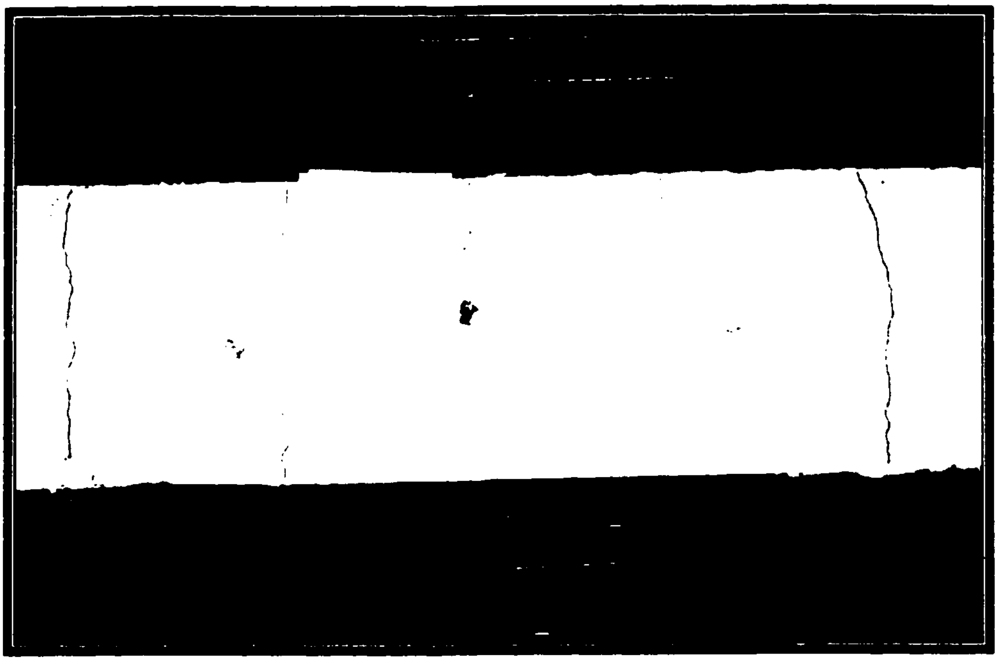

Figure A.21 Cracking due to Thermal Gradient and Mechanically Applied Moment in Beam PoLCS.2

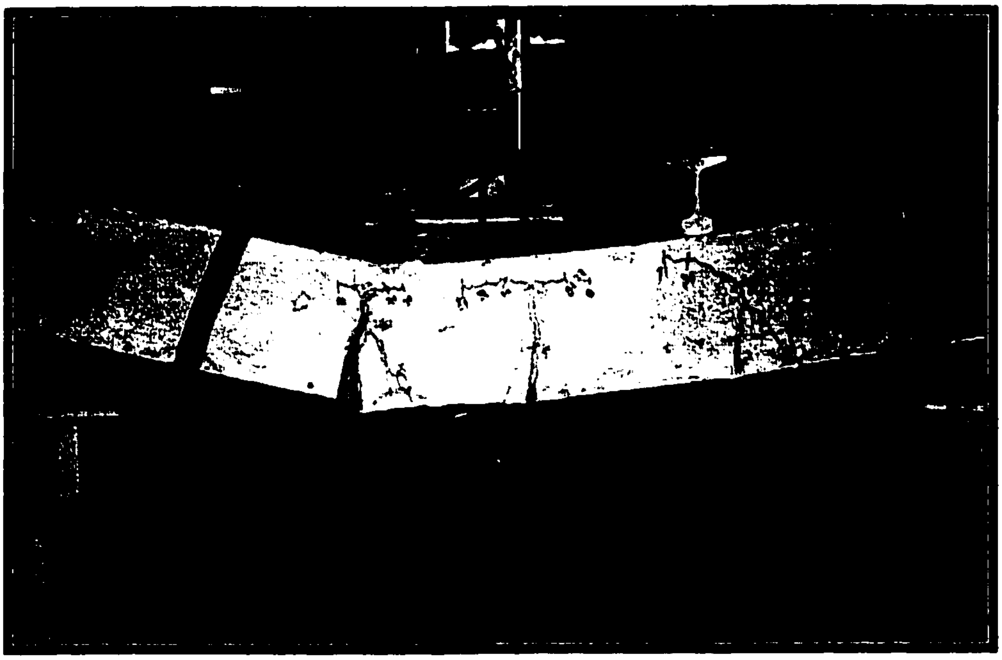

Figure A.22 Beam PoLCS.2 at Failure

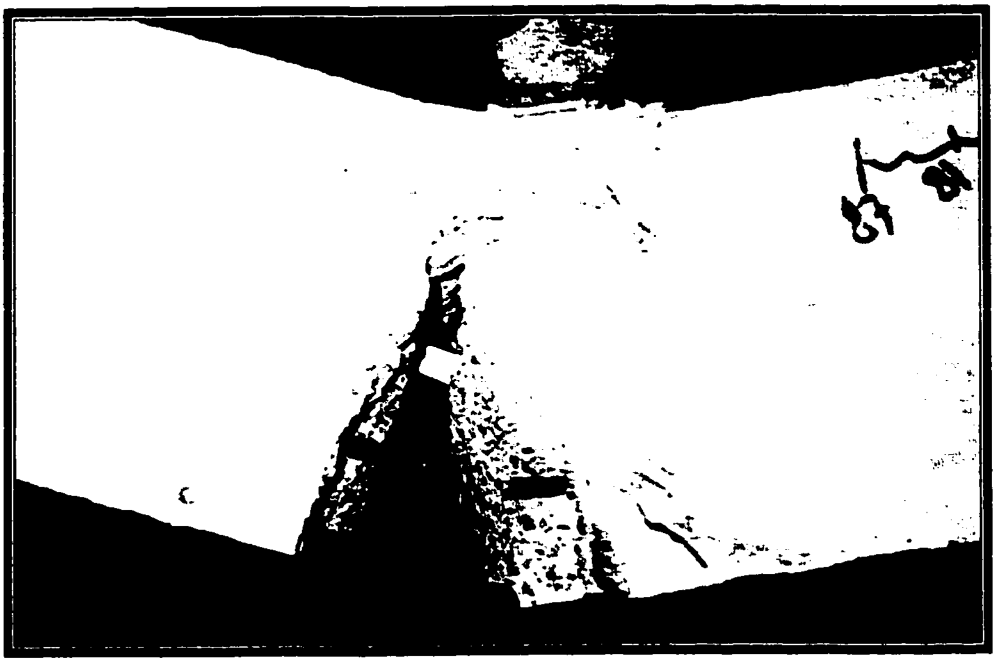

Figure A.23 Close-up View of Failure of Beam PoLCS.2

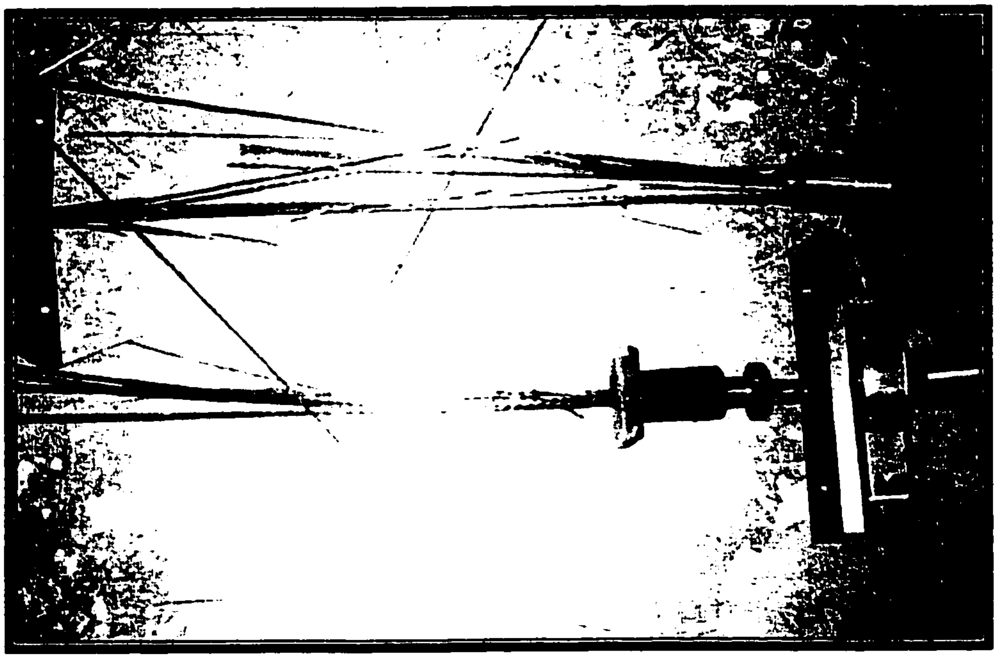

Figure A.24 Broken Cable in Beam PoLCS.2

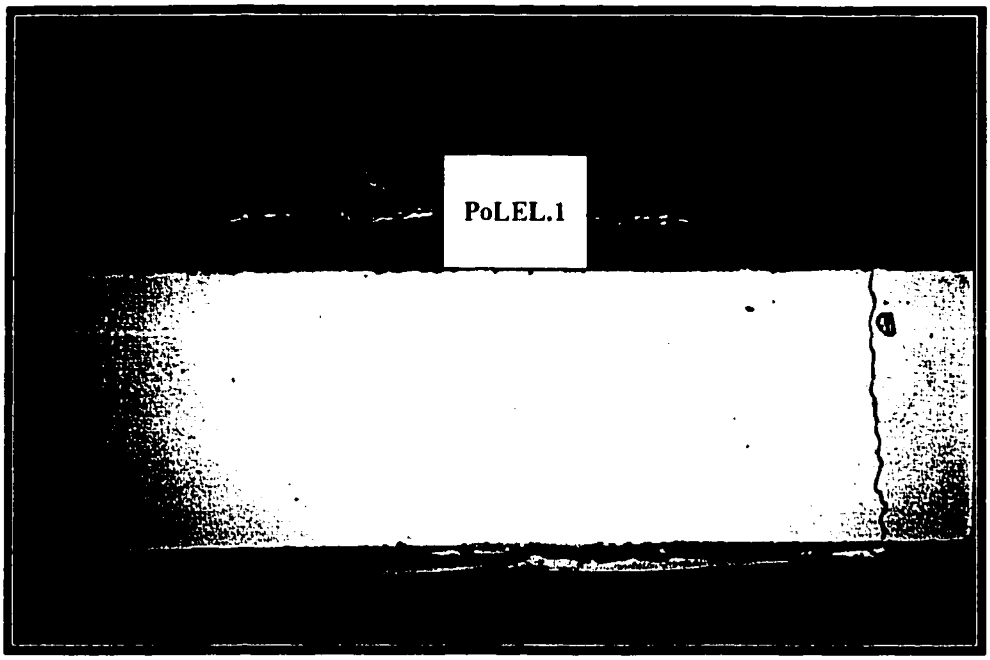

Figure A.25 Cracking due to Thermal Gradient and Mechanically Applied Moment in Beam PoLEL.1

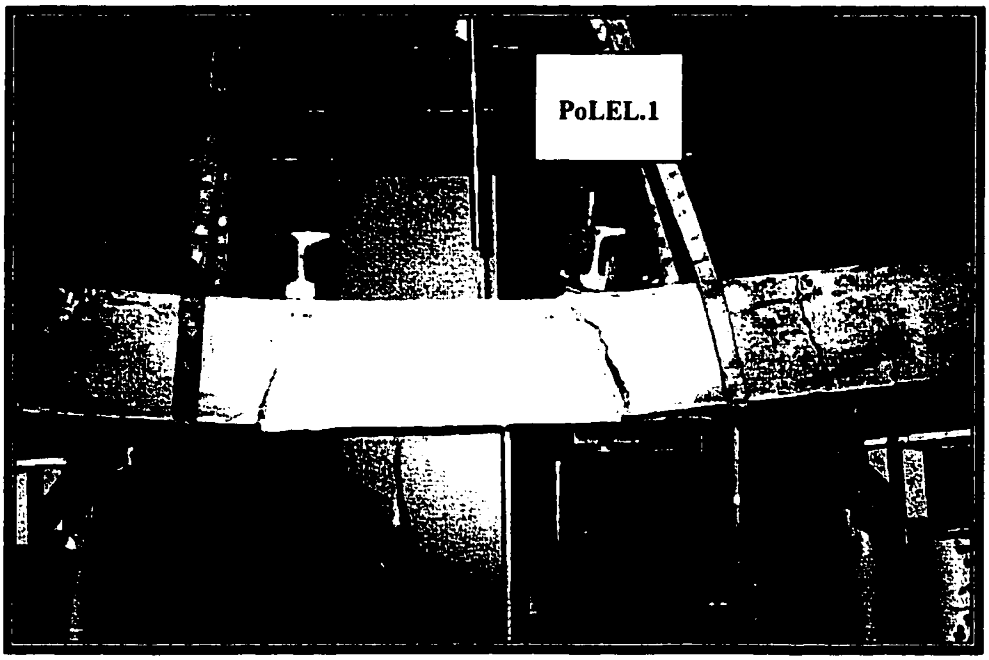

Figure A.26 Beam PoLEL.1 at Failure

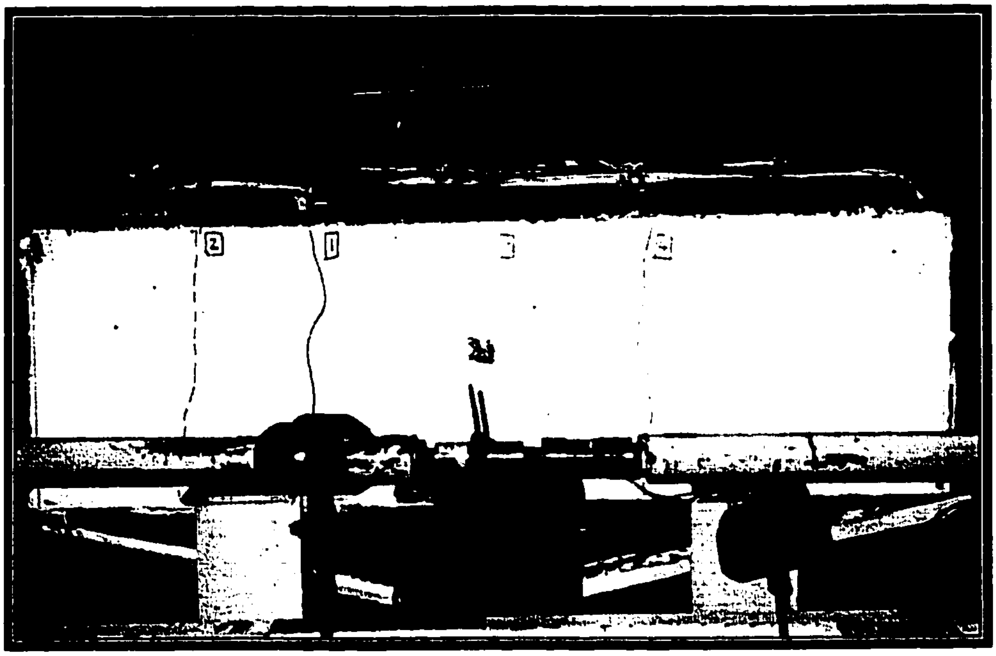

Figure A.27 Cracking due to Thermal Gradient and Mechanically Applied Moment in Beam PoSCS.2

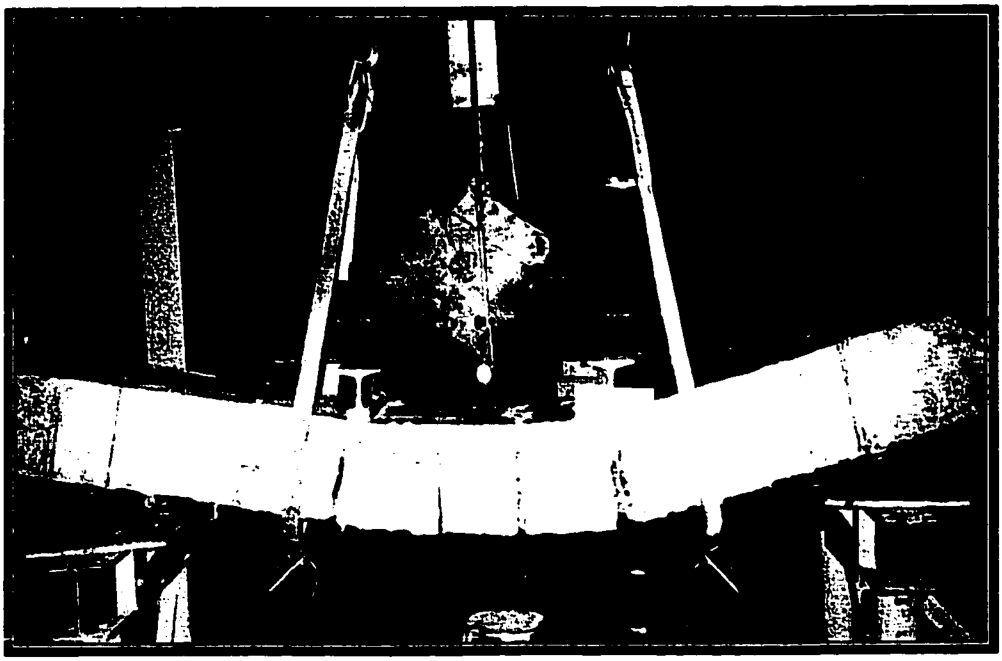

Figure A.28 Beam PoSCS.2 at Failure

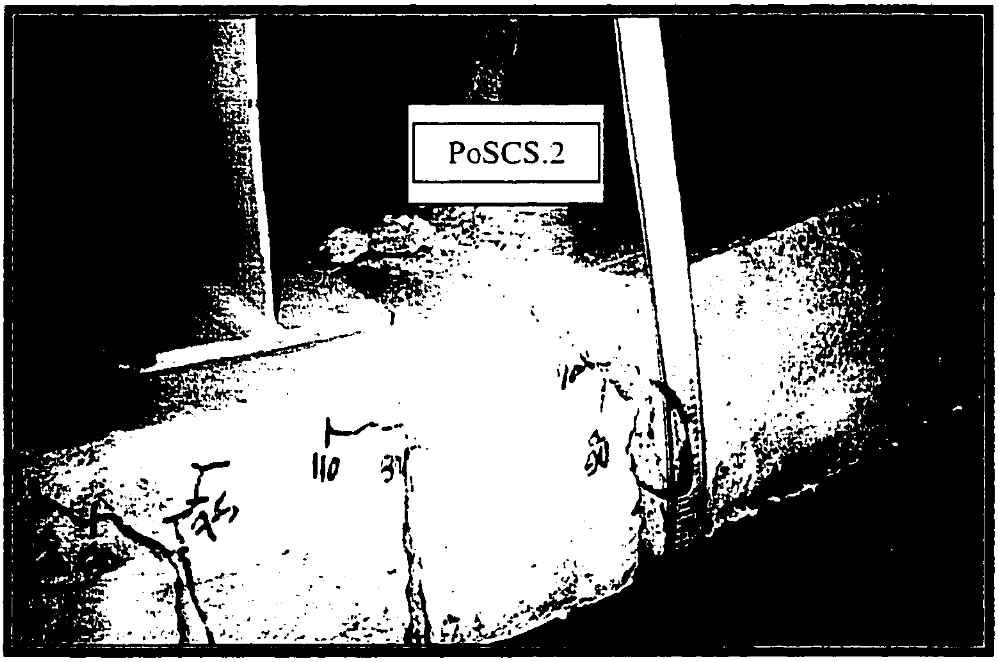

Figure A.29 Close-up View of Failure of Beam PoSCS.2